Effect of corrosion on the mechanical properties of the corroded reinforcement and the residual structural performance of the corroded beams

Wenjun Zhu

Université de Toulouse

THÈSE

En vue de l'obtention du

DOCTORAT DE L'UNIVERSITÉ DE TOULOUSE

Délivré par :

Institut National des Sciences Appliquées de Toulouse (INSA de Toulouse)

Cotutelle internationale avec:

Présentée et soutenue par :
Wenjun ZHU
le jeudi 13 mars 2014

Titre :

Effet de la corrosion sur les propriétés mécaniques de l'armature corrodée et la performance structurale résiduelle des poutres corrodées

---

École doctorale et discipline ou spécialité :
ED MEGEP : Génie civil

Unité de recherche :
Laboratoire Matériaux et Durabilité des Constructions de Toulouse

Directeur(s) de Thèse :

M. Raoul FRANÇOIS

Jury :

M. Alain MILLARD (CEA Saclay)	Rapporteur
M. Christophe PETIT (Université de Limoges)	Rapporteur
M. Dario CORONELLI (Politecnico di Milano, Italia)	Examinateur
M. Bruno CAPRE (Oxand SA)	Examinateur
M. Jean-Paul BALAYSSAC (Université de Toulouse)	Examinateur
M. Raoul FRANÇOIS (Université de Toulouse)	Examinateur

Auteur: Wenjun ZHU

Titre: Effet de la corrosion sur les propriétés mécaniques de l'armature corrodée et la performance structurale résiduelle des poutres corrodées

Thèse de doctorat de l'Institut National des Sciences Appliquées de Toulouse

Spécialité: Génie civil

RÉSUMÉ

Cette thèse s'intéresse à l'étude l'effet de la corrosion sur les propriétés mécaniques des armatures corrodées et les performances mécaniques résiduelles des poutres corrodées. L'étude est basée sur deux poutres corrodées notées B2CL2 et B2CL3, conservés respectivement 26 ans et 28 ans en ambiance saline. Deux poutres non corrodées B2T2 et B2T3 conservées en conditions ambiantes ont également été testés afin d'identifier l'effet de la corrosion indépendamment du vieillissement.

Les propriétés mécaniques des armatures corrodées ont été étudiées par des essais de traction. La limite d'élasticité et résistance à la rupture ont été étudiées sur la base de la section transversale résiduelle évaluée par perte de masse. Les résultats ont montré que les effets de la corrosion sur la diminution ductilité étaient très importants. La forme de la section transversale résiduelle apparait comme étant un paramètre essentiel affectant la ductilité de l'armature.

Les performances résiduelles en flexion des poutres corrodées ont été étudiées. Les résultats montrent que la corrosion réduit la capacité portante et de façon plus significative, la flèche maximale à rupture en raison d'un changement de mode de rupture. La diminution de la charge de plasticité apparait en relation avec la perte de section d'acier tendu due à la corrosion

Des poutres de portées courtes ont été réalisées à partir des poutres corrodées après les essais de flexion. Les tests mécaniques ont été effectués en flexion pour vérifier la réponse des poutres courtes corrodées. Les poutres courtes corrodées ont péri en flexion avec une bonne ductilité tandis que les poutres courtes non corrodées ont péri comme prévu en cisaillement suivant un mode de rupture fragile, qui a montré que la corrosion de l'armature pouvait modifier les modes de défaillance.

Les produits de corrosion ont été recueillis à partir de l'armature corrodée de B2Cl3. Des expériences XRD et TG ont été menées afin d'identifier la composition des produits de corrosion. Le coefficient d'expansion des produits de corrosion a été déduit, ce qui pourrait être utile pour les recherches futures concernant le mécanisme de fissuration du béton d'enrobage.

Mots clés: chlorures, corrosion, ductilité, béton armé, flexion, effort tranchant

Thèse soutenue le 13 Mars 2014 à l'INSA de Toulouse devant la commission d'examen composée de :

Mr. Alain MILLARD (CEA Saclay)	Rapporteur
Mr. Christophe PETIT (Université de Limoges)	Rapporteur
Mr. Raoul FRANÇOIS (Université de Toulouse)	Examinateur
Mr. Dario CORONELLI (Politecnico di Milano, Italia)	Examinateur
Mr. Bruno CAPRE (Oxand SA)	Examinateur
Mr. Jean-Paul BALAYSSAC (Université de Toulouse)	Examinateur

Author: Wenjun ZHU

Title: Effect of corrosion on the mechanical properties of the corroded reinforcement and the residual structural performance of the corroded beams

PhD thesis at l'Institut National des Sciences Appliquées de Toulouse

Specialty: Civil Engineering

ABSTRACT

The thesis aims to study the influence of chloride corrosion on the mechanical properties of the reinforcement and RC beams. The experiments were based on two corroded beams named B2Cl2 and B2Cl3, with a corroded age of 26 years and 28 years respectively. Two non-corroded beams B2T2 and B2T3 which were cast in the same condition and same time were also tested in order to make clear the corrosion effect.

The mechanical properties of the corroded reinforcement were investigated by the tension tests. The yield strength and ultimate strength were studied based on the residual gravimetrical cross-section. The results found that the impact of corrosion on the ductility was more significant than that of the strength. The shape of residual cross-section was considered to be in deep relationships with the ductility of the reinforcement.

The flexural performances of the beams were studied. The results showed that the corrosion deteriorated the capacity and the ductility of the corroded beams. The corrosion degree of reinforcement was found in linear with the residual yield capacity of the corroded beams.

The short-span beams were formed from the corroded beams after bending tests. Mechanical tests were carried out directly to check the response of the corroded beams. The corroded short-span beams failed in bending mode with good ductility while the non-corroded beams performed a brittle shear failure mode, which showed that the corrosion of reinforcement could change the failure modes.

The corrosion products were collected from the corroded reinforcement of B2Cl3. XRD and TG experiments were conducted so as to identify the composition of the corrosion products. The expansive coefficient of the corrosion products was deduced, which could be helpful for the further research on the cracking mechanism of the concrete cover.

Key words: chloride corrosion residual ductility mechanical properties residual strength shear bending expansion coefficient

Dedication

TO MY BELOVED PARENTS

ACKNOWLEDGEMENT

This thesis was carried out at the Laboratoire Matériaux et Durabilité des Constructions de l'Institut National des Sciences Appliquées de Toulouse and l'Université Paul Sabatier de Toulouse III – Université de Toulouse.

First of all, I would like to thank CSC (China Scholarship Council) who financed my thesis during 2010.9-2014.2. Then the academic research life in France became true, which was a pleasant and memorable experience in my career.

I would like to express my deep appreciation and special thanks to my supervisor Mr. Raoul FRANÇOIS for his enthusiastic support and guidance throughout out my doctoral program. His fruitful comments and valuable suggestions kept me motivated during this research. It is a great honor to finish this program under his help.

I am grateful to Mr. David CLELAND who is a professor in Queen's University, Belfast, UK for the precious discussions and advices during my research, which is helpful to achieve my publications and dissertation.

I am also grateful to Mr. Dario CORONELLI who is a professor in Politecnico di Milano, Milano, Italy, for the patience to discuss and improve my investigation, which is of great importance for my publications and dissertation.

I would like to thank Mr. Alain MILLARD, Mr. Christophe PETIT, Mr. Dario CORONELLI, Mr. Bruno CAPRA and Mr. Jean-Paul BALAYSSAC for agreeing to be the reviewers of my dissertation. All the advices and suggestions from the reviewers will be appreciated.

I would like to show my special thanks to Mr. Gilles ESCADEILLAS and all the technicians and other staffs of LMDC, their kind help and positive attitude send me considerable encouragement to get over all the

difficulties I have met during the last three years.

I must also acknowledge all my friends in Toulouse, including Chinese and other international friends. They provided me the brand new cultures and customs, which colored my experience and enriched my knowledge in France.

Last but not least, I would like to express my sincerely appreciation to my family. Thanks for their endless encouragement, prayer and support, all of these will be cherished in my life.

TABLE OF CONTENTS

LIST OF TABLES

LIST OF FIGURES

RÉSUME

La corrosion des armatures des structures en béton est un énorme problème économique pour le monde entier.

Le béton est sans doute la meilleure protection de l'acier vis-à-vis de la corrosion en raison du pH élevé de sa solution interstitielle présente dans la porosité. Cependant, il existe deux causes principales d'amorçage de la corrosion : la diminution du pH de la solution interstitielle due à la carbonatation (réaction du gaz carbonique avec les hydrates du béton conduisant à la formation d'un acide faible) qui permet la corrosion de l'acier, ou rupture local du film passif recouvrant l'acier en raison de la présence d'un taux minimum d'ions chlore (figure 1).

Figure 1 : corrosion de l'acier

Une fois que la phase de propagation de la corrosion est active, les détériorations de la structure sont caractérisées par un éclatement du béton d'enrobage, résultant du caractère expansif des produits de corrosion, et s'accompagnent d'une réduction de la section des aciers ainsi que d'une perte d'adhérence acier-béton. Comparativement, la corrosion due aux chlorures est plus dangereuse que celle due à la carbonatation à cause de son développement rapide et le risque de rupture soudaine pour le cas des environnements sévères. Les principaux facteurs environnementaux mis en cause sont les chlorures provenant de l'eau de mer ou de

l'air marin et l'utilisation de sels fondants pour le déverglaçage des routes.
La corrosion conduit à la détérioration du comportement mécanique des structures, qui est fonction de leur état de corrosion. La majeure partie des études consacrées à la durée de vie considère que le critère de fin de service correspond au démarrage de la phase de propagation de la corrosion. Pourtant, cet instant ne signifie pas que la performance de la structure est mise en cause. Les recherches menées au LMDC montrent que la phase de propagation de la corrosion peut représenter une part importante de la durée de vie des ouvrages en béton armé. Ne considérer que la phase d'initiation semble représenter donc une démarche trop conservative. Ainsi, pouvoir prédire l'évolution du comportement mécanique des structures en béton armé au cours de leur vieillissement est un objectif d'importance majeure pour les maîtres d'ouvrage afin de prévoir éventuellement des réparations, le renforcement de la structure, un programme de maintenance ou, au contraire, la destruction et le remplacement de l'ouvrage.

L'objectif de la thèse est donc de caractériser expérimentalement des effets d'une corrosion sévère sur les propriétés mécaniques des structures en béton armé exposées en atmosphère saline afin de prévoir leur durée de vie résiduelle.
L'étude de la phase de propagation de la corrosion et de ses conséquences sur le fonctionnement mécanique en service ou à rupture, est basée sur l'analyse du vieillissement d'éléments en béton armé, et plus particulièrement sur l'analyse exhaustive de deux poutres corrodées notée B2CL2 et B2CL3 （figure 2）. Ces poutres font parties d'un ensemble d'éléments de trois mètres longueur, conservés depuis respectivement 26 ans et 28 ans en ambiance saline et sous différentes intensités de chargement en flexion trois points. Il s'agit donc de conditions de vieillissement très proches de celles des structures réelles. Cette partie expérimentale est la suite d'un programme de vieillissement du béton armé démarré en 1984 à Toulouse, et dont le support en était la thèse de doctorat de Raoul François. Il a bénéficié d'un financement de l'AFREM (Association Française de Recherche et d'Etudes sur les Matériaux) et de l'AFB (Association Française du Béton) qui ont depuis fusionnées pour donner naissance à l'AFGC (Association Française du Génie Civil). L'objectif initial de l'étude était de comprendre les relations existantes entre la fissuration de service (structurale) du béton armé et la corrosion des armatures. En effet, les règlements de calcul (de l'époque) limitaient l'ouverture des fissures structurales afin d'obtenir une durée de vie suffisante en environnement agressif sans que ces mesures s'appuient sur des bases expérimentales suffisamment pertinentes.

(a) Poutres corrodées B2Cl2 (26 ans)

(b) Poutres corrodées B2Cl3 (28 ans)

Figure 2: poutres corrodées

Le vieillissement des poutres et leur dégradation progressive par la propagation de la corrosion ont permis de réaliser à différentes échéances des études sur les conséquences mécaniques de la corrosion pour le comportement en service ou à rupture des poutres en béton armé (Thèses d'Arnaud Castel et de Ruijin Zhang pour les poutres de type B ; thèses de Thierry Vidal, Inamullah Khan et Vu Hiep Dang pour les poutres de type A)

La phase de propagation de la corrosion avait débuté presque en même temps pour les poutres de type B à faible enrobage (1 cm) que pour les poutres A à fort enrobage (4cm) avec dans ce dernier cas des fissures de corrosion démarrant à l'intersection entre fissures de flexion et armatures tendues (figure 2). Cependant la corrosion des poutres B a démarré à la fois au niveau des armatures tendues et des armatures comprimées alors que dans le cas des poutres A les armatures tendues ont été d'abord corrodées bien avant que la corrosion démarre également sur les armatures comprimées.

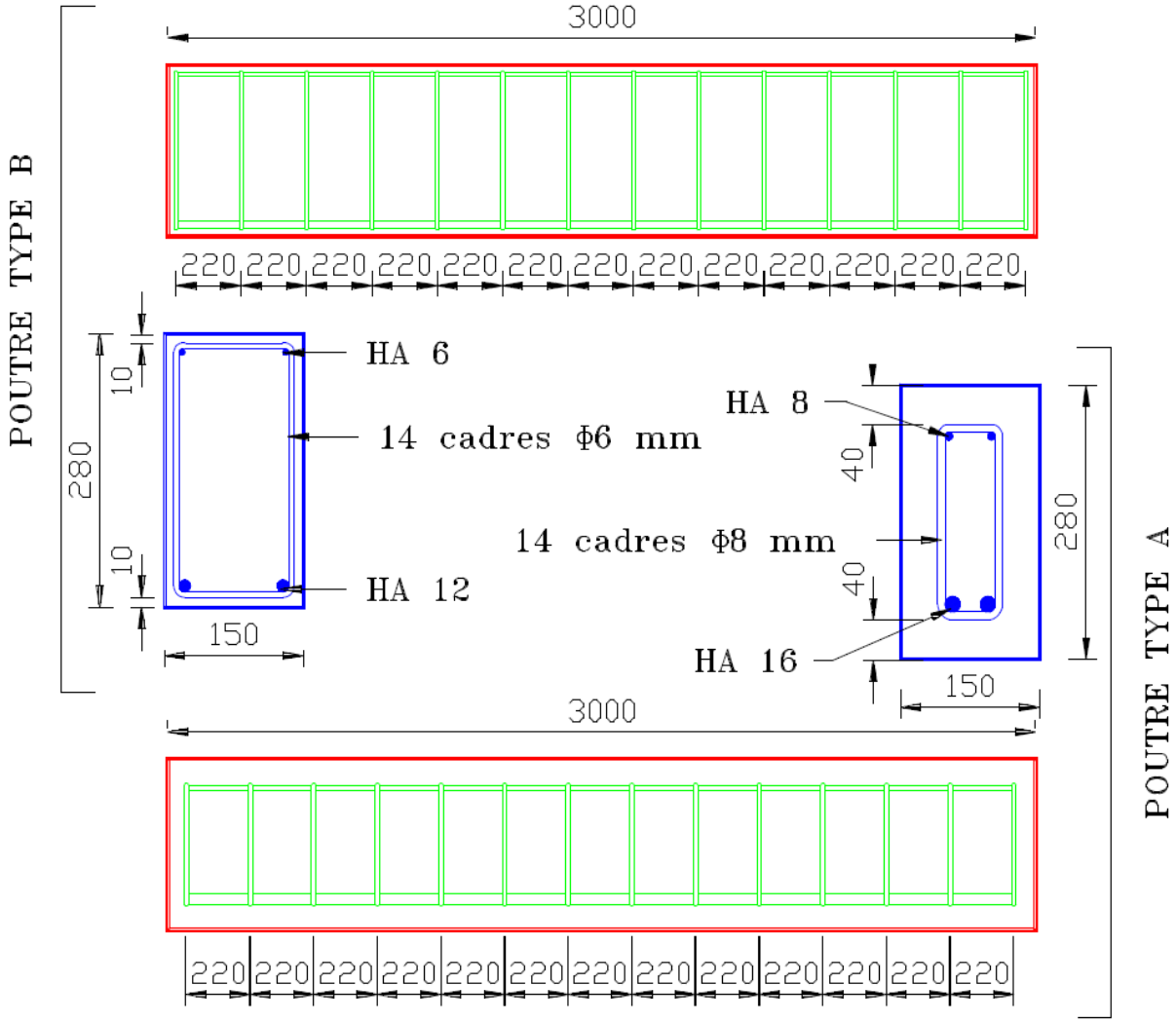

Figure 2: plan de ferraillage des deux types de pout

Le choix de restitution des résultats obtenus dans cette thèse est de proposer outre une analyse bibliographique sur la propagation de la corrosion et ses conséquences mécaniques, une succession de chapitre basée sur des articles publiés ou en relecture.

Le premier chapitre correspond à l'introduction générale de la thèse.

Le second chapitre correspond à une bibliographie sur les conséquences de la corrosion des armatures sur le comportement mécanique des structures en béton armé. On discute des résultats concernant la modification des propriétés mécaniques des armatures en acier en traction en terme de contrainte de plastification, contrainte de traction à rupture et allongement maximal à rupture. On fait également le bilan des études sur la modification de l'adhérence acier-béton liée à la corrosion des armatures. Puis la modification du comportement global : réponse en flexion et réponse vis-à-vis de l'effort tranchant sont

ensuite présentées. Les différentes méthodes utilisées pour mesurer le taux de corrosion sont également discutées. Les différentes techniques pour induire la corrosion : accélération sous champ électrique, conditions naturelles, sont également discutées.

Le troisième chapitre rappelle le programme expérimental mis en place en 1984 par R. François.

Le quatrième chapitre présente l'étude de l'impact de la corrosion sur les propriétés mécaniques de l'acier. En effet, après avoir testé les poutres jusqu'à la rupture, les barres d'acier corrodées ont été récupérées des poutres corrodées B2CL2 et B2CL3 ainsi que des poutres non corrodées B2T2 et B2T3. Les barres d'armature ont été nettoyées en utilisant une solution de Clark ANSI / ASTM G1-72 afin d'éliminer tous les produits de corrosion. Le degré de corrosion des armatures a été évalué en mesurant la perte de diamètre à l'aide d'un pied à coulisse après le retrait complet des produits de corrosion. Il est très difficile de mesurer la perte précise du diamètre de cette manière à cause de la forme de la surface de l'armature corrodée qui est très tortueuse et varie considérablement suivant la longueur de la barre. Par conséquent, la perte de poids de la barre d'acier a également été utilisée pour calculer la perte de diamètre (mesurée sur des segments de barres de quelques mm de longueur).

Figure 3 : les barres d'acier testées

Les barres d'acier ont été testées en traction en utilisant une machine de capacité 250 kN (figure 3). Deux LVDT ont été utilisés pour mesurer l'allongement des barres d'acier. La longueur de base pour la mesure de l'allongement était de 200 mm pour chaque barre d'acier. Les résultats obtenus sont utilisées pour tracer les diagrammes de contrainte-déformation pour chaque échantillon testé. En utilisant des diagrammes contrainte-déformation, la limite élastique, la résistance à la rupture et l'allongement des barres d'acier ont été comparées pour les barres corrodées et non corrodées.

Les contraintes nominales ont été calculées en utilisant le diamètre nominal de la barre d'acier. Les contraintes réelles ont été calculées de deux manières différentes. La première méthode utilise le diamètre réduit mesuré avec le pied à coulisse. Pour éviter la difficulté de mesure avec un pied à coulisse dans le cas de piqures qui ne réduisent pas le diamètre de façon uniforme, une deuxième méthode basée sur la perte de masse de la barre d'acier corrodé, a été utilisée. Voici ci-après quelques conclusions tirées des résultats expérimentaux.

La limite d'élasticité nominale de barres diminue avec le degré de corrosion des armatures en relation avec le fait que la corrosion réduit la section transversale. Toutefois, lorsque la section transversale réduite a été utilisée à la place de section nominale, il a été remarqué que la limite d'élasticité vraie de toutes les barres corrodées et non corrodées avaient la même valeur. On peut dire que la corrosion ne modifie pas la limite élastique des barres d'acier. La contrainte à la rupture nominale diminue avec le degré de corrosion des armatures en relation avec le fait que la corrosion réduit la section transversale. Cependant, la contrainte vraie à rupture des aciers corrodés augmente par rapport aux témoins. Pour toutes les barres non corrodées, le rapport entre la contrainte à la rupture et la limite d'élasticité est d'environ 1,13. Dans le cas des barres corrodées, ce rapport est très supérieur dans un intervalle de 1,3 à 1,6. Ce résultat est lié en partie au mode de calcul des contraintes : nominales pour les barres non corrodées sans tenir compte de l'effet de striction, en fonction de la section « vraie » pour les armatures corrodées avec une striction également non prise en compte mais qui est très fortement réduite en raison de la nature fragile de la rupture des aciers corrodés.

Les barres corrodées n'ont pas montré le plateau plastique au-delà de la limite élastique et de plus le phénomène d'écrouissage est plus marqué avec une augmentation de la contrainte à rupture (figure 4). Cependant l'allongement à rupture est considérablement réduit pour toutes les armatures corrodées. C'est potentiellement le problème le plus important lié à la corrosion, en effet presque toutes les barres d'acier corrodées ont une déformation à la rupture en dessous de la valeur minimale (0,05) requise par l'Eurocode 2 pour les aciers de classe B. Ce point peut compromettre la requalification des structures corrodées.

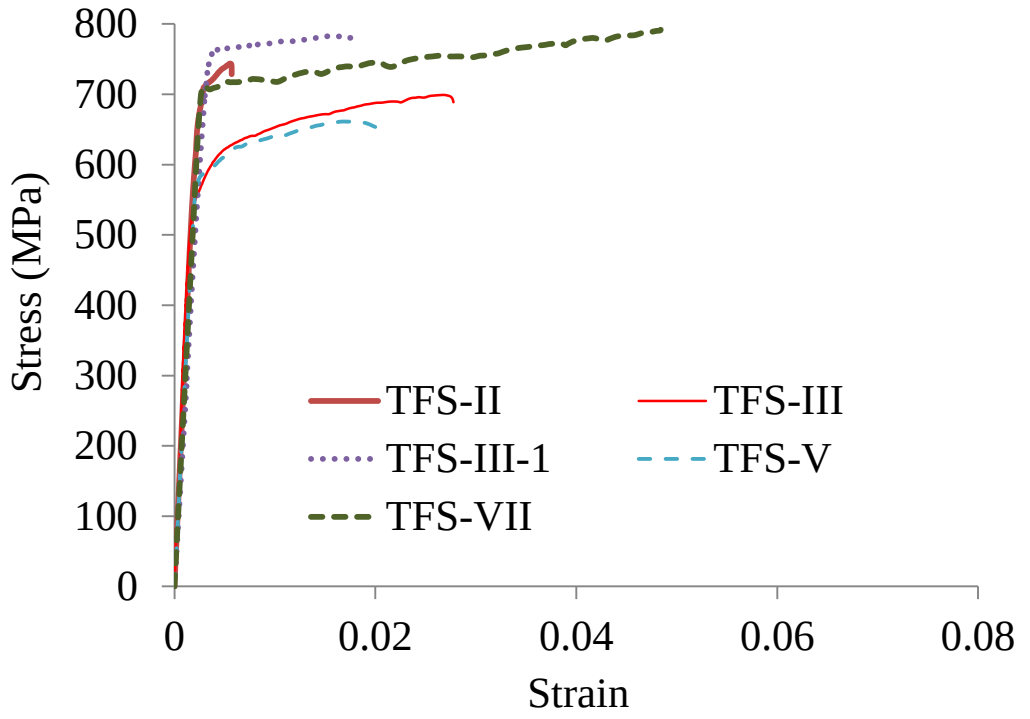

Figure 4 : réponse de barres corrodées

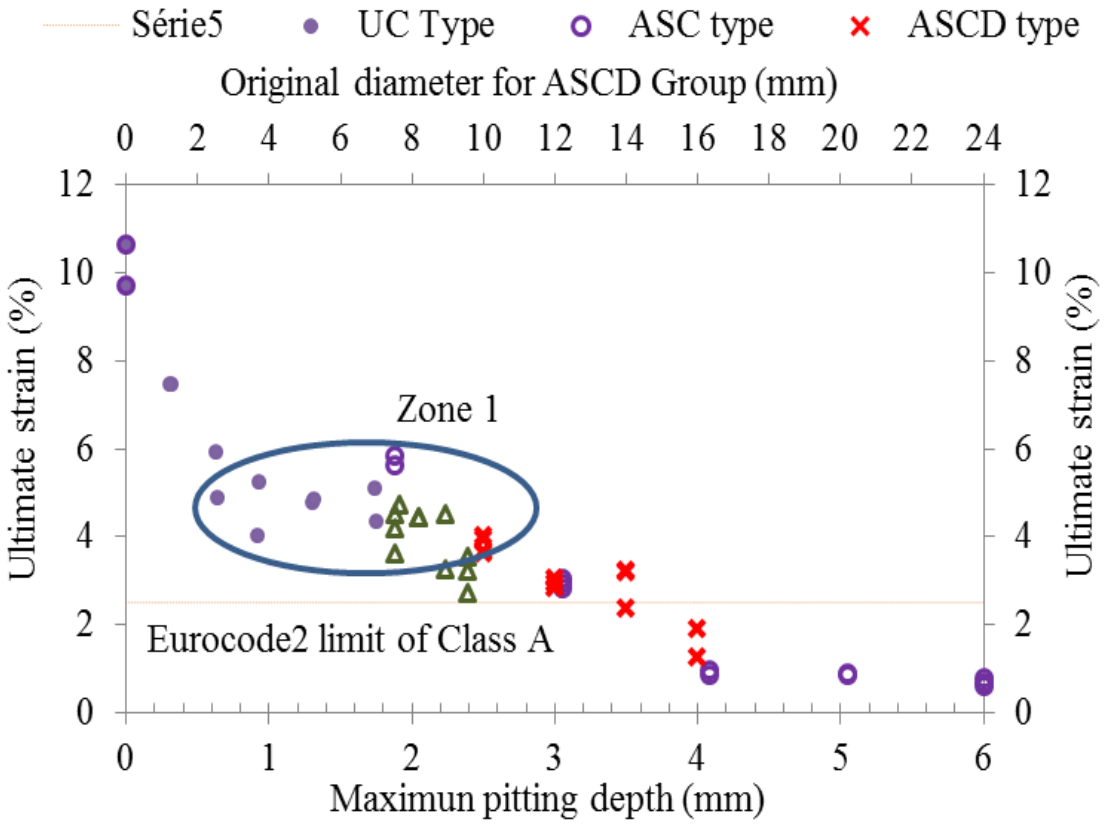

Figure 5 : Influence de la forme de la perte de section, de la profondeur d'entaille et du diamètre sur l'allongement maximal à rupture.

Des essais complémentaires simulant différents types de perte de section : axisymétrique,

pour une corrosion « uniforme », dissymétrique, pour une piqure localisée et partiellement symétrique, pour représenter deux piqures diamétralement opposées de taille différentes ; ont été réalisés. Ces essais ont permis de confirmer le rôle important de la « forme » de l'entaille créée par la corrosion sur la réponse ductile (figure 5).

Le cinquième chapitre concerne les résultats expérimentaux obtenus à partir des essais de mécaniques réalisés sur 2 poutres issues du programme expérimental mis en place en 1984 par R. François. Ce chapitre présente l'étude de l'évolution du faciès de corrosion des armatures et ses conséquences sur le comportement mécanique en service du béton armé. Le travail expérimental est consacrée à l'étude exhaustive de deux poutres, notées B2CL2 et B2CL3 âgées respectivement de 26 ans et de 28 ans et soumises à l'effet couplé du chargement et de la corrosion en atmosphère saline, avec en particulier l'évaluation de la fissuration due à la corrosion, la distribution de la corrosion mesurée par les pertes de section le long des armatures ainsi que l'évolution du comportement mécanique à rupture. Deux poutres témoins de même age que les poutres corrodées sont aussi testés : B2T2 et B2T3.

Les cartes de fissuration des poutres corrodées B2CL2 et B2CL3 après 26 et 28 ans d'exposition en ambiancé saline ont été tracées. En plus des fissures transversales de flexion, qui ont résulté de la flexion trois points initiale, qui sont localisées dans la partie centrale de la traction de la poutre, beaucoup de fissures de corrosion ont également été observées le long des armatures tendues, des armatures comprimées ainsi qu'un développement de la fissuration transversale due à la corrosion des cadres d'effort tranchant. On note également de larges zones de délamination qui sont présentes à la fois le long des armatures tendues et le long des armatures comprimées. De larges zones proches des appuis sont également concernées.

Les cartes de corrosion ont également été élaborés (figure 6), qui montrent l'étendue de la corrosion sur les barres longitudinales tendues FS (barre antérieure) et BS (barre postérieure). Les cartes sont tracées dans deux directions: l'orientation vers le bas pour le côté de l'acier directement exposé aux fissures et à solution saline et la direction vers le haut dans laquelle la face d'acier a une couverture de béton beaucoup plus épaisse. Il est constaté que l'attaque de corrosion n'est pas uniforme. Beaucoup de piqûres de corrosion ont été observés de façon hétérogène sur les barres et la perte maximale de section des armatures tendues atteint 43% au niveau des piqûres de corrosion les plus importantes. Les armatures « comprimées » présentent également une corrosion très développée et non uniforme avec des pertes locales de sections dépassant largement 50% de la section initiale.

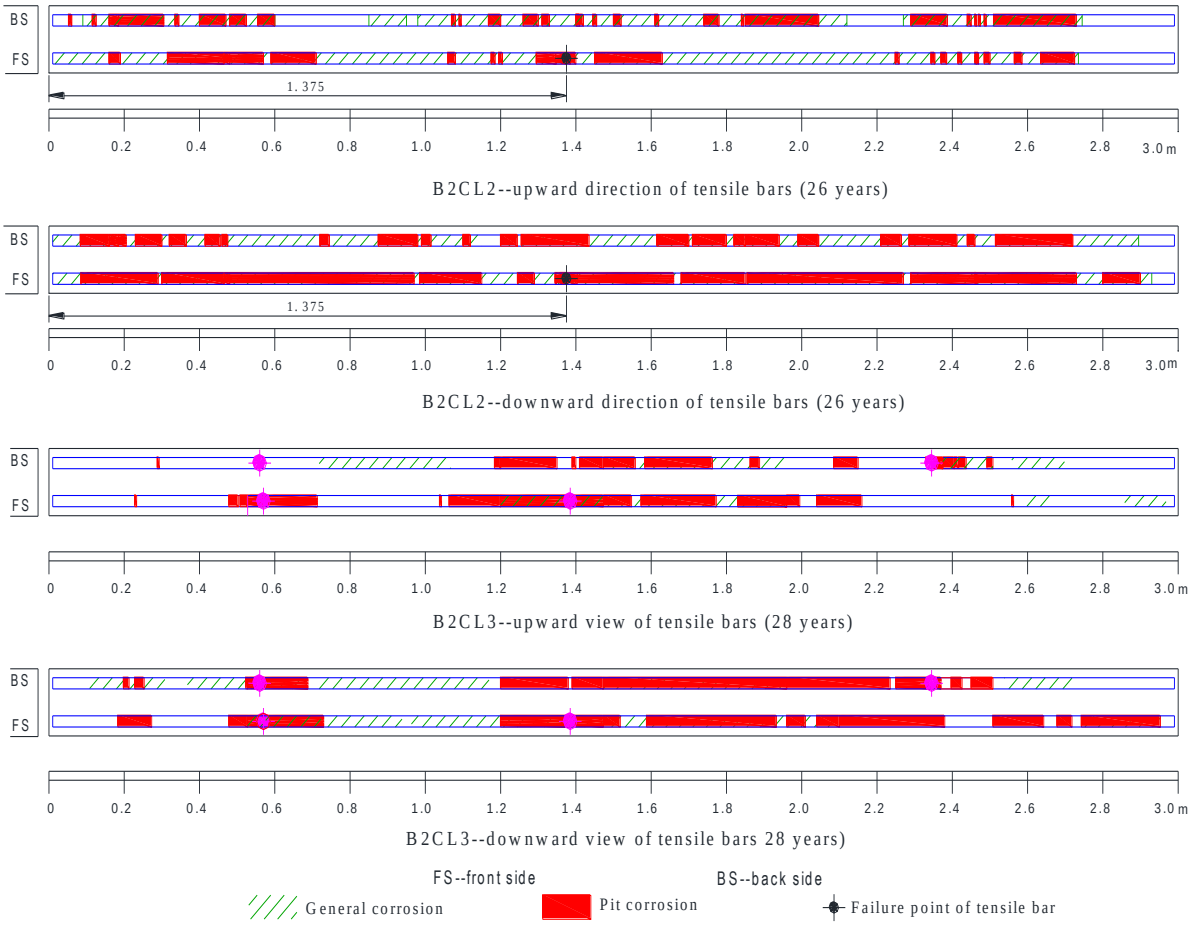

Figure 6: corrosion sur les barres longitudinales tendues

Au cours des essais de flexion, il a été observé que la corrosion avait largement réduit la flèche maximale à rupture des poutres et modifié le type de rupture passant de l'écrasement du béton comprimé pour le témoin à la rupture fragile des aciers tendus pour les poutres corrodées. Cela implique que la corrosion affecte non seulement la résistance des poutres, mais aussi induit une fragilité dans leur comportement. Par conséquent, les grandes déformations, qui se produisent dans les structures en béton-armé en flexion avant la rupture, ne se produiront pas dans le cas d'un renforcement très corrodé, éliminant ainsi l'avertissement le plus souhaitable avant la défaillance de la structure. Des diminutions de 57% et 72% de la flèche ultime des poutres corrodées ont été enregistrées par rapport aux poutres témoins, ce qui indique clairement que la corrosion affecte directement le comportement ductile des poutres en béton armé et peut changer le mode de défaillance des poutres en béton. Le modèle de Castel et al a été utilisé pour prendre en compte la perte de ductilité des aciers tendus. Dans ce modèle, la diminution de la ductilité est liée à la perte maximale de section d'acier.

Les charges de plastification et ultime des poutres corrodées ont également été réduite par rapport aux poutres témoins. Logiquement, une réduction de 1% de la section d'acier due à la

corrosion conduit à une réduction de 1% de la charge de plastification. Cependant, on constate expérimentalement que la capacité ultime est moins réduite avec des valeurs de 0,65% et 0,9%, pour 1% de perte de section d'armatures tendues.

Il a été conclu que le comportement mécanique d'une poutre corrodée diffère de son comportement avant la corrosion de trois façons principales: une diminution de la capacité portante caractérisé par un changement dans le mode de défaillance du béton, une réduction de la flèche maximale à rupture liée au comportement fragile de l'acier corrodé, et une diminution de la rigidité globale due à la corrosion des barres et la perte d'adhérence acier-béton. Ce dernier point n'étant pas le plus important et pouvant varier en fonction de la fissuration transversale.

Le sixième chapitre s'intéresse à l'étude de la cinétique de corrosion tout au long du programme expérimental initié en 1984. La variabilité des résultats obtenus pour les contraintes de plastification et ultime des aciers corrodés est également utilisée pour prévoir le comportement mécanique des poutres corrodées. L'utilisation de la limite élastique vraie après corrosion permet de prédire la charge de plastification des poutres corrodées (figure 7).

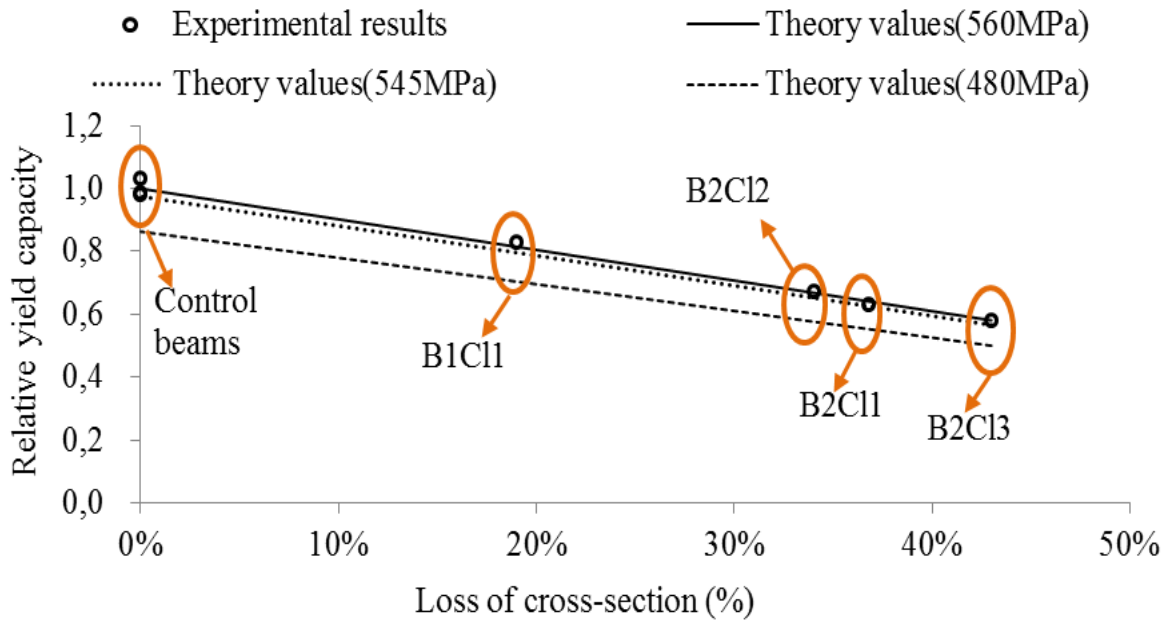

Figure 7 : Evolution de la charge de plastification en fonction de la perte de section due à la corrosion et comparaison avec les valeurs prévues en fonction des contraintes moyennes et caractéristiques de plastification des aciers corrodés.

L'utilisation de la contrainte ultime vraie après corrosion permet de prédire la charge ultime des poutres corrodées (figure 8).

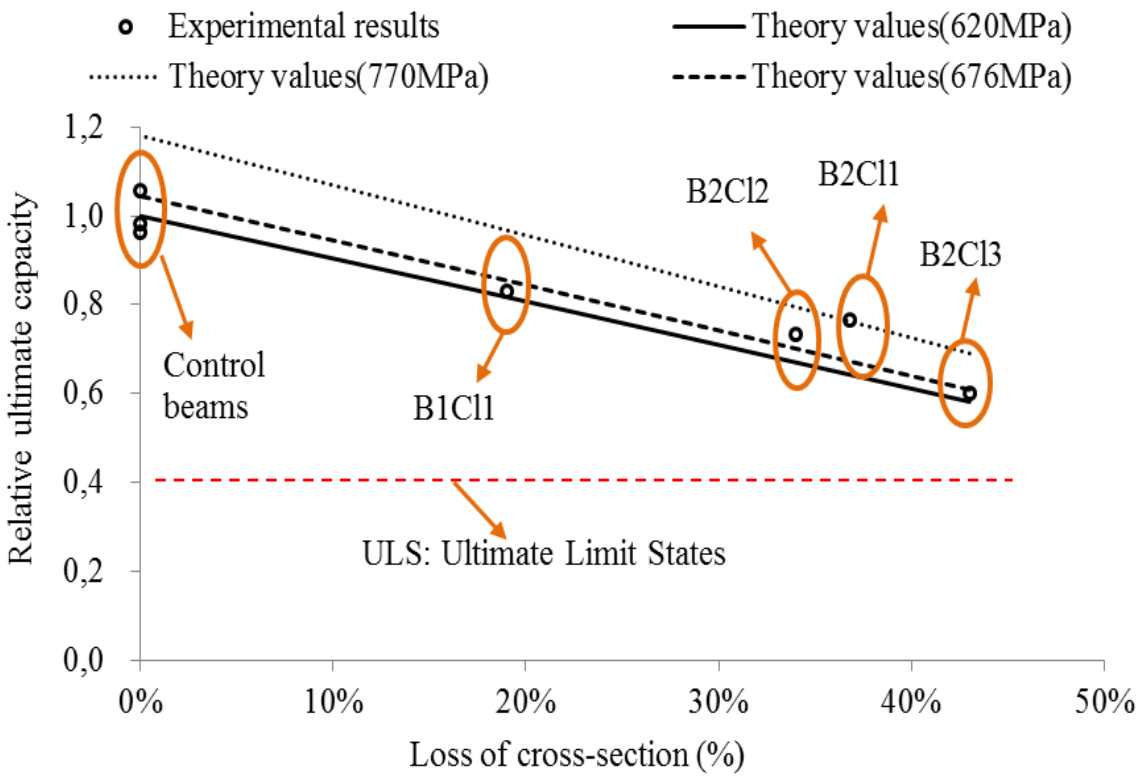

Figure 8 : Evolution de la charge ultime en fonction de la perte de section due à la corrosion et comparaison avec les valeurs prévues en fonction des contraintes moyennes et caractéristiques à rupture des aciers corrodés.

Une synthèse des intensités de corrosion calculées en fonction de la perte maximale de section d'armatures montre que la vitesse moyenne de corrosion est de l'ordre 1.4 $\mu A/cm^2$ pendant tout le processus de corrosion (cf figure 9). Ce résultat confirme que la phase de propagation de la corrosion est très longue et devrait être prise en compte dans les modèles de prédiction de la durée de vie. Il reste évidemment à définir réglementairement et suivant le contexte, le critère de fin de durée de vie : cependant si l'on considère la capacité ultime résiduelle supérieure à la charge de dimensionnement à l'ELU, la durée de vie prévue est de 45 ans ce qui correspond à 5 ans d'initiation et 40 ans de propagation de la corrosion.

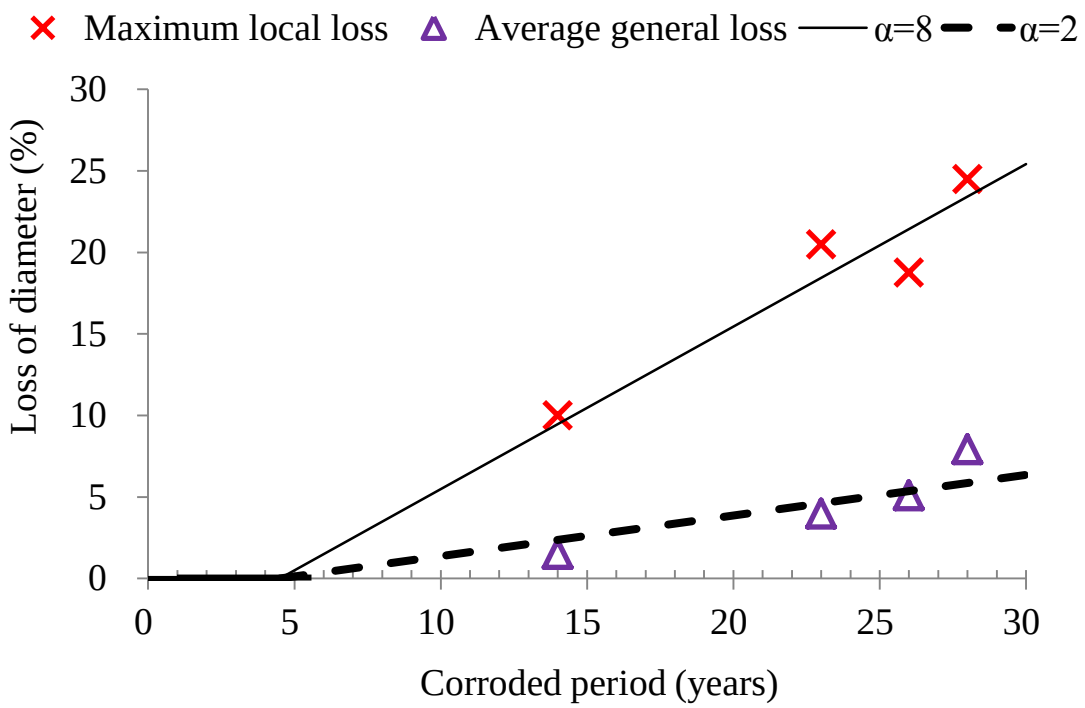

(a) la vitesse moyenne de corrosion pendant tout le processus de corrosion

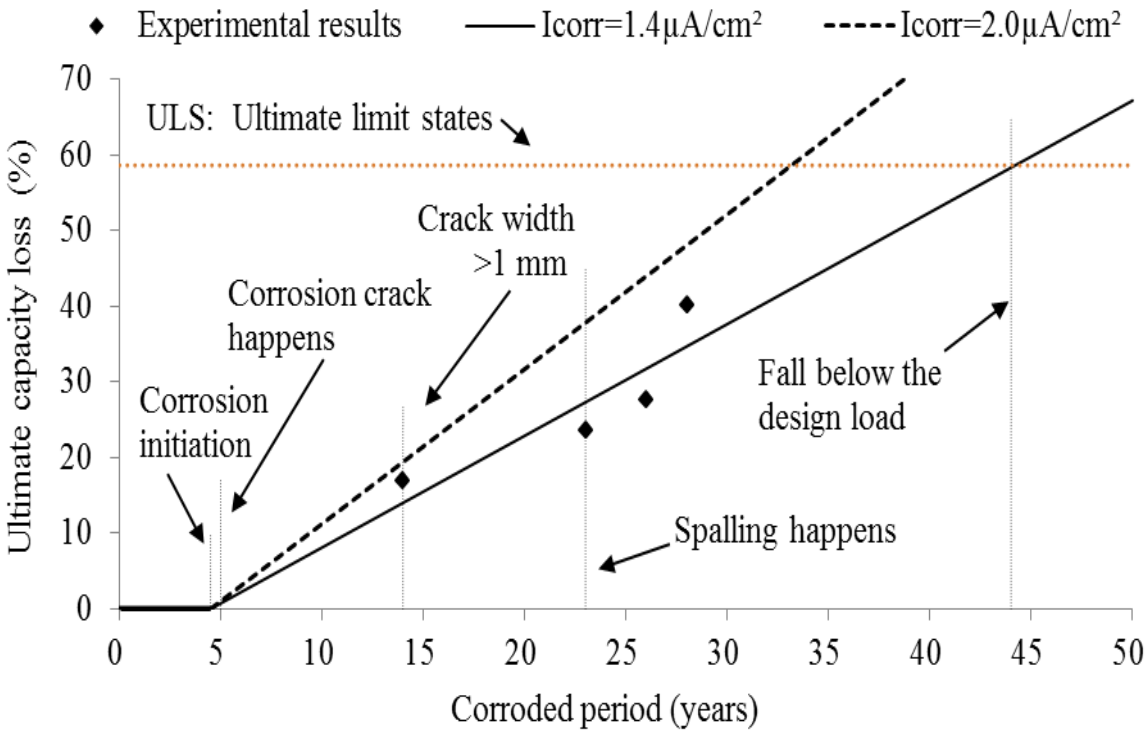

(b) Evolution de la durée de vie

Figure 9 : Evolution de la perte de capacité portante des poutres de type B en fonction de la dure d'exposition en ambiance saline.

Le septième chapitre présente l'étude expérimentale et analytique de quatre poutres courtes

très corrodées, critiques vis-à-vis du cisaillement, pour évaluer le comportement au cisaillement des poutres endommagées par la corrosion à long terme. Ces quatre poutres sont extraites des poutres B2CL2 et B2CL3 qui ont été coupées en poutres critiques au cisaillement avec une portée entre appuis de 950 mm (B2CL2-1 et B2CL2-2), 1000 mm (B2CL3-1) et 840 mm (B2CL3-2) . Des poutres témoins de même portée sont également testées en flexion 3 points.

Les poutres corrodées présentent de larges délaminations le long des armatures tendues qui pourraient a priori laisser penser à un ancrage insuffisant des armatures. Cependant les résultats expérimentaux ont montré un bon comportement de l'adhérence acier-béton avec qui peut s'expliquer soit par un confinement apporté par les réactions d'appuis refermant les fissures induites par la corrosion ou bien une adhérence suffisante sur le pourtour du périmètre de la barre opposé à la zone délaminée due à une corrosion non uniforme (corrosion naturelle) et la présence des cadres d'effort tranchant qui apportent également un confinement. Ce résultat est important car contredit la majorité des études existantes basées sur de la corrosion accélérée sous champ électrique.

Une autre surprise des études sur poutres courtes critiques vis-à-vis de l'effort tranchant est le fait que les poutres corrodées présentent une meilleure ductilité (un plus grand allongement à rupture) que les poutres témoins, ce qui est totalement opposé aux résultats de l'étude du comportement mécanique des poutres « longues » en flexion. Ce paradoxe apparent s'explique par un changement de mode de rupture induit par la corrosion. En effet, les poutres courtes témoins périssent comme prévu sous l'effet de l'effort tranchant : fissures inclinées à 45° près des appuis ; ce qui est un mode de rupture fragile. En revanche, la perte de section d'acier induite par la corrosion conduit à une plastification précoce en zone centrale et à un palier plastique typique du comportement en flexion. En dépit d'une fragilité accrue des aciers tendus corrodés, le mode de rupture en flexion reste moins fragile que celui en cisaillement d'effort tranchant (figure 10).

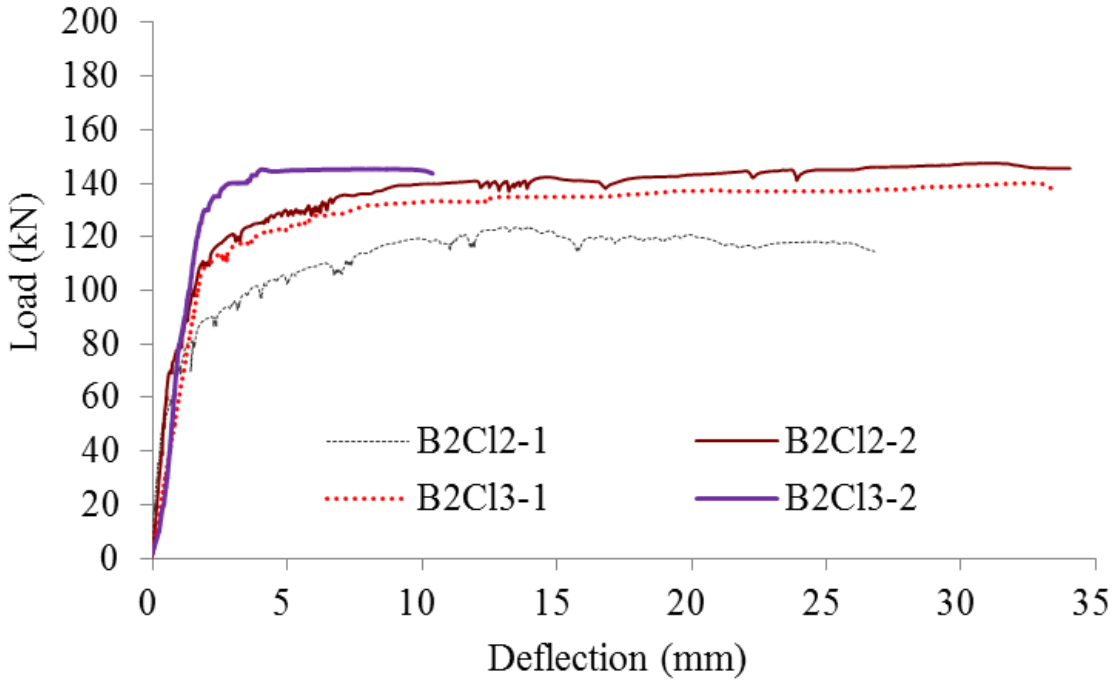

(a) réponse force-flèche des poutres corrodées

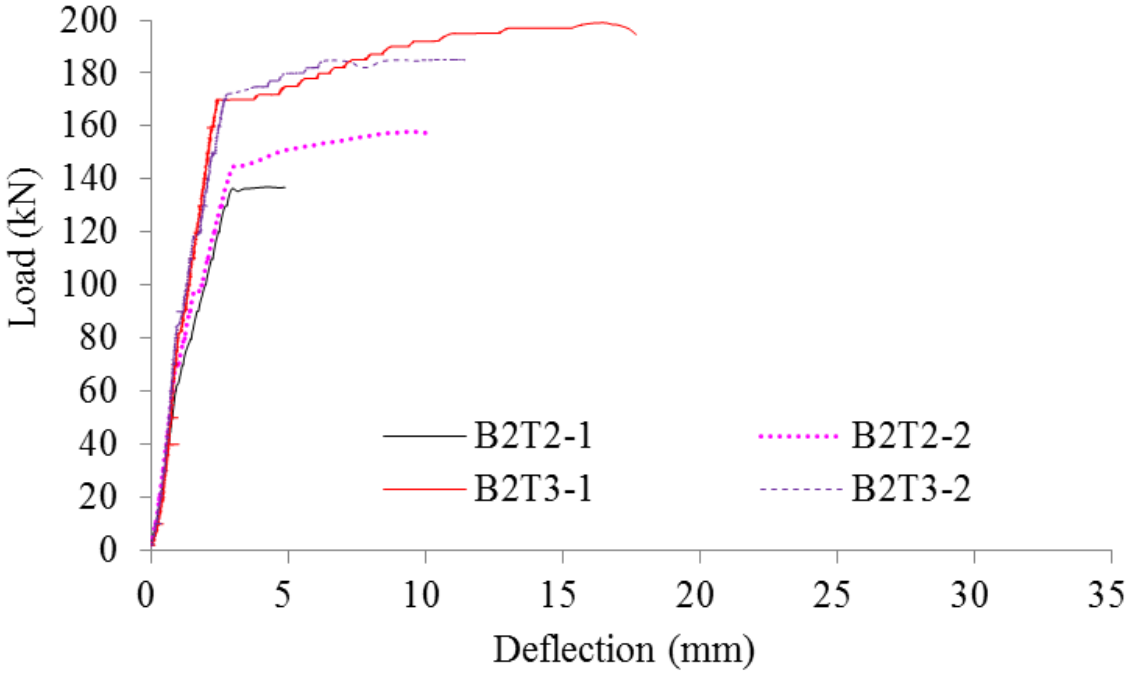

(b) réponse force-flèche des poutres témoins

Figure 10 : réponse force-flèche des poutres courtes corrodées et témoins

On constate que les poutres corrodées ont un comportement typique de flexion alors que les témoins présente une influence marquée de l'effort tranchant

Le huitième chapitre s'intéresse à la composition des produits de corrosion afin de prévoir les coefficients d'expansion de la rouille en corrosion naturelle et ainsi aider à la modélisation de la création des fissures induites par la corrosion.

La thèse se termine par une conclusion générale (chapitre 9) qui confirme la complexité du phénomène de corrosion des armatures, ainsi que la complexité de ses conséquences sur le comportement mécanique des structures.

La corrosion modifie la loi de comportement de l'acier en traction, avec une augmentation apparente du coefficient d'écrouissage qui modifie le ratio entre la contrainte ultime et la contrainte élastique de l'acier. Mais plus important encore, la corrosion réduit l'allongement maximal à rupture ce qui conduit à une rupture prématurée et fragile de l'acier et donc de l'élément en béton armé. Les caractéristiques résiduelles de l'acier apparaissent ainsi ne plus respecter les prescriptions des codes de calcul tels que l'Eurocode 2 et posent clairement le problème de la requalification des structures corrodées.

Le comportement vis-à-vis de la résistance en flexion confirme que la perte de section d'armatures est le paramètre essentiel qui contrôle le changement de capacité vis-à-vis du palier plastique ou de la charge ultime. La prise en compte du changement de ductilité des aciers tendus en raison de la corrosion peut aussi permettre de prédire la flèche maximale à rupture.

Le comportement vis à vis de l'effort tranchant déjà complexe dans le cas des structures saines, apparait au moins aussi complexe en présence de corrosion. Les méthodes classiques de dimensionnement apparaissent largement insuffisantes pour prévoir le comportement de la structure saine et encore plus éloignée en présence de corrosion. Les calculs basés sur un treillis bielle de compression-tirant semblent beaucoup plus réalistes. Cependant, un travail important sur la modélisation reste à faire.

CHAPTER ONE

INTRODUCTION

1.1 Background

Corrosion of reinforcement in concrete elements is one of the global problems which affect considerable reinforced concrete (RC) constructions [1-2]. The corrosion of reinforcement results in premature cracking and even spalling of the concrete cover which leads to the deterioration of the concrete elements and ultimate structural collapse [3]. Corroded RC elements become a more and more important concern to many transportation agencies and building officials all over the world [4]. The estimate for the maintenance and repair costs for corroded RC infrastructures is over several billion dollars in America [5]. Similar problem also happens to all other developed countries and developing countries. Extensive attentions are required to the corrosion process of the RC elements and the residual performance of the corroded constructions.

Generally speaking, concrete is in an alkaline environment which can protect the reinforcement from corrosion attacking [6]. Nevertheless, when the concrete members are in a chloride environment such as marine environment or de-icing condition, the passive layer of reinforcing can be destroyed. Corrosion of the reinforcement spreads gradually once the oxygen and moisture reach the surface of the steel bars [7-8].

At the beginning of the corrosion process, the corrosion products, whose volumes are much higher than that of the original steel bars [9], can fill into the space between the steel and the concrete. However, with the development of the corrosion, the expansion tensile stress appears in concrete and results in the cracking of concrete cover [10]. The corrosion of reinforcement will obviously modify the mechanical performance of the concrete constructions, including the load-bearing capacity and ductility [11]. The influence of the corrosion can’t be ignored to re-evaluate the mechanical performance of existing RC constructions.

During last three decades, a considerable amount of research work has been carried out on the corrosion problems of RC elements [9, 12-13]. The influence of steel corrosion can be drown mainly in the following: 1) reduction of the cross-section of the reinforcing bars; 2) loss of the bond between the steel bars and concrete; 3) volume expansion which can generate splitting stress in the concrete, causing cracking and spalling of the concrete cover; 4) change in ductile properties of steel bars.

All these factors referred above cause the reduction of structural response of corroded RC beams. Hanjari et al. [14] have checked the effect of corrosion on the behaviour of RC structures by analyzing the causes and mechanisms of the reinforcement corrosion. Stewart [15] has investigated the mechanical effects of pitting corrosion, including on flexural and shear reinforcement, which can significantly affect the structural reliability, while greater corrosion loss can lead to brittle fracture. Torres-Acosta et al. [16] have found that 10% loss of cross-section at the most serious pitting corrosion corresponds to a decrease of as much as 60% in the flexural capacity. Val [17] has studied the effect of corrosion influence on flexural and shear capacity and reliability. The pitting corrosion and general corrosion are considered. The results show that corrosion of stirrups has a significant impact on the reliability on RC beams. Higgins et al. [18] investigate the impact of corrosion of stirrups on the shear capacity of the corroded RC beams and indicate that corrosion reduces shear capacity and overall deformation of the corroded beams. Many other programs about the corrosion influence of on the mechanical performance of the corroded beams have been conducted in the last three decades all over the world.

However, most of the research is carried out with accelerated process such as the impressed current or adding the mixture of $CaCl_2$, as the natural corrosion will cost a long period. The problems of the accelerated corrosion are that the research results can not represent the statue of real corrosion. Moreover, the results between different research programs vary from each other. No agreement has been reached about the field of the detailed deterioration of corroded RC constructions, as most of the programs are conducted under different conditions. This increases the difficulty of the application of the research results.

Only a few criteria can be found in this area. Dura Crete Final Technical Report [19] defined the end of Service Limit State (SLS) when corrosion cracking of concrete cover reaches a certain allowable crack width. The value of 0.3 mm has been estimated as critical for visual aspects of RC structures. To avoid the risk of spalling of concrete cover, which is considered as an unacceptable condition as it is susceptible to endanger human life due to the probability for pieces of concrete to fall down, a maximal crack width of 1.0 mm is proposed as SLS criteria. About Ultimate Limit State (ULS) criteria, it is described as follow: load carrying capacity is reduced enough due to ongoing corrosion by further cross-sectional loss. And in this case, the reduction of the safety margin between design load and ultimate capacity is unacceptable and leads to a real risk of failure.

Nowadays, more and more RC constructions rise up in the coastal cities all throughout the world. It is necessary to make some more contribution to make up the leakage of corrosion influence on the RC elements. Some more investigations are still required on the corrosion

process and the residual structural performance of the RC elements in long-term period under a natural corroded environment.

1.2 Statement of the problem

Based on the conclusion of Torres-Acosta et al. [16] and Zhang et al [20], the cracking of corroded beams doesn't mean that the RC beams will fail at the same time. In fact, the corrosion degree is still relatively light when the cracking happens to the concrete [21, 22]. The residual load-bearing capacity of corroded structures is in relation with the maximum loss of cross-section in the most stressed parts of the concrete structures. Because real on-site corrosion induced by chloride contamination of concrete leads to very heterogeneous damage with some strong local loss of cross-section (corrosion pits), it is required to have access to long term natural corroded RC elements. Indeed, common technique to accelerate corrosion through impressed current leads to uniform corrosion totally non representative of real corrosion.

Moreover, for safety reasons, it is also necessary that corroded structure could maintain a sufficient ductility: i.e. to sustain large displacement before collapse. But because chlorides induce corrosion leads to pitting, the ductility of steel bar is reduced and can modify the response of corroded RC structures. This aspect is not taken into account directly in design standards since ductility is considered to be sufficient in both minimum steel cross-section and minimum ultimate elongation. But during the corrosion process, both steel cross-section and ultimate elongation decrease leading to change in failure mode of corroded structure from ductile to brittle.

Another aspect which is poorly studied at this moment is the change in shear capacity due to corrosion of both transverse and longitudinal reinforcement. Indeed, shear failure is always critical because of its brittleness.

1.3 Project motivation

This project of long-term corrosion experiments has been in progress since 1984 at Laboratoire Matériaux et Durabilité des Constructions (L.M.D.C.) in Toulouse, in southwestern France. The destination of this project is to further identify the steel corrosion process in the concrete beams under service load in chloride environment and the influence of corrosion on the residual mechanical performance.

All the beams are cast in real industry dimension. No $CaCl_2$ is applied in the concrete mixtures. And no impressed current is adopted during the whole process. Indeed, all the

corroded beams are exposed to the chloride environment, which is formed by the salt fog generated by four sprays located in top corners of a confined room. This is considered to be climate accelerated corrosion.

The cracking process of the corroded beams is depicted in different periods. The mechanical experiments are carried out on the beams in the late period to study the residual response of the corroded beams and the influence of the corrosion of the reinforcement. With a long-term observation, the corrosion process and the impact on the residual mechanical performance can be drawn more accurately.

1.4 Scope of the thesis

The configuration of the experimental tests performed on corroded beams is shown in Figure 1-1, including mechanical tests and physical investigations. It should be noted that all the mechanical experiments are also carried out on the non-corroded beams to identify the influence of corrosion.

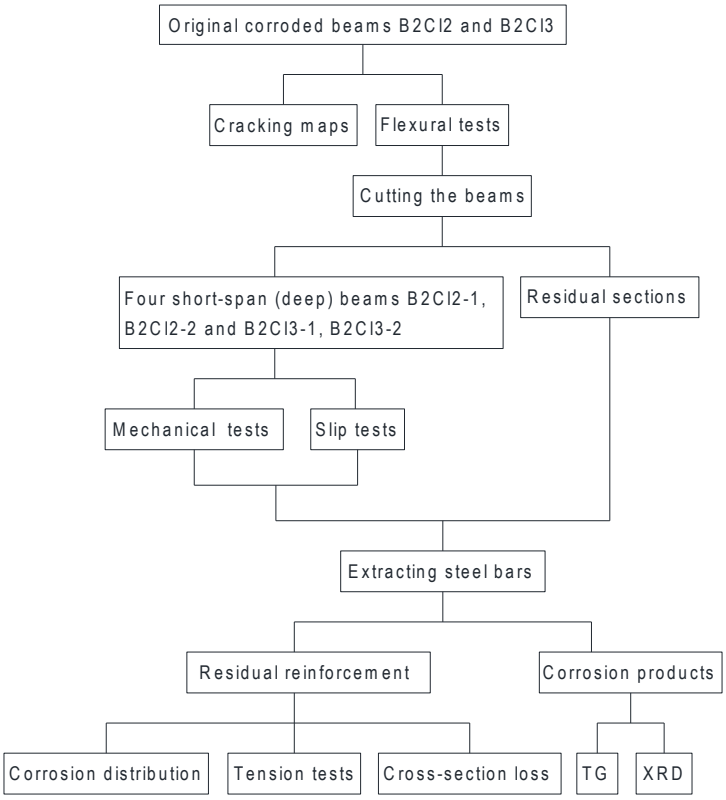

Figure 1-1 Configuration of all the experiments about the corroded beams

Having been stored in corroded environment for a long time, the corroded beams were highly corroded. Cracking of the concrete cover happened to the concrete cover almost all over the

span. Spalling also occurred to the concrete cover, especially in the middle of the tension section. The cracking and spalling of the corroded beams in different periods was described carefully, including the configuration of the longitudinal cracks and transversal cracks. The crack width was also measured by microscope with an accuracy of 0.01 mm.

The mechanical experiments were carried out on the original corroded beam B2Cl2 in 2010 and B2Cl3 in 2012. The beams were loaded in a three-point loading system. The force was recorded throughout the loading process until the beams were ruptured. The deflection at the mid-span of the beams was also detected by a linear variable differential transformer (LVDT).

To study the shear capacity, it was decided to make bending tests with short-span configuration using both end parts of corroded beam extracted from the beams after the bending tests. Indeed, only the central part of initial corroded beams was damaged during the 3 points bending tests. Then, the damaged sections were discarded and two short-span beams were formed. During the mechanical tests on the short-span beams, the slips of the longitudinal tension bars were recorded by another four LVDTs so as to check the bond and anchorage properties despite that large spalling happened to the concrete cover.

After the mechanical tests, the corroded steel bars were extracted by destroying the residual corroded beams. The corrosion products were cleared away from the residual steel bars by Clarke's solution [23]. The corrosion distribution was depicted along the steel bars, including pitting corrosion and general corrosion. The corroded longitudinal bars were then cut into small pieces to check the mass loss. The gravimetric cross-section loss of the steel bars was deduced along each piece.

The mechanical properties of the corroded bars were studied by the tension tests. The strength and elongation were compared with the non-corroded bars. The residual cross-section configuration was checked carefully and was found to be an important factor which influences the ductility of the corroded bars. In order to make clear the relationship between the shape of residual steel cross-section and change in ductility, some simulations on the non-corroded bars were carried out.

Theoretical results of the beams, including the original beams and the short-span beams, were deduced with the help of the strength results of the tension bars. The theoretical results were compared with the experimental results, which could be helpful for the further understand of the residual structural performance of the corroded constructions.

1.5 Outline of the thesis document

Chapter Two reviews the research work based on available literatures about the corrosion of

RC elements. Chapter Three outlines of the program which can date back from 1984 in the laboratory and this thesis is part of the long project. Chapter Four investigates the mechanical properties of the corroded bars and the influence of residual cross-section shape of reinforcement on the ductility of the steel bars. Chapter Five studies the flexural performance of the corroded beams with the help of the non-corroded beams. Chapter Six concludes the structural performance of the beams conducted in different ages of this program. Chapter Seven mainly discusses the residual structural behavior of the corroded short-span beams. The failure modes of the corroded beams can change from shear to bending gradually due to the corrosion of the reinforcement. Chapter Eight examines the composition of corrosion products. The expansion coefficient of the corrosion products is also deduced.

1.6 References

[1] Schiessl, P. (1988). "Corrosion of steel in concrete." Report of the TC60-CSC RILEM, Chapman and Hal, London, 204

[2] American Concrete Institute (ACI) Committee 365. (2002). "Service life prediction- state-of-art report." ACI365.1R-00, American concrete Institute, Farmington Hills, MI, 44

[3] Broomfield, J., (1997), Corrosion of steel in concrete: understanding, investigating and repair, E&FN Spon, London, 264

[4] Chung L.; Najm H.; Balaguru P., Flexural behavior of concrete slabs with corroded bars, *Cem Concr Compos*, 2008, 30(3), 184-93

[5] ASCE Report Card for America's Infrastruture. Progress Report September 2003, p. 1-7.

[6] Almusallam A. A.; Effect of degree of corrosion on the properties of reinforcing steel bars, *Construct Build Mater*, 2001, 15(8), 361-8

[7] Coronelli D., Gambarova P., Structural assessment of corroded reinforced concrete beams: modeling guidelines. *J Struct Eng ASCE.*2004, 130(8), 1214-24

[8] Auyeung Y. B., Balaguru P., Chung L., Bond behavior of corroded reinforcement bars. *ACI Mater J.* 2000, 97(2): 214-20

[9] Tuutti K.; Corrosion of steel in concrete, Report 4, Swedish Cement and Concrete Research Institute, Stockholm, Sweden, April 1982, p.82

[10] Andrade C., Alonsa C., Molina F. J., Cover cracking as a function of bar corrosion: Part I- Experimental test. *Mater Struct*, 1993, 26(8): 453-64

[11] Mangat P.; Elgarf M., Flexural strength of concrete beams with corroding reinforcement. *ACI Struct J* 1999, 96(1): 149-58

[12] Page, C.L.,Corrosion and its control in reinforced concrete, Sixth Sir Frederic Lea

Memorial Lecture. *ICT Yearbook:* 1998-1999, Institute of Concrete Technology, Crowthorne, 1999, 37-51.

[13] Du Y., Clark L. A., Chan A. H., Impact of reinforcement corrosion on ductile behavior of reinforced concrete beams, *ACI Struct J.*2007; 104(3): 285-293

[14] Hanjari K. Z., Kettil P., Lundgren K., Analysis of mechanical behaviour of corroded reinforced concrete structures. *ACI Struct J.* 2011; 108(5): 532-41

[15] Stewart M. G., Mechanical behaviour of pitting corrosion of flexural and shear reinforcement and its effect on structural reliability of corroding RC beams. *Struct Safety*. 2009; 31(1): 19-30

[16] Torres-Acosta A. A.; Navarro-Gutierrez S.; Terán-Guillén J., Residual flexure capacity of corroded reinforced concrete beams, *Eng Struct*, 2007, 29(6): 1145-52

[17] Val D. V., Deterioration of strength of RC beams due to corrosion and its influence on beam reliability, *J Struct Eng*, 2007, 133(9), 1297-306

[18] Higgins C., Farrow III W. C., Tests of reinforced concrete beams with corrosion-damaged stirrups, *ACI Struct. J.*, 2006 103(1): 133-41

[19] DuraCrete (2000) The European Union—BriteEuRam III, DuraCrete final technical report, Document BE95-1347/R17

[20] Zhang, R., Castel, A., François, R., Serviceability limit state criteria based on steel–concrete bond loss for corroded reinforced concrete in chloride environment. *Mater Struct*, 2009, *42*(10), 1407-21.

[21] Vidal T., Castel A., François R., Corrosion process and structural performance of a 17-year-old reinforced concrete beam stored in chloride environment, *Cem Concr Res* 2007; 37(11): 1551-61

[22] O'Flaherty F. J.; Mangat P. S.; Lambert P., Browne E. H., Effect of under-reinforcement on the flexural behaviour of corroded beams, *Mater Struct*, 2008, 41(2): 311-21

[23] ASTM G1-03, 2003, Standard practice for preparing, cleaning, and evaluating corrosion test specimens, ASTM International, West Conshohocken, PA, 7

CHAPTER TWO

Mechanical performance of the corroded beams and the properties of the residual corroded bars ─ Literature review

2.1 Introduction

This chapter provides a summary of the previous literature pertaining to the background and different aspects of the present research work about the corrosion of reinforced concrete (RC) beams. The discussion of the corrosion influence on the RC beams is mainly divided into four parts as following:

The first part deals with the mechanical properties of the steel bars which are extracted from the corroded beams [1–3]. As the residual steel bars play a most important role in the deterioration of structural performance of corroded beams, it is interesting to pay more attention to the residual mechanical behaviour of the corroded bars. Indeed, the distribution of cross-section loss of the corroded steel bars is investigated by many researchers. The mechanical properties of the corroded bars are also studied widely, including the impact of corrosion on elongation and capacity of the steel bars.

The second part is about the residual flexural performance of common RC beams which are corroded by impressed current in laboratory conditions or/and by adding $CaCl_2$ in the mixture of the concrete composition [4–7]. The corrosion of reinforcement leads to the mass loss of the tension bars, the deterioration of the bond and the cracking of the concrete. The mechanical properties of the corroded beams are influenced subsequently. Indeed, the residual structural performance is also investigated by the researchers all over the world, including the serviceability, the ductility and the ultimate capacity of the residual beams [8].

The third part mainly focuses on the research work about the mechanical performance of the short-span beams. The influence of corrosion on the stirrups, tension reinforcement the variations of the shear span to effective depth ratio are also considered in different programs. Moreover, some models about the prediction of the load-carrying capacity of the corroded deep beams were also introduced [9, 10].

The fourth part is mainly fixed on the previous research on the physical and chemical properties of the corrosion products. The compositions of the corrosion products are identified. The expensive coefficient of the corrosion products are deduced which can be helpful to the further research on the influence of corrosion process on the mechanical

performance of RC structures [11, 12].

2.2 Corrosion distribution and mechanical properties of the residual corroded steel bars

In RC construction, the compressive strength of concrete is strong, but the tension strength is weak, about one tenth of the value of the compressive strength. The tension strength of the reinforcement is much stronger than that of the concrete. The reinforcement plays a vital role to sustain the tension strength in the RC constructions.

For the corroded RC constructions, reinforcement is important enough for the serviceability and safety. As referred already, when corrosion happens to the reinforcement, the residual cross-section of the steel is damaged inevitably. It's still necessary to pay enough attention to the distribution of residual reinforcement and the influence of corrosion on the mechanical properties of the steel bars, as the properties of the corroded reinforcement are considered as the most important factors on the residual mechanical performance of the corroded RC constructions.

Up to now, considerable studies have been carried out on the issue about the corrosion distribution and the influence of chloride-induced corrosion of steel bars. In this section, the previous research about the influence of corrosion on the mechanical performance of the reinforcement will be presented.

2.2.1 Corrosion distribution of the corroded bars

Due to the attack of chloride ions, corrosion happens to the reinforcement subsequently. As a result, the cross-section and the surface of the reinforcement are damaged. Due to the different corrosion factors, the corrosion distribution of the corroded bars varied significantly in both the transversal cross-section and longitudinal surface.

Apostolopoulos et al. [13] conducted a program about the corrosion consequences of the reinforcement using accelerated laboratory corrosion tests in salt spray environment. The experiments were conducted for the steel BSt 420 of DIN 488-1 without concrete. The nominal diameter of the bars was 10 mm. the bars were cut with the specimen length of 250 mm and gauge length of 150 mm. The specimens were pre-corroded using accelerate laboratory corrosion tests in salt spray environment. The corrosion processes of the reinforcement during different periods were shown in Figure 2-1. In the figure, (a) represented for the surface of non-corroded bars. (b) showed the pitting corrosion appeared to the rib root gradually with a corrosion period of 10 days. (c) corresponded to a corrosion period of 20 days, which showed that the corrosion developed from the rib root to the zone between the

ribs gradually, then the corrosion pattern got transformed from pitting corrosion to general corrosion (uniform corrosion). (d) showed the corrosion degree got increased significantly and the ribs disappeared due to the corrosion when the corrosion lasted for 30 days.

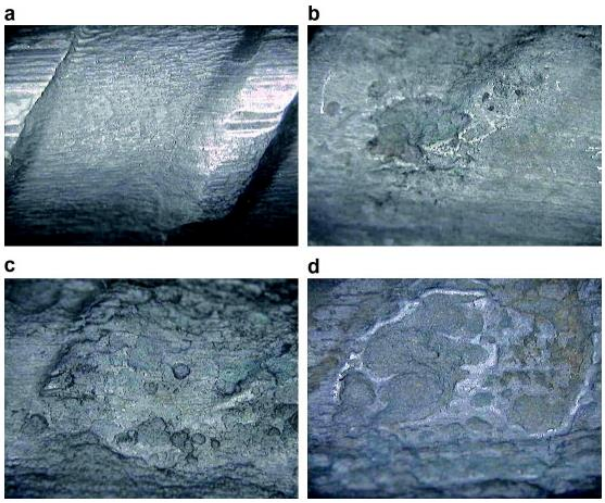

Figure 2-1 Corrosion distribution of the reinforcement[13]

Du et al. [14] investigated the corroded reinforcement with expected amount of corrosion of 5, 10, 15 and 20%. 78 single bare bars and 30 bars embedded in concrete were included in the experiment and electrochemical technique was applied to accelerate the corrosion process of reinforcement. The results showed that the cross-section of the corroded bar was no longer round and varied considerably along the circumference and its length. Figure 2-2 shown the residual diameter of bar along the length corresponding to a typical corroded bar with the original diameter of 8 mm. The results showed that the corrosion distribution was rather irregular and stochastic along the length.

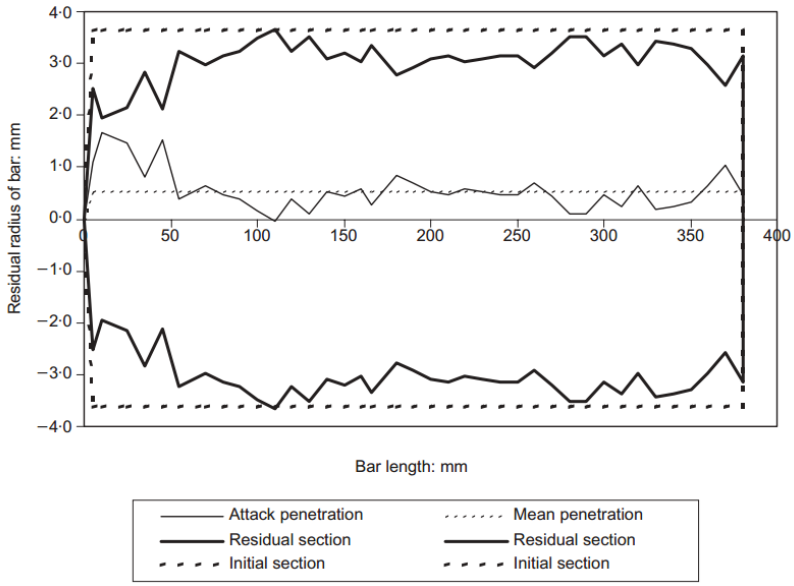

Figure 2-2 Residual radius of corroded bar with original diameter of 8 mm[14]

Malumbela et al. [15] carried out the experimental program with partial corrosion in the beams by impressed current method. 20 quasi-full-scale RC beams were involved. The beams were tested under five different degrees of service load: 0%, 1% (low deflection), 8% (high deflections but no flexural cracks), 12 and 16% (high deflections and flexural cracks) of the ultimate load-bearing capacity of a non-corroded beam. Steel corrosion was limited to tensions bars and only in the middle part of the bars with a span of 700 mm.

The residual mass of the corroded tension bars were measured and the mass loss of the tension bars along the beam was shown in Figure 2-3. The results showed that the mass loss in the middle zone was more significant than other zones, and the distribution was not stochastic as that of nature corrosion.

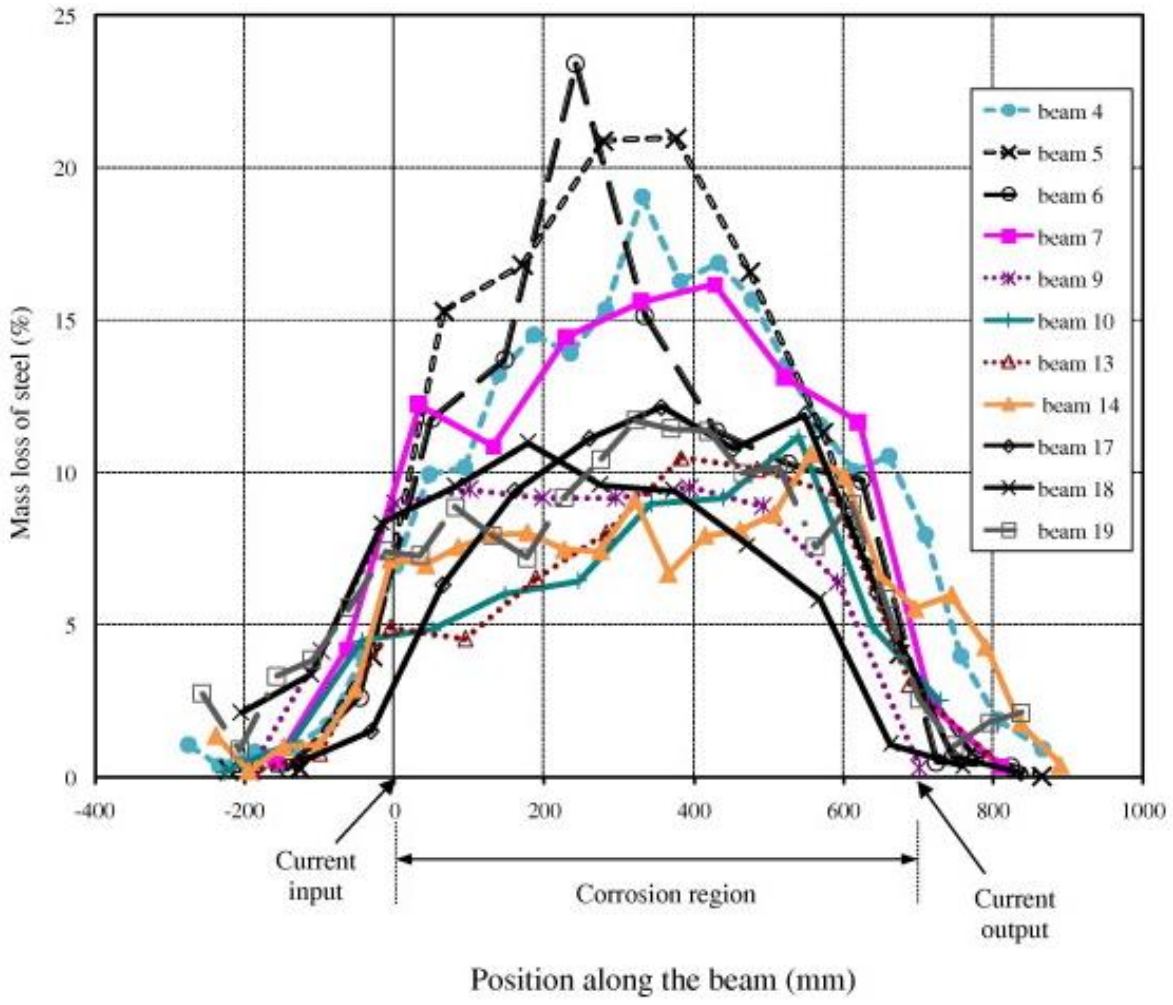

Figure 2-3 Variation of mass loss of bars along the beam[15]

Moreover, some models about the corrosion distribution of the transversal cross-section of the corroded bars were also investigated by the experimental test. Zhao et al. [16, 17] investigated the residual reinforcement corroded in wetting and drying cycles in an environmental chamber and tried to analyze the non-uniform distribution of the residual cross-section of the

corroded reinforcement based on Gaussian. Cao et al. [18] examined the reinforcement corroded by half-cell potential measurement and then made some numerically simulation by employing the Finite Element Method (FEM). But from the viewpoint of the corrosion distribution, no agreement had been reached. The corrosion distribution of the corroded reinforcement was still considered as stochastic.

2.2.2 Influence of corrosion on the strength of steel bars

Relative small research programs have been undertaken on the corrosion impact on the mechanical properties of the corroded reinforcement, including the yield strength and the ultimate strength.

Almusammam [1] conducted an experimental program about the residual properties of corroded reinforcement. The steel bars with original diameter of 6 mm and 12 mm were embedded in the concrete specimens. The specimens were partially immersed into 5% sodium solution in a tank, but the reinforcement was above the solution. A current of 2 mA/cm^2 was applied to the reinforcement so as to accelerate the corrosion process. When the reinforcements were supposed to be corroded in the predicted degree, the corroded reinforcements were extracted by destroying the specimens. The Clarke's Solution was used to clear away the corrosion products. The tension experiments were carried out on the residual steel bars.

The tensile strength of the corroded bars could be deduced by two ways due to the cross-sections adopted. One was the nominal cross-section of the reinforcement. The tensile strength calculated in this way was named nominal tensile strength. As the corrosion reduced the cross-section significantly, the residual cross-section which made the contribution to the tensile performance was much smaller than that of the nominal cross-section. The tensile strength deduced by the residual cross-section was considered to be closer to the true situation. As a result, the tensile strength of the second way was the actual tensile strength. The impact of corrosion degree on the tensile strength was shown in Figure 2-4 for the reinforcement with diameter of 6 mm and Figure 2-5 for the reinforcement with diameter of 12 mm.

The results showed that corrosion reduced the nominal tensile strength obviously. However, there was little influence on the actual tensile strength. The reduction of the nominal tensile strength was due to the cross-section loss of the corroded reinforcement.

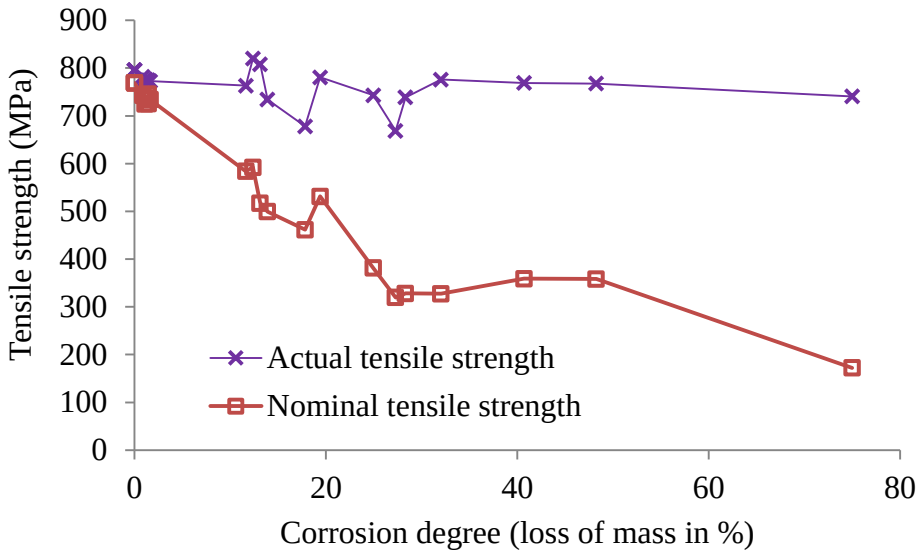

Figure 2-4 Corrosion influence on the tensile strength (6 mm)[1]

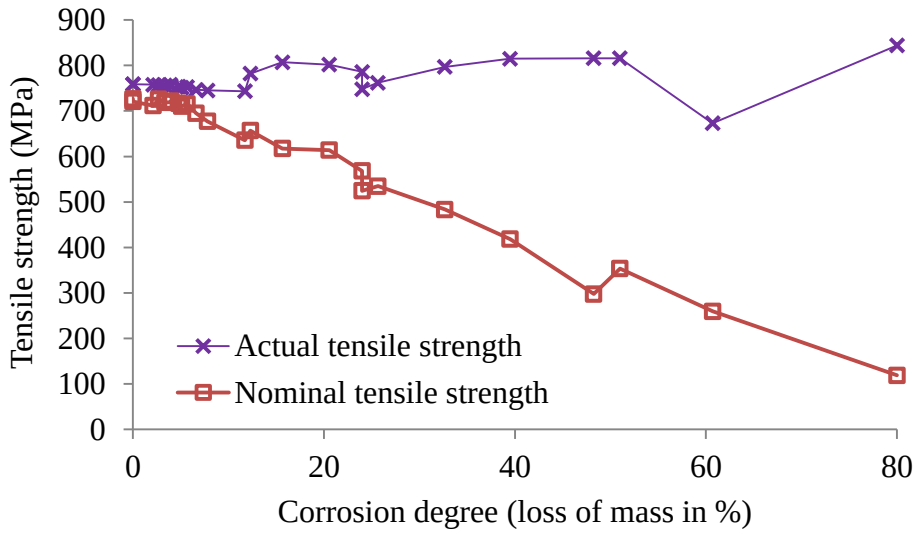

Figure 2-5 Corrosion influence on the tensile strength (12 mm)[1]

Apostolopoulos C. A. et al. [3, 19, 20] carried out a series of experiments on the corrosion of reinforcement based on steel bars S400 and S500. The nominal diameter was 8 mm. In the corrosion process, the bare reinforcements were stored in salt spray environment. The salt spray with 5% NaCl solution was applied in the corrosion program. The bars were fetched when the corrosion bars were in different corrosion degrees. The salt deposits were cleared away from the surfaces of the corroded bars by clean running water and the corrosion products were washed by Clarke's solution.

The tensile tests were carried out on the corroded bars so as to investigate the residual mechanical properties of the corroded reinforcement. The experimental results are shown in

Figure 2-6. The comparison of the nominal ultimate tensile strength and actual ultimate tensile strength is shown the same conclusion as Almusammam [1]. The influence of corrosion on the nominal ultimate tensile strength was significant. But the actual ultimate strength was almost stable even when the corrosion degree increased.

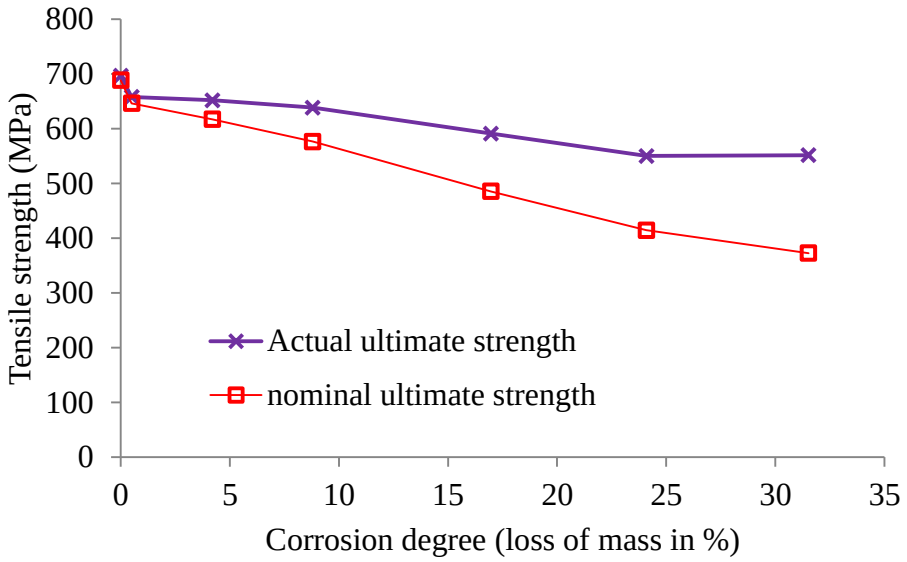

Figure 2-6 Effect of corrosion degree on the tensile strength of the corroded bars[3, 19, 20]

Cairns et al. [2] conducted a program to study the mechanical properties of the corrosion-damaged reinforcement. Both the artificial corrosion and accelerated corrosion were investigated. For the artificial corrosion, the bars were damaged by removing a section of the cross-section to get the corrosion degree of 5%, 10%, 20%, 30%, 40% and 50%. The defect in the residual cross-section was in curve as shown in Figure 2-7. The tests were undertaken on deformed B500B bars with the diameter of 12, 16, 20, and 24 mm. For the accelerated corrosion damage, 25 plain round bars of 16 mm diameter were tested. The bars were embedded in concrete and then subjected to corrosion by impressed current. The specimens were transferred into the corrosion condition with one day of spraying salt solutions and six days at a relative humidity of approximately 70%. When the corrosion reached the designed corrosion degree, the bars were extracted and mechanical tests were carried out.

The yield strength and ultimate strength of the corroded bars were calculated by the residual cross-section with the section-loss at the largest pit. The typical results of the bars corroded by impressed current were shown in Figure 2-8. Both the yield strength and ultimate strength of the corroded bars were almost the same even though the corrosion degree increased from 0% to 8%, which was close to the conclusion of Almusammam and Apostolopoulos at al.

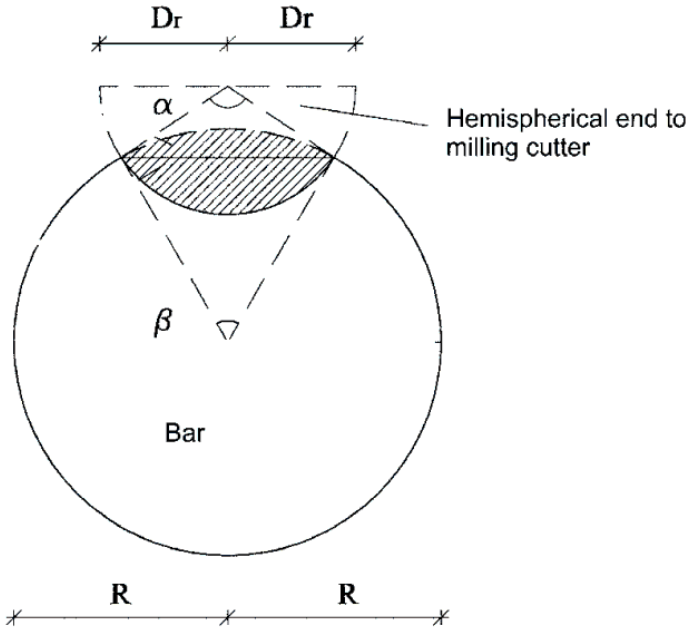

Figure 2-7 Schematic of machined defect geometry[2]

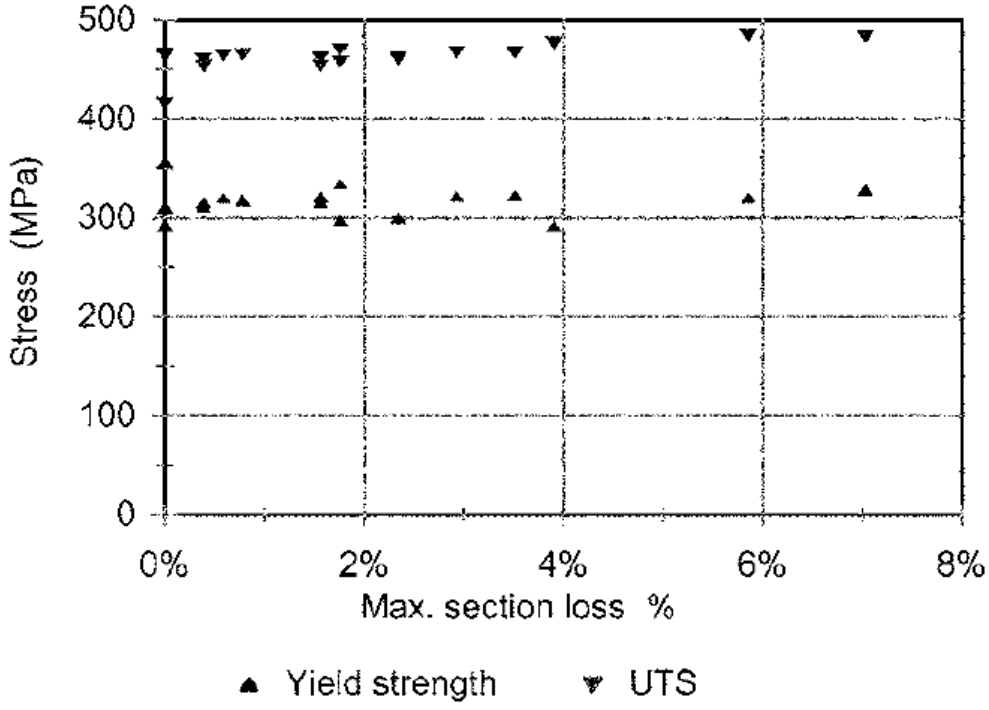

Figure 2-8 Tension strength of bars with accelerated corrosion[2]

However, the results of bars with artificial mechanical defect showed that the yield strength and ultimate strength of the corrosion was different. As shown in Figure 2-9, the yield strength and ultimate strength were deduced by the residual gravimetric cross-sections. The strength of the bars with artificial corrosion decreased with the corrosion levels. Based on the mechanical results, the stress could be related to the corrosion degree as follow:

$$f_y = \left(1.0 - \alpha_y \cdot Q_{corr}\right) \cdot f_{y0} \qquad (2\text{-}1)$$

$$f_u = (1.0 - \alpha_u \cdot Q_{corr}) \cdot f_{u0} \qquad (2\text{-}2)$$

Where:

f_y represents the yield strength of the corroded bars;

f_u represents the ultimate strength of the corroded bars;

f_{y0} represents the yield strength of the non-corroded bars;

f_{u0} represents the ultimate strength of the non-corroded bars;

Qcorr is the percentage of average section loss;

α_y and α_u are the empirical coeffeicients.

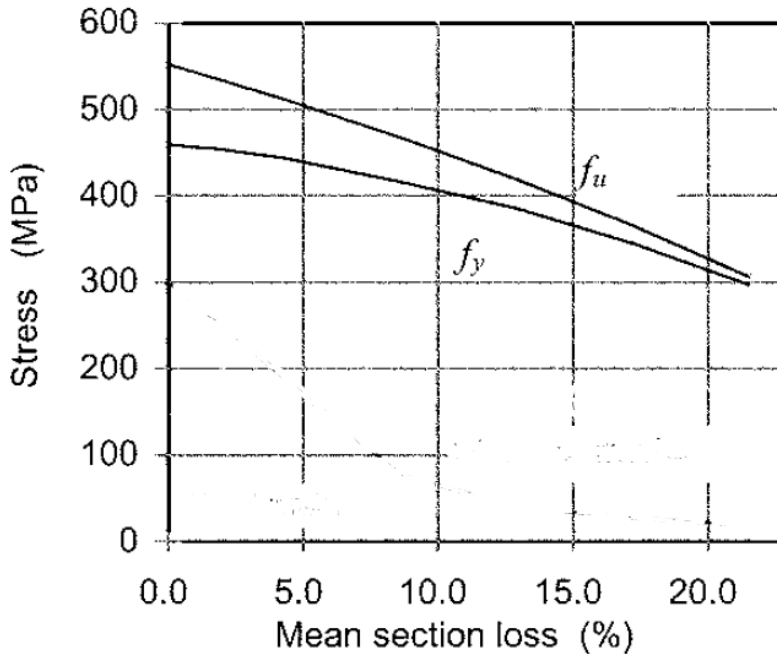

Figure 2-9 Actual tension stress of steel bars with artificial corrosion[2]

Similar to the results of artificial corrosion bars of Cairns [2], Du et al. [14] performed some experimental tests with both accelerated and simulated corrosion experiments on bare bars and bars embedded in concrete. The corrosion condition was introduced in last section. The residual strength of both bare bars and corroded bars embedded in concrete were shown in Figure 2-10 and Figure 2-11.

Figure 2-10 showed the relative value of both the yield strength and ultimate strength which were determined by the average corroded cross-sectional area. The distributions of the results were scattered. But the trend line agreed with the equations (2-1) and (2-2). For Figure 2-11, it was necessary to point out that the letters in legend R represented the plain bar, T

represented ribbed bar, RC standed for plain bar embedded in concrete, and TC corresponded to ribbed bar embedded in concrete.

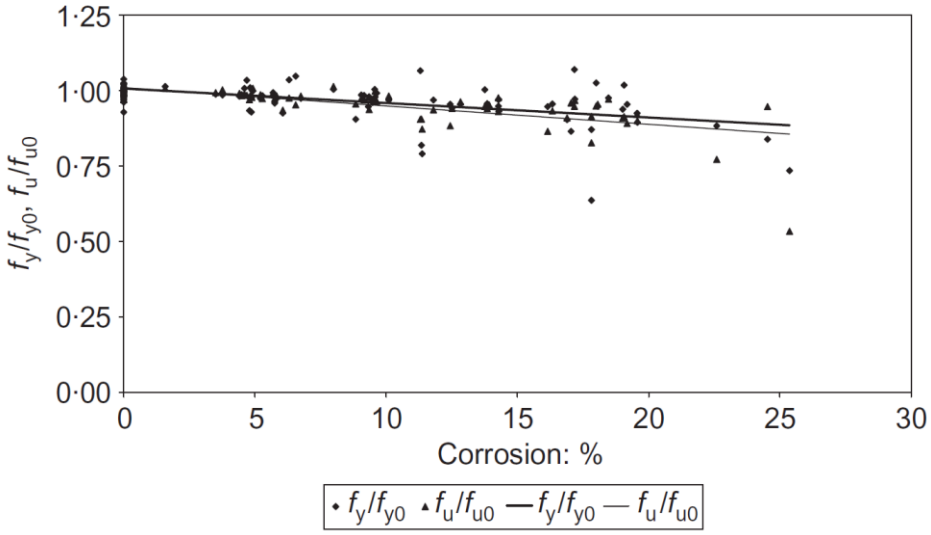

Figure 2-10 Residual strength of corroded bare bars[14]

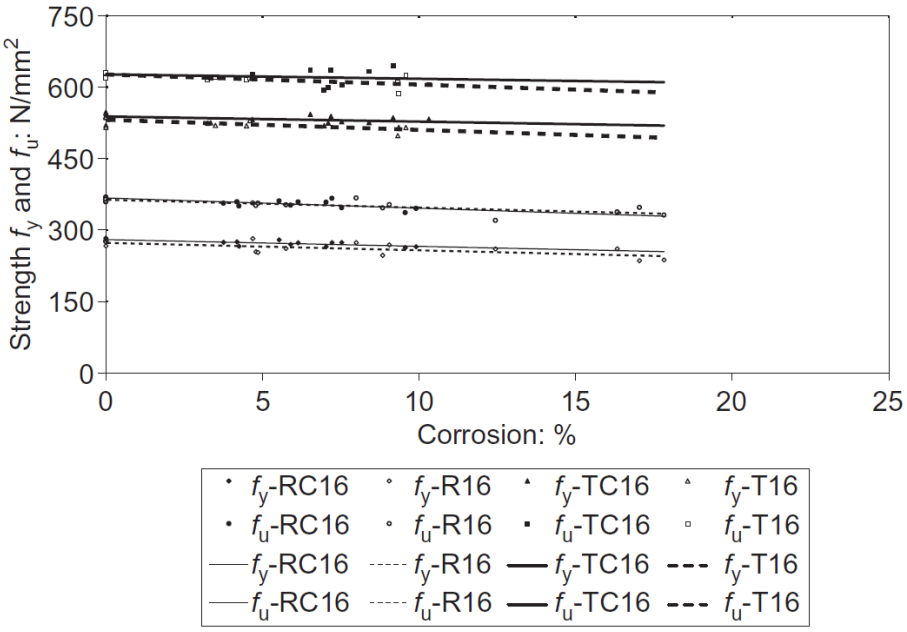

Figure 2-11 Residual strength of corroded bars embedded in concrete[14]

Lee et al. [21] also investigated the corrosion induced by carbonation and chloride with the help of impressed current. The results were also agreed with equations (2-1) and (2-2). The differences between different research programs showed that more experimental work were required for the further research so as to make clear the influence of corrosion on the residual mechanical properties of the corroded bars.

2.2.3 Influence of corrosion on the ductility of steel bars

Ductility is defined as the ability of a structure to resist against environmental attacks without its performance to drop below a minimum acceptable limit [13]. Ductility of the reinforcement is a most important characteristic which makes the main contribution to the ductility of the RC constructions. Corrosion of the reinforcement is considered to be the most serious problem which deteriorates the durability of the RC constructions. The influence of corrosion leads to the reduction of the cross-section of the steel bars, deterioration of the bond between the concrete cover and the reinforcement, cracking of the concrete cover and even results in threaten to the safety of the whole RC structures.

Recently, the ductility of the corroded RC constructions has drawn considerable attention. However, the research about the corrosion influence on the ductility of the corroded steel bars is still limited. Only a few literatures can be found at this moment. So it is necessary to make some investigation about the influence of corrosion on the ductility of corroded reinforcement.

Almusammam [1] conducted a study to assess the effect of corrosion degree of the reinforcement on the mechanical properties, the ductility was also studied. The experiment was carried out to the reinforcements which were corroded in different degrees by impressed current and salt solution. The tension tests were undertaken to the corroded steel bars. The load-elongation curves for the steel bars with diameter of 6 mm are shown in Figure 2-12. The percentages in the graphs corresponded to the corrosion degree which was measured by the mass loss of the residual bars.

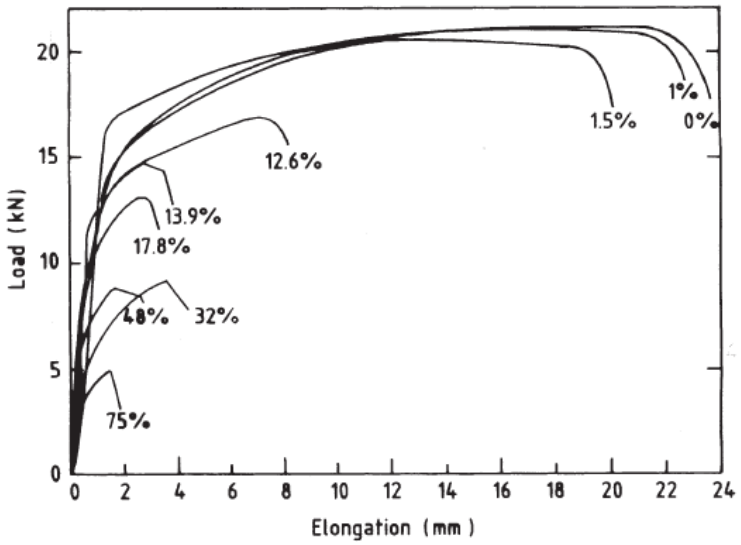

Figure 2-12 Tension results of bars corroded by impressed current (diameter 6 mm)[1]

The elongation of the reinforcement got reduced significantly with the increase of the corrosion degree. For the steel bars with corrosion degree smaller than 12%, the plastic plateau was clear when the steel bars reached yield value, which showed that the ductility of the steel bars was still strong. However, when the corrosion degree reached 12.6%, the elongation of the reinforcement reduced sharply. Finally, the failure mode of the corrosion reinforcement was also changed due to the increase of the corrosion degree. The steel bars performed from ductile behavior to brittle behavior gradually.

Apostolopoulos et al. [3, 19, 20] carried out the experimental tests on the corroded reinforcement on the steel bars S400 and BSt 500s as referred in above sections. The results of the elongation to fracture (ultimate strain) and the corrosion degree of the reinforcement were shown in Figure 2-13 and Figure 2-14 respectively. According to the two figures, the elongation to fracture of the corroded reinforcement got reduced significantly with the increase of the corrosion degree. Moreover, the elongation decreased more significantly for the steel bar BSt 500s than S400 when the reinforcement were in the same corrosion degree, which showed that the ductility was reduced more seriously in this condition.

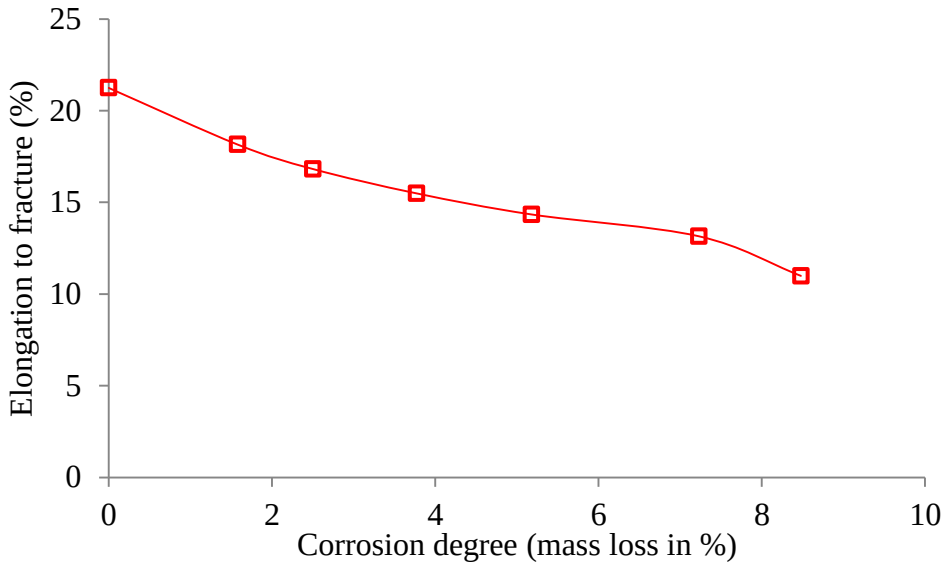

Figure 2-13 Effect of natural corrosion on elongation (steel bar S400)[3, 19, 20]

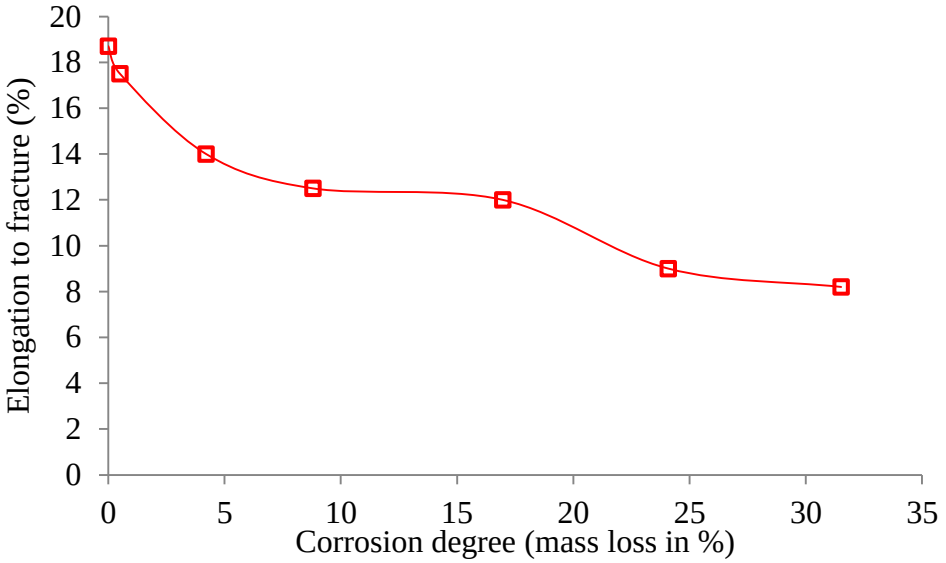

Figure 2-14 Effect of natural corrosion on elongation (steel bar BSt 500s)[3, 19, 20]

Du et al. [14, 22] got the similar conclusion based on electrochemical technique as shown in Figure 2-15. The ultimate extension of the corroded bars got reduced significantly with the increase of the corrosion degree. When the corrosion degree increased from 0% to 16.3%, the force reduced from 55kN to 45 kN, with about 18% loss of yield capacity. However, the extension got reduced from 11.8 mm to 3.8 mm, about 68% loss of ductility, much more serious than the loss of yield capacity.

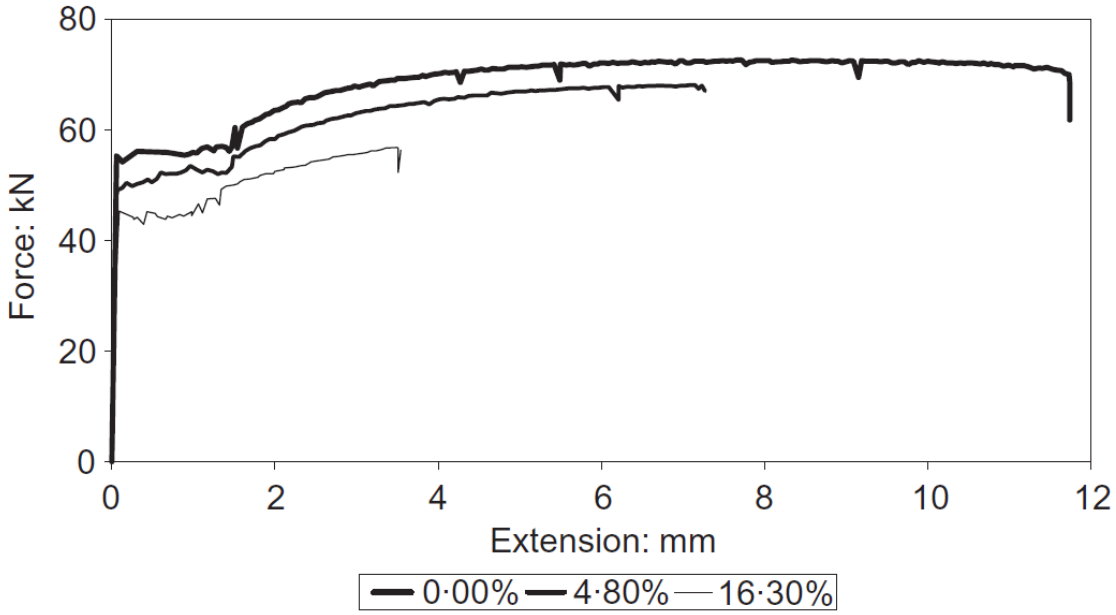

Figure 2-15 Force-extension curves of bars in different corrosion degrees[14]

Though many investigations on the residual mechanical properties of the corroded bars have been carried out broadly by the researchers all over the world up to now, there are still some

deficiencies existed:

(1) Most of the corrosion was induced by accelerated method of impressed current or by mechanical defect directly. However, these conditions would be different from the natural corrosion. As the corrosion induced by impressed current mainly caused uniform (general) corrosion, while the natural corrosion resulted in pitting corrosion. The influence of pitting corrosion and general corrosion on the mechanical properties of the reinforcement was unknown.

(2) The residual cross-section or the cross-section loss of the corroded steel bars was measured by different ways. Some program adopted the value got from vernier caliper directly. This method would overestimate the cross-section loss and result in the calculated strength higher than the actual strength. Some program used the drainage to measure the residual volume of the corroded bars. it was a good idea to measure the corrosion distribution along the length of the corroded bars. However, as the surface of the corroded bars was rather irregular and many micro-porous existed around the surface. It increased the possibility that the air stayed in the micro-porous when the bars were immersed into the water. As a result, the volume of the residual bars was overestimated, and the strength of the corroded bars was underestimated subsequently. So it was still a different way to make clear the precise residual cross-section.

(3) The corrosion results varied from different corrosion program as discussed about the strength of the corroded bars. Some found that the corrosion influence on the mechanical properties was small. But some discovered that the mechanical properties of the corroded bars were changed significantly.

Based on the viewpoints discussed before, it's necessary to carry out some more experimental tests based on the natural corroded bars, which would be helpful to compared with the simulated corrosion results and improve the applicability of the results.

2.3 Flexural performance of the corroded RC beams

During corrosion process of the reinforcement, the corrosion products are created. The volume expansion of corrosion products leads to the cracking of the concrete cover decreasing the confinement of the reinforcement and the bond between the reinforcement and the concrete gets reduced obviously. As a result, the residual load-bearing capacity of the corroded beams is deteriorated significantly.

2.3.1 Load-carrying capacity of the corroded RC beams

Rodríguez et al. [23–25] made some investigations about the relationships between the residual flexural capacity of the corroded beams and the residual cross-section of the reinforcement. In the program, 30 RC beams with the dimension of 2300×200×150 mm were cast. The corroded beams were tested by the impressed current and corroded up to 600 μm for the reinforcement. Some serious pitting corrosion was found in the test.

The mechanical results were recorded and compared with the theoretical results calculated by Eurocode 2 [26] as shown in Figure 2-16. In order to find the influence of corrosion to the RC beams, two predicted results were made subsequently: one results took account of the residual cross-section of the corroded tension reinforcements and the nominal cross-section of the concrete beams; the other results were based on the residual cross-section of the corroded tension bars and the damaged cross-section without the contribution of the concrete cover. The experimental results were close to the values deduced by the first method. The results calculated from the second method were conservative when compared to the experimental results.

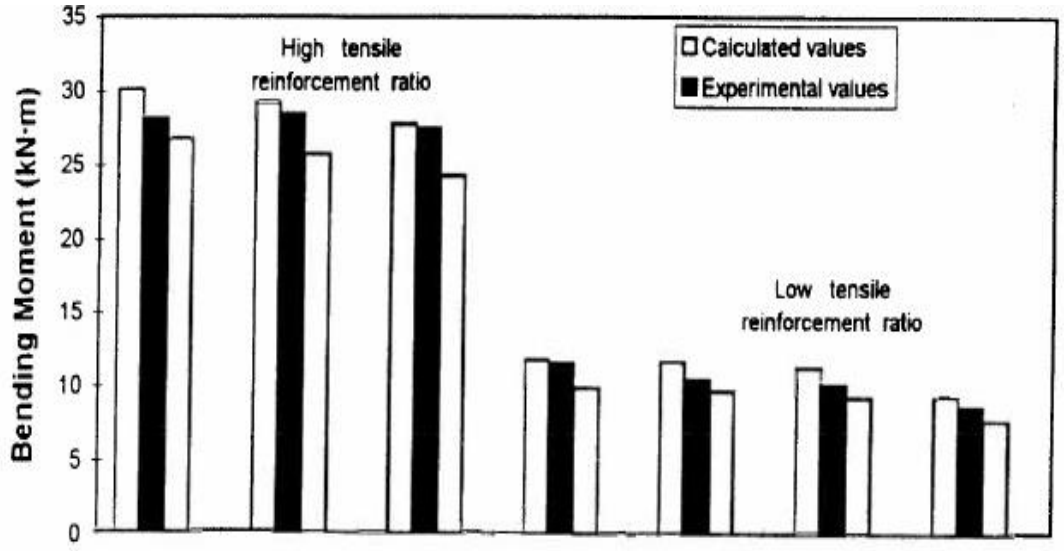

Figure 2-16 Flexural capacities of beams corroded by impressed current[25]

Azad et al. [8] made an effort to develop a model based on the experimental data to predict the residual flexural capacity of the corroded RC beams. The data were got from 56 specimens of RC beams which were dealt with a varying degree of impressed current to accelerate the corrosion process. According to the experimental results of the corroded beams, it was found that the corrosion current density and corrosion period is the vital factor impacting the flexural behaviour of a corroded beam. Part of the typical experimental curves

of load-deflection results is shown in Figure 2-17.

Based on the experimental results, two-step procedure was proposed to predict the residual flexural capacity of the corroded beams: the moment capacity was deduced by residual cross-section of the reinforcement; the correction factor was considered. The detailed expressions are shown as follow:

$$M_{res} = \beta \cdot M_{th,c} \quad (2\text{-}3)$$

$$\beta = \frac{A}{(I_{corr} T)^m D^n} \quad (2\text{-}4)$$

Where:

$M_{th,c}$ is the moment capacity calculated by residual cross-section of tension bars;

M_{res} is the residual flexural capacity;

β is the factor stand for combined effect of the bond loss and loss of flexural strength;

m, n are constants and A is a dimensional constant. The detailed information can be found in reference [8]

I_{corr} is the corrosion current density;

T is the corrosion period;

D is the original diameter of the tension bars.

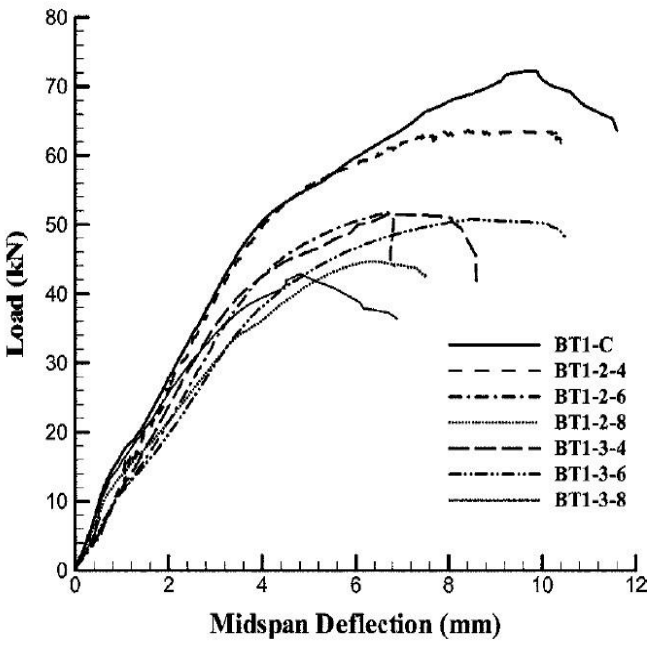

Figure 2-17 Typical load-deflection curves of beams corroded by impressed current[8]

Torres-Acosta et al. [27] also contributed to the residual flexural capacity of the corroded beams. The investigation was based on the beams with the dimension of 100×150×1500 mm.

chlorides were applied during the casting process. Then the corroded beams were subjected to a constant current of 80 μA/cm^2 for a period of 50-180 days. Part of the experimental results is shown in Figure 2-18.

The experimental results showed that the maximum depth of the pitting corrosion of the reinforcement played a most important role in the flexural performance of the corroded beams. The average diameter loss of 0.06 and 0.2 decreased the residual capacity about 30%-40%. But if the corrosion is in deep pitting corrosion, the reduction of the flexural capacity of the corroded beams could reach as much as 60%.

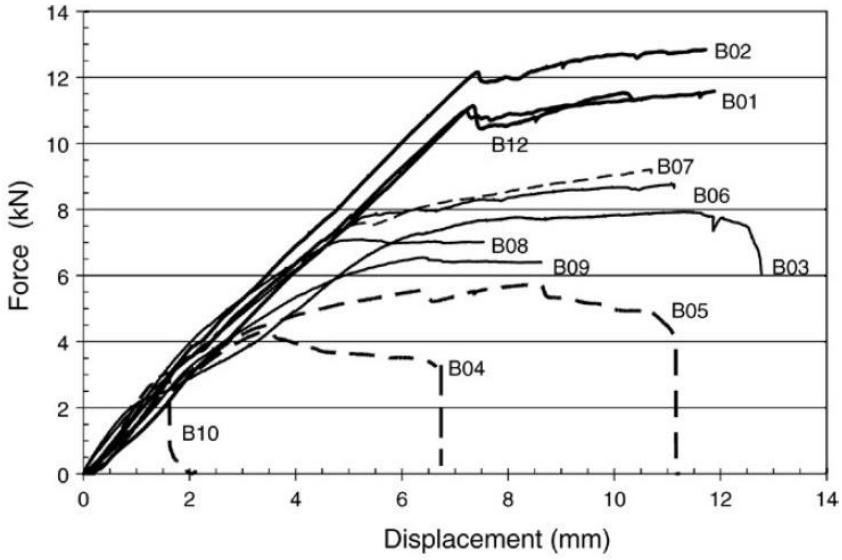

Figure 2-18 Typical experimental results of the corroded beams (impressed current)[27]

Considerable research programs have been carried out about the corrosion influence on the flexural capacity of the corroded beams. However, most of the programs used accelerated corrosion by the impressed current or/and by adding the mixture of $CaCl_2$, which resulted in the differences between the experimental results and RC constructions existed in marine environment.

Moreover, due to the different programs [8, 24, 27–36], the corrosion current applied in the RC beams varied from 80 μA/cm^2 to 10400 μA/cm^2, which would lead to variable consequences on the corrosion pattern. The differences of the corrosion conditions in the simulation and variations of the corrosion results increased the difficulties of the applicability of the research results. In fact, Otieno et al. [37] found the variation of natural corrosion rate in was in a limited range from 0.1 μA/cm^2 to 1-2 μA/cm^2 based on the examinations the beams exposed to cyclic wetting and drying with NaCl solution which was considered to be close to the natural corrosion. The corrosion rate in this condition was much smaller than that

used in the accelerated experiments. Moreover, Yuan et al. [38] also found that galvanic method lead to a corrosion on the whole surface of the steel bar (uniform corrosion pattern) and then is not representative of natural corrosion, as natural corrosion of chloride environment usually resulted in pitting corrosion more seriously, and corrosion distribution usually concentrated in one side of the bar close to the exposure surface.

2.3.2 Ductility of the corroded RC beams

Ductility is one of the most important properties of the concrete structures. The deflection at the mid-span of the corroded beams is considered as an important parameter to study the ductility of the beams.

Mangat et al. [30] investigated the ductility of the corroded beams based on 111 under-reinforced concrete beams. The beams were cast with a dimension of 910×150×100 mm. The beams were corroded in different corrosion degrees induced in increments, ranging from 1.25 to 10% at corrosion rates of 1, 2, 3, 4 mA/cm^2. But before the accelerated corrosion was applied to the reinforcement, the beams were precured for different periods of up to 1 year. Then four-point loading system was used to the beams so as to check the residual performance of the corroded beams. The results showed that the corrosion reduced the deflection of the RC beams significantly. When the corrosion degree increased from 0% to 10%, the deflection reduced from 13 mm to 3 mm. the failure of the corroded beams transformed from ductile response to brittle response.

Yuan et al. [38] conducted a program to discover the influence of corrosion on the residual structural performance of the RC beams by both the corrosion accelerated with impressed current and natural corrosion. The mechanical experiments on the corroded beams were shown in Figure 2-19. The results showed that the corrosion of the main steel bars in the beams could deteriorate the load-bearing capacity and ductile characteristic significantly. The failure of the corroded beams was also transferred from ductile to brittle mode. Different corrosion properties on the surface of the steel bar were the main reasons that caused the different structural behavior of the concrete beams.

However, it should be pointed out that the experimental results of Yuan et al. showed the beams corroded by galvanostatic method (G Method) showed a more brittle performance than that corroded by artificial climate environment (A. C. E.). This was quite different from the conclusion of Torres-Acosta et al. [27], as Torres-Acosta found that the general corrosion play a more important role for the beams corroded by impressed current. But the pitting corrosion of the reinforcement would lead to the brittle performance of the corroded beams.

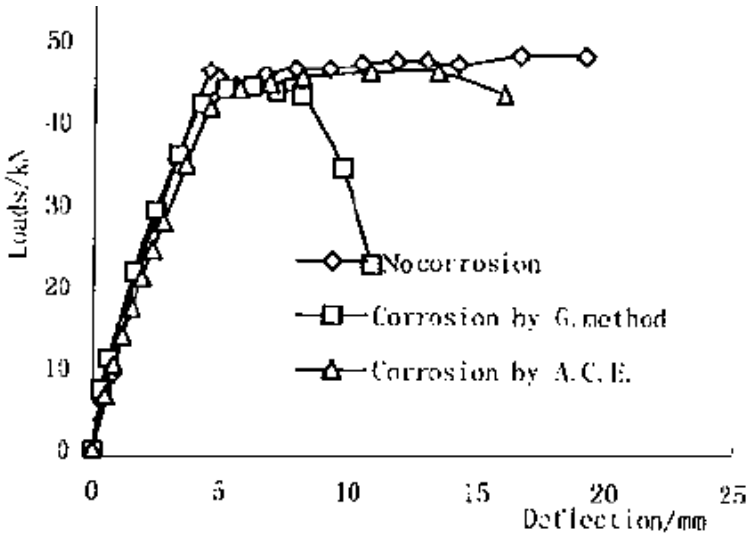

Figure 2-19 Load-defection curves of beams corroded in different method[38]

Cabrera [39] carried out a program based on a series of slabs with the dimension of 100×300×200 mm. Electrochemical system were applied to the slabs so as to accelerate the corrosion of the reinforcement. Mechanical experiments were carried out to the corroded and non-corroded samples. The mid-span deflections were recorded before failure. The results were shown in Figure 2-20. The deflection ratio was the ratio of the deflection of the corroded beam divided by the deflection of the non-corroded beam loaded to the service load. The service load is defined as the ultimate load multiplied by 0.6. The results showed that the corrosion had significant influence on deflection of the beams. According to the experimental results, a 1% mass loss of the corroded beams corresponded to an increase of mid-span deflection about 5%.

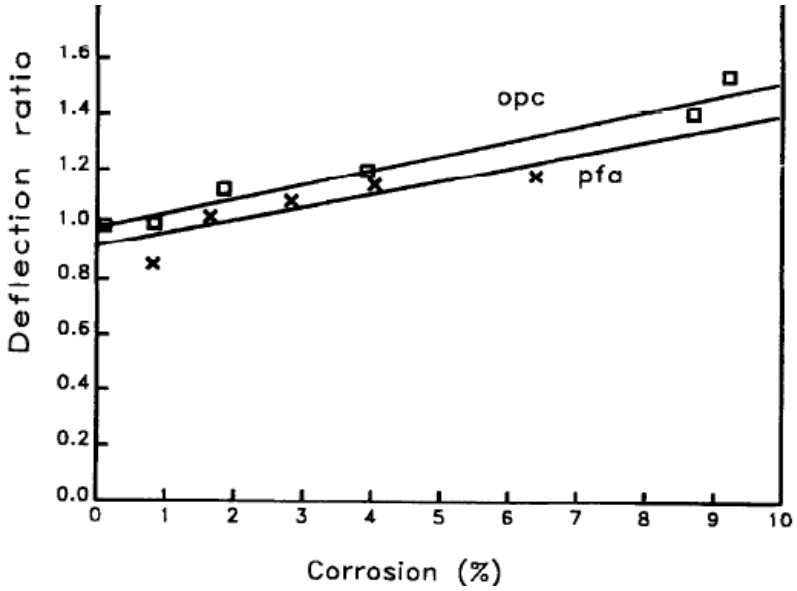

Figure 2-20 Relationship of deflection ratio and corrosion degrees of series I beams [39]

From the experimental work carried out by different programs and literatures available at this moment, the corrosion influenced the mechanical performance significantly. Some researchers found that the ductility of the corroded beams got reduced and the failure of the corroded beams transferred from ductile failure mode with a large mid-span deflection to a brittle failure mode with only a few limited deflections gradually. As the brittle response of the RC constructions might result in collapse without any prediction, this should be avoided definitely. More attention should be paid to the reduction of the ductility of the corroded construction.

2.4 Shear behaviour of the corroded RC beams

RC beams are usually designed to rupture from the compression zone in bending failure mode after yielding of tensile reinforcement. However; during the corrosion process, the stirrups are also corroded. Sometimes the corrosion is more serious than that of longitudinal bars due to the short distance from the surface of the beam. The transversal cracks happen to the cross-section of the RC beam. Moreover, both the transversal cracks and longitudinal cracks may happen to the compressive concrete. As a result, shear resistance of the corroded RC beams is reduced significantly. It also becomes an important parameter for the evaluation of corroded RC beams.

2.4.1 Influence of corrosion on shear performance of corroded beams

Rodríguez et al. [23–25] carried out some experiments on corroded beams which were cast with high tension reinforcement ratio of 1.5%. The diameter of the stirrups in the beams was 6 mm with the spacing of 170 mm. The influence of corrosion on the shear capacities of the beams were investigated during the tests.

The theoretical results were deduced by standard method (cross-sectional method) in Eurocode 2 [26]. However, considering the corrosion cracks happened to concrete cover both in tension and compressive zones, the theoretical calculation of the shear capacity were carried out in three ways: one was deduced by the nominal cross-section of the beam; while the other way was deduced by the residual cross-section by considering the damaged zones, the concrete cover at the compressive zone was not considered in the detailed residual cross-section; in the third method, the corroded RC beams deteriorated more serious were considered, and the concrete cover in compressive zone and two vertical sides were excluded, which meant that only the parent concrete contributed to the shear resistance in the mechanical performance.

The comparison of the experimental results and the theoretical results in three methods are shown in Figure 2-21. The results showed that the corrosion did reduce the shear capacity as experimental results were smaller than that of the calculated results based on nominal cross-section. However, the theoretical results due to the parent concrete in the third method were relatively conservative.

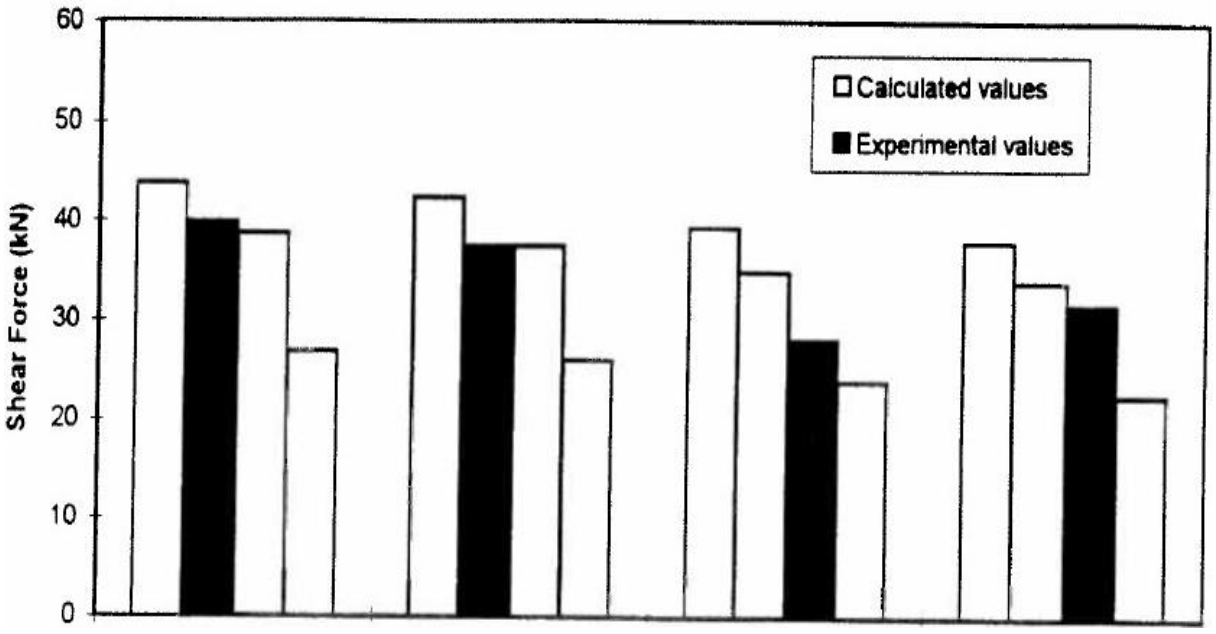

Figure 2-21 Shear capacity of the corrosion beams (with different cross-sections)[25]

Wang et al. [40, 41] carried out a program about the experimental tests on the shear performance of the RC beams with corrosion in partial length of the reinforcement in the tension section. Fourteen beams in total, eight RC beams with partially corroded length, four RC beams with partially unbounded length and two non-corroded beams treated as the control beams, were cast in the program. The mechanical performance of the RC beams was studied carefully. The experimental results were shown in Table 2-1. The experimental results showed that the failure modes and relative capacity varied due to the partially non-bonded and corroded length in different RC beams. When the corrosion degree is small (10%), the load-bearing capacity of the corroded beams was close to that of the non-corroded beams, which showed that the influence of the corrosion on the ultimate capacity was relatively small. However, when the corrosion degree was high (25%), the reduction was significant, which should not be ignored.

Table 2-1 Experimental results of the beams corroded by impressed current [40]

RC test Specimen	Bond-perfect RC beam				Test result		Relative load capacity ratio $\frac{F_{P,ult}}{F_{cru}^{f}}$
	Flexural capacity (kN)		Shear capacity (kN)	Failure mode	Ultimate capacity $F_{P,ult}$(kN)	Failure mode	
	F_{yie}^{f}	F_{ult}^{f}					
BC2.0	164.78	214.35	149.74	Shear 1	182.1	Shear 1	0.850
B2.0-200-0	166.14	226.44	156.84	Shear 1	179.4	Shear 1	0.792
B2.0-200-10	171.38	231.39	152.69	Shear 1	202.8	Shear 2	0.876
B2.0-200-25	170.28	221.62	156.02	Shear 1	143.4	Shear 2-S	0.647
B2.0-300-0	165.11	204.87	155.11	Shear 1	202.4	Shear 1	0.988
B2.0-300-10	171.75	234.85	156.34	Shear 1	218.9	Shear 2	0.932
B2.0-300-25	172.61	243.40	143.37	Shear 1	104.3	Shear 2-S	0.429
BC3.0	121.78	182.63	116.74	Shear 1	116.4	Shear 1	0.637
B3.0-300-0	114.33	154.99	105.77	Shear 1	129.6	Flexural	0.836
B3.0-300-10	113.90	138.71	110.39	Shear 1	111.5	Shear 2-S	0.804
B3.0-300-25	116.22	157.74	110.85	Shear 1	84.9	Shear 2	0.538
B3.0-450-0	117.65	156.30	106.07	Shear 1	131.6	Shear 1	0.842
B3.0-450-10	115.32	149.69	110.82	Shear 1	105.0	Shear 2-S	0.701
B3.0-450-25	116.63	161.68	107.37	Shear 1	49.1	Shear 3	0.304

Failure mode shear 1: yielding and/or fracture of the stirrup in the middle of the shear span;
Failure mode shear2: shear compression failure;
Failure mode shear 2-s: splitting along the corrosion cracks
Failure mode shear3: brittle diagonal tension shear failure;

2.4.2 Analytical model of deep beams

Up to now, several analytical models are proposed to evaluate the shear capacity of the beams. In this section, the typical models will be introduced.

Cross-sectional method by ACI 318-08 [42]

According to ACI-318-08, for a beam with web reinforcement, the shear capacity of the deep beam includes the contribution of concrete and the stirrups. The calculation is based on the following equations:

$$V_R = V_C + V_S \qquad (2\text{-}5)$$

$$V_C = 2\sqrt{f_c'}\,b_w d \qquad V_S = \frac{A_V f_y d}{s} \qquad (2\text{-}6)$$

Where:

V_R is the total shear capacity;

V_C is the shear resistance of the concrete;

V_S is the shear resitance of the shear reinforcement and stirrups;

f_c' specified compressive strength of concrete;

Bw web width, or diameter of circular section;

d distance from extreme compression fiber to centroid of longitudinal tension reinforcement, but need not be less than 0.80h for circular sections and prestressed members;

Av area of shear reinforcement within a distance, or area of shear reinforcement perpendicular to flexural tension reinforcement within a distance for deep flexural members;

fy specified yield strength of nonprestressed reinforcement;

s spacing of shear or torsion reinforcement measured in a direction parallel to longitudinal reinforcement.

Cross-sectional method by Eurocode 2 [26]

In Eurocode 2, the design value for the shear resistance V_{Rd} of a RC beam with vertical shear reinforcement (stirrups) is the smaller value of the following equations:

$$V_{Rd,s} = \frac{A_{sw}}{s} z f_{ywd} cot\theta \qquad (2\text{-}7)$$

$$V_{Rd,max} = \alpha_{cw} b_w z v_1 f_{cd} / (cot\theta + tan\theta) \qquad (2\text{-}8)$$

Where:

A_{sw} is the cross-sectional area of the shear reinforcement;

s is the spacing of the stirrups;

z is the inner lever arm;

θ is the angle between the concrete compression strut and the beam axis perpendicular to the shear force;

bw is the minimum width between tension and compression chords;

fcd is the design value of concrete compression strength;

f_{ywd} is the design yield strength of the shear reinforcement;

v_1 is a strength reduction factor for concrete cracked in shear;

α_{cw} is a coefficient taking account of the state of the stress in the compression chord;

Strut and tie model to predict the strength of the corroded deep beams [9]

The struct and tie model is also adopted in Eurocode 2. Azam et al. carried out an experimentally investigation on different corrosion levels (0%, 5% and 7.5%). Six beams were subjected to artificial corrosion whereas two beams acted as control un-corroded and then all the beams were tested in three point bending. The results showed that corrosion of properly anchored longitudinal steel reinforcement didn't have any adverse effect on the behaviour of shear critical RC deep beams. Corrosion changed the load transfer mechanism to a pure arch action and as a result the load carrying capacity was improved. A strut and tie model was proposed to predict the failure loads of shear-critical RC deep beams with corroded longitudinal bars as follow:

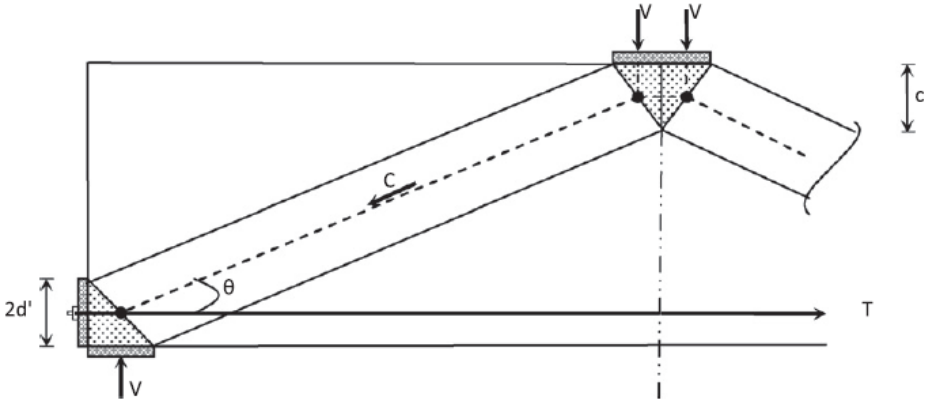

Figure 2-22 Strut and tie model for deep beams[9]

The shear strength of the corroded deep beams was the smaller value of the following calculations:

$$P = 2V = 2 \cdot C \cdot sin\theta = 2 \cdot [(0.6f_c') \cdot w_c \cdot b] \cdot sin\theta \qquad (2\text{-}9)$$

$$P = 2V = 2 \cdot T \cdot tan\theta = 2 \cdot [As^* \cdot f_y] \cdot sin\theta \qquad (2\text{-}10)$$

Where:

P is the failure load of the corroded deep beams;

V is the reaction at the support (shear force);

C is the compression force in the strut;

θ is the angle between strut and tie;

$0.6f_c'$ is the limiting stress in the strut, f_c' is the compressive strength of concrete;

$w_c \cdot b$ is the area of the strut (w_c is the width of the strut, b is the width of the beam);

T is the tension force in the tie;

As^* is the residual cross-section of the corroded steel bars;

f_y is the yield strength of the steel bars.

Based on eight medium-scale reinforced concrete beams with corrosion levels of 0%, 5%, 7.5% in impressed current method, Azam et al. [9] found the experimental results matched the simplified model well. The analytical model predicted that the failure mode of the deep beams could transfer from splitting of compression strut to yielding of longitudinal reinforcement at higher concrete strengths and corrosion levels.

However, it should be pointed out that the corrosion of the deep beams was based on the impressed current, and the experimental tests were limited. More experimental tests were still required to improve the models.

2.4.3 Bond and anchorage of the corroded beams

Bond and anchorage is also an important parameter for the deep beams. Due to the corrosion of the reinforcement, the bond and anchorage got reduced subsequently. The properties of bond and anchorage were usually tested by pull-out tests.

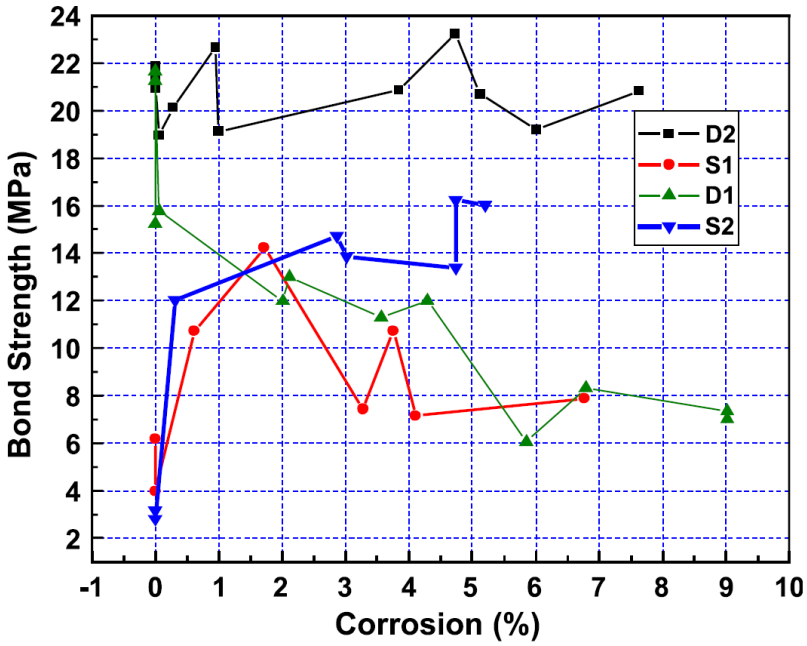

Figure 2-23 Effect of corrosion on the bond of reinforcement(Impressed current) D1: deformed without stirrups; D2: deformed with stirrups; S1: smooth without stirrups; S2: smooth with stirrups [43]

Fang et al. [43] conducted the pullout tests to evaluate the effects of corrosion on bond strength and bond-slip behavior of corroded RC samples. The specimens were cast with deformed bars and plain bars in different reinforcement corrosion degrees between 0 and 9%. The influence of stirrups on the anchorage of the corroded reinforcement was also considered in the tests. Part of the experimental results was showed in Figure 2-23. The bond reduced significantly in the samples without stirrups when corrosion increased, which showed that the stirrups played a vital role for the bond of the corroded reinforcement.

Hanjari et al. [44, 45] undertook pull-out tests on beam-end specimens with long embedment length to investigate the global behavior of an anchored bar when the concrete cover had cracked and spalled off due to corrosion. The experimental results showed that the stirrups played a very important role in the anchorage of the corroded bars. In fact, the stirrups provided the main source of confinement when the corrosion-induced cover cracking happened to the samples.
Based on the previous literatures, the bond and anchorage of the natural corroded beams will be investigated in this dissertation as the extension research work.

2.5 Composition of corrosion products

In chloride environment, the reinforcement got corroded and corrosion products are created. According to the previous literatures [11, 46, 47], the main constituents of rust are iron oxides, iron oxyhydroxides. The volume of the corrosion products is much larger than that of the original steel, as a result, the expansive volume will produce the stress to the concrete and finally the corrosion crack occurs to the concrete cover. So the composition and the physical properties of the corrosion products were considered as an important way to understand the cracking process of the corroded RC beams.
Jaffer et al. [11, 48] investigated the characterization of chloride-induced corrosion products. Both the composition and the distribution of the corrosion products at the rebar-concrete interfaces and on crack surfaces were examined. The chemical compositions and the unit volume of the corrosion products were shown in Figure 2-24. According to the figure, the volume of corrosion products could range from about 1.8 to 6.2 times larger than that of the original steel reinforcement.

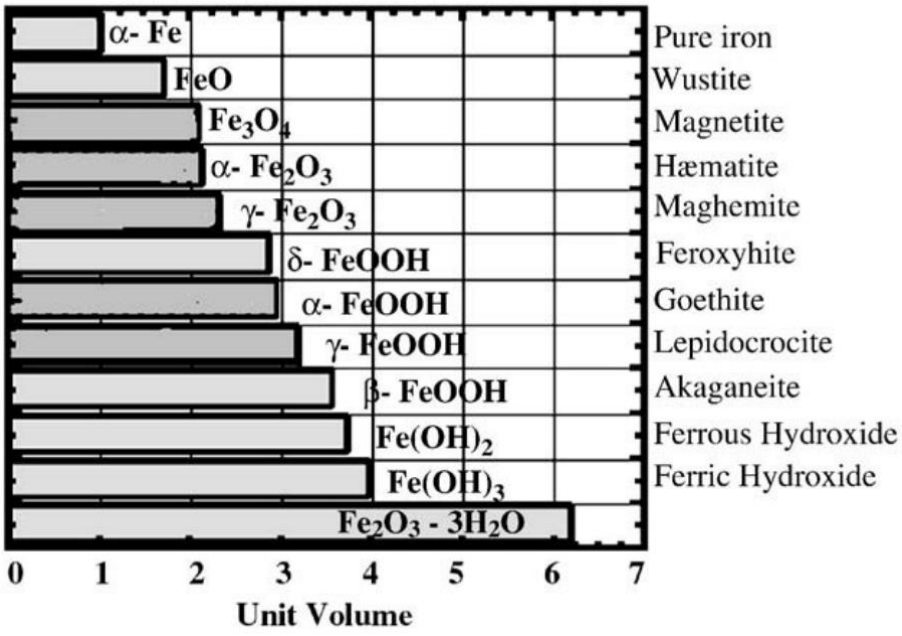

Figure 2-24 Corrosion products of iron [11]

Zhao et al. [12, 17, 49–51] investigated the composition and expansion properties of the corrosion products based on the X-ray diffraction and thermal analysis. The corrosion products were collected from the RC constructions exposed in marine environment in different regions. Finally, the rust expansion coefficients corresponding to different environments were proposed as shown in Table 2-2.

Table 2-2 Rust expansion coefficients corresponding to different environments[12]

Environment factors		Humidity (water)		
		High	Middle	Water
Oxygen supplement	High	3.3	3.1	2.9
	Middle	3.2	3.0	2.8
	Low	3.1	2.9	2.6

According to Table 2-2, the corrosion products could range from 2.6 to 3.3 due to different corrosion environment, which could be interesting for the further research on the cracking initiation of the corroded RC elements.

2.6 Summary of presented research method about corrosion

As discussed above, a considerable amount of research has been conducted on the corrosion of concrete beams during last few decades. But the weak point of most of the corrosion processes used in the research is that they were accelerated either by the application of an impressed

current or by including an admixture of $CaCl_2$ in the concrete [52]. Very limited studies dealing with the behavior of naturally corroded structures can be found at this moment. A summary of tests done to assess the residual capacity of corroded beams is shown in Table 2-3. Almost all studies use impressed current to accelerate corrosion. One main difference between the behavior of RC beams artificially corroded and naturally corroded is the ultimate deflection which is not modified in case of artificial corrosion but strongly reduced in case of natural corrosion. The reason can be that artificial corrosion leads to uniform corrosion [53] which is not the case for natural corrosion. Moreover, Otieno et al. [37] and Yuan et al. [38] have concluded that corrosion accelerated in artificial chloride environment such as cycle of wetting-drying is similar to that of corrosion in natural environment. This point is very important since as mentioned by Yuan et al. [38] different corrosion characteristics on the surface of steel are the main reasons that cause differences of structural behaviour between methods of inducing corrosion.

Corrosion rate is also an important parameter to predict the actual performances of corrosion affected RC structures. Impressed current used in accelerated corrosion study varies [8, 24, 27-34, 59, 60] from 80 $\mu A/cm^2$ to 10400 $\mu A/cm^2$ leading to different consequences on the corrosion pattern. For natural corrosion, the corrosion rate also varies from one structure and exposure condition to another. Nevertheless, the variation of Icorr [37] is in a limited range from 0.1 $\mu A/cm^2$ to 1-2$\mu A/cm^2$. Then results obtained from exposition to cyclic wetting and drying with NaCl are closed from natural corrosion.

Yuan et al. [38] have shown that galvanic method leads to a corrosion on the whole surface of steel bar and then is not representative of natural corrosion. The effect of sustained loading was clearly established in terms not only of the presence of mechanical cracks but also of damage at the interfaces between re-bars and concrete. Nevertheless, the effect of the load intensity was only reported for the short term and was not significant at long term. The effect of load on the corrosion process has also been studied by Yoon et al. [30] and Malumbela et al. [63], whose studies demonstrate not only the influence of the load but also an effect of the load level. Nevertheless, if as expected non-corroded beams failed by yielding followed by crushing of concrete; it is quite surprisingly that all corroded beams failed also by yielding of steel following by concrete crushing: these results seem to indicate that impressed electrical current used in the experimental process has led to generalized corrosion which does not allow to put in evidence the loss of ductility due to corrosion pits which appears with natural corrosion process.

Table 2-3 Summary on the mechanical behavior of corroded concrete members

Authors	Time	Beams	Environment	Corrosion condition	Loading condition
Tachibana et al.[54]	1990	RC		Galvanostatic	Corrosion prior to loading
Ting et al. [6]	1991	RC		Numerical simulation	
Cairns et al. [5]	1993	RC		Simulation of corrosion through reinforcement exposed	
Almusallam et al. [29]	1996	RC		Impressed current	Corrosion prior to loading
Rodriguez et al. [24]	1997	RC		Impressed current	Corrosion prior to loading
Mangat et al. [30]	1999	RC		Impressed current	Corrosion prior to loading
Castel et al. [55]	2000	RC	Chloride	Natural corrosion	Simultaneous corrosion and load
Yoon et al. [31]	2000	RC		Impressed current	Simultaneous corrosion and load
Capozucca et al. [32]	2003	RC		Impressed current	Corrosion prior to loading
Torres-Acosta et al. [33]	2004	RC		Impressed current	Simultaneous corrosion and load
El Maaddawy et al. [34]	2005	RC		Impressed current	Simultaneous corrosion and load
Du et al. [28]	2007	RC		Impressed current	Corrosion prior to loading
Azad et al. [8]	2007	RC		Impressed current	Corrosion prior to loading
Torres-Acosta et al. [27]	2007	RC		Impressed current	Corrosion prior to loading
Vié D. et al. [56]	2007	RC & pre-stressed	Chloride	Natural corrosion	Corrosion prior to loading
Vidal et al. [57]	2007	RC	Chloride	Natural corrosion	Simultaneous corrosion and load
Zhang et al. [58]	2009	RC	Chloride	Natural corrosion	Simultaneous corrosion and load
Malumbela et al. [59]	2009	RC		Impressed current	Simultaneous corrosion and load
Ababneh et al. [60]	2011	RC	Chloride		Loading prior corrosion
Khan et al. [61]	2011	RC	Chloride	Natural corrosion	Simultaneous corrosion and load
Dang et al. [62]	2013	RC	Chloride	Natural corrosion	Simultaneous corrosion and load

2.7 Conclusions

This chapter mainly presents a general background about various researches on chloride corrosion of RC beams. The mechanical properties of the corroded bars, the corrosion influence on the load-carrying capacity and ductility, the flexural and shear performance of the corroded beams. At last, the expansive properties of the corrosion products were also introduced briefly. It was worth pointing out that although a series of corrosion programs had been carried out all over the world, there were still some drawbacks to be improved:

(1) The major work on the corrosion of the RC constructions is based on the experiments accelerated by impressed current and/or adding $CaCl_2$ during the casting period. The destination is that the corrosion was increased significantly and the experiment period is shortened greatly. However, the differences between natural corrosion and electro chemical corrosion are unclear which made a reduction to the application of the research results.

(2) Most of the programs were carried out separately. As a result, the research conclusions varied from different programs. It was worth conducting a system experiments covering from the composition of the corrosion products to the cracking process, from the mechanical properties of the corroded bars to the residual structural performance of the corroded beams;

(3) The simulations of corrosion in RC beams are usually conducted with smaller dimensions. Though the dimensions are usually scaled, the influence of the sizes on the corrosion propagation and the residual mechanical performance could not be ignored.

(4) Most of the corrosion programs are undertaken without service load. In fact; for the RC constructions in aggressive environment, the corrosion process usually happens to the RC elements which are under service load. If possible, the consideration of the service load in the corrosion process will increase the value and reliability of the research conclusions.

(5) It was also popular that part of the RC beam is submerged into the saline solution as the corrosion conditions, which is not the exposure condition of the existed building. But for the RC constructions in marine environment, the RC elements are situated in the saline fog. In this condition, the RC elements are submerged into the fog in all the exposure surfaces. It can be different from the simulations by submerging into the solution with only part of the RC beams or just one tension surface in aggressive environment. The program to predict the service time in this simulation needs more experiments to make clear the influence of exposure conditions.

2.8 References

[1] Almusallam A. A., Effect of degree of corrosion on the properties of reinforcing steel bars. *Constr Build Mater* 2001;15(8): 361–8.

[2] Cairns J., Plizzari G. A., Du Y., Law D. W., Franzoni C., Mechanical properties of corrosion-damaged reinforcement. *ACI Mater J,* 2005;102(4): 256-64.

[3] Apostolopoulos C. A., Papadopoulos M. P., Tensile and low cycle fatigue behavior of corroded reinforcing steel bars S400. *Constr Build Mater* 2007; 21(4): 855–64.

[4] Kong F. K., Reinforced Concrete Deep Beams. Taylor & Francis; 2006.

[5] Cairns J., Zhao Z., Behaviour of concrete beams with exposed reinforcement. *Proceedings of the Institution of Civil Engineers: Structures and bridges*, 1993, 99(2): 141-54.

[6] Ting S. C,, Nowak A. S., Effect of reinforcing steel area loss on flexural behavior of reinforced concrete beams. *ACI Struct J* 1991; 88(3), 309-14.

[7] Río O., Andrade C., Izquierdo D., Alonso C., Behavior of Patch-Repaired Concrete Structural Elements under Increasing Static Loads to Flexural Failure. *J Mater Civ Eng* 2005; 17(2): 168–77.

[8] Azad A. K., Ahmad S., Azher S. A., Residual strength of corrosion-damaged reinforced concrete beams. *ACI Mater J* 2007; 104(1): 40-7.

[9] Azam R, Soudki K. Structural performance of shear-critical RC deep beams with corroded longitudinal steel reinforcement. *Cem Concr Compos* 2012; 34(8): 946–57.

[10] Zararis P., Shear Compression Failure in Reinforced Concrete Deep Beams. *J Struct Eng* 2003; 129(4): 544–53.

[11] Jaffer S. J., Hansson C. M., Chloride-induced corrosion products of steel in cracked-concrete subjected to different loading conditions. *Cem Concr Res* 2009; 39(2): 116–25.

[12] Zhao Y., Ren H., Dai H., Jin W., Composition and expansion coefficient of rust based on X-ray diffraction and thermal analysis. *Corros Sci* 2011; 53(5): 1646–58.

[13] Apostolopoulos C. A., Papadakis V. G., Consequences of steel corrosion on the ductility properties of reinforcement bar. *Constr Build Mater* 2008; 22(12): 2316–24.

[14] Du Y. G., Clark L. A., Chan A. H. C., Residual capacity of corroded reinforcing bars. *Mag Concr Res* 2005; 57(3): 135–47.

[15] Malumbela G., Moyo P., Alexander M. Influence of corrosion crack patterns on the rate of crack widening of RC beams. *Constr Build Mater* 2011; 25(5): 2540–53.

[16] Zhao Y., Hu B., Yu J., Jin W., Non-uniform distribution of rust layer around steel bar in concrete. *Corros Sci* 2011; 53(12): 4300–8.

[17] Zhao Y., Karimi A. R., Wong H. S., Hu B., Buenfeld N. R., Jin W., Comparison of uniform and non-uniform corrosion induced damage in reinforced concrete based on a Gaussian description of the corrosion layer. *Corros Sci* 2011; 53(9): 2803–14.

[18] Cao C., Cheung M. M. S., Non-uniform rust expansion for chloride-induced pitting corrosion in RC structures. *Constr Build Mater* 2014; 51: 75–81.

[19] Apostolopoulos C. A., Papadopoulos M. P., Pantelakis S. G., Tensile behavior of corroded reinforcing steel bars BSt 500s. *Constr Build Mater* 2006; 20(9): 782–9.

[20] Apostolopoulos C. A., Kappatos V., Tensile properties of corroded embedded steel bars B500c in concrete. *Int J Struct Integr* 2013; 4(2): 275–94.

[21] Lee H., S., Noguchi T., Tomosawa F., Evaluation of the bond properties between concrete and reinforcement as a function of the degree of reinforcement corrosion. *Cem Concr Res* 2002; 32(8): 1313–8.

[22] Du Y. G., Clark L. A., Chan A. H. C., Effect of corrosion on ductility of reinforcing bars. *Mag Concr Res* 2005; 57(7): 407–19.

[23] Rodriguez J., Ortega L. M., Casal J., Diez J. M., Assessing structural conditions of concrete structures with corroded reinforcement. Concr Repair Rehabil Prot Ed RK Dhir MR Jones E FN Spon Lond 1996: 65–78.

[24] Rodriguez J., Ortega L., Casal J., Load carrying capacity of concrete structures with corroded reinforcement. *Constr Build Mater* 1997; 11(4): 239–48.

[25] Rodriguez J., Ortega L. M., Casal J., Diez J. M., Corrosion of reinforcement and service life of concrete structures. *Durab Build Mater Compon* 1996; 7(1): 117–26.

[26] Institution BS. Eurocode 2: Design of Concrete Structures: Part 1-1: General Rules and Rules for Buildings. British Standards Institution; 2004.

[27] Torres-Acosta A. A., Navarro-Gutierrez S., Terán-Guillén J., Residual flexure capacity of corroded reinforced concrete beams. *Eng Struct* 2007; 29(6): 1145–52.

[28] Du Y., Clark L. A., Chan A. H., Impact of reinforcement corrosion on ductile behavior of reinforced concrete beams, *ACI Struct J.*, 2007; 104(3): 285-93.

[29] Almusallam A., Al-Gahtani A., Aziz A., Dakhil F., Rasheeduzzafar. Effect of Reinforcement Corrosion on Flexural Behavior of Concrete Slabs. *J Mater Civ Eng* 1996; 8(3): 123–7.

[30] Mangat P. S., Elgarf M. S., Flexural strength of concrete beams with corroding reinforcement. *ACI Struct J* 1999; 96(1): 149-58.

[31] Yoon S., Wang K., Weiss W. J., Shah S. P.., Interaction between loading, corrosion, and serviceability of reinforced concrete, *ACI Mater J;* 2000; 97(6): 637-44

[32] Capozucca R, Cerri MN. Influence of reinforcement corrosion—in the compressive

zone—on the behaviour of RC beams. *Eng Struct* 2003; 25(3): 1575–83.

[33] Torres-Acosta A. A., Sagues A. A., Concrete Cracking by Localized Steel Corrosion–Geometric Effects. *ACI Mater J* 2004; 101(6): 501-7.

[34] El Maaddawy T., Soudki K., Topper T., Long-term performance of corrosion-damaged reinforced concrete beams. *ACI Struct J* 2005; 102(5): 649-56.

[35] Malumbela G., Moyo P., Alexander M., Behaviour of RC beams corroded under sustained service loads. Constr Build Mater 2009; 23(11): 3346–51.

[36] Ababneh A., Sheban M., Abu-Dalo M., Effectiveness of Benzotriazole as Corrosion Protection Material for Steel Reinforcement in Concrete. *J Mater Civ Eng* 2012; 24(2): 141–51.

[37] Otieno M., Beushausen H., Alexander M., Prediction of corrosion rate in reinforced concrete structures – a critical review and preliminary results. *Mater Corros* 2012; 63(9): 777–90.

[38] Yuan Y., Ji Y., Shah S. P., Comparison of two accelerated corrosion techniques for concrete structures, *ACI Struct J.*, 2007; 104(3), 344-7.

[39] Cabrera J. G., Deterioration of concrete due to reinforcement steel corrosion. *Cem Concr Compos* 1996; 18(1): 47–59.

[40] Wang X. H., Li B., Gao X. H., Liu X. L., Shear behaviour of RC beams with corrosion damaged partial length. *Mater Struct* 2012; 45(3): 351–79.

[41] Wang X. H., Gao X. H., Li B., Deng B. R., Effect of bond and corrosion within partial length on shear behaviour and load capacity of RC beam. *Constr Build Mater* 2011; 25(4): 1812–23.

[42] 318 AC. Building Code Requirements for Structural Concrete (ACI 318-08) and Commentary. American Concrete Institute; 2008.

[43] Fang C., Lundgren K., Chen L., Zhu C.. Corrosion influence on bond in reinforced concrete. *Cem Concr Res* 2004; 34(11): 2159–67.

[44] Coronelli D., Hanjari K. Z., Lundgren K., Rossi E., Severely Corroded Reinforced Concrete with Cover Cracking: Part 1. Crack Initiation and Propagation. In: Andrade C, Mancini G, editors. Model. Corroding Concr. Struct., Springer Netherlands; 2011, p. 195–205.

[45] Hanjari K. Z., Coronelli D., Lundgren K., Severely Corroded Reinforced Concrete with Cover Cracking: Part 2. Anchorage Capacity. In: Andrade C, Mancini G, editors. *Model. Corroding Concr. Struct.*, Springer Netherlands; 2011, p. 207–17.

[46] Caré S., Nguyen Q. T., L'Hostis V., Berthaud Y., Mechanical properties of the rust layer induced by impressed current method in reinforced mortar. *Cem Concr Res* 2008; 38(8):

1079–91.

[47] Cook D. C., Spectroscopic identification of protective and non-protective corrosion coatings on steel structures in marine environments. *Corros Sci* 2005; 47(10): 2550–70.

[48] Marcotte T. D., Characterization of chloride-induced corrosion products that form in steel-reinforced cementitious materials, Ph. D. Thesis in Mechanical Engineering, 2001, University of waterloo: Waterloo, Canada.

[49] Zhao Y., Yu J., Wu Y., Jin W., Critical thickness of rust layer at inner and out surface cracking of concrete cover in reinforced concrete structures. *Corros Sci* 2012; 59: 316–23.

[50] Zhao Y., Yu J., Jin W., Damage analysis and cracking model of reinforced concrete structures with rebar corrosion. *Corros Sci* 2011; 53(10): 3388–97.

[51] Wong H. S., Zhao Y. X., Karimi A. R., Buenfeld N. R., Jin W. L., On the penetration of corrosion products from reinforcing steel into concrete due to chloride-induced corrosion. *Corros Sci* 2010; 52(7): 2469–80.

[52] Xu J., Jiang L., Wang W., Jiang Y., Influence of $CaCl_2$ and NaCl from different sources on chloride threshold value for the corrosion of steel reinforcement in concrete, *Construct Build Mater.* 2011; 25(2): 663-9

[53] Zhu W. J., François, R., Effect of corrosion pattern on the ductility of tensile reinforcement extracted from a 26-year-old corroded beam, *Advances in Concrete Construction*, 2013, 1(2):121-37

[54] Tachibana Y., Maeda K. I, Kajakawa Y., Mechanical behaviour of RC beams damaged by corrosion of reinforcement, Applied Science, 1990: 178-87

[55] Castel A., François R., Arliguie G., Mechanical behaviour of corroded reinforced concrete beams—Part 1: experimental study of corroded beams, *Mater Struct*, 2000, 33(9): 539-44

[56] Vié D., Poupard O., Bilan des essais sur corps d'épreuve, *Revue européenne de génie civil*, 2007, 11(1-2): 55-95

[57] Vidal T., Castel A., François R., Corrosion process and structural performance of a 17-year-old reinforced concrete beam stored in chloride environment, *Cem Concr Res* 2007; 37(11): 1551-61

[58] Zhang R., Castel A., François R..Serviceability Limit State criteria based on steel-concrete bond loss for corroded reinforced concrete in chloride environment, *Mater Struct* 2009; 42(10): 1407-21

[59] Malumbela G., Moyo P., Alexander M., Behaviour of RC beams corroded under sustained service loads, *Construct Build Mater*, 2009, 23(11): 3346-51

[60] Ababneh A., Sheban M. A., Abu-Dalo M. A., Effectiveness of benzotriazole as corrosion protection material for steel reinforcement in concrete, *J Mater in Civ Eng*, 2011, 24(2): 141-51

[61] Khan I., François R., Arnaud Castel. Mechanical behavior of long-term corroded reinforced concrete beam, *Modelling of corroding concrete structures* 2011; 5(10): 243-58

[62] Dang V. H., François, R., Influence of long-term corrosion in chloride environment on mechanical behaviour of RC beam, *Eng Struct*, 2013, 48: 558-68

[63] Malumbela G., Moyo P., Alexander M., Longitudinal strains and stiffness of RC beams under load as measures of corrosion levels, *Eng Struct.* 2012; 35: 215-27

CHAPTER THREE

Experimental program of the corrosion process of the RC beams exposed to natural aggressive environment

3.1 Introduction

This program of long-term corrosion of reinforcement in RC beams has been carried out by François [1] since 1984 in Laboratoire Matériaux et Durabilité des Constructions (L.M.D.C.) in Toulouse, southwest of France. The program was financially supported by l'AFREM (Association Française de Recherche et d'Etudessur les Matériaux) and l'AFB (Association Française du Béton) which was reformed to l'AFGC (Association Française du Génie Civil) in the later period. The destination of this program was to improve the knowledge about the corrosion process of reinforcement in RC beams that were exposed to the aggressive environment and the influence of service load on the corrosion initiation and propagation during the corrosion period. The mechanical performance of the corroded beams was also investigated during different periods.

A series of full-scale RC beams were cast and stored in the chloride environment continually. This chapter presents a detailed description of the test specimens built for this research program. The characteristics of the materials, the conservation conditions and the corroded situations are introduced. Moreover, part of previous literature about the continually experimental results which has been observed during the 26-28 years is also described here.

3.2 Test specimens

In this program, 36 RC beams were cast in 1984. All the beams were loaded and then stored in corroded environment with chloride fog spraying in the continually cycles; which were treated to be the corroded beams. Another 36 beams with the same materials and compositions, the same configurations were cast but stored in the normal laboratory conditions, which were considered to be the non-corroded beams (control beams). The corrosion process of the research program was carried out by the comparison of the differences of the observation results between the corroded beams and non-corroded beams during the whole experimental period.

3.2.1 Configurations

All the beams were cast with the dimension of 3000 mm × 280 mm × 150 mm. The configurations were shown in Figure 3-1. It was a typical size of elements applied in the construction industry of the casting time. Both 10 mm and 40 mm were considered for different beams as the depth of the concrete cover, which meant that 16 beams were cast with the cover of 10 mm and 16 beams were cast with the cover of 40 mm. It should be pointed out that 10 mm of the concrete cover was the minimum value required by French regulations [2] in 1984. The beams with the concrete cover of 40 mm were labeled Type A as shown in the figure, while the beams with the concrete cover of 10 mm were labeled Type B.

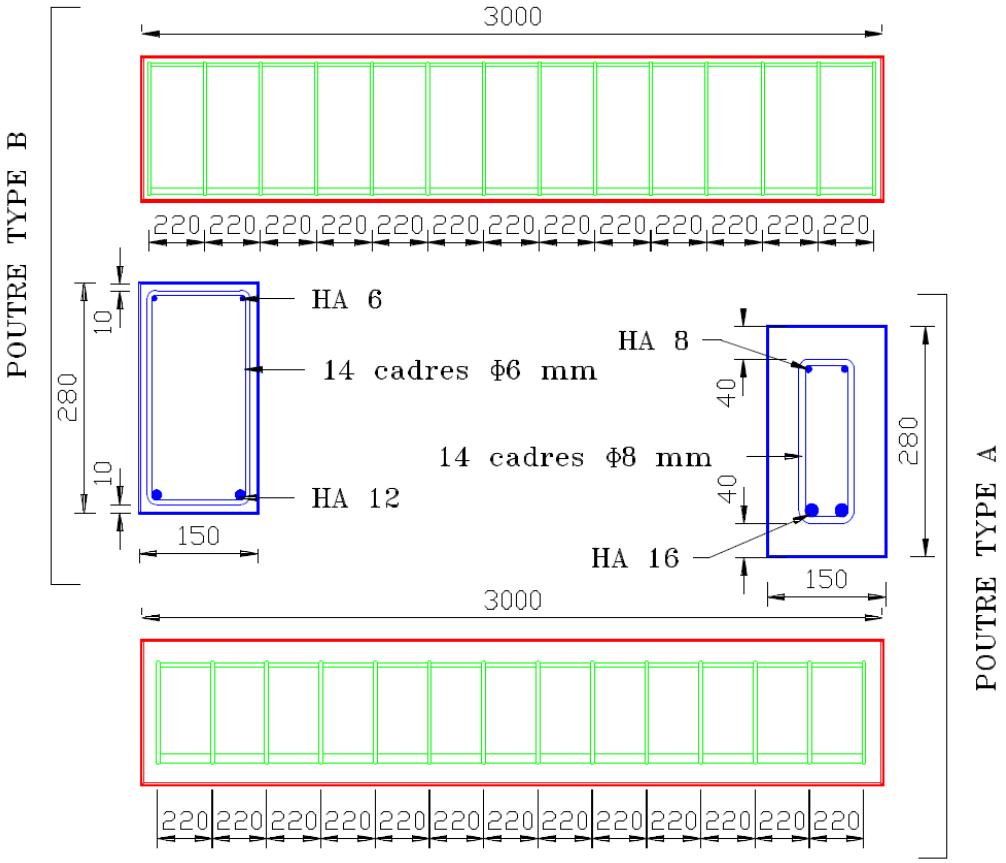

Figure 3-1 Configuration of the beams for Type A and Type B

The diameter of the reinforcement was also different for the two types of the beams. For Type A, the diameter of tension bars (longitudinal bars in the bottom of the beam) was 16 mm; the diameter of the compressive bars (longitudinal bars in the top of the beam) and stirrups was 8 mm. However, for Type B, the size of the reinforcement was smaller than that of Type A. The diameter of the tension bars was 12 mm; the diameter of the compressive bars and the stirrups was 6 mm. It should be pointed out that there was no hook for all the longitudinal bars.

3.2.2 Materials

The cylindrical specimens, with the diameter of 110 mm and height of 220 mm, were fabricated at the time of casting the beams. The specimens were then stored in the curing room for 28 days. Experimental tests were carried out on the specimens in order to get the mechanical properties of the concrete.

According to the compression tests on the cylindrical specimens, the average compressive strength of the concrete was 45 MPa. The elastic modulus was 32 GPa. The tensile strength was 4.7 MPa, which was tested by splitting test on the cylindrical specimens. The porosity was about 15.2%. There formed steel bars were adopted for all the reinforcements, including the longitudinal bars and stirrups. Moreover, the reinforcement belonged to the high yield strength bars, with the nominal yield strength of 500 MPa.

3.2.3 Compositions

The composition of the concrete and the chemical compounds presented in the cement are given in Figure 3-1. It's worth noting that the initial idea of this program was to realize concrete for real structural application such as bridges and building. So the concrete adopted in this experiment was not in poor quality. The ratio of water to cement was designed to be 0.5. However, the water content could be reduced in the casting process in order to achieve a constant workability of 70 mm in the slump test.

Table 3-1 Concrete composition and chemical compounds of the cement

Mix composition							
Rolled gravel (silica+limestone)					5/15 mm		1220 kg/m^3
Sand					0/5 mm		820 kg/m^3
Portland cement: OPC HP (high perform)							400 kg/m^3
Water							200 kg/m^3
Cement composition	SiO_2	Al_2O_3	Fe_2O_3	CaO	MgO	SO_3	Na_2O
Weight (%)	21.4	6.0	2.3	63.0	1.4	3.0	0.5

3.2.4 Loading system

A three-point loading system was applied to the beams according to coupling a beam of Type A and a beam of Type B together. As shown in Figure 3-2, the load was controlled by the strain measurement of the loading system.

Two levels of the load were applied: the moment at the mid-span of the beams was 13.5 kN·m which corresponded to the maximum load versus durability in an aggressive environment for the beams in Type A and the maximum load versus resistance for the beams in Type B according to French code [2]. The load was marked as level 1 and the beams under level 1 were named A1 and B1 respectively; the moment at the mid-span was 21.2 kN·m which corresponded to the maximum load versus resistance for the beams in Type A and 80% of the failure load and equal to twice the design service load in aggressive environment. The beams loaded in level 2 were named A2 and B2 respectively.

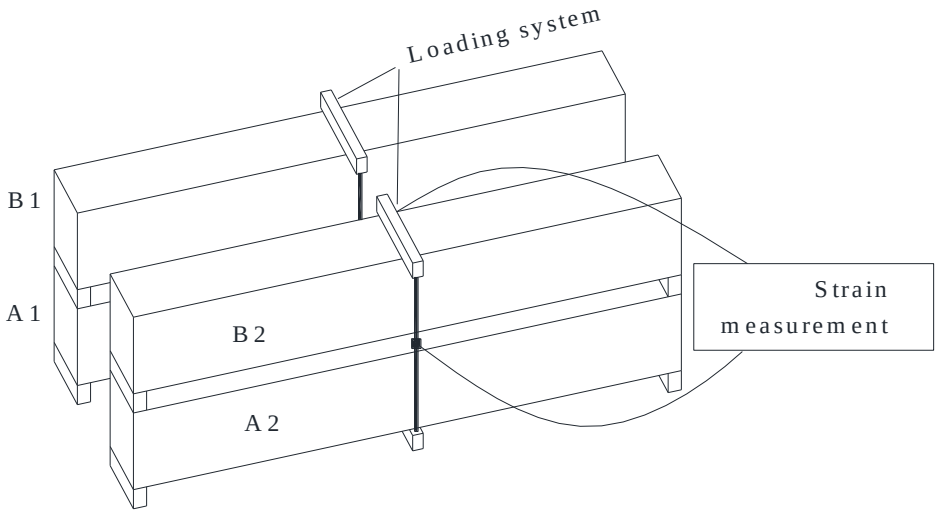

Figure 3-2 Loading system of the beams

3.2.5 Conservation environment

The beams were transferred to a chloride environment, which was formed by the salt fog generated by four sprays located in top corner of a confined room as shown in Figure 3-3. The fog was made by a solution of 35 g/l NaCl, which was the same to the salt concentration of sea water. In order to improve the understanding of the chloride corrosion effect on the reinforcement and the concrete beams, the non-corroded beams were kept in a laboratory room, with R.H. of 50% and a temperature of 20°C throughout the program.

Having been stored in the saline fog for 6 years, the corroded beams were transferred to wetting-drying cycles (Table 3-2) so as to accelerate the corrosion process. It should be pointed out that the loading system was allowed to monitor the decrease of the force applied due to creep of concrete. The load was re-adjusted periodically during the first years. Moreover, a spring system of the loading device was allowed to accept some increase in beam deflection without affecting the load [3]. Nevertheless, the loading device suffered in the

aggressive environment the monitoring system stopped giving load information after 6 years. After 19 years of storage, it was decided to perform mechanical tests on the beams, the loading system was removed. However, because of the high chloride content [4] and storage in outside conditions, corrosion continued to propagate.

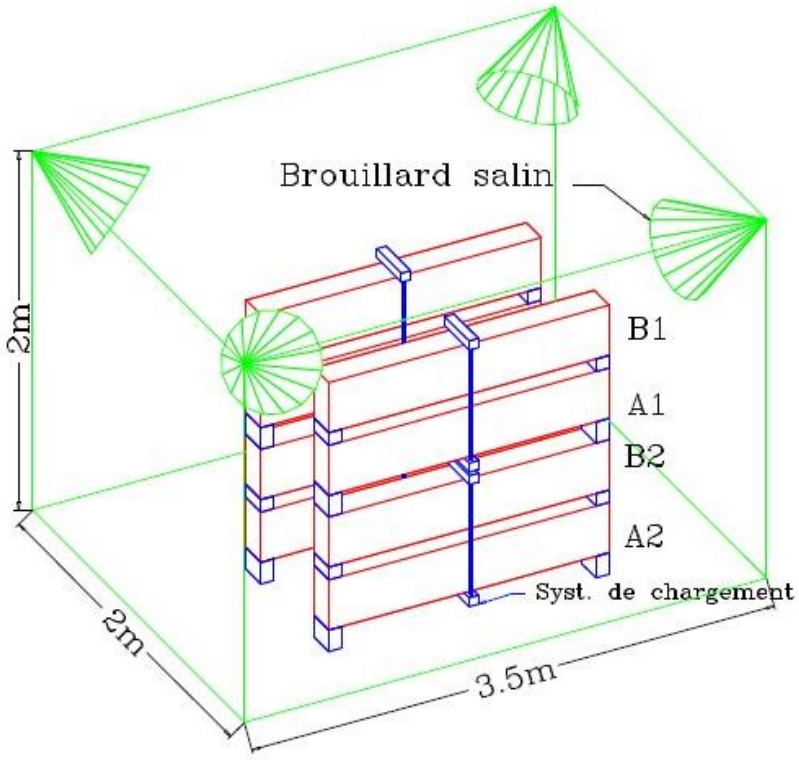

Figure 3-3 Storage of the chloride environment

Table 3-2 Wetting-drying cycles of the corroded beams

Period (years)	Spraying state	Loading conditions	Conservation conditions	Temperature (°C)
0-6	continuous spraying	loaded	confined room	about 20 °C
6-9	WDC	loaded	confined room	about 20 °C
9-19	WDC	loaded	confined room	CSWF
19-26	stop spraying	unloaded	confined room	CSWF
26--present	WDC	unloaded	confined room	CSWF

*WDC: wetting-drying cycles for one week respectively;

*CSWF: climate of south-west France, ranging from 5.1 to 21.3°C average value per month

3.2.6 Corrosion propagation

At different stages of the long-term period, several kinds of the experimental studies have

been conducted by observations and mechanical tests without destroying the beams. A series of relative literatures about the beams have been published. Zhang et al. [5] and Vidal et al. [6] have tried to predict the corrosion degree by the corrosion crack width. Khan et al. [7] and Dang et al. [8] have investigated the deterioration of the corroded beams in Group A. Castel et al [9] have studied the mechanical behavior of beams from group B with respectively 14 years and 23 years of aging in chloride environment.

Parts of the research results about the objective beam of this thesis, corroded beam B2Cl2, in the previous stages will be presented in this section. The label B2 stands for beams in Type B and loaded in the second load level. Cl means the corroded beams, while for the non-corroded beams, the symbol is T. The last figure means the series number in the same condition. For example, B2Cl2 means the corroded beam in Type B under the second load level. Instead, the corresponding non-corroded beam is named B2T2.

The cracking maps of B2Cl2were described in 28 days, 6 years, 14 years, 17 years and 23 years, including the transversal cracks which were induced mainly by the applied load and the longitudinal cracks which were mainly due to the corrosion of reinforcement. The results were presented in Figure 3-4 to Figure 3-8. The corrosion cracking propagation of B2Cl2 could be checked clearly in different stages. Moreover, the mechanical tests were also carried out in the corresponding stages under service load. The load-deflection curves of B2Cl2 in different stages were shown in Figure 3-9.

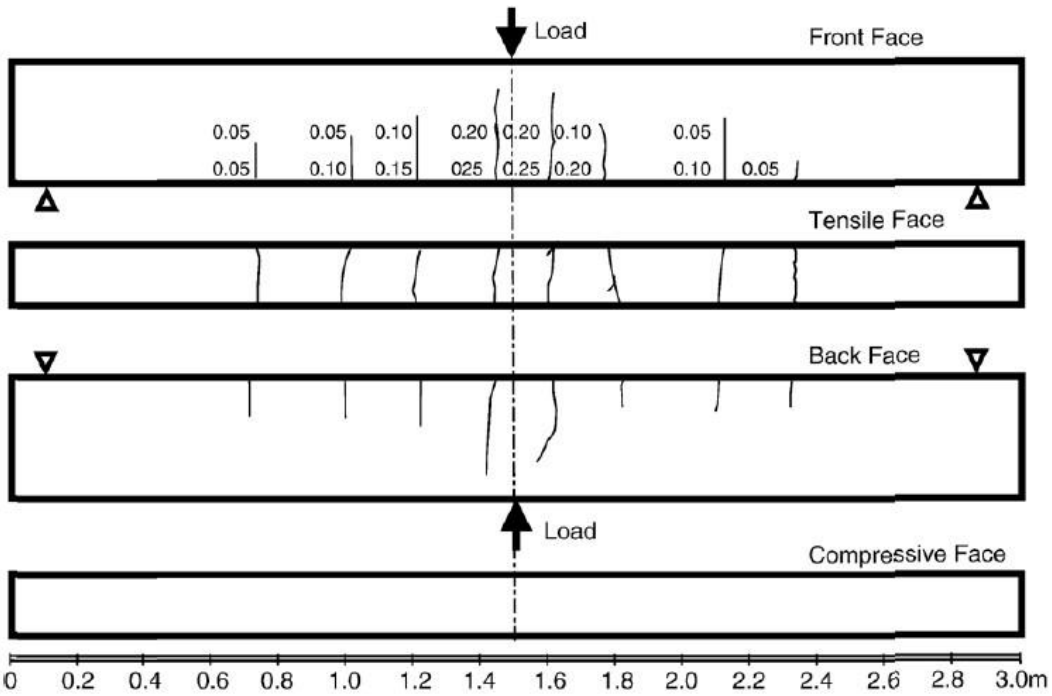

Figure 3-4 Cracking maps of beam B2Cl2 after 28 days of storage[4]

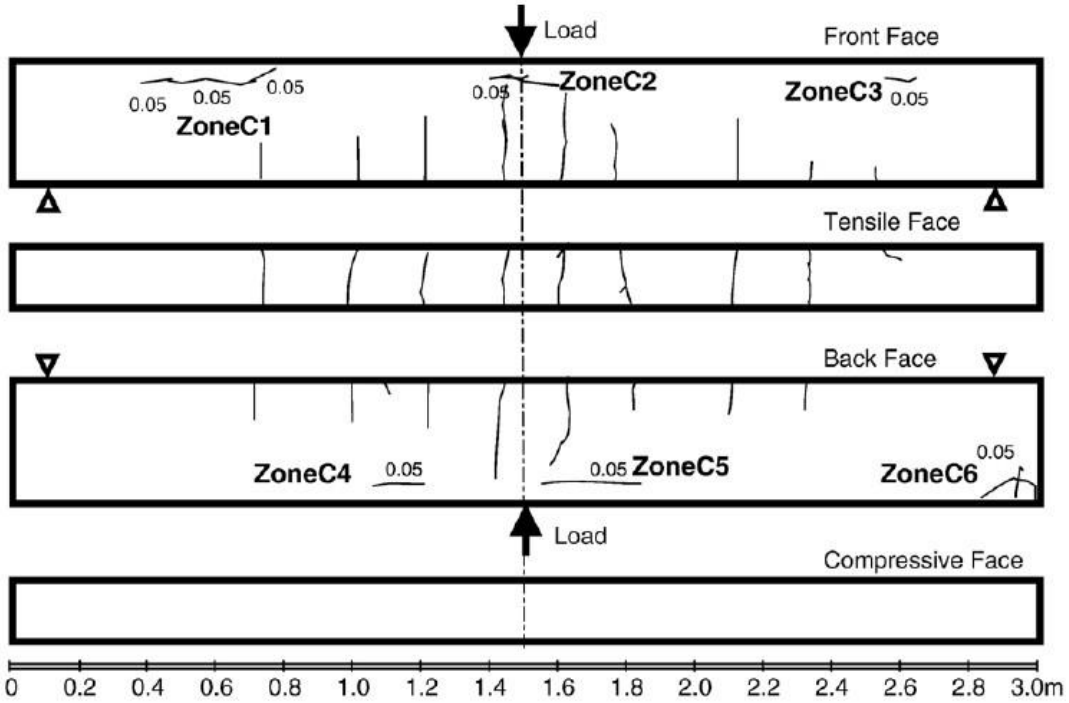

Figure 3-5 Cracking maps of beam B2Cl2 after 6 years of storage[4]

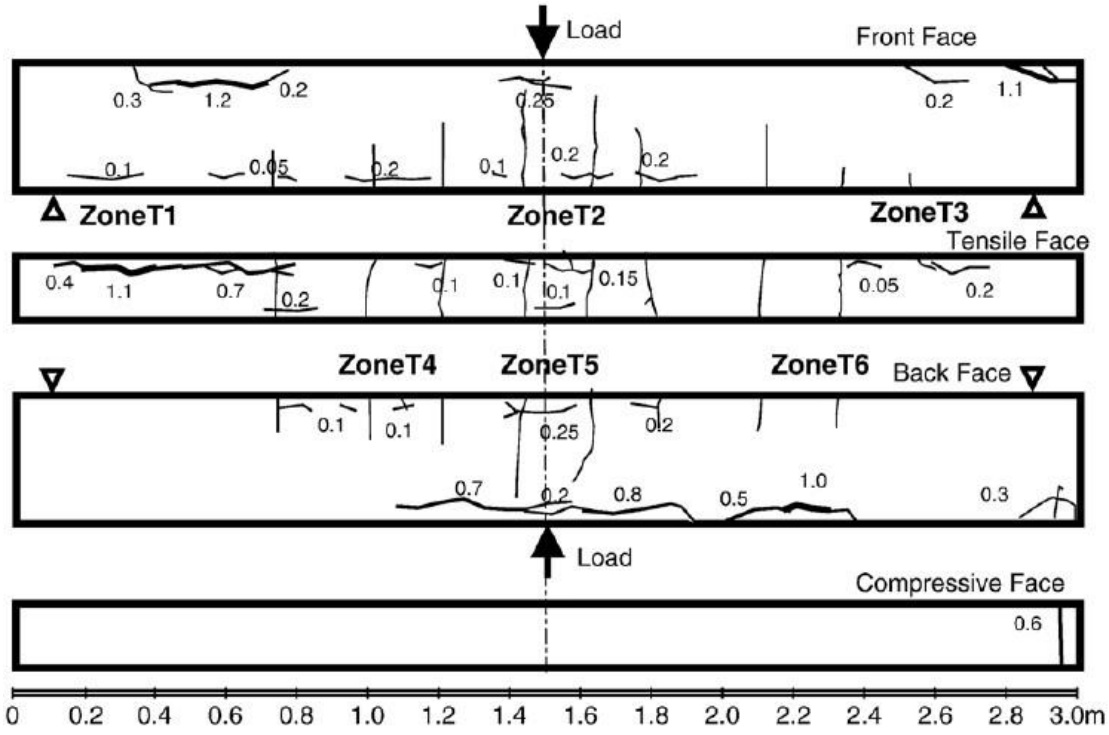

Figure 3-6 Cracking maps of beam B2Cl2 after 14 years of storage[4]

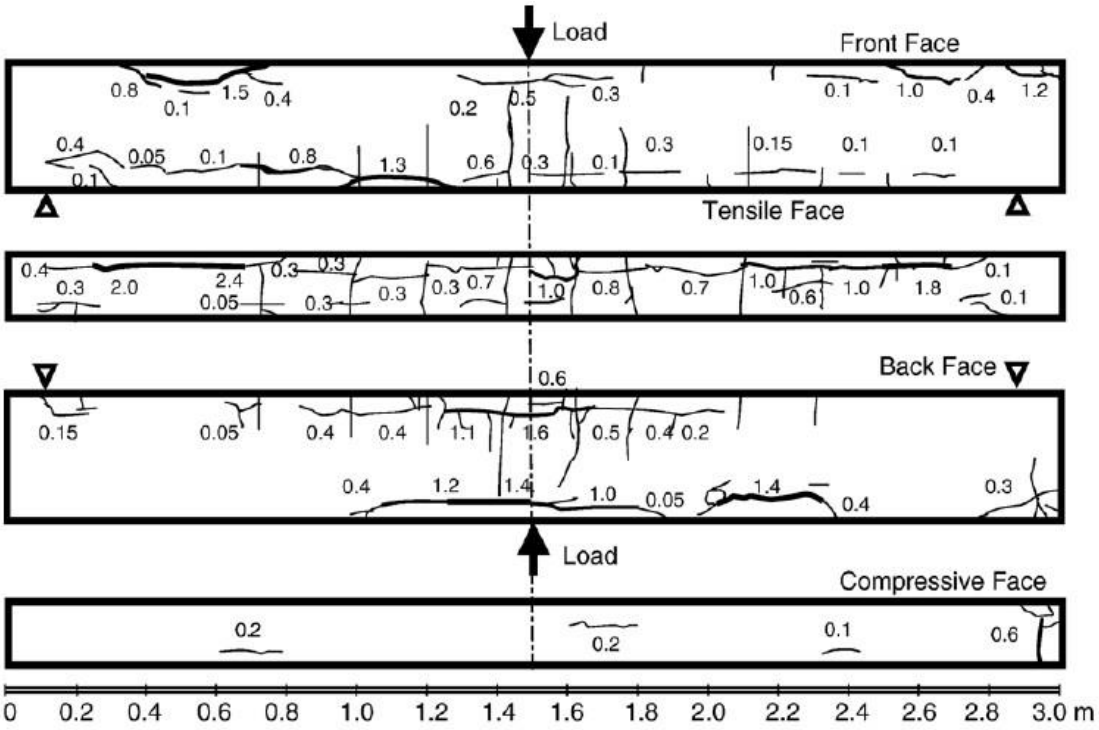

Figure 3-7 Cracking maps of beam B2Cl2 after 17 years of storage[4]

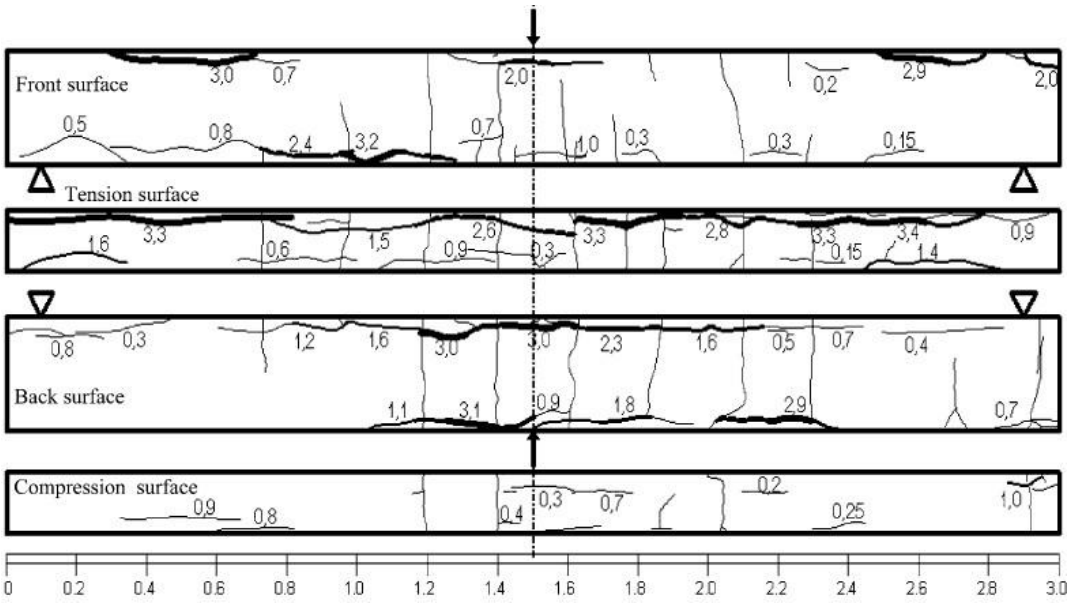

Figure 3-8 Cracking maps of beam B2Cl2 after 23 years of storage[10]

3.3 Conclusion and prospect

Based on this program, the previous research was mainly conducted on the mechanical performance of the corroded beams under service load, the chloride content during the corrosion period, cracking process and the relationship of crack width and the cross-section loss of the reinforcement. In this thesis, the flexural capacity, the shear capacity, and the

residual mechanical properties of the corroded reinforcement will be investigated.

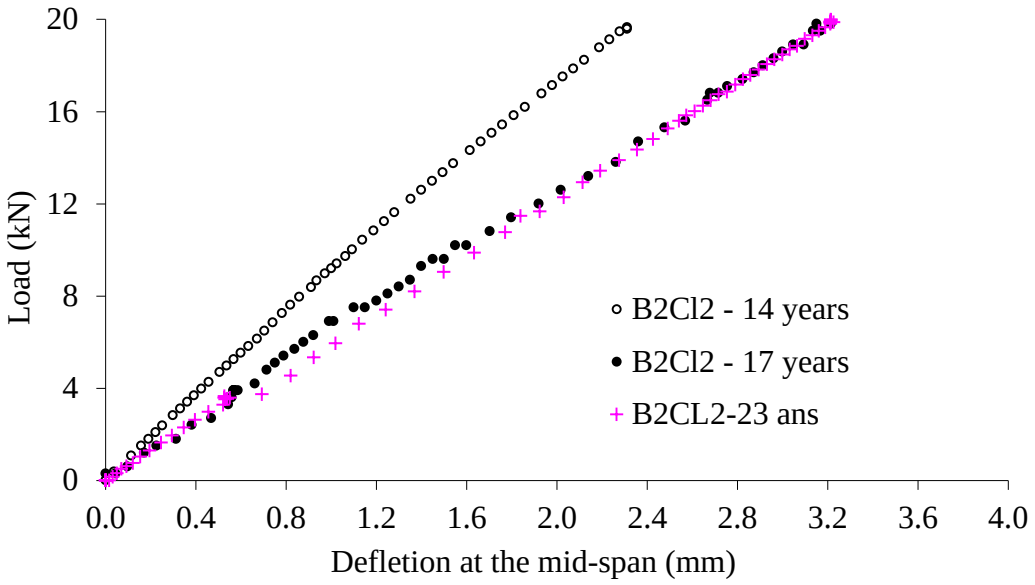

Figure 3-9 Curves of load-deflection for beam B2Cl2 in different stages

3.4 References

[1] François R., "Béton armé : corrélation entre fissuration et corrosion", PHd of Toulouse Université, France, Juin 1987.

[2] B.A.E.L. (1983) *French regulations for reinforced concrete structures*

[3] François R., Ringot E., Force sensor based on strain measurement to record the load applied to RC beams (in French), GAMAC INFO, n°2-3, pp. 21-28, 1988

[4] Vidal T., Castel A., François R., Corrosion process and structural performance of a 17-year-old reinforced concrete beam stored in chloride environment, *Cem Concr Res* 2007; 37(11) :1551-61

[5] Zhang R., Castel A., François R.. Concrete cover cracking with reinforcement corrosion of RC beam during chloride-induced corrosion process, *Cem Concr Res* 2010; 40(3): 415-25

[6] Vidal T., Castel A., François R.. Analyzing crack width to predict corrosion in reinforced concrete, *Cem Concr Res* 2004; 34(1): 165-74

[7] Khan I., François R., Arnaud Castel. Mechanical behavior of long-term corroded reinforced concrete beam, *Modelling of corroding concrete structures* 2011; 5(10): 243-58

[8] Dang V. H., François R. Influence of long-term corrosion in chloride environment on mechanical behaviour of RC beam, *Eng Struct*, 2013, 48: 558-568

[9] Castel A., François R., Arliguie G., Mechanical behaviour of corroded reinforced concrete beams—Part 1: experimental study of corroded beams, *Mater Struct*, 2000, 33(9): 539-44

[10] Zhang R., Castel A., François R., Serviceability Limit State criteria based on steel-

concrete bond loss for corroded reinforced concrete in chloride environment, *Mater Struct* 2009; 42(10):1407-21

CHAPTER FOUR

Mechanical properties of the corroded bars and the influence of residual cross-sectional shape on the ductility of the steel bars

The mechanical properties of the corroded bars are investigated in this chapter. The main attention is fixed on the following two parts:

Tension tests were carried out to investigate the effect of the corrosion pattern on the ductility of tension bars extracted from a 26-year-old and a 28-year-old corroded reinforced concrete beams. The tensile behavior of corroded bars with different corrosion patterns was examined, as were the non-corroded bars extracted from two non-corroded beams of 26-year-old and 28-year-old respectively. The results show that corrosion leads to an increase in the ratio of the ultimate strength over the yield strength, but reduces the ultimate strain at maximum force of the reinforcement. Both the corrosion pattern and the corrosion intensity play an important role in the ductile properties. The asymmetrical distribution of the corrosion around the surface is a decisive factor, which can influence the ultimate strain at maximum force more seriously.

Based on the mechanical properties of the corroded bars, the residual cross-section shape was found in deep relationship with the ductility of the steel bars. Three corrosion simulation types were proposed to investigate the influence of residual cross-section shape on the ultimate strain of the steel bars. The same experimental tests were carried out on the three corrosion simulation types with different residual cross-section shapes, including both the uniform cross-section loss and non-uniform cross-section loss. The results showed that the residual cross-section shape and the different cross-section loss played an important role on the ductility of the bars. The steel bar with symmetrical distribution of residual cross-section performed a better ductility when the corrosion degrees of the steel bars were in the same condition.

4.1 Introduction

The corrosion of reinforcement, which commonly happens in a chloride environment, is considered to be one of the major problems for the deterioration of reinforced concrete structures, which has been the object of great attention from both researchers and engineers [1-3]. Corrosion damage of the reinforcement can not only reduce the cross-section of the steel bar but also produce stress in the concrete around the bar which can gradually result in cracking or even spalling of the concrete cover as the volume of the corrosion products increases [4]. Considerable resources are expended to repair and rehabilitate deteriorating concrete structures [5]. It has been reported that, in the USA, such repair and rehabilitation costs over $20 billion per year [6].

Much research work has done to deal with this corrosion problem, especially the corrosion of reinforcement. Ahmad [7] has reviewed reinforcement corrosion in concrete structures and assessed the causes and extent of corrosion of reinforcements, so as to predict the residual behavior of a corroded structure exposed to an aggressive environment. Apostolopoulos et al. [8] noted the increase in steel stress at corroded cross-sections, and also observed reduction of the ductility. Stewart [9] and Maslehuddin et al. [10] have also investigated the influence of corrosion on the mechanical properties of the reinforcement in different conditions. However, most research has concentrated on the yield strength and ultimate strength based on the nominal diameter without considering the loss of cross-section due to corrosion [11-12].

In fact, relatively less work has been done on natural corrosion and the ductility of corroded steel bars [13]. The ductility and the minimum cross-section of the tension bars are the two key elements that determine the ductile behavior of corroded RC structures.

4.2 Tension tests on corroded bars

After 26 years, the corroded beam B2Cl2 from the aggressive environment and the non-corroded beam B2T2 were broken to provide access to the tension bars of both beams. Then seven samples were taken from different parts of the two tension bars as shown in Figure 4-1. The details of the corroded and non-corroded samples are shown in Table 4-1. The length of effective range is the distance between fixed points of LVDT as shown in Figure 4-2.

A 250-kN-capacity machine was used to carry out the tension test as shown in Figure 4-2. Two LVDTs distant of about 200 mm (Ler) measured the elongation of the tension bar. The tensile properties of the bars were calculated from the results of the tensile test.

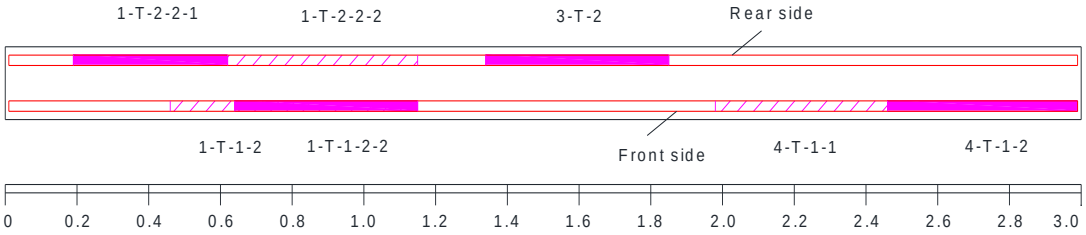

Figure 4-1 Locations of the tension samples from corroded beam B2Cl2

Figure 4-2 Uniaxial tension tests on the bars

Table 4-1 Details of the tension bars

	Location	Label	Length of sample (mm)	Effective range (mm)	Mass (g)	Mass/metre of length (g/m)
Corroded bars	Front side	1-T-1-2	662.58	201	512.25	772.9
	Front side	1-T-1-2-2	479.22	201	374.43	780.5
	Front side	4-T-1-1	615.76	201	480.78	780.8
	Front side	4-T-1-2	509.86	230	411.21	806.5
	Rear side	1-T-2-2-1	447.02	224	359.70	804.7
	Rear side	1-T-2-2-2	487.10	216	402.12	825.5
	Rear side	3-T-2	430.80	201	334.14	775.6
Non-corroded bars	Front side	B2T-1-2	580	200	510.65	887.8
	Rear side	B2T-2-2	557	201	493.04	887.8

4.3 Corrosion of the corroded bars

4.3.1 Corrosion distribution

The corroded tension bars were put into Clarke's Solution ANSI/ASTM G1-72 to clean the

corrosion products. Then the corrosion distribution was drawn in pitting corrosion and general corrosion (Figure 4-4) from the top view and bottom view as shown in Figure 4-3(b).

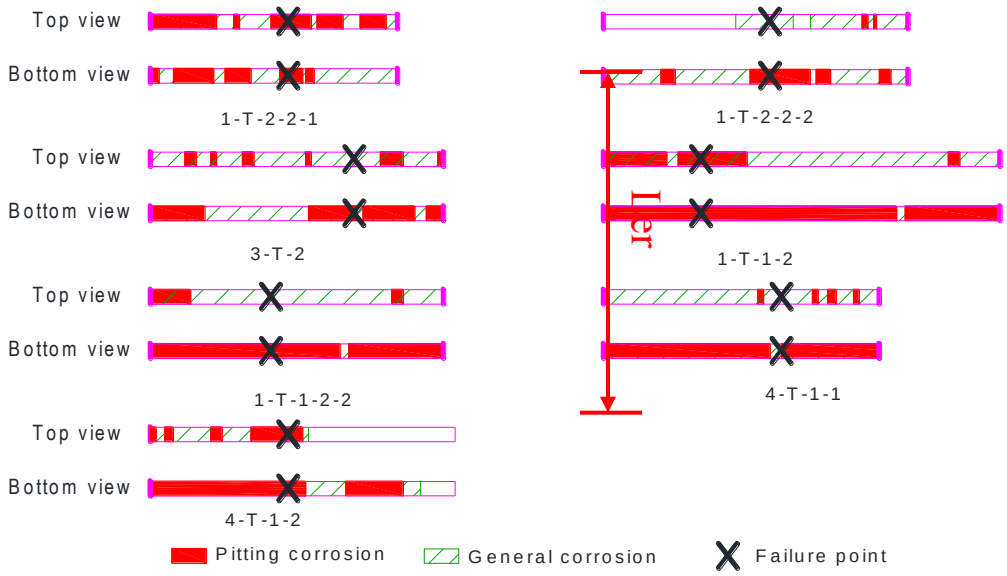

(a) Corrosion distribution in the tension samples

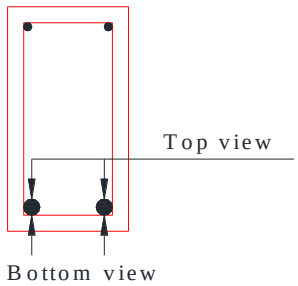

(b) The two directions of viewing

Figure 4-3 Corrosion distribution

4.3.2 Loss of cross-section of the corroded tension samples

Tension samples were cut into small pieces so that the average mass loss of the bars could be determined. The length of the small pieces depended on the corrosion pattern and the corrosion distribution as shown in Figure 4-3(a). The aim was to make sure that the residual mass of the steel was uniform throughout the length of each piece. The shortest length could be less than 5 mm.

It should be pointed out that the plastic residual deformation of the corroded bars during the tension test was assumed to be very limited due to the brittle failure. The nominal mass was calculated by Equation (4-1). The mass loss of the corroded bars was measured and the loss of cross-section was deduced by the loss of mass by Equation (4-2):

$$m_0 = \rho \cdot A_s \cdot L \qquad (4\text{-}1)$$

$$\Delta A_s = \frac{m_0 - m}{m_0} \cdot A_s \qquad (4\text{-}2)$$

Where:

ρ (g/cm^3) is the density of the steel bars, considered to be 7.85g/cm^3.

L (mm) is the length of each piece of the steel bars, measured with a vernier caliper.

ΔAs (mm^2) is the average cross-section loss of the small piece of bar.

As (mm^2) is the nominal cross-section of the steel bars.

m (g) is the residual mass of the small pieces of the corroded bars.

m_0 (g) is the nominal mass of the steel bars.

(a) Comparison of general corrosion

(b) Comparison of pitting corrosion

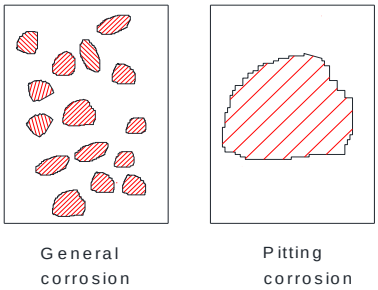

(c) Schematic plan of different corrosion patterns

Figure 4-4 General corrosion and pitting corrosion of the bars

4.4 Experimental results

4.4.1 Loss of cross-section of the corroded bars

As shown in Figure 4-3, the corrosion distribution was different according to the viewing direction. However, due to the long duration of exposure to the chloride environment, corrosion had developed along almost the whole length of the samples. The distribution was not uniform, neither in pattern nor in corrosion level. Pitting corrosion refers to large local loss of cross-section and general corrosion refers to a cluster of small pits (Figure 4-4). Both

general and pitting corrosion existed on most surfaces of the corroded bars. But pitting corrosion was more serious in the bottom view than the top view, which was due to the smaller depth of the concrete cover and the fact that corrosion induced by natural processes is not uniform. The greatest loss of cross-section corresponded to pitting corrosion. Then, the failure point during tension tests was always located in a general corrosion zone with serious pitting depth.

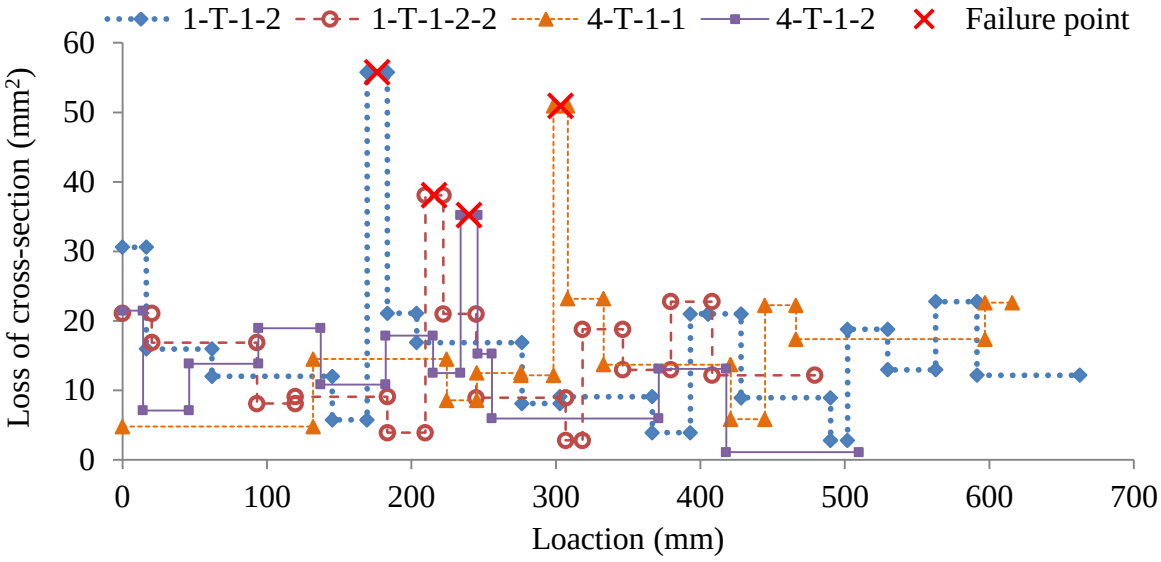

(a) Loss of cross-section of the front side tension bars

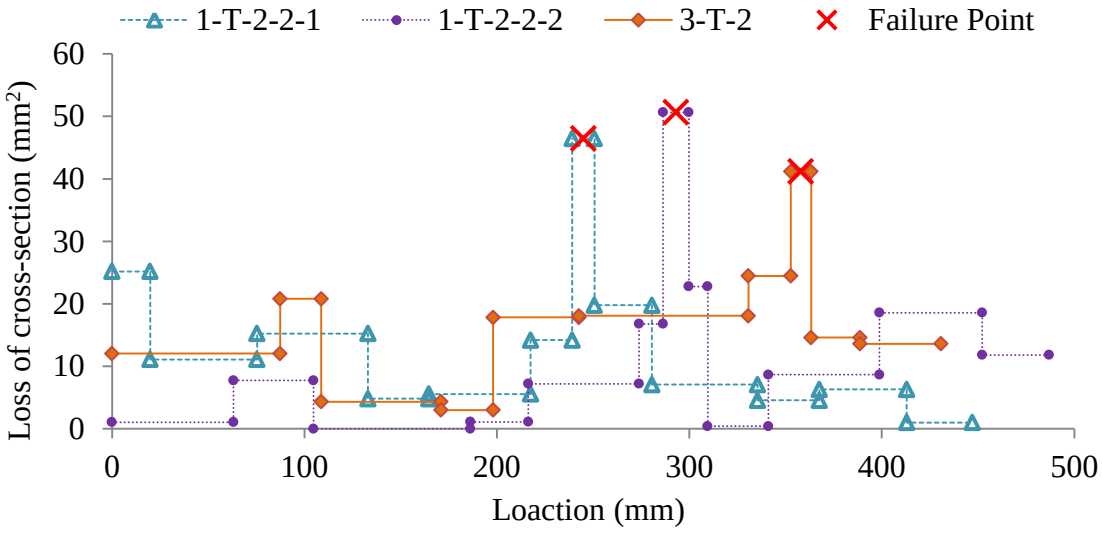

(b) Loss of cross-section of the rear side tension bars

Figure 4-5 Loss of cross-section of the corroded tension bars

As shown in Figure 4-5, the loss of cross-section appeared practically throughout the length of the corroded bars. The maximum loss of cross-section reached as much as 56 mm^2 for the

samples from the front side tension bar and 51mm^2 for the samples of the rear side tension bar. It should be noted that, along tension bars, the variation of the loss of cross-section was very significant, reaching 50% of the initial cross-section in some places, and failure always occurred at the location with maximum pitting corrosion.

4.4.2 Tension tests

The stress and strain curves for the tension bars are shown in Figure 4-6. The stress was calculated by the force and the effective cross-section at the failure point, while the strain was deduced from the average deformation over the effective length (Ler) of about 200 mm. Indeed, as the failure location was unknown, it was impossible to choose a given short length of bar to measure the deformation. However, the inconsistency between local stress and global strain calculations is acceptable since the change in elongation beyond the yielding stress was due to necking in the failure zone of non-corroded steel bar and it is the change in failure mode from ductile behavior with necking to brittle behavior without necking which reduced the corroded steel elongation. This change was of cause evaluated for a given based length, but it would not significantly be modified with a change in based length.

The shape of tension curve for corroded bars differed from the curve for the non-corroded bar in that, like diagrams for cold-formed steel, they lacked a well-defined yield point. Then yield stress in calculated as 0.2% proof strain. The curves for the nine bars were not identical (Figure 4-6). The ductility of the corroded bars was strongly reduced, but the ultimate stress of the corroded bars increase in comparison with the non-corroded bars as shown in Table 4-3.

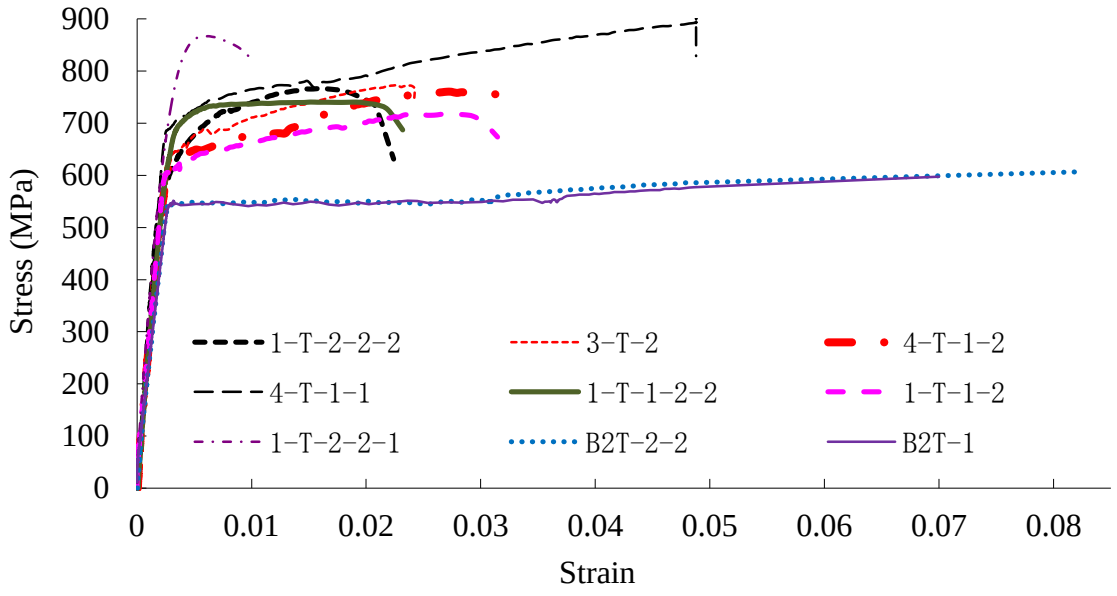

Figure 4-6 Stress-strain curves of the tension tests

4.5 Properties of the corroded bars

4.5.1 Residual cross-section of the failure points

The failure points of the steel bars were sawed carefully so that their mechanical properties could be investigated effectively. Part of the failure points are shown in Figure 4-7 and Figure 4-8. The failure points of the corroded bars occurred at locations with serious pitting corrosion.

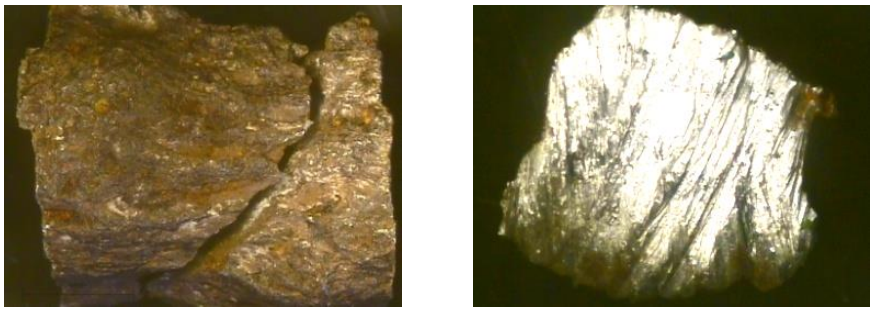

(a) 4-T-1-1

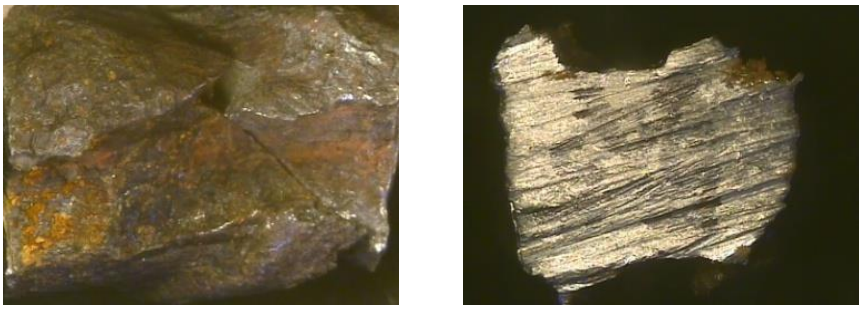

(b) 1-T-2-2-2

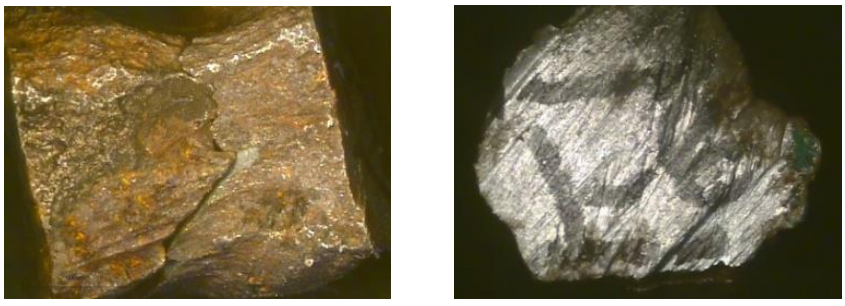

(c) 1-T-2-2-1

Figure 4-7 Failure points of the corroded bars

By comparison with the non-corroded bars, most of the corroded bars had at least one obvious groove corresponding to corrosion pits. As a result, the cross-section of the corroded bars was no longer circular, which made it rather complicated to measure. So the cross-section of the corroded bars was calculated from the residual mass measured on small pieces, which was

considered to give a closer estimate of the true residual cross-section than the residual diameter measured using a vernier caliper. The corroded bars showed much smaller elongation at fracture location during the tension test and exhibited more brittle behavior than the non-corroded bars, which were ductile and showed necking at failure (Figure 4-8).

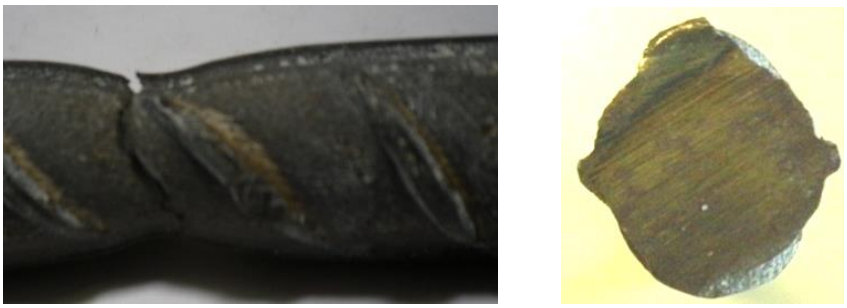

Figure 4-8 Failure point of the non-corroded bar B2T-1-2 with necking phenomena

4.5.2 Characteristics of the steel bars

The ductility of the corroded bars will be discussed on the basis of the experimental results. The loss of cross-section and the pit depth of the corroded bars at the failure point will be considered as the main factors. According to Eurocode 2 [14], the reinforcement should have adequate ductility as defined by the ratio of the tension strength to the yield strength, f_u/f_y, and the elongation at maximum force, ε_u (ultimate strain), indicated in Table 4-2.

Table 4-2 Properties of reinforcement according to Eurocode 2

Product form	Bars and de-coiled rods		
Class	A	B	C
Characteristic yield strength fyk (MPa)	400 to 600		
Minimum value of f_u/f_y	≥1.05	≥1.08	≥1.15 and ≤1.35
Characteristic strain at maximum force, ε_u(%)	≥2.5	≥5.0	≥7.5

The properties of the steel bars are shown in Table 4-3. In comparison with the non-corroded bars, the properties of the corroded bars had been changed tremendously, including the yield strength, the ultimate strength and the ratio f_u/f_y, the ultimate strain at maximum load ε_u.

The yield strength was about 530 MPa for the non-corroded bars as shown in Table 4-3, which was slightly higher than the nominal value but still in the 400-600 MPa range defined by Eurocode 2. However, for the corroded bars, the yield strength ranged from 580 MPa to 750 MPa. The corrosion had significantly influenced the yield strength of the bars, which

finally appeared to be outside the range prescribed by Eurocode 2 as defined in Table 4-2. For the ultimate strength and the ratio of f_u/f_y, all the values of the corroded bars were over the non-corroded bars. The reason could be due to the different deformation performance of the bars and the cross-section which was adopted for the calculation of the stress.

As discussed before, necking behavior was the most significant factor between the corroded bars and non-corroded bars when the bars reached yield strength. The residual cross-section was adopted for the corroded bars. As the corroded bars showed brittle response, there is almost no necking then the use of the residual cross-section allow a good approximation of ultimate stress. But, for the non-corroded bars, the necking could not be ignored. However, the cross-section used in the calculation of stress is the nominal one which is correct for yield stress, but will resulted in underestimating the effective ultimate stress due to the necking with reduce the effective cross-section at failure. In order to take into account of this necking effect, 20% reduction was considered as a first approach for the residual cross-section of the non-corroded bars. They would be treated as nominal ultimate strength f_u(without reduction) and effective ultimate strength f_{ue} (with reduction) respectively. At the same time, the nominal value of the non-corroded bars could stand for the limit of pure brittle behavior of the tension tests, while the effective value could be considered as the ductile response.

Table 4-3 Properties of the steel bars calculated from the tension test

	Samples	Yield f_y (MPa)	Ultimate strength		f_u/f_y	f_{ue}/f_y	Ultimate strain ε_u (%)
			f_u(MPa)	f_{ue}(MPa)			
Corroded bars	1-T-1-2	525	717		1.37		2.5
	1-T-1-2-2	502	740		1.47		1.5
	4-T-1-1	581	890		1.53		4.8
	4-T-1-2	498	760		1.53		2.7
	1-T-2-2-1	558	854		1.53		0.6
	1-T-2-2-2	542	766		1.41		1.6
	3-T-2	474	772		1.63		2.28
Non-corroded bars	B2T-1-2	532	592	710	1.11	1.33	7.0
	B2T-2-2	539	601	721	1.12	1.34	8.2

4.5.3 Ratio of tensile strength to yield strength (f_u/f_y) and ultimate strain (ε_u)

Figure 4-9 shows the relationship between the ratio of ultimate tensile strength and yield strength including (f_u/f_y and f_{ue}/f_y) and the loss of cross-section. For the corroded bars, the

value f_u/f_y was really in scattered distribution and no law could be drawn.

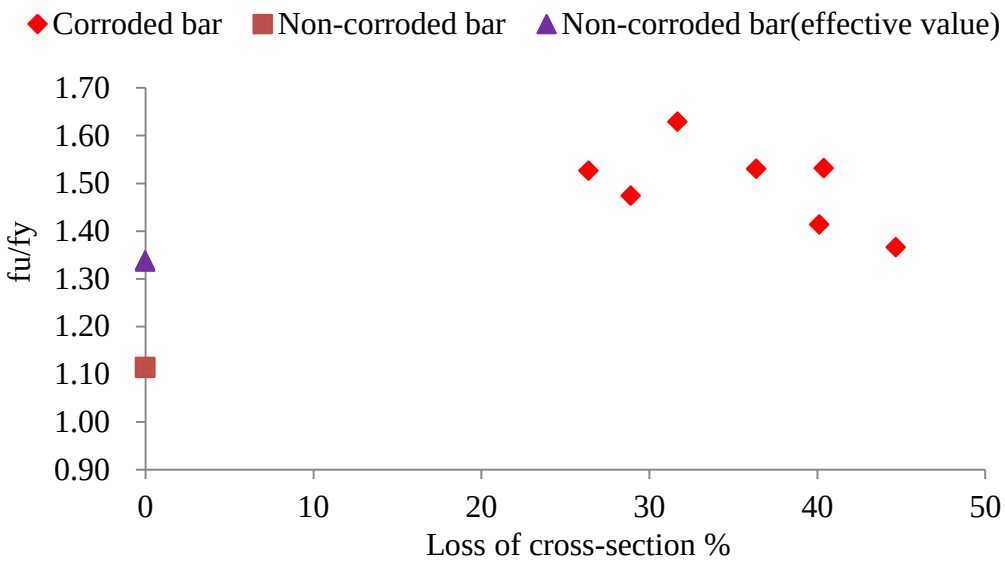

Figure 4-9 Ratio of ultimate stress to yield stress of the steel bars

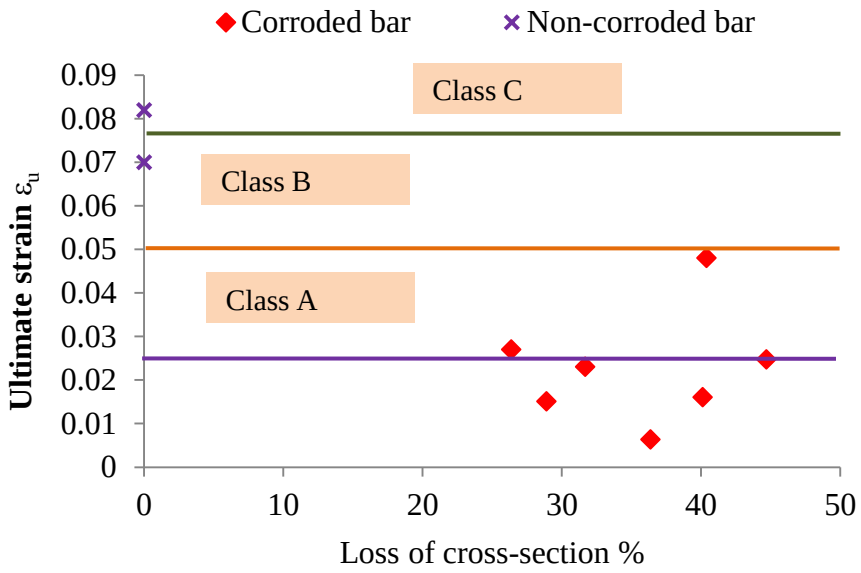

Figure 4-10 Ultimate strain of the steel bars

Figure 4-10 shows that the ultimate strain ε_u is reduced in relation with loss of cross-section due to corrosion. For the non-corroded bars, the ultimate strain corresponds at least to Class B while, for the corroded bars, the ultimate strain is mostly below the Class A threshold. Even though some of the results are higher than the Class A threshold, the residual ductility of the corroded bars is not sufficient according to Table 4-2. In Table 4-3, all the corroded bars have stronger yield strength and ultimate strength than that of the non-corroded bars, but over half of the corroded bars' ultimate strain is too weak to reach the threshold value of 2.5%, which means that ductility would be the determinant factor for highly corroded bars, and the brittle

behavior of the steel bars would require special attention to assess the quality of the existence corroded structures.

4.5.4 Loss of cross-section and ultimate strain at maximum force (ε_u)

A. Castel et al. [15] carried out tension tests on notched re-bars, which showed a significant reduction in ductility. They proposed a model of corroded bar behavior (equation (4-3)) between the loss of cross-section c% and the ratio of ultimate elongation of corroded bar to ultimate elongation of a non-corroded bar.

$$\frac{\varepsilon_{ucorr}}{\varepsilon_u} = e^{-0.1c\%} \qquad \text{But the value should not be less than 0.2} \qquad (4\text{-}3)$$

J. Cairns et al. [16] also conducted research on both the effect of notches in steel bars and steel damage due to an accelerated corrosion process. In order to compare the results of A. Castel et al. and J. Cairns et al.'s tests, the curve of the reference/damaged sample ultimate strain versus the loss of cross-section is plotted in Figure 4-11.

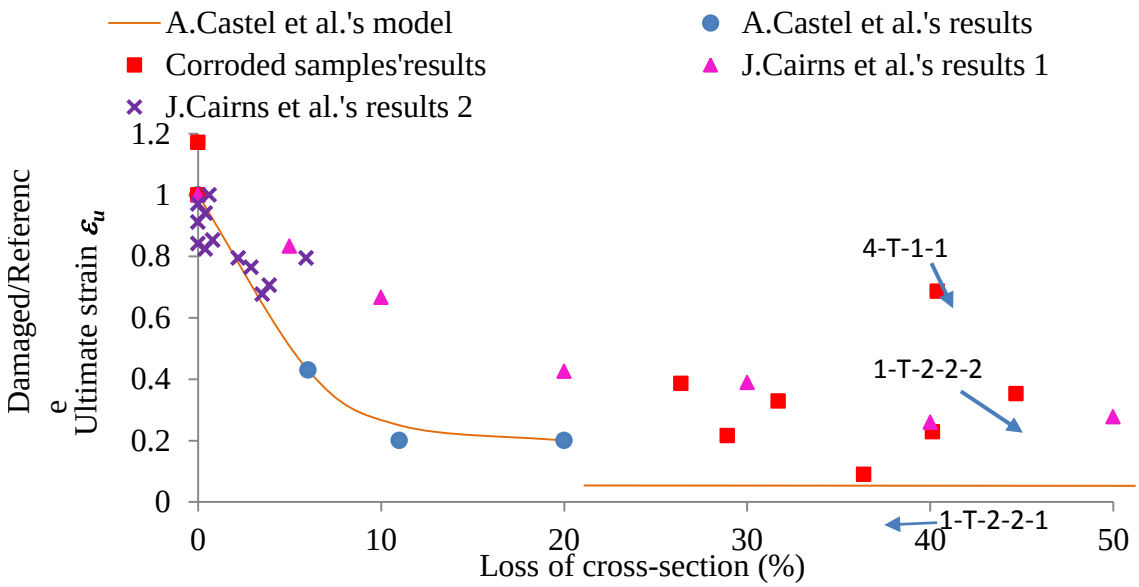

(J. Cairns et al.'s results 1 were achieved using artificial notches
J. Cairns et al.'s results 2 were found using impressed current to accelerate corrosion)

Figure 4-11 Evolution of ultimate strain versus the steel cross-section reduction

According to Figure 4-11, Cairns' results 2 match Castel's model well. Nevertheless, Cairns' results 1 are above Castel's model, but the results support the proposal that the minimum ratio of damage/reference ultimate strain should be 0.2. The experimental results presented in this section were also compared with Castel's model. They appeared generally conservative,

which is logical since notches have a constant shape, unlike real pits, which can be more or less pointed as shown in Figure 4-12. Thus, the damage/reference ultimate strain ratio for corroded bar 1-T-2-2-1 is below 0.2 but is almost 0.7 for 4-T-1-1.

4.5.5 Effect of cross-section corrosion pattern on ductility of steel bar

Corrosion leads to a decrease in the ultimate elongation but there is high scatter on the loss of cross-section and the depth of pitting corrosion of steel bars. The explanation could be that the cross-sectional corrosion pattern at the failure point is very variable. The corrosion pattern of 1-T-2-2-1 was the sharpest, as shown in Figure 4-12. A huge corrosion pit appears in only one side of the steel bar while, for other bars, the corrosion is more or less distributed all around the perimeter of the cross-section (e.g. for sample 4-T-1-1), so the ultimate strain is the highest of all the corroded bars. Castel's model was built using notched re-bars. The residual cross-sections are highly asymmetric and close to sample 1-T-2-2-1.This would result in an eccentricity of the center of gravity of the cross-section to the force axis, which could induce local bending and reduce the ultimate strain, and then lead to conservative results.

The shape and distribution of pitting corrosion in a steel cross-section would play a very important role in the reduction of ultimate elongation. Sharper, deeper pitting corrosion will lead to more pronounced concentration for the strain and stress and more brittle failure will occur. Stress concentration leads to partial yielding of the cross-section and, according to the fracture mechanics theory, when the whole cross-section of the steel bar reaches the elastic limit, a large part of yielding reserve has already been consumed, which leads to premature rupture of the bar [15-17].However, it is worth noting that the effect of such asymmetry would be less significant for a bar embedded in concrete than one tested in air. As the corrosion products can fill into the corrosion zones, the bond and constraint from the concrete around the bar could make some contribution to the mechanical performance.

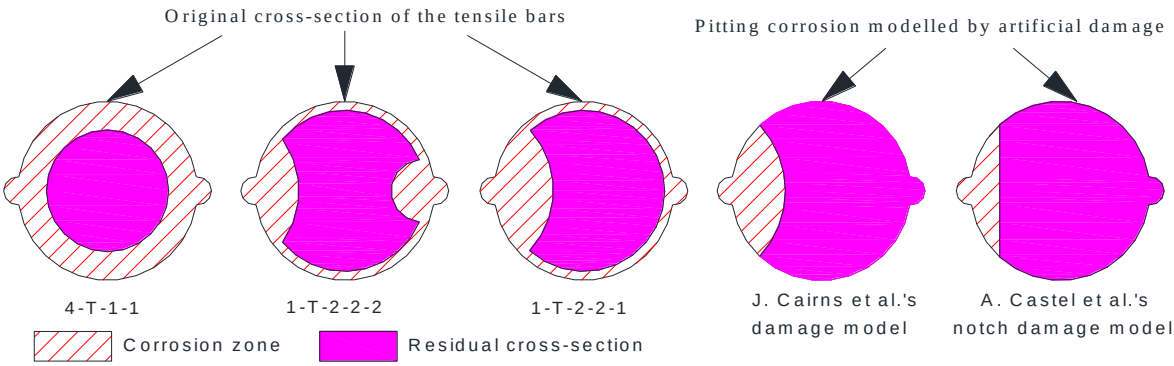

Figure 4-12 Corrosion distribution in the cross-section at failure point
(The true residual cross-section was shown in Figure 4-7 and Figure 4-8)

An equivalent steel concept [18] was defined to judge the overall steel ductility. Nevertheless, because of the large scatter on the value of effective cross-section after corrosion and then high yield stress recorded, the use of this concept would not be useful because due to antagonist evolution of yield stress with corrosion and ultimate strain.

4.5.6 Global mechanical behavior of the beam B2Cl2 and B2T

The mechanical behavior of beam B2Cl2, with the corroded bars, and the non-corroded beam B2T are shown in Figure 4-13. Both the yielding capacity and the ultimate capacity of beam B2Cl2 are reduced significantly by the corrosion of the steel bars, these trends agree well with the tension results of the corroded bars in Figure 4-6. However, the ratio of ultimate capacity to yield capacity, Fu/Fy, for non-corroded beam B2T is 1.12. While the ratio of ultimate capacity to yield capacity for the corroded beam B2Cl2, F'u/F'y, is 1.25, much higher than that of the non-corroded beam. Thus, the difference in post-yielding behavior found on steel bars leads to a modification of the post yielding performance of the corroded beam

The ductility of the beam is reduced almost to half of that of the non-corroded beam, which is more serious than the reduction of the capacity. The ratio of ultimate deflection between the corroded beam B2Cl2 and non-corroded beam B2T2, D/D', is 53.6%, which means that the deflection of the corroded beam was almost half that of the non-corroded beam.

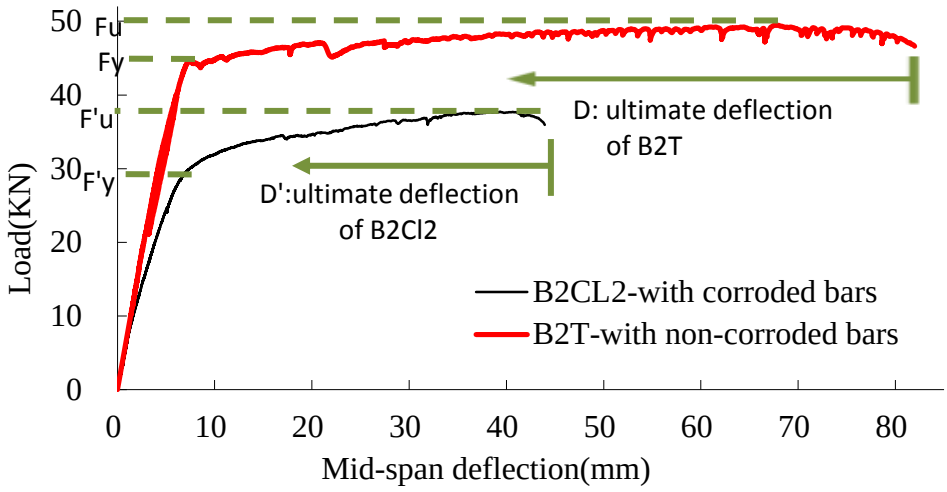

Figure 4-13 Force-deflection curves for the beam

4.6 Simulation of corrosion on the non-corroded bars

A series of corrosion simulations are set up to the non-corroded bars in order to investigate the influence of the residual cross-section shape on the ductility of the steel bars. In this section,

three types of corrosion simulations are set up by removing part of cross-section in the non-corroded bar with a saw and a ground machine in different degrees.

4.6.1 Residual cross-section shape simulations

In the middle of the non-corroded bars, different residual cross-section shapes were created as shown in Figure 4-14. The bars with original diameter d0 were treated as no corrosion. Both uniform corrosion and non-uniform corrosion (pitting corrosion) were made.

The uniform corrosion was polished around the perimeter by a ground machine and then classified into UC type (uniform corrosion). The non-uniform corrosion was achieved by sawing the bars directly. They were conducted in two ways, including cross-section loss in one side and in two sides symmetrically, classified as ASC type (asymmetrical corrosion) and SC type (symmetrical corrosion) respectively. Different corrosion depths which were marked as d1 and d2 were made to simulate the variable corrosion degrees. G_0 corresponded to the original gravity centre of the cross-section. G′ was the residual gravity centre of the damaged cross-section. e was the eccentricity between G_0 and G′. The tension tests were applied to all the steel bars subsequently.

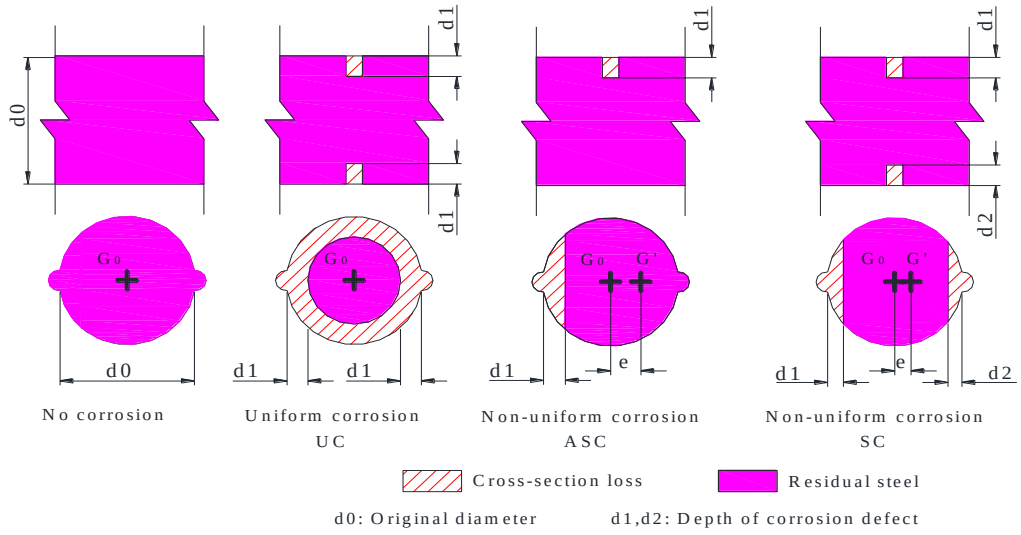

Figure 4-14 Residual cross-section of the corrosion simulations

4. 6.2 Tension tests and results of the bars in UC type

For UC type, the uniform corrosion was manufactured to the bars with original diameter of 12 mm, the same to the natural corroded steel bars. Different corrosion degrees ranged from no corrosion loss to 50% corrosion loss were ground as uniform corrosion bars in UC type.

Moreover, the residual cross-section was in circle shape which was absolutely symmetrical as shown in Figure 4-14. The corrosion depth was measured by vernier caliper with an accuracy of 0.02 mm. The tension tests were carried out and the results of all the specimens are shown in Table 4-4.

Table 4-4 Tension results of uniform corrosion of bars in UC type

Specimen	d0 (mm)	ΔAs0 (mm^2)	Simulated corrosion (%)	d1 (mm)	ΔAs (mm^2)	Asres (mm^2)	ε_u (%)
U1	12	113.10	0	0	0	113.10	10.65
U2	12	113.10	0	0	0	113.10	9.70
U3	12	113.10	10.22	0.32	11.56	101.53	7.47
U4	12	113.10	9.91	0.31	11.26	101.89	7.46
U5	12	113.10	19.75	0.63	22.33	90.76	5.92
U6	12	113.10	20.05	0.64	22.67	90.43	4.86
U7	12	113.10	28.32	0.92	32.02	81.07	4.01
U8	12	113.10	28.60	0.93	32.34	80.75	5.23
U9	12	113.10	38.77	1.31	43.85	69.25	4.76
U10	12	113.10	39.16	1.32	44.29	68.81	4.83
U11	12	113.10	49.47	1.74	55.95	57.15	5.09
U12	12	113.10	49.83	1.75	56.35	56.75	4.32

Asres: Residual cross-section d1: Depth of uniform corrosion

The corrosion degree and the ultimate strain of the steel bars are shown in Figure 4-15. The ultimate strain got reduced from about 10% to 5% when the cross-section loss was smaller than 20%. But the corrosion degree had little influence on the ultimate strain of the uniform corrosion simulation types when the cross-section loss got over 20%.

Moreover, the ultimate strain of the bars in UC type was much higher than that of the natural corroded bars even though in the interval of 40%-50% cross-section loss as shown in Figure 4-6, which could be due to the irregular residual cross-section caused by the natural corrosion. The results supported the point that the uniform corrosion due to impressed current reduced the ductility of steel bars only in a relative light degree compared with natural corrosion.

Figure 4-16 shows one of the typical stress-strain curves of the uniform corrosion bars in UC type and the original bar with the same diameter of 12mm. The configuration of the two curves was quite close to each other. Nevertheless, compared to the Figure 4-6, the post

yielding behaviour was quite different from the natural corrosion bars. There was an obvious plateau stage after the yield and the strain hardening behavior was significant.

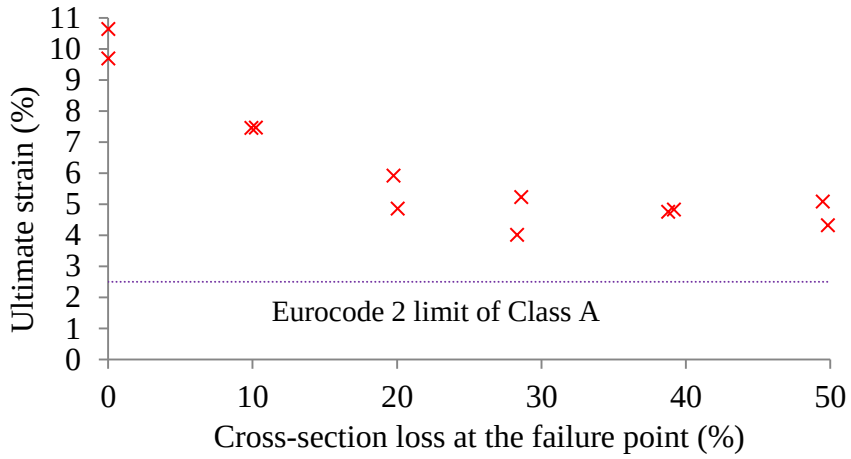

Figure 4-15 Influence of corrosion degrees on ultimate strain of the bars in UC type

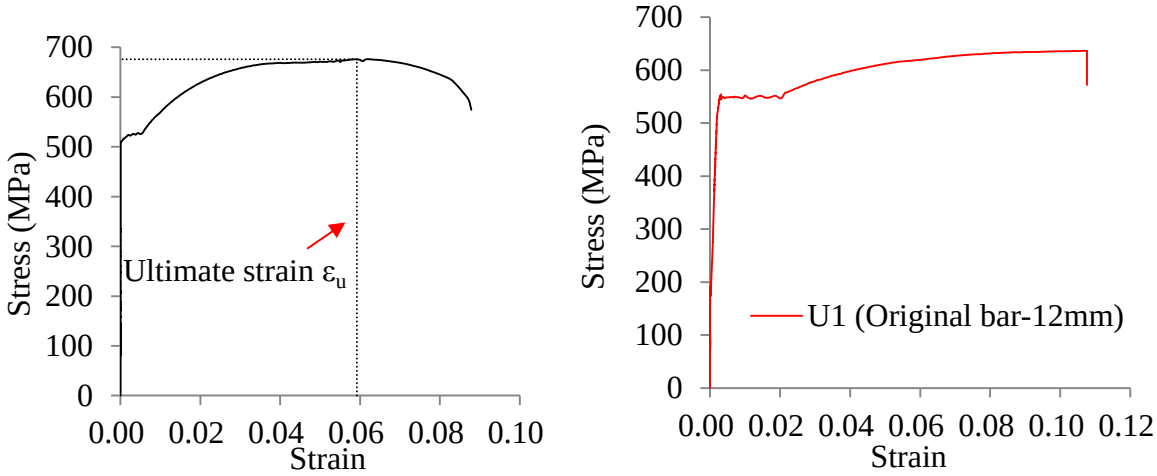

(a) Typical curve of UC type (Bar U5) (b) Original bar with diameter of 12mm

Figure 4-16 Comparison of the stress-strain curves of bars in UC type and original bar

4.6.3 Tension tests and results of the bars in ASC type

In order to make the investigation of pitting corrosion influence on the ductility of the steel bars, one side notch was made by the saw and marked as ASC type as shown in Figure 4-14. The maximum depth of the defect d1 was shown in Figure 4-14 and measured by vernier caliper. Then the cross-section loss ΔAs1 and residual cross-section Asres could be deduced based on the original cross-section. Different corrosion degrees from 0 to 50% cross-section loss were curved. The tension experiments were conducted and the results about the bars in ASC type are shown in Table 4-5.

Table 4-5 Tension results of non-uniform corrosion in one side (ASC type)

Specimen	d0 (mm)	As0 (mm^2)	Corrosion (%)	d1(mm)	e (mm)	ΔAs1 (mm^2)	Asres (mm^2)	ε_u (%)
L1-0-1	12	113.10	0	0	0	0	113.10	10.65
L1-0-2	12	113.10	0	0	0	0	113.10	9.70
L1-1-1	12	113.10	10	1.88	0.47	11.31	101.79	5.85
L1-1-2	12	113.10	10	1.88	0.47	11.31	101.79	5.64
L1-2-1	12	113.10	20	3.05	0.95	22.62	90.48	3.06
L1-2-2	12	113.10	20	3.05	0.95	22.62	90.48	2.93
L1-2-3	12	113.10	20	3.05	0.95	22.62	90.48	2.82
L1-3-1	12	113.10	30	4.08	1.43	33.93	79.17	0.96
L1-3-2	12	113.10	30	4.08	1.43	33.93	79.17	0.85
L1-4-1	12	113.10	40	5.05	1.92	45.24	67.86	0.86
L1-4-2	12	113.10	40	5.05	1.92	45.24	67.86	0.89
L1-5-1	12	113.10	50	6.00	2.42	56.55	56.55	0.62
L1-5-2	12	113.10	50	6.00	2.42	56.55	56.55	0.79
L1-5-3	12	113.10	50	6.00	2.42	56.55	56.55	0.68

The relationships of ultimate strain and the corrosion degree of the bars in ASC type are shown in Figure 4-17. The ultimate strain of the bars decreased significantly from about 10% to 1% when the cross-section loss ranged from 0 to 30%. Nevertheless, for higher loss of cross-section, the ultimate strain kept relatively stable. The reduction trend of the experimental results was close to that of UC type in Figure 4-15 though the detailed ultimate strain was much smaller. It should be pointed out that when the cross-section loss of bars in ASC type was over 30%, the ultimate strain was smaller than 1%. The ductility of the bars in this condition would not be acceptable according to Eurocode 2.

Moreover, it was obvious that the ultimate strain of ASC type was smaller than the results of UC type even in condition of the bars in the same corrosion degree. This could be attributed to the residual cross-section shape. For UC type, the cross-section loss was uniformly located around the perimeter. However, the cross-section loss was just in one side for ASC type. That meant that the residual cross-section distribution of bars ASC type was asymmetric. As a result, the ultimate strain of bars ASC type was weaker than the results of UC type in the same condition. The results shown that the ultimate strain of the steel bars could be influenced by both the corrosion degree and cross-section distribution.

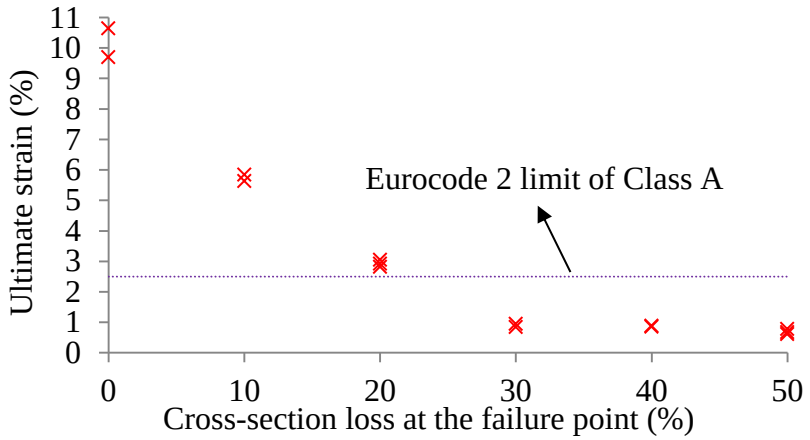

Figure 4-17 Influence of corrosion degrees on ultimate strain of the bars in ASC type

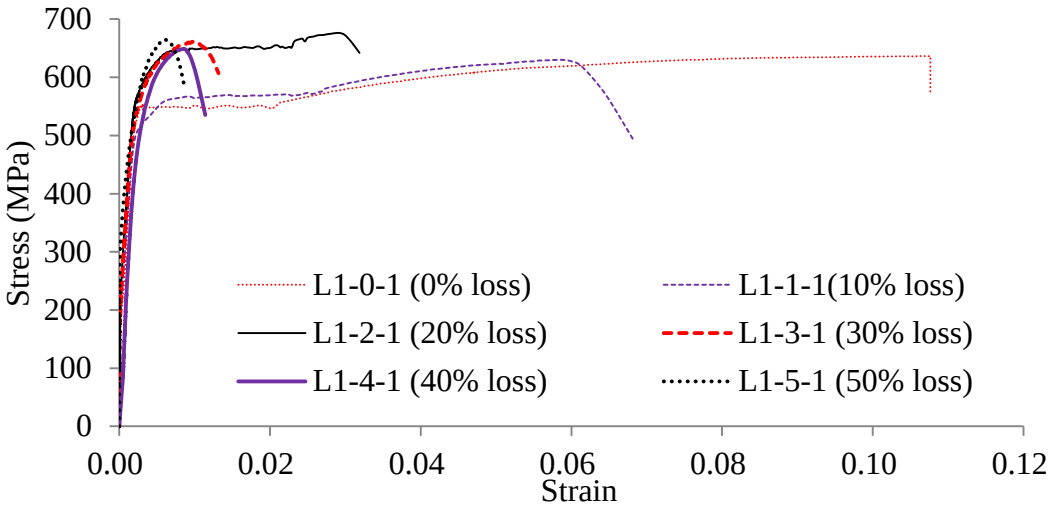

Figure 4-18 Stress-strain curves of non-uniform corrosion bars in ASC type

Stress-strain curves of the one-side corrosion bars in ASC type are showed in Figure 4-18. No typical curves for the bars in ASC type could be found, as the configurations of the curves changed obviously with the increase of the corrosion degrees. When the cross-section loss was smaller than 30%, the strain of the steel bars was sensitive to the corrosion degree. The elongation of the bars got reduced sharply with the increase of the corrosion degree. Moreover, the plateau stage and the strain hardening behaviour disappeared when the cross-section loss reached 30%. As a result, the ultimate strain of the bars was smaller than 1%. The bars became brittle, which was a problem for safety serviceability.

4.6.4 Tension tests and results of SC type

SC type was used to investigate the influence of the asymmetric notches on the ductility of the steel bars. The diameter of all the steel bars in SC type was 12mm. Two-side mechanical defects were made by the saw as shown in Figure 4-14. The depths of the two defects were

marked as d1 and d2 respectively. The corresponded cross-section loss was marked as ΔAs1 and ΔAs2. The total cross-section loss was 20%. However, the detailed cross-section loss of the two defects ΔAs1 and ΔAs2 was determined by the depth of the defects. A series of steel bars were made with the variation of the ratios of ΔAs1 and ΔAs2 in SC type. The tension experiments were applied and the results were shown as Table 4-6. The ultimate strain was still between 2.5% to 5% when the total cross-section loss was 20%.

Figure 4-19 shows the relationships of cross-section loss ratio and the ultimate strain of SC corrosion simulation types. Though all the bars were with 20% cross-section loss in total, the ultimate strain was still different from each other due to the variable ratios of the two defects. Firstly, when the ratio of the cross-section loss of the two defects increased, the ultimate strain of the steel bars in SC types also improved. The reason could be attributed to the fact that the increase of cross-section loss ratio could lead to more symmetrical distribution of the residual cross-section. When the ratio reached 1, the two defects were in the same value, which meant that the cross-section loss of the two defect parts were located equably at the two sides. As a result, the steel bars performed a better elongation during the tension experiments.

ASC type with notch in only one side could be treated as the limit state when the ratio of ΔAs1 and ΔAs2 in SC type was 0. Finally, the ultimate strain of ASC type was much smaller than all the other bars in Figure 4-19.

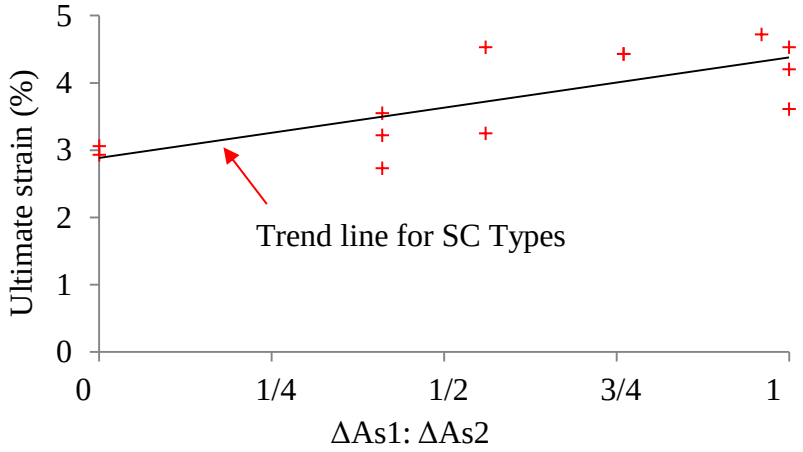

Figure 4-19 Influence of 20% corrosion on ultimate strain for SC type

The configuration of stress-strain curves of all the steel bars in SC type are closed to each other. One typical stress-strain curve of bar L2-5-1 is shown in Figure 4-20. The plateau stage after yield was still clear and the strain hardening behaviour is obvious. In fact, the whole performance was quite close to that of the original bars as showed in Figure 4-16(b). But the elongation of the steel bars got reduced more significant than that of the uniform corrosion of UC type even the steel bars were in the same corrosion degree of 20%.

Table 4-6 Tension results of non-uniform corrosion in two sides (SC type)

Specimen	d0 (mm)	As0 (mm^2)	Corrosion (%)	d1 (mm)	ΔAs1 (mm^2)	d2 (mm)	ΔAs2 (mm^2)	ΔAs1:ΔAs2	e (mm)	Asres (mm^2)	ε_u (%)
L2-1-1	12	113.10	20	1.88	11.31	1.88	11.31	1:1	0	90.48	4.53
L2-1-2	12	113.10	20	1.88	11.31	1.88	11.31	1:1	0	90.48	3.61
L2-1-3	12	113.10	20	1.88	11.31	1.88	11.31	1:1	0	90.48	4.20
L2-2-1	12	113.10	20	1.85	11.07	1.91	11.55	0.96:1	0.02	90.48	4.72
L2-3-1	12	113.10	20	1.70	9.79	2.05	12.83	0.76:1	0.13	90.48	4.43
L2-3-2	12	113.10	20	1.70	9.79	2.05	12.83	0.76:1	0.13	90.48	4.43
L2-4-1	12	113.10	20	1.50	8.16	2.23	14.46	0.56:1	0.26	90.48	4.53
L2-4-2	12	113.10	20	1.50	8.16	2.23	14.46	0.56:1	0.26	90.48	3.25
L2-5-1	12	113.10	20	1.30	6.62	2.39	16.00	0.41:1	0.39	90.48	3.55
L2-5-2	12	113.10	20	1.30	6.62	2.39	16.00	0.41:1	0.39	90.48	2.73
L2-5-3	12	113.10	20	1.30	6.62	2.39	16.00	0.41:1	0.39	90.48	3.22
L2-6-1	12	113.10	20	0	0	3.05	22.62	0	0.95	90.48	3.06
L2-6-2	12	113.10	20	0	0	3.05	22.62	0	0.95	90.48	2.93
L2-6-3	12	113.10	20	0	0	3.05	22.62	0	0.95	90.48	2.82

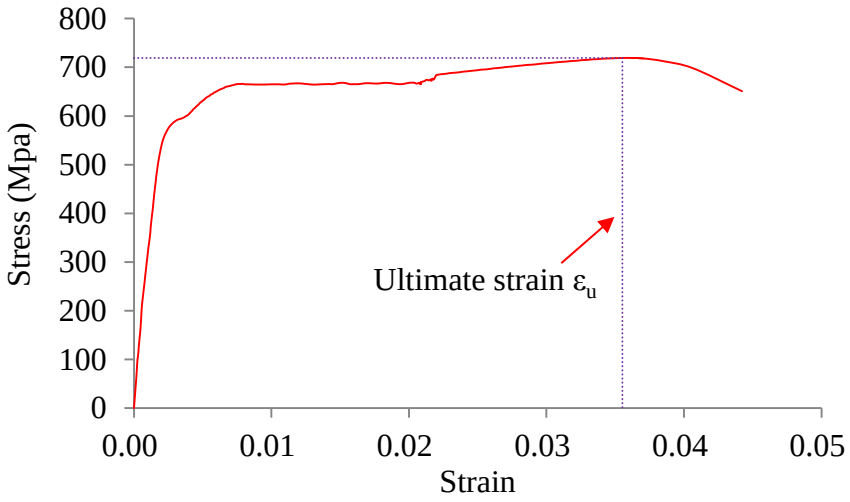

Figure 4-20 Typical stress-strain curve of SC type (L2-5-1)

4.6.5 Tension tests and results of steel bars with different diameters

The steel bars with different diameters ranged from 10mm to 16mm were carried out as ASC type and labeled as ASCD type. The defect of 20% cross-section loss was made by the saw for all the steel bars so as to check the influence of the diameter on the ultimate strain. The tension tests were undertaken on the steel bars and the results were shown in Table 4-7.

Figure 4-21 shows the relationships of original diameter of the bars and the ultimate strain of the tension results. When the diameter was smaller, the ultimate strain was better even all the still bars were in the same corrosion degree of 20% cross-section loss. However, it should be pointed out that the pitting depths were different due to the differences of the original diameters. When the diameter was larger than 16mm, the ultimate strain was already smaller than 2%, which was not acceptable by Eurocode 2.

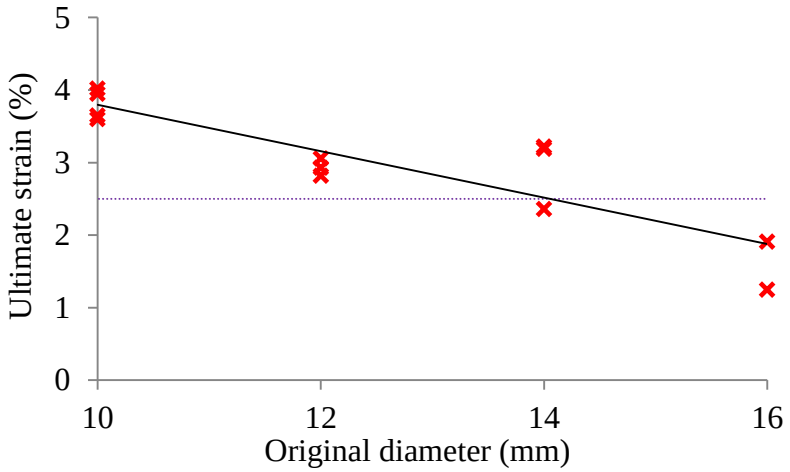

Figure 4-21 Ultimate strain of the steel bars with different diameters

Table 4-7 Tension results of bars with different diameters (ASCD type)

Specimen	d0 (mm)	As0 (mm^2)	Corrosion degree (%)	d1 (mm)	e (mm)	ΔAs1 (mm^2)	Asres (mm^2)	ε_u (%)
L10-2-1	10	78.54	20	2.54	0.79	15.71	62.83	4.02
L10-2-2	10	78.54	20	2.54	0.79	15.71	62.83	3.95
L10-2-3	10	78.54	20	2.54	0.79	15.71	62.83	3.65
L10-2-4	10	78.54	20	2.54	0.79	15.71	62.83	3.60
L12-2-1	12	113.10	20	3.05	0.95	22.62	90.48	3.06
L12-2-2	12	113.10	20	3.05	0.95	22.62	90.48	2.93
L12-2-3	12	113.10	20	3.05	0.95	22.62	90.48	2.82
L14-2-1	14	153.94	20	3.56	1.11	30.79	123.15	2.36
L14-2-2	14	153.94	20	3.56	1.11	30.79	123.15	3.19
L14-2-3	14	153.94	20	3.56	1.11	30.79	123.15	3.22
L16-2-1	16	201.06	20	4.07	1.26	40.21	160.85	1.25
L16-2-2	16	201.06	20	4.07	1.26	40.21	160.85	1.91

Part of tension tests of the steel bars of different diameters in ASCD type notch is shown in Figure 4-22. The elongation of the steel bars reduced with the increase of the diameter when the cross-section was of 20% loss of notch effect. When the original diameter of the steel bars was smaller than 14 mm, the plateau of the stress-strain curves was obvious and the steel bars performed a good ductile behaviour. However, when the diameter reached 16 mm, the plateau got disappeared. As a result, th Eurocode 2 limit of Class A ance in the tension experiment.

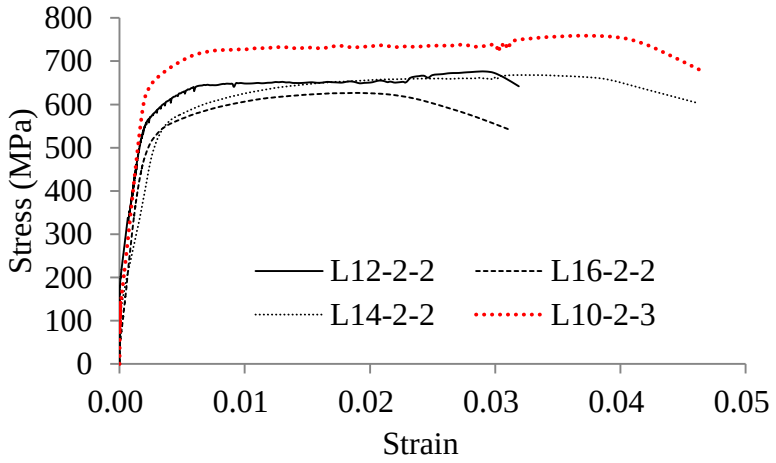

Figure 4-22 Typical stress-strain curves of bars of ASCD type with different diameters

4.7 Discussion about the simulation results

4.7.1 Comparison of the three simulation types

The results of three simulation types with 20% cross-section loss were drawn in Figure 4-23, including the uniform corrosion (UC type), one side corrosion (ASE type) and two side corrosion (SC type).

The ultimate strain of the uniform corrosion bars in UC type was the best, which was about 5%. On the contrary, the ductility of the one side corrosion in ASC type was the weakest, with a value of about 3% ultimate strain. The shape of residual cross-section could explain this phenomenon. UC type was in uniform corrosion. The distribution was more equable then SC type, with the corrosion distributed in two sides. Then ASC type came the last, as also the corrosion distributed only in one side. The symmetrical distribution of the residual cross-section shape lead to a better ductility.

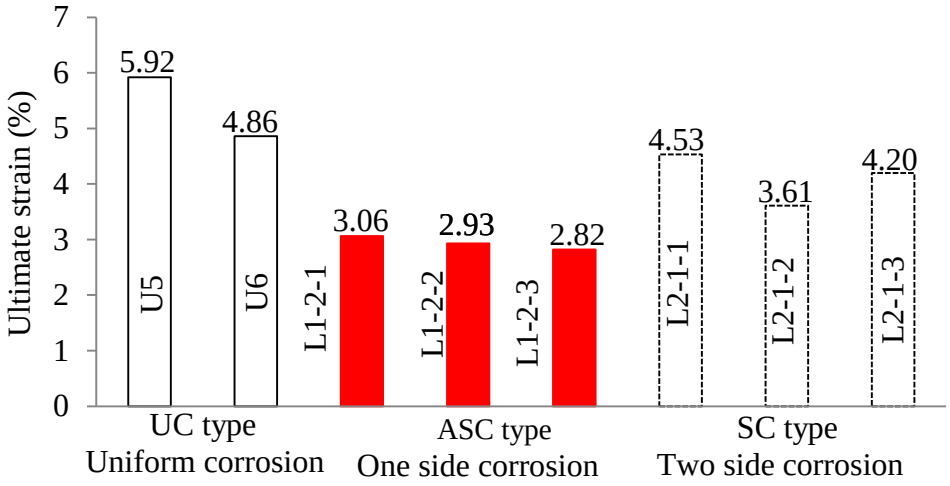

Figure 4-23 Results for different simulation types with 20% cross-section loss

4.7.2 Influence of pitting depth on the ultimate strain of all the simulated bars

The pitting depth of the simulated bars varied due to the corrosion degrees and the original diameters. The influence of maximum pitting depth on the reduction of ultimate strain was shown in Figure 4-24. It should be pointed out that the maximum pitting depth for UC type was considered as the depth of the corrosion defect d1. For the SC type, the maximum pitting depth was the larger corrosion defect of d2 as shown in Table 4-6. The original diameter of all the bars was 12 mm except for ASCD type whose diameter varied as shown in the Figure 4-24.

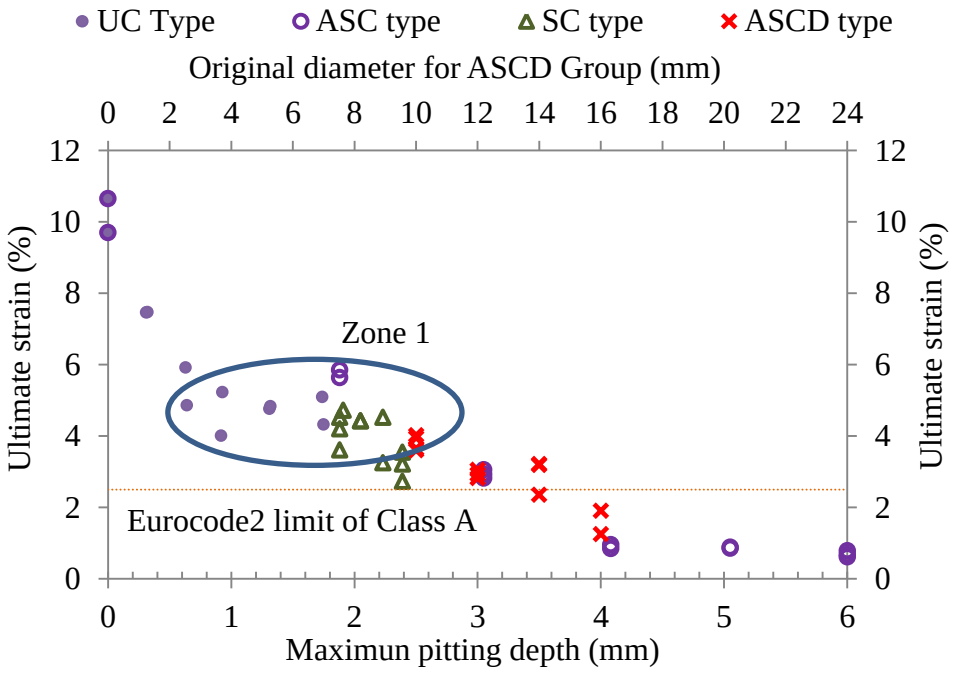

Figure 4-24 Relationships of pitting depth and ultimate strain of all the bars

According to Figure 4-24, it was easy to find the ultimate strain of the simulated bars reduced with the increase of maximum pitting depth. It was worth pointing out that the residual ultimate strain was influenced by the corrosion types significantly. For example, the ultimate strain in zone 1 was about 5%, but the maximum pitting depths of the steel bars varied from 0.6 mm to 2.54 mm. This was due to the fact that the maximum pitting depths of the steel bars corresponded to different residual cross-section due to the variable corrosion types. The residual cross-section of steel bars in UC type was smallest when the maximum pitting depth was the same to the other types.

4.7.3 Stress distribution in residual cross-section of steel bars

Figure 4-25 shows the stress distribution in residual cross-section of the steel bars. As shown in the figure, the stress was uniform in the cross-section for no corrosion and UC type (with residual cross-section symmetrical distribution). Nevertheless, the stress increased sharply at the residual cross-section near notch zone for ASC type and SC type. The stress concentrated in the zone near the notch significantly. Moreover, for the bars in ASC type, the eccentric of gravity centre increased the concentration of stress in the notch boundary zone. As a result, the ultimate strain of the steel bars in UC type was better, and then followed by the steel in SC type. The steel bars in ASC type showed most significant brittle performance in the tension experiment. In fact, even for ASC type, the eccentric increased with the corrosion degree. As a result, the brittle performance played a more important role when the corrosion degree grew.

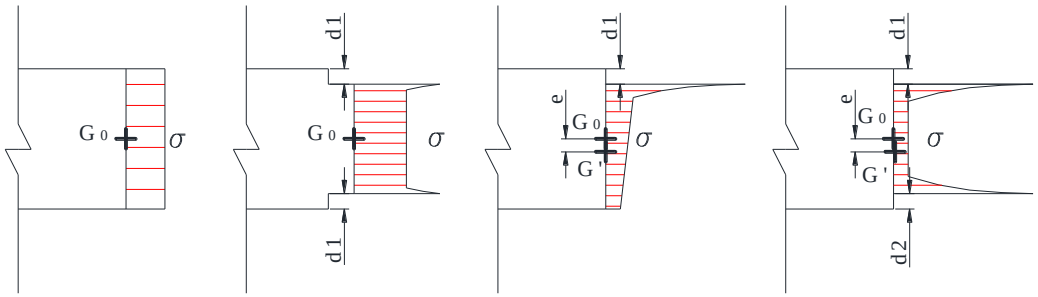

Figure 4-25 Stress distribution of the steel bars in three types

For the steel bars in the same degree, when the diameter increased, the eccentric got larger, which led to a more asymmetric distribution of the stress in the residual cross-section as shown in Figure 4-26. The corrosion degree for the two bars was 20%. When the original diameter was 10 mm, the eccentric was only 0.79 mm. However, the eccentric reached 1.26

mm for the bar with diameter of 16 mm. The increase of the eccentric resulted in the increase of the strength at the edge when the average stress of the cross-section was the same, which finally cause the stress concentration and lead to the failure of the bars with the decrease of the elongation in the tension experiment.

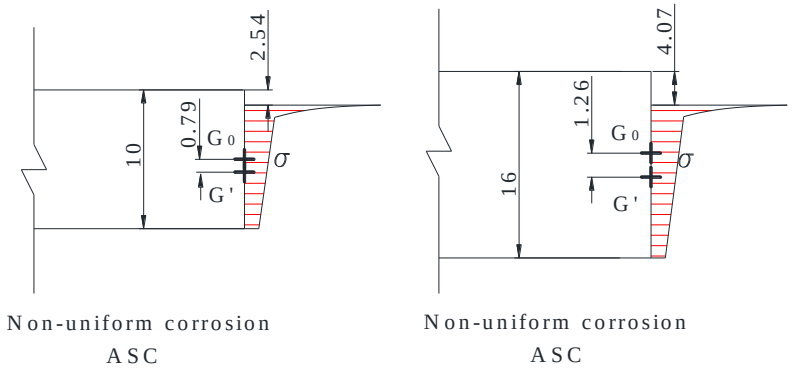

Figure 4-26 Stress distribution of steel bars with different diameters

4.7.4 Strength comparison of the corroded bars and simulated bars

The yield strength and ultimate strength of the simulated bars are shown in Figure 4-27, including the simulated bars with diameter of 12 mm in UC type and ASC type. The results showed that the yield strength of all the bars was close to each other. However, the ultimate strength varied significantly. The ultimate strength of the simulated bars in UC type and ASC type was about 660 MPa. But the ultimate strength of natural corroded bars distributed rather irregularly. The average value was also much larger than the simulated value. One possible and relevant explanation is the influence of necking phenomenon. Indeed, control steel bars exhibit ductile behavior with a strong necking phenomenon before the failure, while corroded steel bar exhibit brittle behavior without necking phenomenon. As a result, the effective cross section at failure is lower to the nominal one for control steel bar because necking reduced the effective steel cross-section. Then the ultimate stress calculated from nominal cross-section for control steel bar is lower than the true ultimate stress calculated from effective true cross-section at failure; On the contrary, the residual cross-section used to calculate the ultimate stress of corroded steel bar is less influence by the necking phenomenon then close to real ultimate stress. As a result, it is probable that ultimate stress is not change by corrosion but the way to calculate the ultimate stress leads to a difference between control and corroded bars.

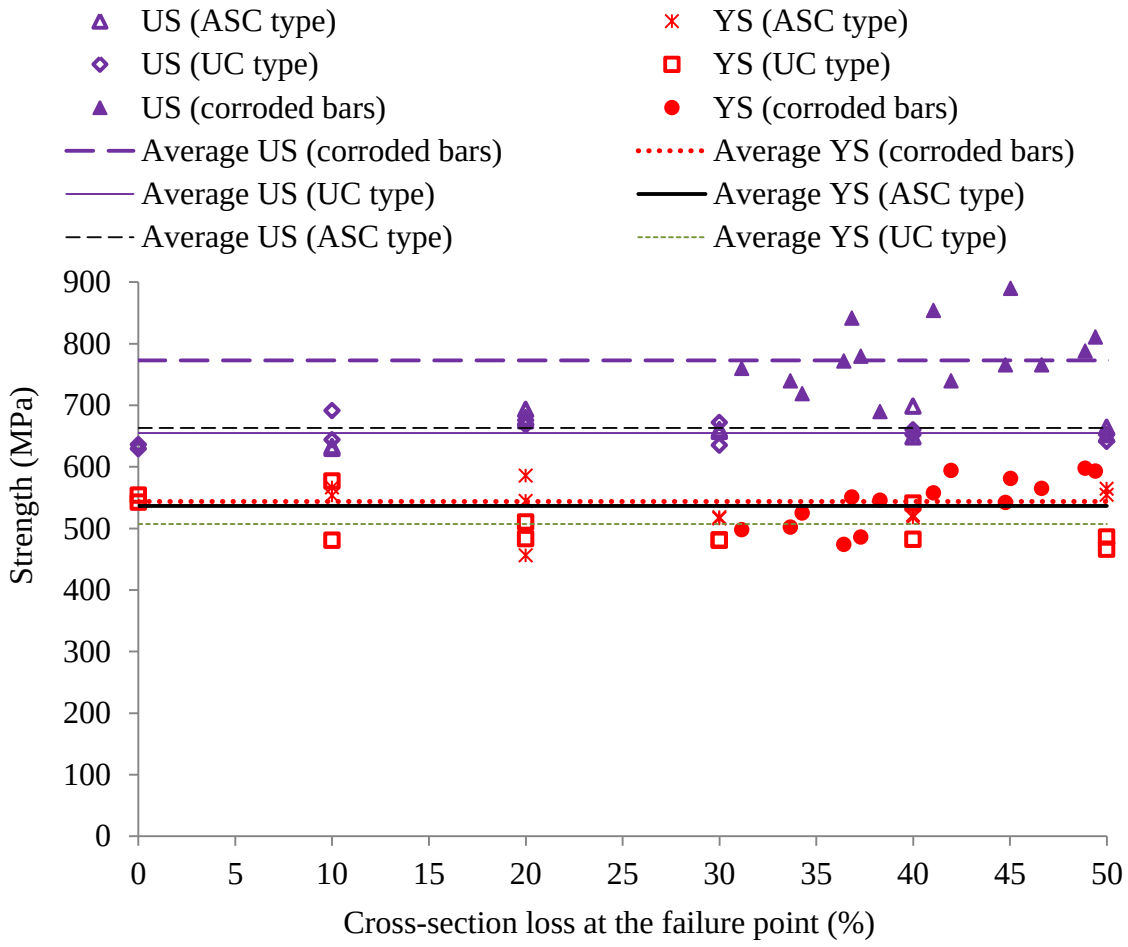

Figure 4-27 Strength comparison of natural corroded bars and simulated bars (UC and ASC types)

4.8 Conclusion

Tension tests were carried out on seven steel bars with different levels of corrosion and two non-corroded bars extracted from two 26-year-old beams to investigate the mechanical behavior of corroded steel bars. The ratio of the tensile strength to the yield stress and the ultimate strain at maximum force (ultimate strain) were studied in relation to the loss of cross-section. In order to better understand the mechanical behavior, the shapes of the cross-sections at the failure points of the tension bars were analyzed carefully.

The nominal ultimate strength and the effective ultimate strength were proposed. All the ratio of the tensile strength to yield stress of both the corroded bars and the non-corroded bars were in Class B and Class C. The ultimate strain was reduced greatly. These results agree with the model by A. Castel et al., although the model is relatively conservative due to the fact that it was built from results obtained with an artificial notch rather than natural pitting corrosion. The loss of cross-section was found to be less important than the shape of the corrosion in the

cross-section, which was considered to be the decisive factor for the ductile behavior of the corroded bars. When the corrosion was distributed uniformly around the cross-section, the steel bar exhibited higher ductility, whereas when the pitting corrosion occurred asymmetrically around the cross-section, the steel bar responded with more brittle behavior. As a result, although the ultimate stress of all the corroded bars was improved, the ductility of most of the corroded bars decreased below the threshold fixed by Eurocode 2. This result shows that the residual ultimate elongation of a corroded steel bar may be the most important parameter effecting reliability as far as the structural performance in bending of an RC structure damaged by corrosion in a chloride environment is concerned.

The results of the simulation show that there was some relationship between the residual cross-section and the ultimate strain. The symmetrical distribution of the residual cross-section performed a better ductile behavior, which showed that the natural corrosion lead to higher ductility due to the asymmetrical distribution of the residual cross-section. With the corrosion degree increase, the ultimate strain of the steel bars could fall below the requirement of Eurocode 2, which should be avoided as it might result in brittle failure of the constructions. Moreover, in the condition of the same corrosion degree, the ductility of the steel bars decreased when the diameter of the steel bars increased.

The residual cross-sectional shape of the steel bars was considered as an important factor to influence the ductility. In the future work, more attention should be paid to the prediction of the residual cross-sectional shape of the bars without damage the residual corroded beams.

4.9 References

[1] Caré S., Nguyen Q.T., L'hostis V., Berthaud Y.. Mechanical properties of the rust layer induced by impressed current method in reinforced mortar. *Cem Concr Res*. 2008, 38(8), 1079-1091

[2] ZHU W.J., François R., Coronelli D.. Effect of corrosion of reinforcement on the coupled shear and bending behaviour of reinforced concrete beam. 6th International Conference on Bridge Maintenance, Safety and Management, Stresa, Lake Maggiore, Italy, July 8-12, 2012,

[3] Bhargava K., Ghosh A. K., Mori Y., Ramanujam S., Model for cover cracking due to rebar corrosion in RC structures, *Eng Struct*. 2006, 28(8) : 1093-109

[4] Wong H. S., Zhao Y. X., Karimi A. R., Jin W. L.. On the penetration of corrosion products from reinforcing steel into concrete due to chloride-induced corrosion. *Corros Sci* 2010, 52(7). 2469-2480

[5] Kreit A., Al-Mahmoud F., Castel A., François R., Repairing corroded RC beam with near-

surface mounted CFRP rods, *Mater Struct* 2011; 44(7): 1205-17

[6] Strategic High Research Program. Concrete and Structure: Progress and Product Update. Washington DC: National Research Council, 1989.

[7] Ahmad S.. Reinforcement corrosion in concrete structures, its monitoring and service life prediction-a review. *Cem Concr Compos*, 2003, 25(4-5): 459-471.

[8] Apostolopous Ch.Alk., Papadopoulus M.P., Pantelakis Sp.G.. Tensile behavior of corroded reinforcing steel bars BSt 500s. *Construct. Build Mater* 2006; 20(9). 782-789.

[9] Stewart M. G., Mechanical behaviour of pitting corrosion of flexural and shear reinforcement and its effect on structural reliability of corroding RC beams. *Struct Safety*. 2009; 31(1) :19-30

[10] Maslehuddin M., Ibrahim I. M., Al-Sulaimani G. J., Al Al-Mana, SNAbduljauwad. Effect of rusting of reinforcing steel on its mechanical properties and bond with concrete. *ACI Mater J* 1990. 87(5): 496-502.

[11] Lee H. S., Cho Y. S.. Evaluation of the mechanical properties of steel reinforcement embedded in concrete specimen as a function of the degree of reinforcement corrosion. *Int J Frat*, 2009, 157(1-2):81-88

[12] Palsson R., SaeedMirza M.. Mechanical response of corroded steel reinforcement of abandoned concrete bridge. *ACI Struct J Technical Paper*. 2002. 99(2):157-162

[14] BS EN 1992-1-1 Eurocode 2, Design of concrete structures-Part 1-1 : General rules and rules for buildings, October 2005

[15] Castel A., François R., Arligue G., Mechanical behaviour of corroded reinforced concrete beams—Part 2 :bond and notch effects, *Mater Struct* 2000; 33(9):545-551

[16] Cairns J., Plizzari G. A., Du Y.G., Law D. W., Franzoni C.. Mechanical Properties of Corrosion-Damaged Reinforcement, *ACI Mater J* 2005; 102(4) :256-64

[17] Almusallam A. A., Effect of degree of corrosion on the properties of reinforcing steel bars, *Construct Build Mater* 2001; 15(8): 361-368

[18] Cosenza E., Greco C., Manfredi G., An Equivalent steel Index in the Assessment of ductility Performances of the Reinforcement, *CEB Bulletin* No.242. 1998.

CHAPTER FIVE

Flexural performance of the corroded beams and non-corroded beams

The flexural performances of the corroded beams B2Cl2 and B2Cl3 are discussed respectively in this section.

The reinforcement corrosion process and the results of experiments on two highly corroded beams B2Cl2 and B2Cl3 subjected to a chloride environment for 26 years and 28 years respectively are presented in this chapter to assess the residual performance of long-term-corrosion-damaged beams. The cracking maps were drawn for the corroded beams, which were then tested by a three-point loading system until failure, as were the non-corroded beams of the same ages. Force displacement curves were recorded for both beams. The corrosion distribution and loss of diameter of the steel bars were studied for the reinforcement. The yield strength, ultimate strength and ultimate strain of the corroded bars were analysed statistically. Both the average value and the characteristic value of the yield strength and ultimate strength were used to calculate the residual capacity of the beams. The changes in yield capacity and ultimate capacity of the corroded beam in comparison with the non-corroded beam are discussed in relation with the damage to the steel reinforcing bars. The behaviour of corroded beam appears to be strongly connected to the behaviour of the corroded steel re-bars.

5.1 Introduction

The corrosion of reinforcement induced by the presence of chloride ions in concrete is considered to be one of the most common reasons for the deterioration of reinforced concrete (RC). During the last few decades, a considerable amount of research has been conducted on the corrosion of concrete beams [1-6].

Hanjari et al. [7] have described the effect of corrosion on the behavior of RC structures by analyzing the causes and mechanisms of the reinforcement corrosion. Stewart [8] has also studied the mechanical effects of pitting corrosion, including on flexural and shear reinforcement, which can significantly affect the mechanical behavior and ductility, while greater corrosion loss can lead to brittle fracture. Nevertheless, relatively less research has been performed to assess the practically important aspect of evaluating the residual structural performance of corroded concrete structures. Torres-Acosta et al. [3] have focused on an experimental investigation of the relationship between the loss of bending capacity and loss of steel cross-section of corroded beams, and reached the conclusion that the maximum pit depth was the most important factor reducing the load bearing capacity of the corroded beams.

To study the natural corrosion, François et al. [9] have built a long-term program concerning the corrosion of concrete beams stored in a chloride environment under service load since 1984. The residual flexural performances of the corroded beams B2Cl2 with the corroded age of 26 years and B2Cl3 with the corroded age of 28 years were investigated in this chapter.

5.2 Experimental program

The corrosion cracks of the corroded beams B2Cl2 and B2Cl3 were checked carefully. In the mechanical tests, the corroded beams and the non-corroded beams were loaded until failure. The residual behavior of the beams would be reported in the following parts.

5.2.1 Cracking map

Before the mechanical test, the cracking maps of the four surfaces of the corroded beams B2Cl2 and B2Cl3 were drawn. The location and configuration of the cracks and the spalling of the concrete cover caused by the aggressive environment were depicted. The widths of the cracks were also measured using a video-microscope.

5.2.2 Mechanical test

The mechanical test of the corroded and non-corroded beams was performed up to rupture by

a three-point loading system. The deflection at the middle of the span was recorded by a linear variable differential transformer (LVDT) digital sensor with an accuracy of 0.01 mm and a capacity of 100 mm.

5.2.3 Corrosion distribution and diameter loss of the steel bars

After the mechanical test, the concrete cover was destroyed and removed so that the bars could be extracted from the corroded beams. The corrosion distribution of the longitudinal bars was drawn for two kinds of corrosion patterns, pitting corrosion and general corrosion.
The corroded bars were immersed in Clarke's solution (ANSI/ASTM G1-72) to clear the corrosion products from the surface of the bars. The diameter loss of the steel bars was measured by vernier caliper with an accuracy of 0.02 mm. The percentage loss of diameter of the stirrups was also calculated.

5.3 Experimental results

Experimental results are presented in this section, including the cracking map of the two corroded beams, the mechanical test results of four beams, the corrosion distribution map of the tensile bars and the compressive bars, the tensile tests of the bars, and the diameter loss of all the corroded bars.

5.3.1 Crack morphology of corroded beams

The crack morphology of the corroded beams B2Cl2 and B2Cl3 is shown in Figure 5-4. The reinforcement configuration of the corroded beam is also indicated so as to identify the relationships between corrosion of the steel bars and cracking behavior. The cracks larger than 1mm are drawn in thicker lines, since concrete cover spalling could occurred as reported in the DuraCrete report [10].
Many longitudinal cracks appeared in the compressive surface in the middle of the span, coinciding with the positions of the steel bars. The widths of these cracks were usually less than 1 mm. Nevertheless, there were some areas of concrete spalling. Corrosion cracks were more developed in the tensile surface, both in frequency and width. Moreover, there were more areas of concrete spalling. In non-spalling zones, corrosion cracks corresponding to tensile bars were almost all wider than 1 mm.
At the bottom of the two vertical surfaces, large longitudinal cracks also developed throughout the span at the locations of the tensile bars. However, the widths of the longitudinal cracks

decreased from the middle of the span to the two supporting ends.

In the web of the beam, the transversal cracks, coinciding with the stirrups, were initially due to the flexural load and located in the central part of the beam but subsequently extended throughout the depth of the beam and connected the cracks of the tensile and compressive surfaces due to stirrups corrosion.

The beams B2Cl2 and B2Cl3 had been highly corroded as shown in Figure 5-4, with cracks and spalling distributed over the whole length, especially in the bottom section with tensile effect. Almost all the main cracks extended along the longitudinal tensile bars, in both the tensile surface and the bottom of the vertical surfaces in the middle of the span. This tended to confirm that long-term sustained bending loading could impact the corrosion of beams. In the tension zone, the tensile bars became corroded more easily, and the expansion of the corrosion products produced stress strong enough to split the concrete and even spall the cover. There were also some major cracks in the compressive area, but their lengths were relatively small and they existed mostly in the middle; only a few cracks lay in the zone above the support.

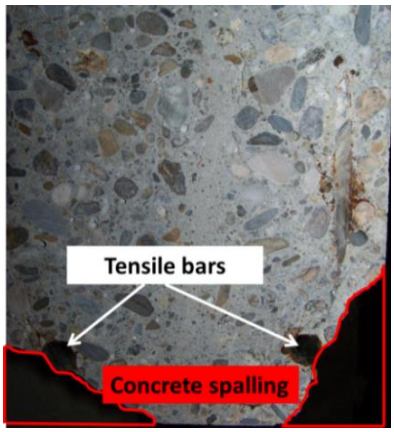

Figure 5-1 Typical cross-section of corroded beam with spalling in the corners

There were large zones with spalling along the beam. Due to the small depth of concrete cover along the longitudinal bars (i.e. 16 mm), spalling areas were located at the corners of the rectangular beam cross-section and there was very limited zone with internal corrosion cracks (Figure 5-1). The transversal cracks were less developed than the longitudinal cracks. They were located in the middle. Almost all the transversal cracks coincided with the stirrups.

5.3.2 Mechanical response of the beams during the test

The mechanical response of the corroded beams was affected by the corrosion significantly. Corrosion changed the failure mode of the beams, from yielding of the tension bars then compressive concrete crushing for non-corroded beam to yielding then brittle failure of one of

the tensioned bras for corroded beam.

With the increase of the load, the cracking of the corroded beams B2Cl2 developed gradually. During the failure process, some new cracks appeared, slowly widening and extending from the bottom to the top of the beam. Two main transversal cracks in the middle of the span, coinciding with the two stirrups nearest the loading node, had obviously formed and widened before the beam yielded (Figure 5-5). Finally, the tensile bar in the front side failed, leading to beam failure as shown in Figure 5-2(a). Similar response happened to corroded beam B2Cl3 as shown in Figure 5-3.

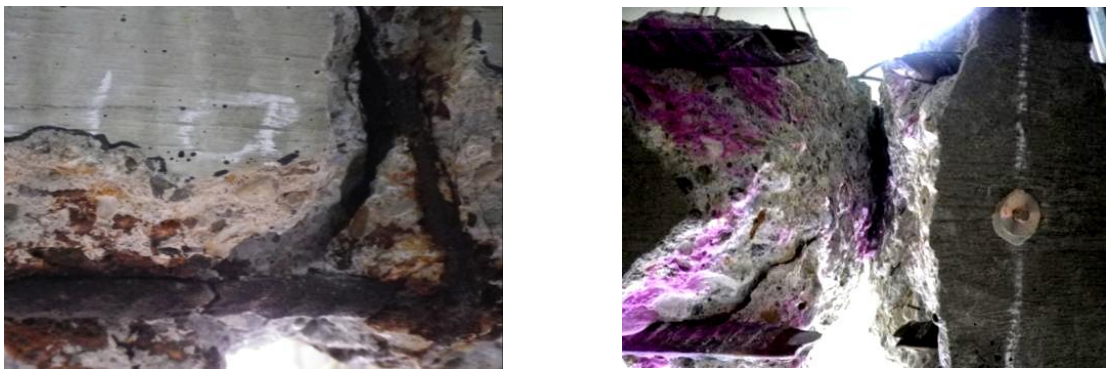

(a) Corroded beam (b) non-corroded beam

Figure 5-2 Failure of the tensile bars during the bending tests: cause of the corroded beam failure, consequence of concrete crushing for non-corroded beam

Figure 5-3 Experimental test on the corroded beam B2Cl3

When the mechanical test was carried out on the non-corroded beams, there were also two main cracks in the middle of the span, paralleling the two stirrups in the middle of the span. However, with the increasing load, another crack appeared between the two main cracks, right in the middle of the span, almost under the loading point, and extended sharply from the tensile zone to the compressive zone. Finally, the three main cracks converged and reached the loading point (Figure 5-5). The compressive concrete crushed under the loading point, leading to the failure of both tensile bars at the location of the late main crack in the middle of the span as shown in Figure 5-2(b).

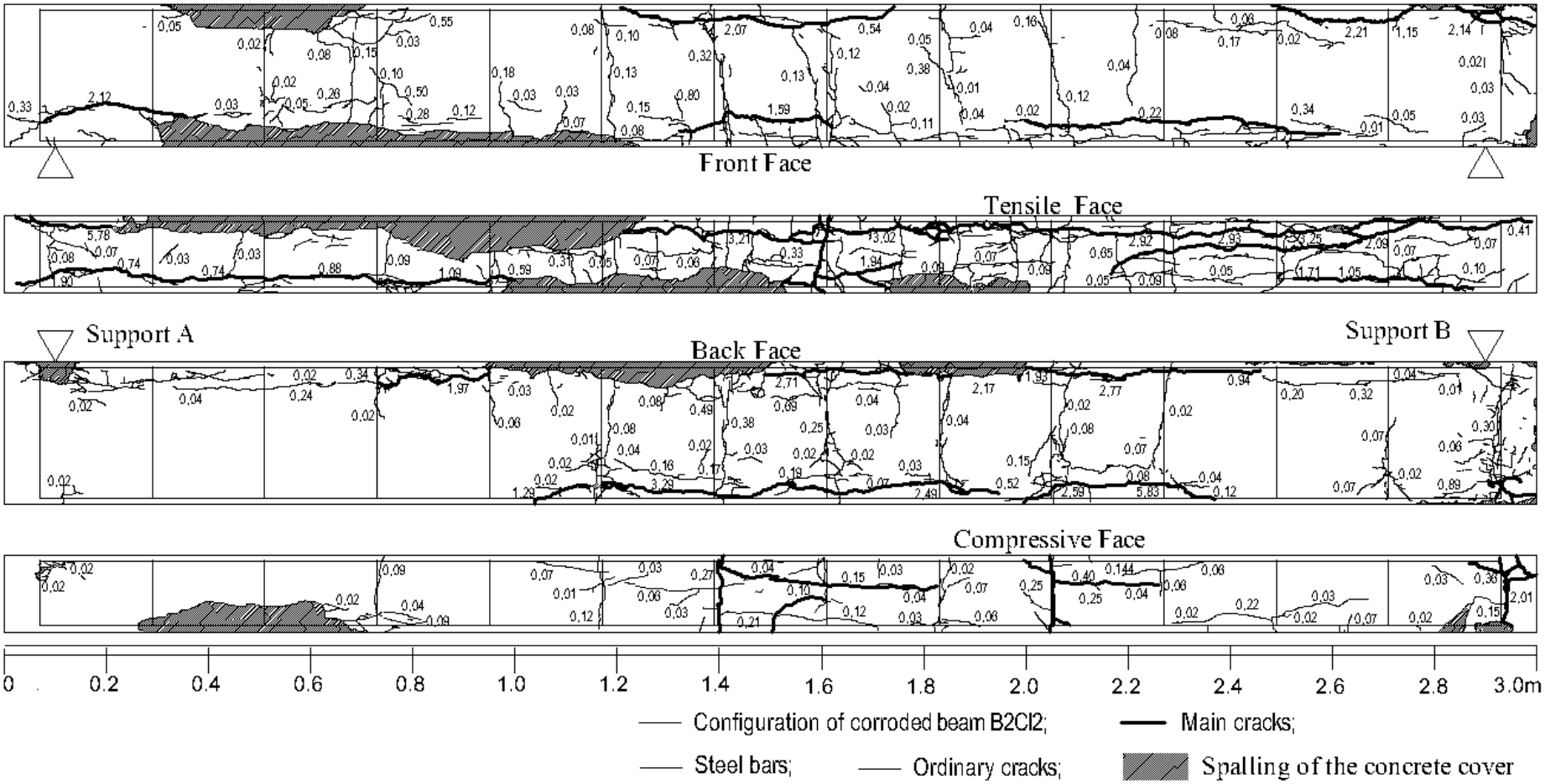

(a) Corroded beam B2Cl2 (26 years)

Figure 5-4 Cracking maps of corroded beams (mm)

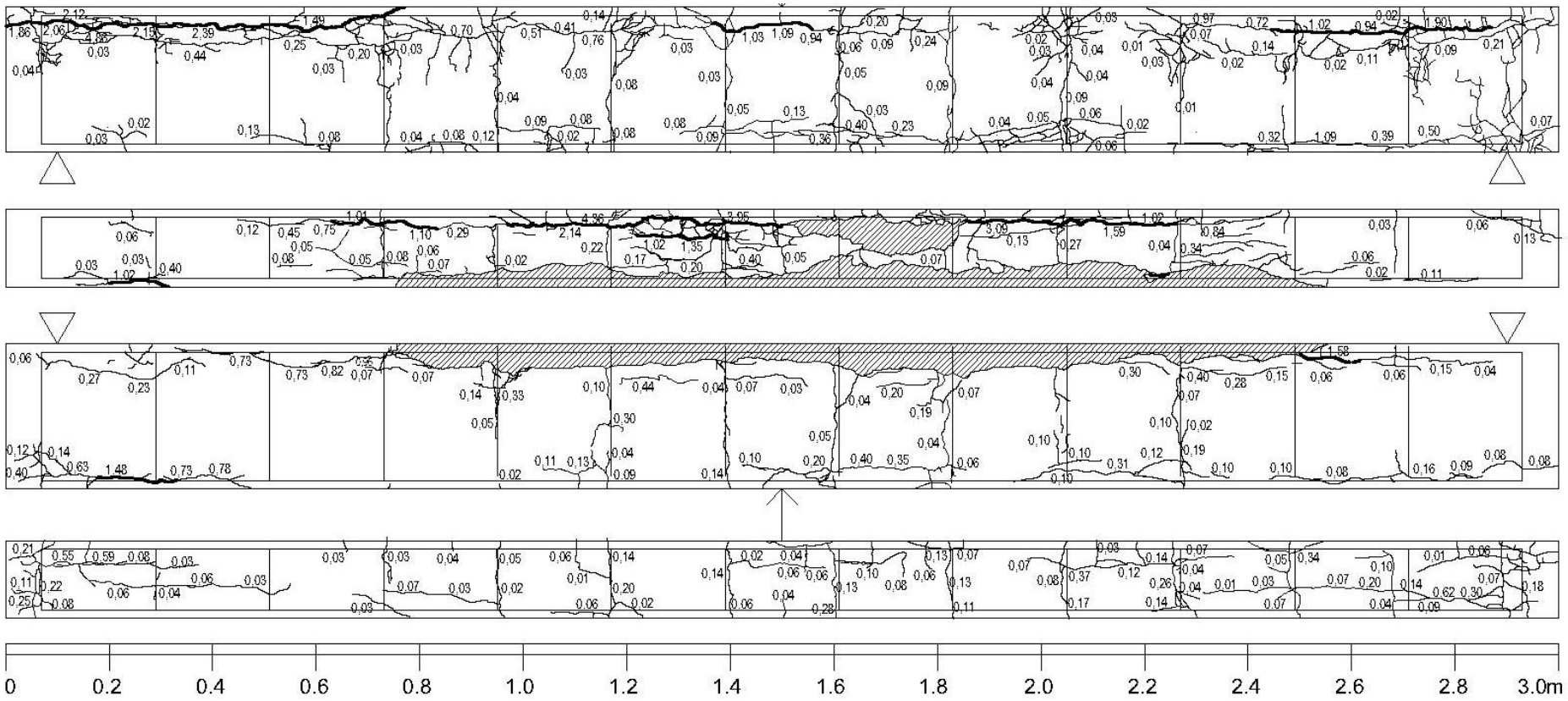

(b) Corroded beam B2Cl3 (28 years)

Figure 5-4 Cracking maps of corroded beams (mm)

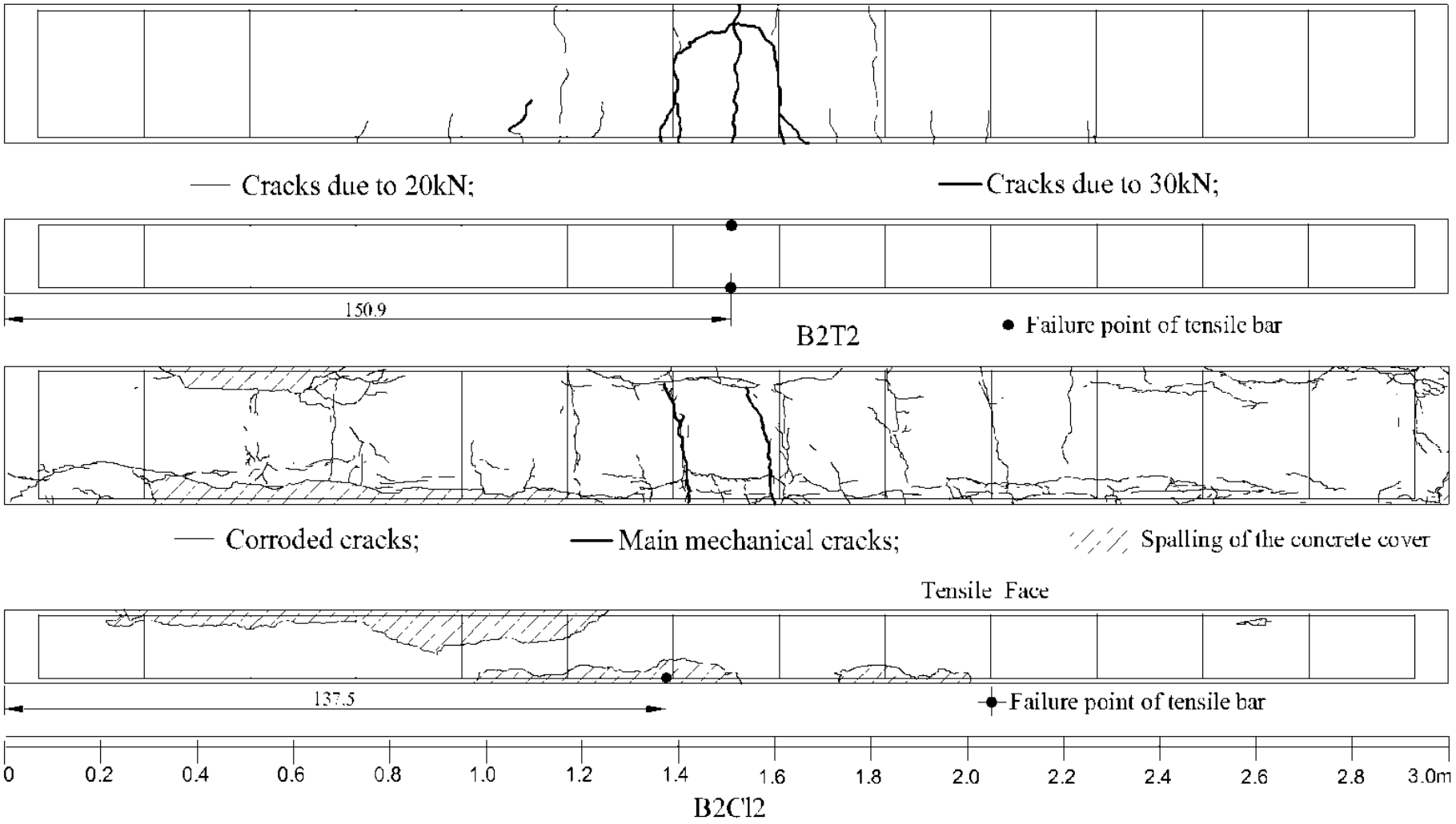

(a) B2T2 andB2Cl2 (26 years)

Figure 5-5 Failure points and main cracks during the bending test

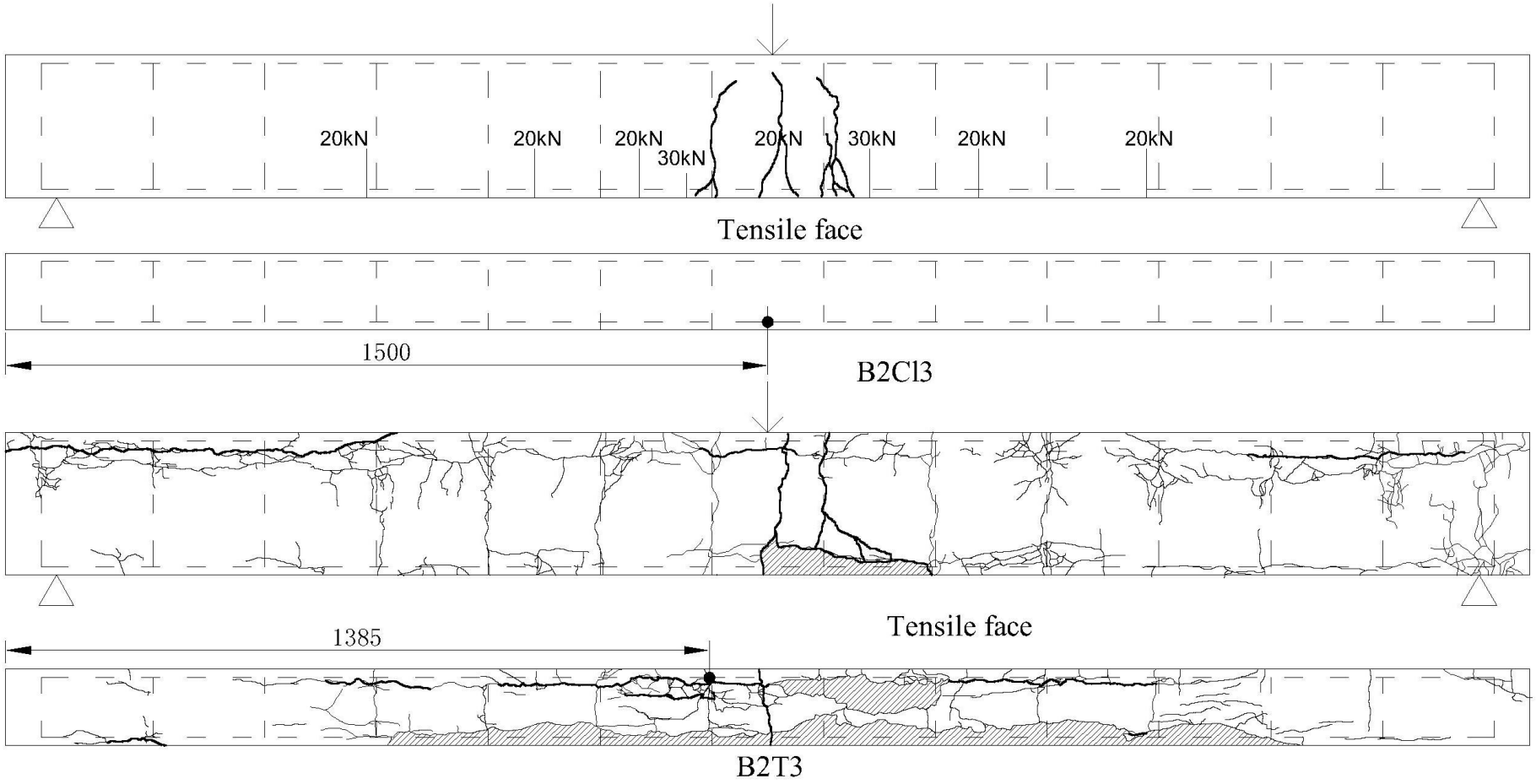

(b) B2T3 andB2Cl3 (28 years)

Figure 5-5 Failure points and main cracks during the bending test

5.3.3 Corrosion distribution in the steel bars

The corrosion maps of the tensile and the compressive bars are plotted in the downward direction and the upward direction in

Figure 5-6 and Figure 5-7, which show that the corrosion is neither uniform all along the bars nor along the perimeter of the bars. This characteristic distinguishes natural corrosion from accelerated corrosion [11-12].

According to the two phases of corrosion propagation defined by Zhang et al. [13], the corroded beams B2Cl2 and B2Cl3 had reached the generalized corrosion phase, which meant that there was corrosion and then loss of cross-section all along the bars, but there were also some zones where pitting corrosion was still significant. In Figure 5-6, for the front side tensile bar, the general corrosion spread over almost all the span except the right support. This coincided with the cracking map (Figure 5-4). The spalling and cracking of the concrete cover sped up the corrosion process of the tensile bars. As a result, the pitting corrosion in the downward was strongly developed and interconnected in most of the zones. However, the pitting corrosion in the upward direction had just appeared in some discrete zones, and most of them could be covered by the general corrosion zones (Figure 5-8).

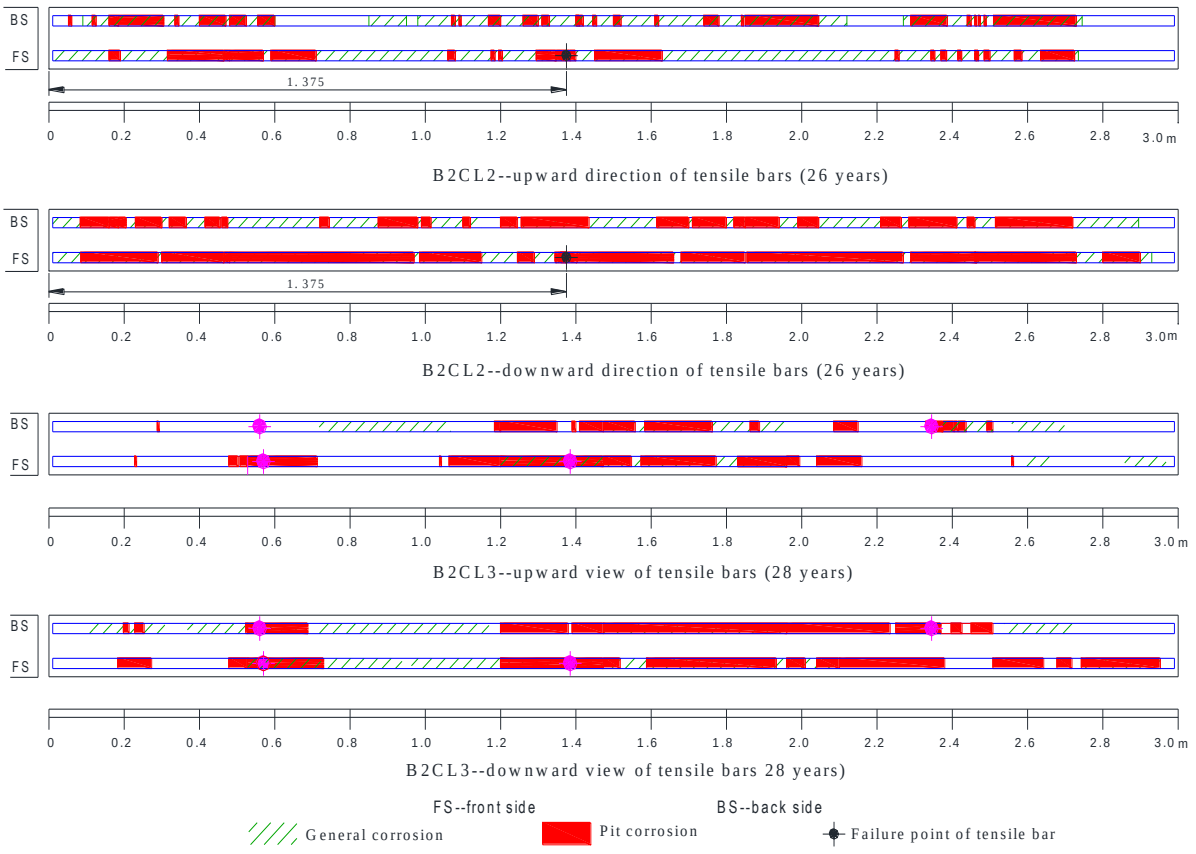

Figure 5-6 Corrosion maps for the tensile bars in the upward and downward directions

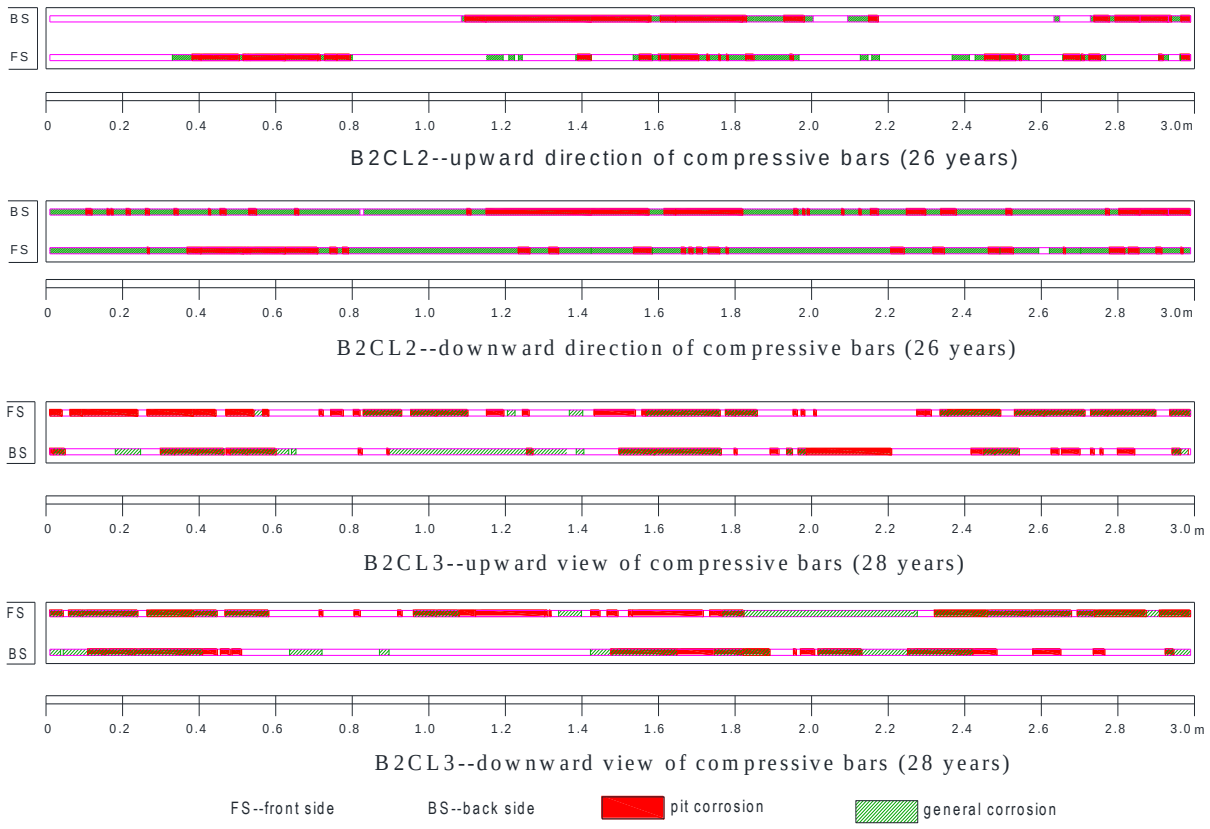

Figure 5-7 Corrosion maps of the compressive bars in upward and downward directions

Compared with the front tensile bar of B2Cl2, the corrosion status of the back tensile bar was less serious, including both general corrosion and pitting corrosion, which also coincided with the cracking and spalling of the concrete cover in Figure 5-4.

Figure 5-7 shows the corrosion distribution in compressive bars. The corrosion in the downward direction was more serious than that in upward direction, both for general corrosion and pitting corrosion, despite the fact that though the distance of the upward direction of the compressive bars was smaller than that of downward direction. This result, which was opposite on the one obtained on tension bars and usually found in natural corrosion process [14], could be explained by the “top-bar” effect. Indeed, “top bar” effect, which corresponded to the voids created under horizontal bars located in the upper part of the beam with regard to casting direction [15], played a more important role in the corrosion process than the distance between the steel surface and concrete cover [16]. These voids had an effect on bond but also on the resistance to corrosion since it modified the buffering effect in pH when depassivation by chlorides occurs. Moreover there was also an effect on the development of corrosion products on the surface of steel bar since the confinement was different along the perimeter.

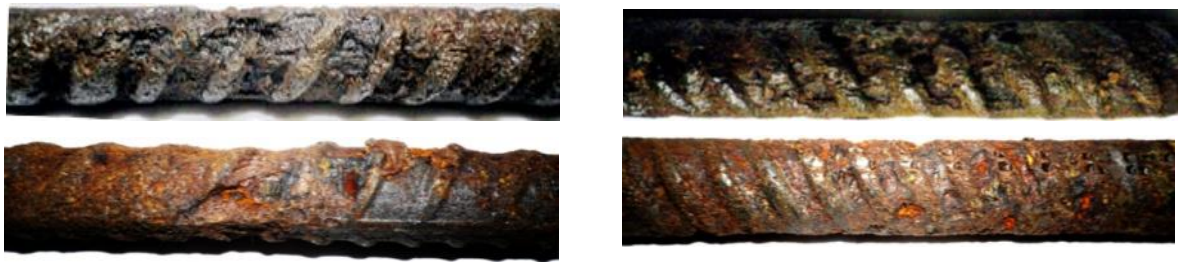

(a) Corrosion distribution of the tensile bars

(b) The non-corroded bar

Figure 5-8 Comparison of the corroded and non-corroded tensile bars

5.3.4 Diameter loss of the tensile bars

The loss of diameter in the corroded bars of B2Cl2 was measured by vernier caliper, including the tensile bars, the compressive bars and the stirrups. The losses are shown in Figure 5-9, Figure 5-10 and Figure 5-11, respectively. As discussed in Chapter Four, the loss of the steel cross-section could be overestimated by the measurement of residual diameter since the shape of residual cross-section was irregular. The mass loss of some small pieces of the steel bar (called coupons) was also measured and is shown in Figure 5-9(b). The length of the steel coupons was depended on the corrosion distribution, with the minimum length being about 5 mm (Figure 4-7).

In Figure 5-9, the diameter loss of the two tensile bars agreed well with the cracking and spalling distribution and the corrosion distribution in Figure 5-6. The diameter loss occurred throughout the length of the two tensile bars. Although the corrosion in the front bar was a little more serious than that of the back one due to delamination of the concrete cover, the distribution trend of the corrosion was almost the same. The pitting corrosion mainly accumulated in three zones for both of the tensile bars, 100-700 mm, 1250-1850 mm, 2300-2700 mm (Figure 5-9). In the first pitting corrosion zone and the third pitting corrosion zone, the diameter loss was greater than in the second zone, but the front side tensile bar failed at the point with the largest loss of diameter in the middle pitting corrosion zone. The failure point occurred in the middle of the tensile bar at the location with severe pitting corrosion, although the diameter loss was a little smaller than for the pitting corrosion in other zones. Interestingly, the diameter loss at the location of the stirrups was relatively smaller than in the areas nearby, which suggested that the stirrups somehow reduced pitting corrosion of the

tensile bars.

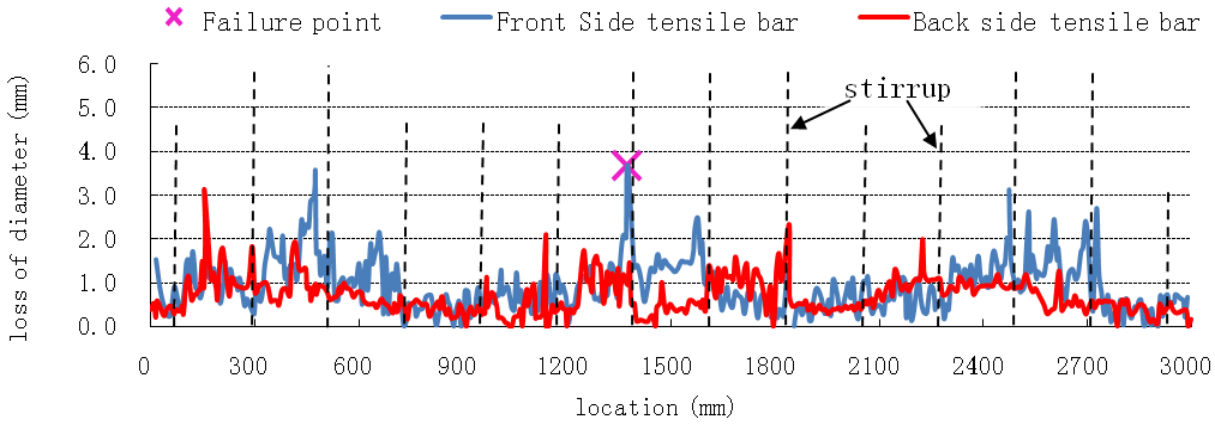

(a) Loss of diameter due to corrosion, from the vernier caliper measurement

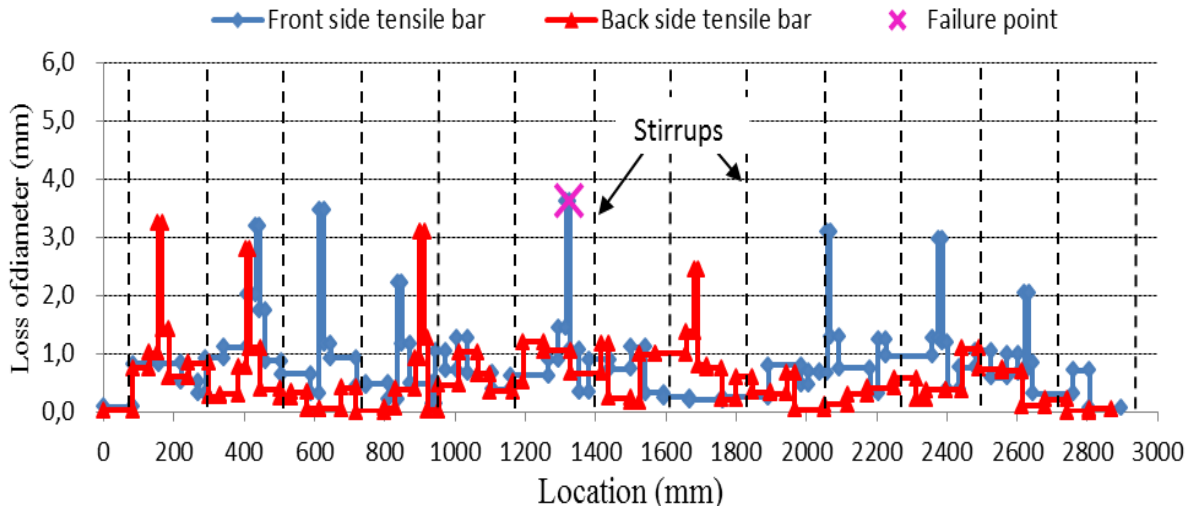

(b) Loss of diameter due to corrosion, from weight measurement

Figure 5-9 Loss of steel cross-section diameter of the tensile bars of beam B2Cl2

In Figure 5-10, the pitting corrosion with the diameter loss was more serious in the compressive bars than that in the tensile bars. The maximum depth of the pitting corrosion for both the compressive bars reached as much as 5mm, with a minimum residual diameter of the compressive bars of only 1 mm. Compared with the maximum diameter loss of 3.5 mm for the tensile bars, this meant that the corrosion in the compressive bars was superior to the tensile bars in spite of the smaller diameter. The explanation could be linked to the “top-bar” effect leading to bad interface quality between the compressive bars and the concrete.

The trend of corrosion distribution was almost the same. The general corrosion depth was about 0.8 mm. While the pitting corrosion was mainly concentrated in two zones, one located

in the middle and the other was near the right support. But the front side compressive bar, as there was a spalling zone near the left support, and pitting corrosion developed in this zone.

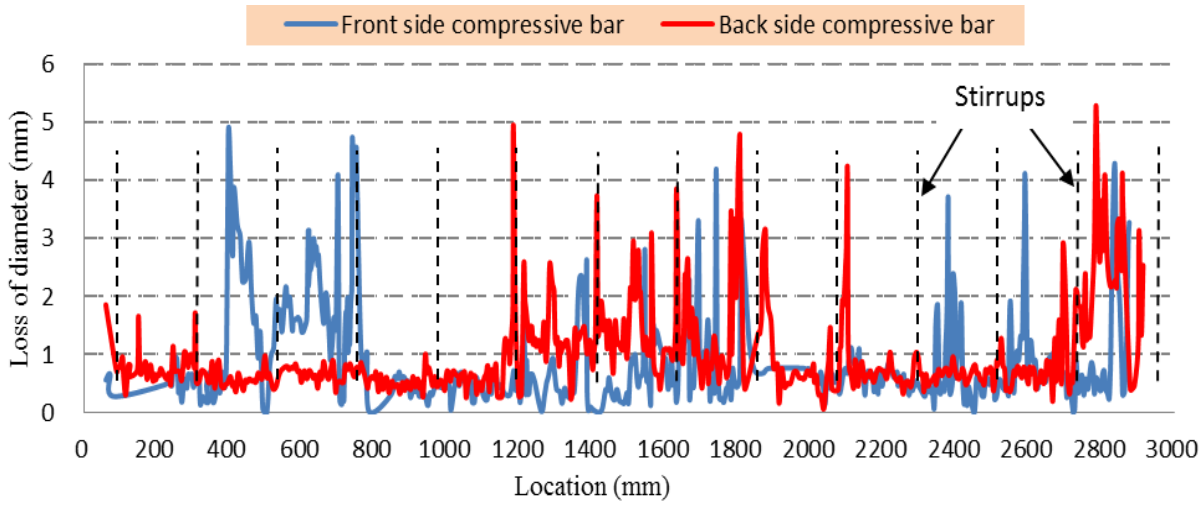

Figure 5-10 Diameter loss of compressive bars by vernier caliper measurement (B2Cl2)

Figure 5-11 shows the percentage diameter loss for all the stirrups. The distribution of the corrosion was irregular. However, for each stirrup, pitting corrosion was more severe in the corner, followed by the bottom part and the top part.

According to the discussion on the diameter loss of the steel bars in B2Cl2, the results got by the gravimetric method were supposed to be better. As the residual cross-section measured by vernier caliper was shown in Figure 5-12, only the area in cross-section hatched as shown in (b) was considered, which would obviously overestimate the cross-sectional loss of the corroded bars. Then the cross-sectional loss of the corroded tensile bars was deduced from the residual mass of the failure location, which had been cut into small pieces as short as 5 mm, and the results were closer to the true residual cross-section. So, for corroded beam B2Cl3, only the cross-sectional loss of the corroded bars calculated by mass loss was presented in Figure 5-13. In the following section, the gravimetric residual cross-section of the corroded bars is used in the calculations concerning the corroded beams.

5.3.5 Results of the mechanical test

The deflections in the mid-span of the two beams were recorded by a numerical sensor so that the load-deflection curves of the mechanical tests could be plotted (Figure 5-14 and Figure 5-15). The response of the beams showed that the corrosion played a very influential role in the mechanical behavior. Some differences could be noted by comparing the corroded beam with the non-corroded beam: the load-bearing capacity, the ultimate deflection had decreased.

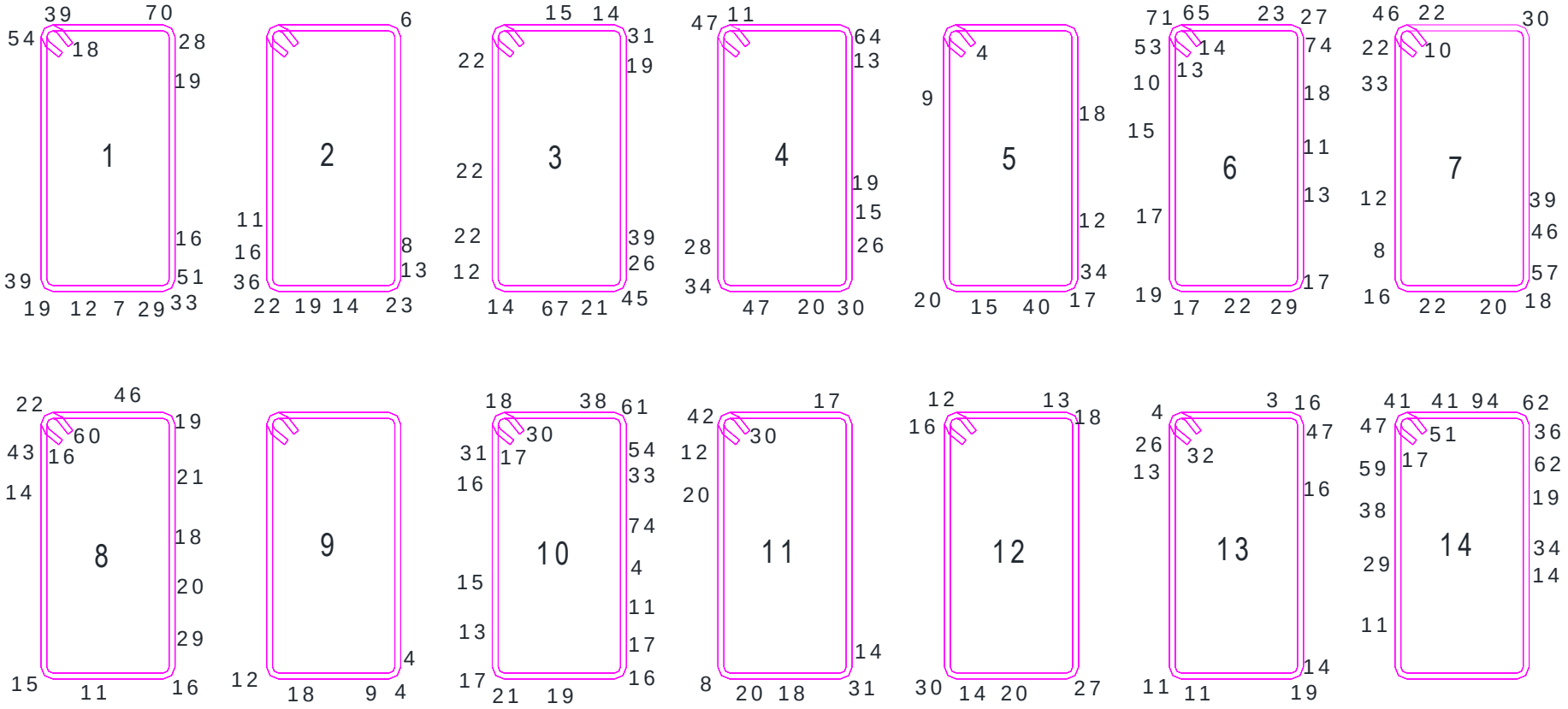

Figure 5-11 Percentage loss of diameter for the stirrups

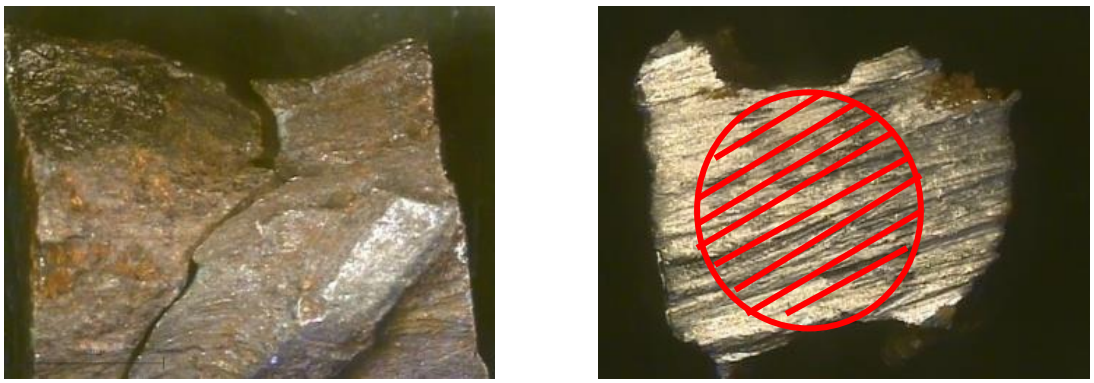

(a) Example of steel piece at the failure point (b) Residual cross-section of corroded bars

Figure 5-12 Example of failure pattern of the corroded longitudinal reinforcement

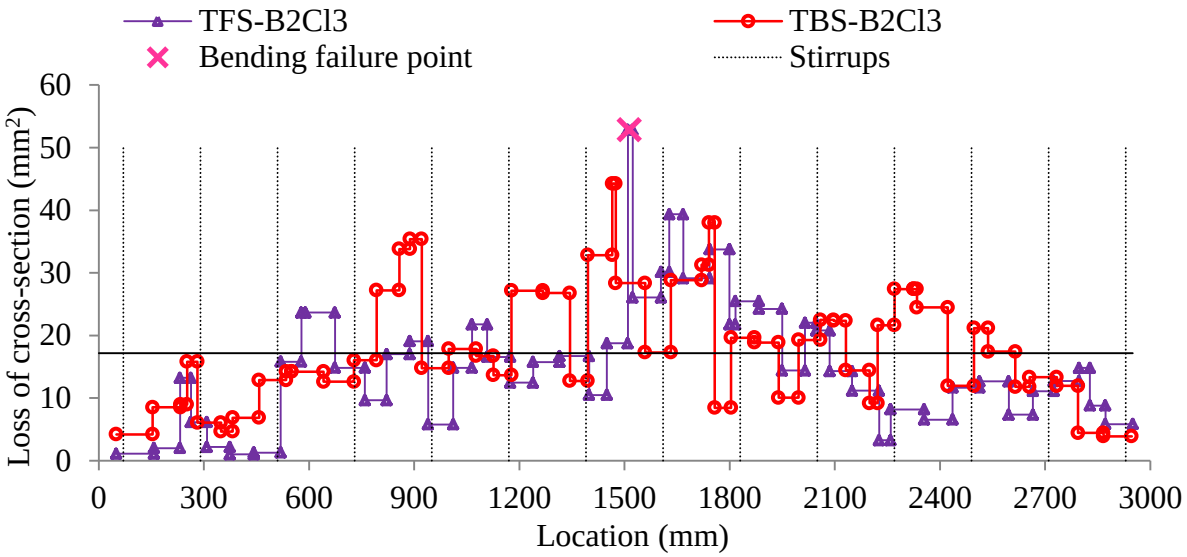

Figure 5-13 Cross-sectional loss of the tension bars of B2Cl3

5.4 Discussion

5.4.1 Classical RC calculation

As already mentioned, both the beams failed with the rupture of the tensile bars. The ultimate load was closely linked to the yielding load, which itself depended on the actual cross-section and the yield strength of the reinforcement. The effect of corrosion on the contribution to the mechanical capacity and the ductility of the corroded beam were considered.

The reduction of cross-section was considered for the two corroded bars at the failure point. For B2Cl2, there were 59 mm^2 and 19 mm^2 of cross-section loss in the two corroded tensile bars (Figure 5-9b), which corresponded to a global loss of cross-section of around 36%.

For the corroded beam B2Cl3, the maximum cross-section losses were 52.8 mm^2 (46.7%) and 44.3 mm^2 (39.1%) for the front bar and back bar respectively. That meant that there was about

43% loss for the two bars. The maximum of cross-section loss of both bars were located between the same stirrups and very close to each other. So they were assumed to be the critical cross-section for each bar.

5.4.2 Curves of the mechanical tests

The force-deflection curves of the mechanical tests on the beams are shown in Figure 5-14 and Figure 5-15. It should be noted that, despite the highly damaged aspect of the corroded beams, with a large spalling zone and large corrosion cracks, the bending capacity was still well above the design load corresponding to ULS (from Eurocode 2) which correspond to a force of 20kN. The mechanical performance of the tensile bars was quite similar to the response of the beams during mechanical tests. For the corroded bars and the corroded beams, both the tensile tests and the bending tests showed the transition period when the load reached the yield value. During this period, the corroded elements manifested a stronger post-yielding behavior but ultimate elongation was sharply reduced by the corrosion. In contrast, no transition existed for the non-corroded bars and non-corroded beams. The loading capacity showed little improvement once the non-corroded bar yielded.

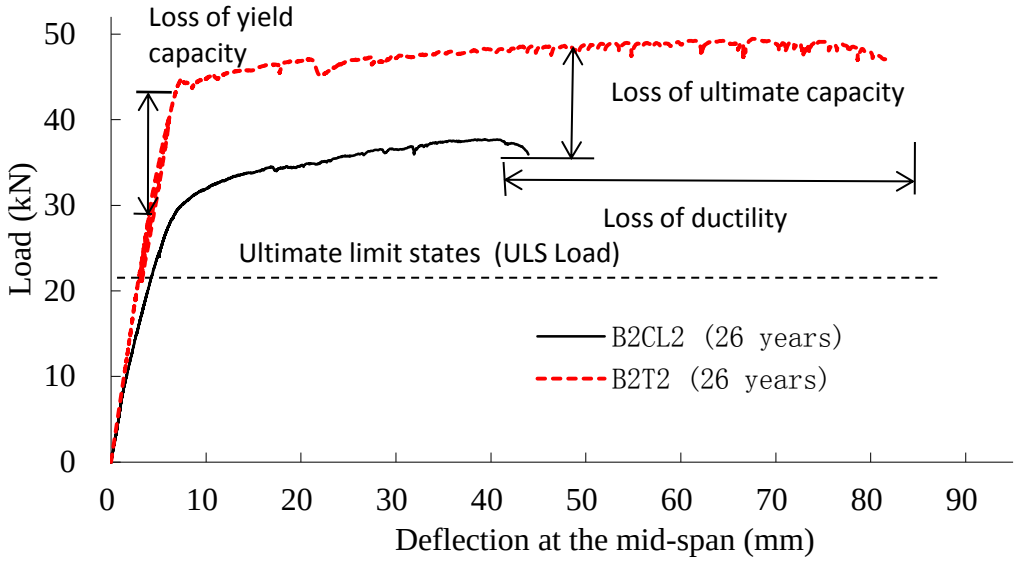

Figure 5-14 Load-deflection behavior of beams B2Cl2 and B2T2 (26 years)

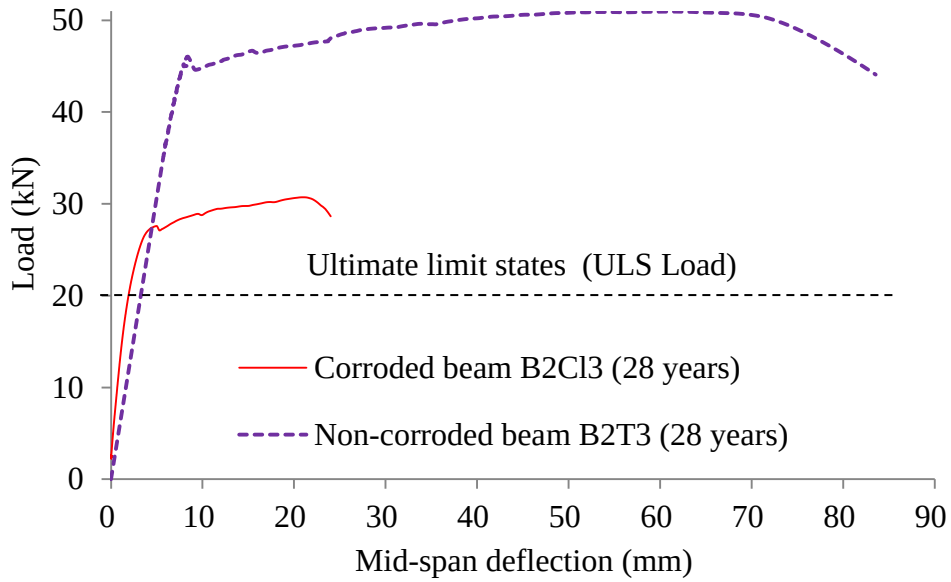

Figure 5-15 Experimental results for the beams B2Cl3 and B2T3 (28 years)

5.4.3 Loss of capacity (yielding and ultimate)

The yielding force of the beams calculated by classical RC models is shown in Table 5-1. The comparison of the results between the experiment tests is also given in the Table 5-1.

According to Table 5-1, the experimental result matched well the calculation well and yielding capacity was in relation with the loss of cross-section. Then the percentage decreased in B2Cl2 and B2Cl3 yielding load for both experiment and calculation coincided with the average maximum reduction in cross-sectional area of corroded steels. This result was similar to previous research results (Rodriguez et al. [5], Zhang et al [17]) and confirms that it was possible to predict the residual loading capacity of a corroded RC beam if the average maximum loss of cross-sectional area of the tensile bars was known in the zone of highest bending moment.

The relative ultimate capacity versus yielding capacity was slightly more important for the corroded beam and could be linked to the post-yielding hardening of corroded steel, which seemed more important than that of non-corroded steel.

According to Table 5-1, the relationship between the ultimate capacity and the level of average steel corrosion could also be deduced. Every 1% cross-section loss of the tensile bars corresponded to 0.67% reduction in the ultimate bending capacity of the beams, which agreed quite well with the findings of Malumbela et al. [18]. The post yielding hardening coefficient of corroded steel which was higher than non-corroded steel, could explained the fact that ultimate capacity was less reduced than yielding capacity.

Table 5-1 Comparison of yielding capacity and results

Beam	B2Cl2	B2T2	B2Cl3	B2T3
Yielding (Experiment value)	30 kN	44 kN	26 kN	47 kN
Yielding (Calculated value)	30.3 kN	40.6 kN	25.5 kN	44.7 kN
Comparison (Calculated value/Experiment value)	101%	92%	98.1%	95.3%
Relative yield loss Exp%	32%		44.7%	
Relative yield loss calc%	25%		43.0%	
Relative loss (cross-section)%	36%		43%	
Ultimate (Experiment value)	37.6 kN	49.2 kN	30.7 kN	50.2 kN
Ultimate (Calculated value)	38.4 kN	45.2 kN	34.4 kN	49.2 kN
Comparison (Calculated value/Experiment value)	102%	92%	112.1%	98%
Relative ultimate loss Exp%	24%		38.8%	
Relative ultimate loss Calc%	15%		30.1%	
Relative loss (cross-section)%	36%		43%	

The yield capacity and ultimate capacity of all the beams are extracted in Figure 5-16 and Figure 5-17 respectively. Figure 5-16 shows the yield capacity of the four beams, two of which were corroded beams aged 26 and 28 years. In comparison with B2T2 and B2Cl2 at the age of 26 years, there was about 32% loss of yield capacity due to the corrosion of the reinforcement, which corresponded to 34% loss of cross-section in the failure zone. As for B2Cl3 and B2T3 at the age of 28 years, the yield capacity loss was 44.6%. The cross-section loss in the failure zone was 43%. This means that 1% gravimetric cross-section loss of the tension reinforcement resulted in about 1% loss of experimental yield capacity of the corroded beams.

The ultimate capacity of the beams is compared in Figure 5-17. The reduction of ultimate capacity was 39% for B2Cl3, with a corroded age of 28 years, and 24% for B2Cl2, with a corroded age of 26 years, which shows that the decrease of ultimate capacity was more serious for greater corroded age. 1% gravimetric cross-section loss of the tension bars led to 0.65% - 0.9% loss of ultimate capacity of the corroded beam, which was smaller than that of the yield capacity loss but is consistent with Malumbela et al.'s results [18]. This phenomenon could be due to the tensile behaviour of the corroded bars, according to previous literature [19], the ratio between ultimate and yield stress fu/fy is modified by corrosion damage to the steel bars.

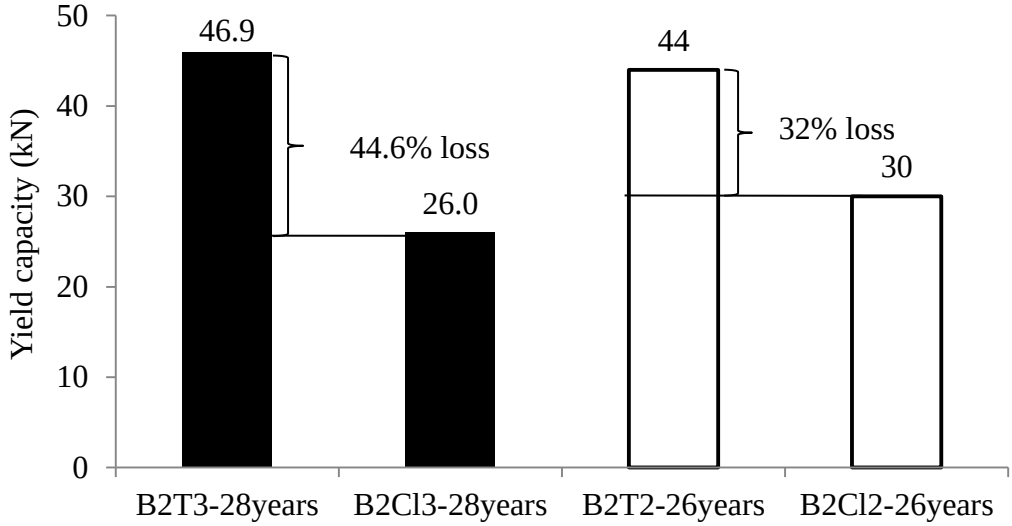

Figure 5-16 Loss of yield capacity of corroded beams

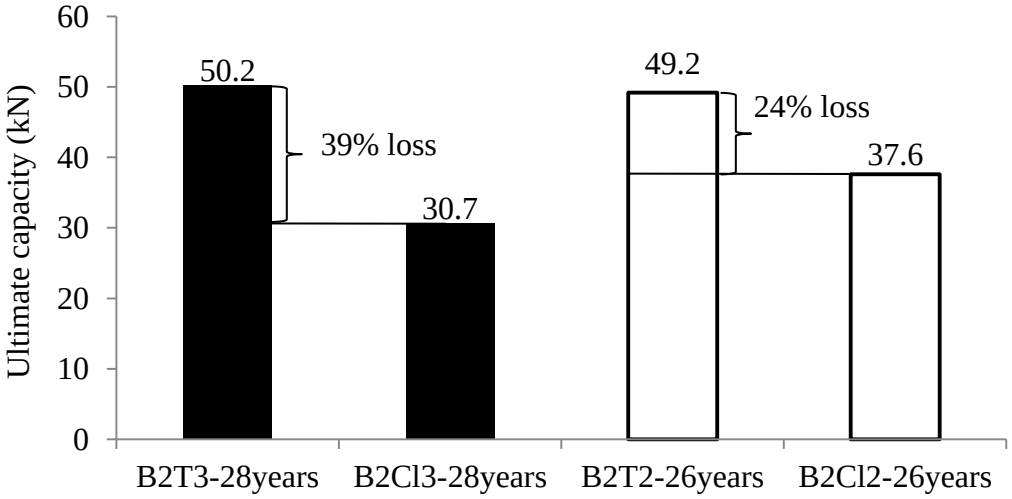

Figure 5-17 Loss of ultimate capacity of corroded beams

5.4.4 Loss of stiffness and deflection

From the load-deflection curves of Figure 5-14 and Figure 5-15, the impact of corrosion on the mechanical behavior of the beams could be calculated and is shown in Table 5-2.

The corrosion had a huge influence on the mechanical characteristics of the corroded beams, resulting in about a quarter loss of ultimate capacity. Nevertheless, the loss of deflection even reached 56.5% and 71.5% respectively, which meant that the ductility of the corroded beam had been reduced most seriously.

For tensile bars, the ultimate elongation decreased from 0.08 for non-corroded steel bar to 0.02-0.03 for corroded steel bars. So corroded steel bars didn't respect the ductility criteria of Eurocode 2 (minimal ultimate elongation = 0.05). To compare the steel bar elongation reached

during the bending test of non-corroded and corroded beams, the strain at failure was computed using the model of RC members developed by Vu et al. [20]. For the non-corroded beam, the concrete compressive strain was 0.004 at beam failure due to concrete crushing, while the tension strain of the steel bar was about 0.002, which was considerably less than the ultimate elongation of steel, but crushing of concrete led to a strong increase of stress in the tensile bar, then its failure. But, for the corroded beam, the steel strain elongation corresponding to beam failure was close to 0.012, while the concrete strain reached 0.002. These values were consistent with the failure mode of the non-corroded beam, but for corroded beam, the steel elongation strain at failure, 0.012, was less than the ultimate elongation recorded in tensile tests performed on corroded steel bar. One explanation was that the failure of beam B2Cl2 and B2Cl3 was due to bar failure at a big pit (around 50% loss of cross-section) with a higher loss of cross section than the pits that induced failure in the direct tensile tests of corroded steel bars. As a result, the ultimate elongation of steel bars with 50% of loss of cross-section was limited to 0.012. Tests performed by François et al. [21] and Cairns et al. [22] support this proposal.

Table 5-2 Loss of deflections

Beams	Deflection	Beams	Deflection
B2Cl2	35.9 mm	B2Cl3	21.0 mm
B2T2	82.6 mm	B2T3	73.8 mm
Differences	46.7 mm		52.8 mm
Relative difference (%)	56.5		71.5

5.5 Conclusion

The experimental tests of the 26-year-old and 28-year-old beams presented in this chapter have confirmed the impacts of corrosion on mechanical characteristics, including the load-bearing capacity and the ductility.

The corrosion of reinforcement changes the failure mode from yielding followed by concrete crushing for non-corroded beam to brittle failure of corroded tension bars which strongly reduced the ductility of the beam. The loss of ductility was in relation with the loss of cross-section of the steel bar at the failure location. Ultimate deflection of the corroded beam was greatly (about 57% and 72%) reduced in comparison with the non-corroded beam. This was because of the reduction of ultimate elongation of the steel bar in tension due to corrosion: the

tensile test performed on corroded bars extracted from the beam showed that ultimate elongation of corroded steel was strongly reduced, the consequence being that the steel bar did not respect the minimal prescription of design codes such as Eurocode 2.

Despite the high corrosion level of beams, the ultimate capacity was still largely above the ULS design load. However, as the corroded steel bars did not respect the ductility prescription of Eurocode 2, beams B2Cl2 and B2Cl3 could not be re-qualified as respecting standards. Thus loss of ultimate elongation of the steel could be the limiting factor for the service life of corroded RC structures. Experimental results confirmed that the loss of capacity was linked to the cross-section loss at the failure location. Corrosion slightly modified the post-yielding hardening properties of steel bars, which led to a difference in yielding capacity versus the ultimate capacity. Corrosion led to large corrosion cracks and spalling, which reduced the bond between re-bars and concrete, thus reducing the bending stiffness of the beams. Nevertheless, this effect was not so obvious as the loss of ductility and loss of capacity.

According to experimental results obtained on corroded or non-corroded beams, the consequences of the loss of 1% of the cross-section of a tension bar are different for yield capacity (also 1%) and ultimate capacity (from 0.65% to 0.9%). Similar conclusions have been drawn by other researchers [3, 40] and the dispersion on both yield and ultimate strength of corroded steel bars shown in this section is not sufficient to explain this difference. A change in the tension behaviour of steel due to corrosion damage could be involved but additional work is needed to understand this phenomenon.

5.6 References

[1] Page, C. L., Corrosion and its control in reinforced concrete, Sixth Sir Frederic Lea Memorial Lecture. *ICT Yearbook:* 1998-1999, Institute of Concrete Technology, Crowthorne, 1999, 37-51.

[2] Du Y., Clark L. A., Chan A. H., Impact of reinforcement corrosion on ductile behavior of reinforced concrete beams, *ACI Struct J.*2007; 104(3):285-293

[3] Torres-Acosta A. A., Navarro-Gutierrez S., Terán-Guillén J., Residual flexure capacity of corroded reinforced concrete beams, *Eng Struct.* 2007; 29(6):1145-52

[4] Tuutti K., Corrosion of steel in concrete. Swedish Cement and Concrete Research Institute, Fo 4.82, Stockholm; 1982, 469

[5] Rodriguez J., Ortega L. M., Casal J., Load carrying capacity of concrete structure with corroded reinforcement. *Construct Build Mater* 1997; 11(4):239-48

[6] Val D. V., Deterioration of strength of RC beams due to corrosion and its influence on

beam reliability. *J Struct Eng ASCE* 2007; 133(9): 1297-306.

[7] Hanjari K. Z., Kettil P., Lundgren K., Analysis of mechanical behaviour of corroded reinforced concrete structures. *ACI Struct J.* 2011; 108(5):532-41

[8] Stewart M. G., Mechanical behaviour of pitting corrosion of flexural and shear reinforcement and its effect on structural reliability of corroding RC beams. *Struct Safety*. 2009; 31(1):19-30

[9] François R., Arliguie G., Influence of Service Cracking on Reinforcement Steel Corrosion, *J Mater Civ Eng* 1998; 10(1):14-20

[10] Dura-Crete (2000) The European Union—BriteEuRam III, *DuraCrete final technical report*, Document BE95-1347/R17

[11] Malumbela G., Moyo P., Alexander M. .Longitudinal strains and stiffness of RC beams under load as measures of corrosion levels, *Eng Struct.* 2012; 35:215-27

[12] Lee H. S., Cho Y.S.. Evaluation of the mechanical properties of steel reinforcement embedded in concrete specimen as a function of the degree of reinforcement corrosion, *Int J Fract,* 2009; 173(1):81-8

[13] Zhang R., Castel A., François R.. Concrete cover cracking with reinforcement corrosion of RC beam during chloride-induced corrosion process, *Cem Concr Res* 2010; 40(3): 415-25

[14] Yuan Y., Ji Y., Shah S. P., Comparison of two accelerated corrosion techniques for concrete structures, *ACI Struct J*, 2007; 104(3), 344-7

[15] Kosmatka S. H., Bleeding significance of tests and properties of concrete and concrete making material, ASTM Special Publication, Philadelphia, STP 169C, 1994, 88-111

[16] Soylev T. A., François R.. Quality of steel-concrete interface and corrosion of reinforcing steel, *Cem Concr Res*, 2003, 33(9) : 1407-15

[17] Zhang R., Castel A., François R..Serviceability Limit State criteria based on steel-concrete bond loss for corroded reinforced concrete in chloride environment, *Mater Struct* 2009; 42(10):1407-21

[18] Malumbela G., Alexander M., Moyo P.. Variation of steel loss and its effect on the ultimate flexural capacity of RC beams corroded and repaired under load, *Construct Build Mater.* 2010; 24(6): 1051-9

[19] Zhu W. J., François, R., Effect of corrosion pattern on the ductility of tensile reinforcement extracted from a 26-year-old corroded beam, *Advances in Concrete Construction*, 2013, 1(2):121-37

[20] Vu N-A., Castel A., François R., "Response of post-tensioned concrete beams with unbonded tendon including serviceability and ultimate state", *Eng Struct,* 2010; 32(2) 556-69.

[21] François R., Khan I., Dang V-H., Impact of corrosion on mechanical properties of steel

embedded in 27-year-old corroded reinforced concrete beams, *Mater Struct*, 2013; 46(6), 899-910

[22] Cairns J., Plizzari G. A., Du Y., Law D. W. and Franzoni C., "Mechanical properties of Corrosion-Damaged Reinforcement", *ACI Mater J.,* 2005; 102(6), 256-64.

CHAPTER SIX Structural performance of RC beams corroded in chloride environment for a long period

This chapter presents experimental work to investigate the influence of chloride corrosion of the reinforcing bars on the residual structural performance of reinforced concrete beams in relation to the corroded period. A mechanical experiment was conducted with a three-point loading system on four corroded beams that had been exposed to a chloride environment for 14 years, 23 years, 26 years and 28 years. The load and deflection at the mid-span were recorded to study the residual mechanical behaviour of the beams. The corroded tensile bars were extracted from the beams to check the cross-sectional loss of the reinforcements. Non-corroded beams, which were cast at the same time and had the same composition, were also tested to highlight the effect of corrosion on the mechanical behaviour of the beams. The results show that the 1% cross-sectional loss of the tension bars corresponded to 1% loss of yield capacity and about 0.84% loss of ultimate capacity. The natural corrosion at the maximum cross-sectional loss corresponded to a corrosion speed of 1.3μA/cm^2/year. The lifetime was also predicted to be 45 years by the average corrosion properties.

6.1 Introduction

Chloride corrosion of reinforcement bars is the major cause of deterioration in reinforced concrete (RC) constructions [1], especially when the structures are exposed to a marine environment or subjected to the application of de-icing salts [2]. The corrosion occurs due to the diffusion of chloride ions, oxygen and water through the concrete cover to reach the reinforcing bars [3].

The impact of reinforcement corrosion on the structural performance of RC structures has received significant attention from researchers and engineers all over the world during the last three decades [4-5]. Corrosion of the reinforcement results in a loss of cross-section and reduces the bond between the longitudinal bars and the concrete. At the same time, as the corrosion products are expansive, the increased volume of corroded products causes the concrete cover to crack along the longitudinal reinforcement and stirrups, and even leads to spalling and delamination [6].

The mechanical performance of RC structures can be significantly influenced by corrosion of their reinforcement, which has an important relationship with the corrosion crack width. Cairns et al. [7] have concluded that a longitudinal crack 1.0 mm wide can correspond to 0.3 mm depth of pitting corrosion in the longitudinal reinforced bars, which is about 10% loss in their cross-section. Torres-Acosta et al. [8] have found that 10% loss of diameter of the tensile bars can result in a decrease of as much as 60% in the flexure load capacity, and Maaddawy et al. [9] have found that 1% mass loss of steel bars leads to a maximum corrosion crack width from 0.08 mm to 0.14 mm.

However, most of these corrosion programmes in laboratory conditions were carried out in the absence of a sustained load during the corrosion process. Malumbela et al. [10] have run a programme of corrosion under service load and found that a 1% cross-sectional loss at the most corroded point of the tensile bars corresponded to 0.7% reduction in the ultimate bending capacity of the beams. Ababneh et al. [11] have investigated the impact of mechanical loading on the corrosion of steel reinforcement and have described the relationship between the mechanical load applied before exposure and the initiation of corrosion. Nevertheless, corrosion of the reinforced concrete was accelerated by impressed current, the effects of which could obviously be different from natural corrosion and thus limit the applicability of these research results.

It should be pointed out that no agreement has been reached on chloride corrosion problems so far. No details can be found in relevant standards [12], although some requirements refer to

the indicative strength of the materials, which does not correspond to inside conditions. The issue of structural safety and chloride-induced corrosion still needs considerable study.

This section mainly describes the mechanical experiments on seriously corroded beams that had been exposed to a chloride environment under service load for 14 years, 23 years, 26 years or 28 years. The residual structural performance of the corroded beam will be compared to that of a non-corroded beam and discussed systematically, including from the points of view of capacity and ductility versus loss of cross-section of the corroded reinforcement and the duration of the corrosion.

6.2 Experimental context

This section considers four seriously corroded beams from Group B of different corroded ages. Detailed information about the beams is shown in Table 6-1. In fact, at different stages, experiments were conducted on the beams in order to check the progress of corrosion and the mechanical performance of the corroded and non-corroded beams [13, 14].

Table 6-1 Presentation of beams

Label	Mser (kN·m)	Type	Age (years)
B1Cl1	14	corroded beam	14
B1T1	14	non-corroded beam	14
B2Cl1	21.2	corroded beam	23
B2Cl2	21.2	corroded beam	26
B2Cl3	21.2	corroded beam	28
B2T2	21.2	non-corroded beam	26
B2T3	21.2	non-corroded beam	28

*Mser (kN·m): bending moment applied at the mid-span of the beams

6.3 Experimental program and experimental results

6.3.1 Observation of the corroded beams

According to previous observations on the beams [13], the first corrosion cracks appeared after 5 years of storage in the chloride environment, then cracks developed and spread all over the concrete cover as shown in Figure 6-1, including longitudinal cracks parallel to the tensile bars in the bottom section and the compressive bars in the top section, and transversal cracks along the stirrups in the middle area of the corroded beams. Some spalling also occurred at

the bottom of the middle zones for beams B2Cl2 and B2Cl3, which had been exposed for 26 and 28 years respectively. Detailed cracking maps, with the configuration and the widths of the cracks, can be found in previous papers about this programme [15].

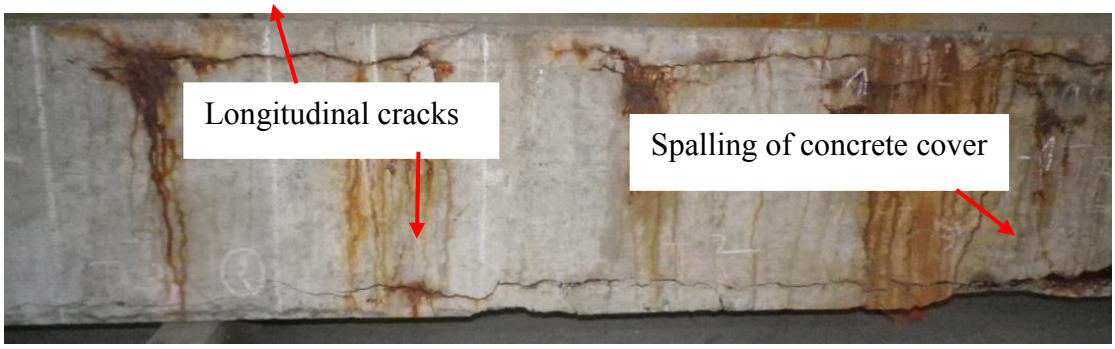

Figure 6-1 Visible damage due to corrosion for beam B2Cl2 at the age of 26 years

6.3.2 Mechanical experiment on the beams

All seven beams described in Table 6-1 were loaded under force control at different times in this programme. The mechanical experiments were carried out using a three-point loading system. During the test, the load was applied in a monotonic way until the beams failed. The deflections at mid-span of the beams were recorded by a linear variable differential transducer (LVDT) with an accuracy of 0.01 mm and a capacity of 100 mm.

All the beams failed in a bending mode. Nevertheless, there were some differences between the failure of corroded beams and non-corroded beams. As described by Castel et al. [16], corroded beam B1Cl1 failed due to the yielding and failure of the tensile bars, while both yielding of the tensile bars and the crushing of the compressive concrete led to the failure of non-corroded beam B1T1. The same failure mode was found in the other corroded and non-corroded beams that were loaded in the present work.

Figure 6-2 shows the failure of corroded beam B2Cl3 and non-corroded beam B2T2. Bending failure mode was modified by the corrosion of the reinforcements. Figure 6-2(a) shows that B2Cl3 failed with considerable spalling and even delamination of the concrete cover at the tensile section in the middle of the beam. Moreover, one of the corroded tensile reinforcements failed in the delamination zone. However, in the compressive section, only some small spalling zones were observed the compressive concrete cover. Figure 6-2(b) shows that the non-corroded beam B2T2 failed by crushing of the concrete and failure of a tensile bar.

(a) Failure of the corroded beam B2Cl3 due to tensile bar rupture

(b) Failure of the non-corroded beam B2T2 due to concrete crushing

Figure 6-2 Failure modes of the beams

6.3.3 Experimental results

The curves of force versus mid-span deflection for the corroded beams and non-corroded beams are shown in Figure 6-3. The capacity and ductility aspects of structural performance were quite different in the corroded beams and the non-corroded beams. The ultimate capacity of B2Cl3 was about 60% of that of the non-corroded beams B2T2 and B2T3. The mid-span deflection of the corroded beams was reduced by more than 50% as the corrosion of the reinforcement led to brittle behaviour. Moreover, the load-bearing capacities of all the non-corroded beams were almost the same while, for the corroded beams, the capacities were significantly reduced and varied from beam to beam. The detailed information about these results is shown in Table 6-2.

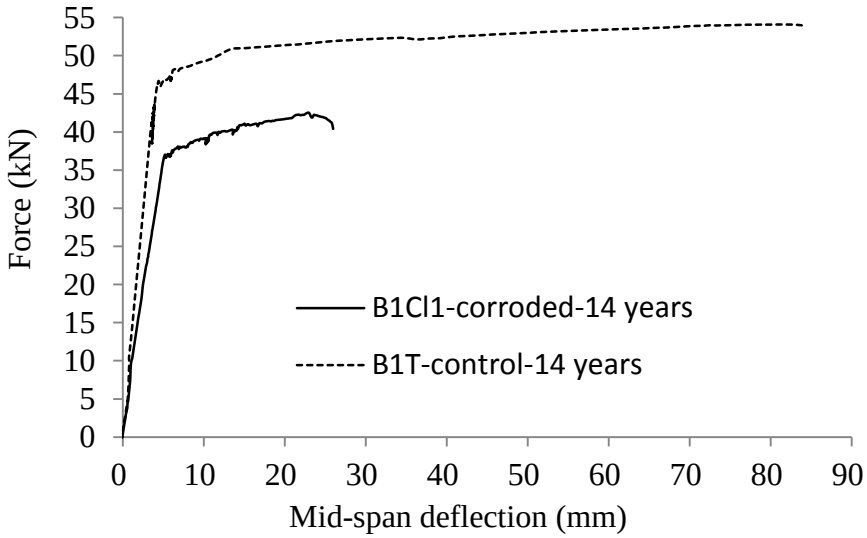

(a) Beams loaded at the age of 14 years

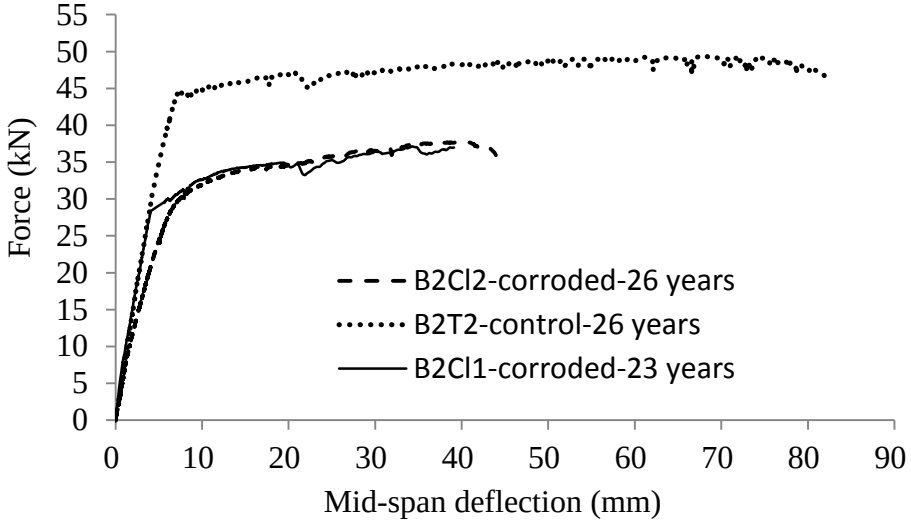

(b) Beams loaded at the ages of 23 and 26 years

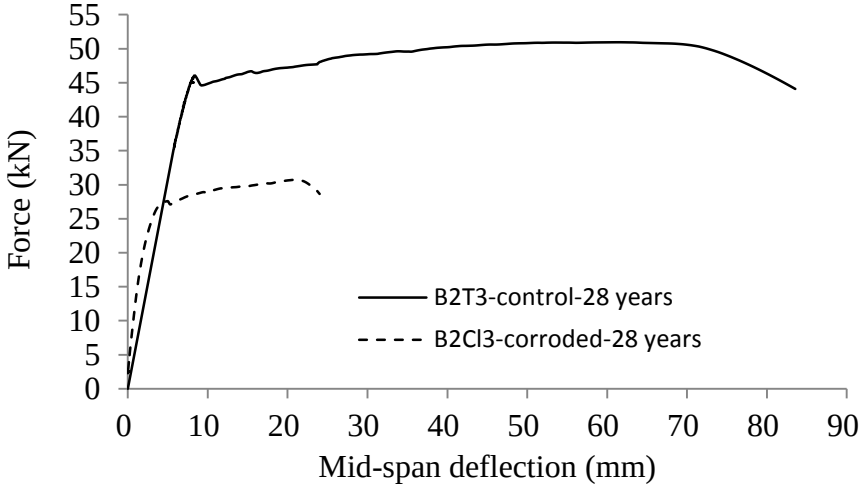

(c) Beams loaded at the age of 28 years

Figure 6-3 Load versus mid-span deflection for corroded and non-corroded beams

Table 6-2 Results of the bending experiments

Label	Yield capacity (kN)	Ultimate capacity (kN)	Elastic deflection (mm)	Ultimate deflection (mm)
B1Cl1	37.0	42.5	5.3	23.0
B1T1	43.8	54.1	3.9	80.8
B2Cl1	28.2	39.1	4.0	37.0
B2Cl2	30.0	37.1	6.3	39.4
B2Cl3	26.0	30.7	3.1	21.0
B2T2	44.1	49.4	7.1	79.8
B2T3	46.0	50.2	8.3	73.8

6.4 Influence of corrosion on structural performance

The structural performance of the corroded and non-corroded beams will be discussed in terms of residual cross-section of the reinforcement and corrosion time in this section. The residual cross-section is difficult to measure because of the irregular shape. A related work [17] discusses different measurement methods, such as investigating the residual diameter by vernier calliper, and by residual mass. Both measurements were made for the corroded bars. However, if the residual cross-section was obtained from the vernier calliper, only the cross-section hatched as in Figure 5-12 was considered, which would obviously overestimate the cross-sectional loss. Then the cross-sectional loss of the corroded tensile bars was deduced from the residual mass of the failure location, which had been cut into small pieces as short as 5 mm as shown in Figure 5-12, and the results were closer to the true residual cross-section. So, in the following section, the gravimetric residual cross-section of the corroded bars is used in the calculations concerning the corroded beams.

6.4.1 Influence of corrosion on yield capacity of the beams

The yield capacity of the seven beams is shown in Table 6-2. According to the tension experiments on the corroded bars from B2Cl2 at 26 years [18] and B2Cl3 at 28 years, the average value of yield strength of the corroded bars from the two beams was almost the same, which meant that the duration of corrosion had almost no impact on the yield strength of the corroded bars. So in the following calculation, the yield strength of the corroded bars of different ages was considered to have the same value. The yield strength of the tensile bars was assumed to have a normal distribution and the results are shown in Figure 6-4.

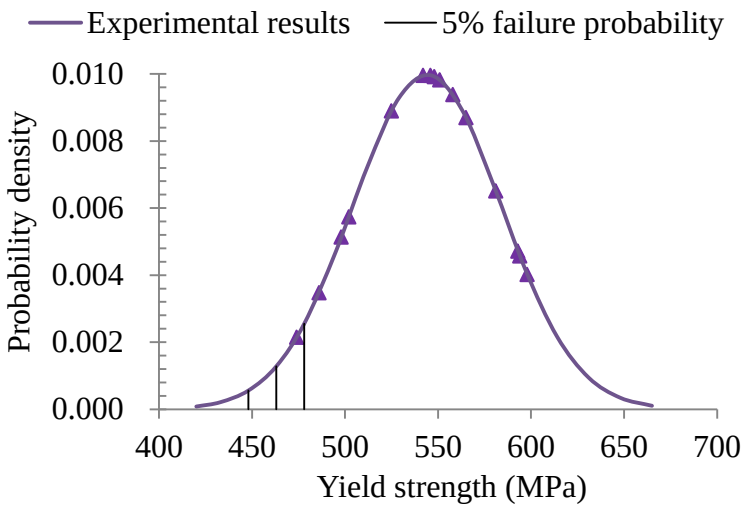

Figure 6-4 Yield strength distribution of the corroded tensile bars

The average yield strength of the corroded bars was 545 MPa, which was calculated from the gravimetric residual cross-section at the failure points. The characteristic yield strength of the corroded bars that corresponded to 5% failure probability according to the statistical analysis on the experimental results was found to be 480 MPa. The yield capacity of the corroded beams was deduced from the average yield strength and characteristic strength of the corroded bars. The results for the relative yield capacity of the beams in relation to the cross-sectional loss of corroded reinforcement are shown in Figure 6-5. It should be pointed out that the yield strength of the non-corroded steel bars was taken to be 560 MPa according to the tensile tests on the tensile bars from non-corroded beams. In Figure 6-5, the experimental results are indeed located in the interval of the results calculated using the characteristic yield strength and average yield strength of the corroded bars.

Figure 6-5 also shows the experimental reduction trend of the yield capacity of the corroded beams with increasing cross-sectional loss of the corroded tension bars. For example, the reduction of yield capacity of corroded beam B1Cl1 was about 19%, corresponding to 20% of the loss of cross-section of the tensile corroded bars, while for corroded beams B2Cl1, B2Cl2, and B2Cl3, the reduction of yield capacity reached respectively 37%, 33% and 42% with loss of 36%, 34% and 43% of the cross-section of the tensile bars. This means that, for the tensile bars, 1% loss of cross-section corresponded to about 1% reduction in the yield capacity of the corroded beams. As a result, the experimental reduction of the yielding capacity shows exactly the same trend as the theoretical reduction of yielding capacity (Figure 6-5).

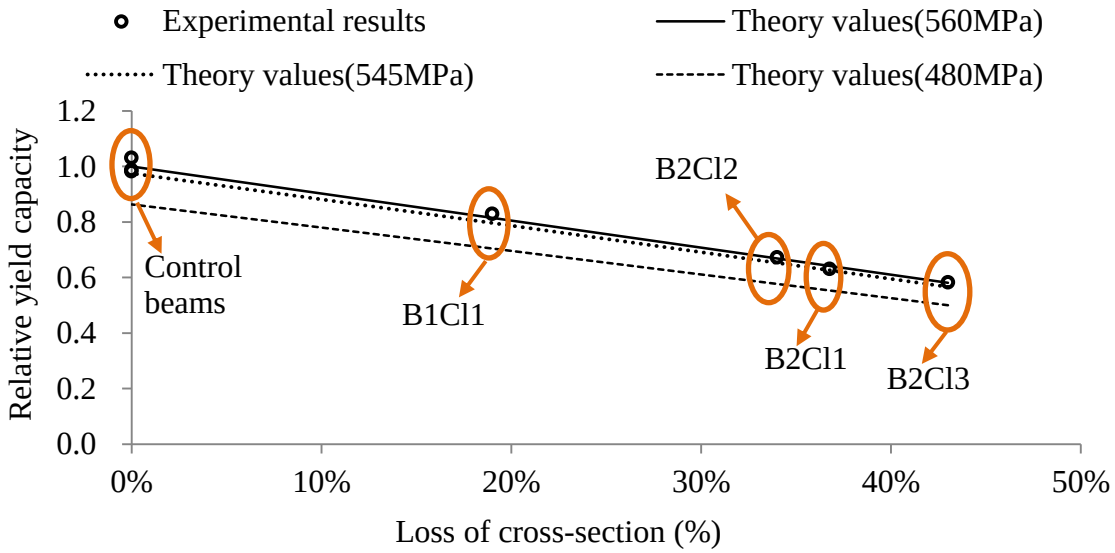

Figure 6-5 Relative yield capacity and cross-section loss of the tension bars

6.4.2 Influence of corrosion on ultimate capacity of the beams

According to the comparison of the experimental results for corroded bars from B2Cl2 and B2Cl3, the average value of ultimate strength was also similar for the two beams. The results of the two beams were analysed together. A normal distribution was assumed for the ultimate strengths of all the corroded bars, as shown in Figure 6-6.

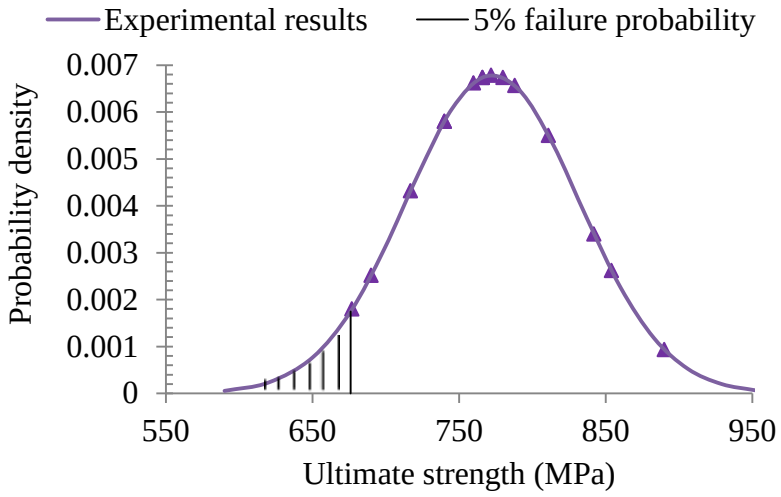

Figure 6-6 Ultimate strength distribution of the corroded tensile bars

According to Figure 6-6, the average ultimate strength of the corroded bars was 770 MPa, while the characteristic ultimate strength corresponding to 5% failure probability was 676 MPa. The characteristic and average ultimate strengths were applied to the corroded beams successively. According to the tensile experiment on the non-corroded bars, their ultimate strength was 620 MPa. The ultimate capacity of the corroded beams and the non-corroded

beams could be calculated by classical bending theories. The ultimate capacities from the experimental results of all the beams were compared with the calculated intervals as shown in Figure 6-7.

The decreasing trend of ultimate capacity of the corroded beams with increasing cross-sectional loss of the tension bars was almost the same as that of the yield capacity of the beams shown in Figure 6-5. The reduction of ultimate capacity was about 17% for B1Cl1 and about 30% for the other three corroded beams in Group B2. As a result, loss of 1% of the cross-section of tension bars corresponded to about 0.8% reduction in the ultimate capacity of the corroded beams.

As the beams were seriously corroded due to their long exposure to the aggressive environment, large cracks and even spalling appeared in the concrete cover. The ultimate capacity of the corroded beams was significantly reduced due to the corrosion of the tensile bars. Nevertheless, it should be noted that the ultimate capacity of all the corroded beams was still over the design load of 20 kN.

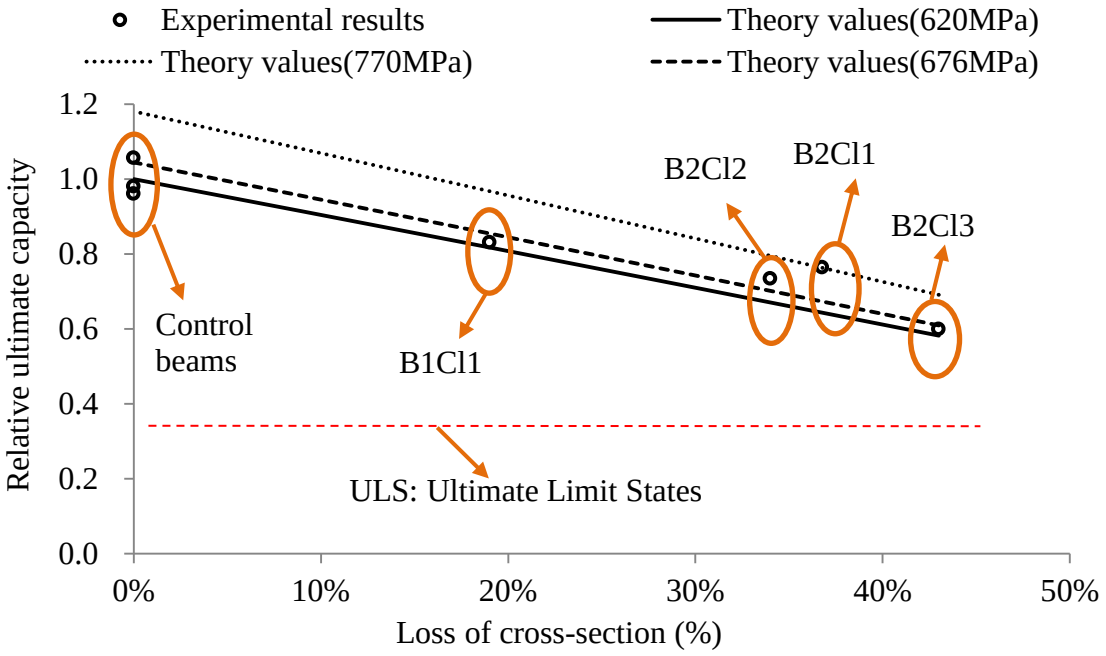

Figure 6-7 Ultimate capacity and the cross-sectional loss of the tensile bars

However, the experimental results were limited to only several beams investigated in this program. In order to make clear the corrosion influence on the load-carrying capacity of the corroded beam and the relationships with the variability of the predicted values, the experimental results of B2Cl2 and B2Cl3 were compared with the results from the previous literatures, including some other programs using corroded by impressed current to accelerate corrosion [8, 10, 19].

According to Torres-Acosta et al. [8], the pitting corrosion was found a good parameter to show the corrosion influence on the residual capacity ratio. The residual capacity ratio was used to study the influence of corrosion on the ultimate capacity of the beams. The relative ultimate capacity was defined as the ratio of ultimate capacity of the corroded beam and non-corroded beam. The average value was the relative ultimate capacity of corroded beams predicted by the average ultimate strength of the corroded tension bars. The characteristic value was the relative ultimate capacity of the corroded beams predicted by the characteristic strength of the corroded tension bars. The corrosion influence on the relative ultimate capacity was shown in Figure 6-8.

As shown in Figure 6-8, most of the experimental results were located between the zone of average value and characteristic value, which showed that the predicted values could well match the experimental results, not only the natural corroded beams but also the beams corroded by impressed current. Nevertheless, it should be pointed out that the results of Torres-Acosta's were over the zone of average value. The reason could be due to the calculation of corrosion degree which was deduced by the maximum pitting depth available in their paper. But for all other results, the corrosion degree was retrieved from the mass loss method. As discussed in previous literature [18], the corrosion degree deduced by the maximum pitting depth got from vernier caliper would overestimate the cross-section loss.

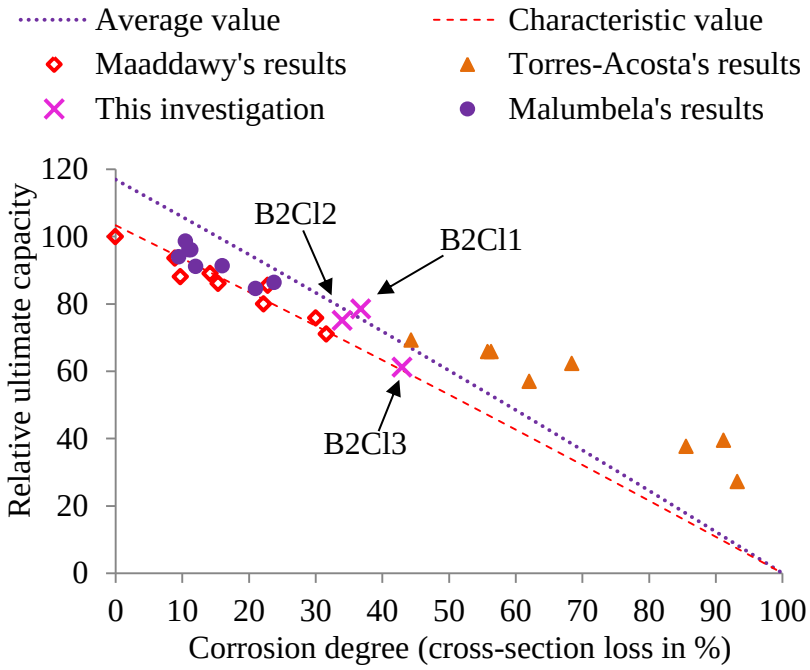

Figure 6-8 Comparison with other investigation results [8, 10 19, 20]

6.4.3 Influence of cross-sectional loss of tension bars on ductility of the beams

The ultimate strain was also extracted from the tensile tests of the corroded bars. The normal distribution of the ultimate strain is shown in Figure 6-9. According to the results, the average value of the ultimate strain was 0.0244. The characteristic ultimate strain corresponding to 5% failure probability was 0.0023.

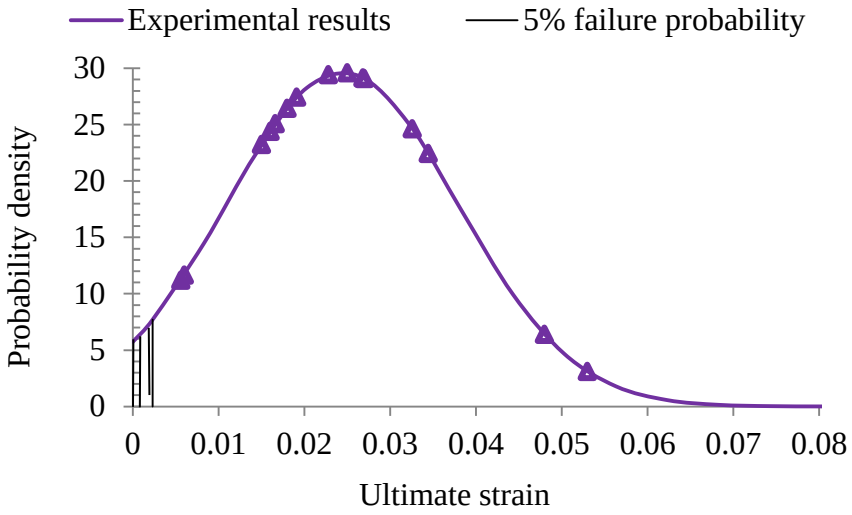

Figure 6-9 Ultimate strain distribution of the corroded tensile bars

The ultimate deflection of the beams was considered as an important index for judging the ductility behaviour of the corroded beams. The theoretical ultimate deflection can be deduced using the non-linear model of Vu et al. [21] at ultimate state. During the calculation, the ultimate strain of the compressive concrete was considered to be 0.0035. The ultimate strain of the non-corroded bars was 0.05. However, the ultimate strain of the corroded bars depended on the cross-sectional loss, which was retrieved from the relative tension tests on the corroded reinforcement of these beams as shown in Figure 6-10. Castel et al. [22] found that the relationship between ultimate strain of the corroded bars and the cross-sectional loss was exponential, as shown below:

$$\frac{\varepsilon_{ucorr}}{\varepsilon_u} = e^{-0.1c\%} \qquad (6\text{-}1)$$

Where:ε_{ucorr} is the ultimate strain of the corroded bar; ε_u is the ultimate strain of the non-corroded bar;c is the percentage cross-sectional loss. It should be noted that the ratio of the two ultimate strains should be no less than 0.2 (corresponding to c% >18%).

Figure 6-10 compares Castel et al.'s model and experimental results from the tensile test performed on re-bars extracted from beams B2Cl2 and B2Cl3. Because all bars tested had

corrosion damage higher than 18%, only the value of the model plateau (0.2 of the relative ultimate strain) could be compared to experimental results. The latter results were largely scattered and the average value was slightly higher that the model value of 0.2. Nevertheless, Castel et al.'s model was used to predict the deflection of beams at failure in relation with the corrosion damage of the reinforcement.

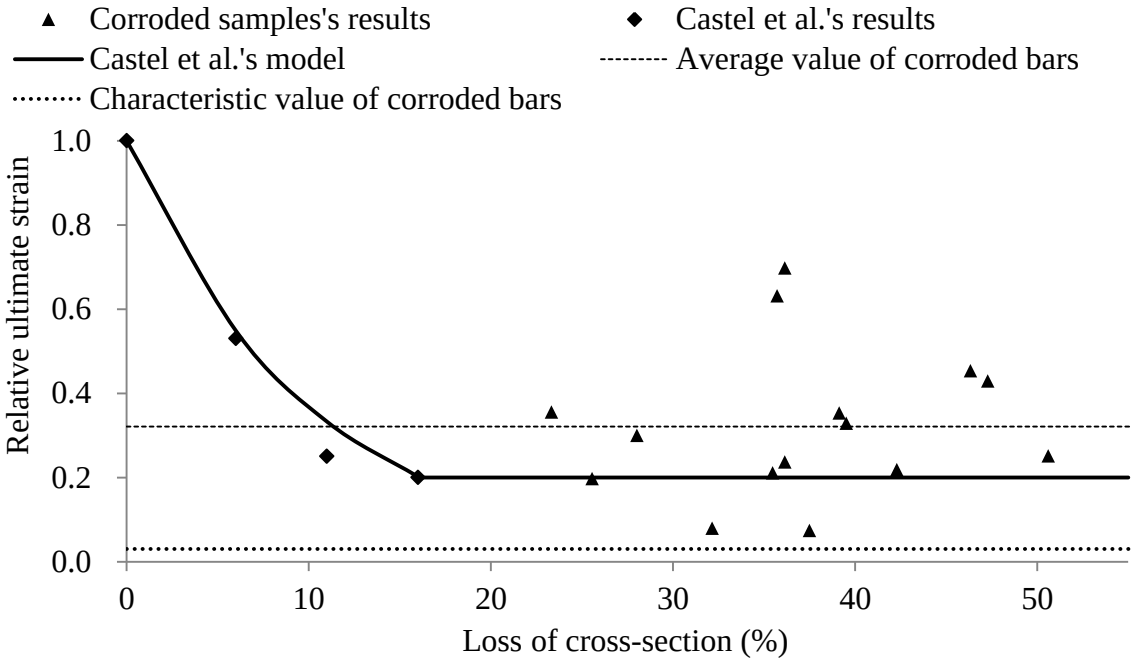

Figure 6-10 Relative ultimate strain of the bars compared to Castel et al.'s model[22]

From the non-linear behaviour of RC beams until failure described by Vu et al. [21], the deflection of the beams could be deduced from the ultimate strain of the concrete and the ultimate strain of the tensile bars. When the beam was assumed to fail due to compression of the concrete, the deflection of the beam could be calculated by the ultimate strain in the concrete of 0.0035. When the beam failed due to rupture of the tensile bars, the deflection of the beam could be calculated using the ultimate strain of the corroded tensile bars calculated from Castel et al.'s model. Moreover, the maximum beam deflection was also plotted according to the average experimental ultimate strain of 0.0244 and characteristic experimental ultimate strain of 0.0023 to compare with the experimental ultimate deflection of corroded beams. The relationships between the ultimate deflection of the corroded beams and the cross-sectional loss of the corroded tensile bars are shown in Figure 6-11.

Figure 6-11 shows that, using Castel et al.'s model, when the cross-sectional loss was smaller than 9%, the beams failed due to concrete crushing in the compressive zone. The experimental results for the control beams were a little higher than the calculated values. This may have been due to a higher ultimate strain of the concrete in compression because of the

long-term storage. However, the experimental results of the non-corroded beams still agreed well with the predicted results. The non-corroded beams failed because of crushing of the compressive concrete, followed immediately by failure of the tension reinforcement. As shown in Figure 6-11, when the cross-sectional loss of the tension reinforcement was higher than 9%, the corroded beams failed due to the rupture of the reinforcement. According to Castel et al.'s model, when the loss was over 18%, the ultimate deflection became relatively stable even though the cross-sectional loss of the tension reinforcement continued to decrease. This agreed well with the experimental results for the corroded beams as all the corroded beams failed by rupture of the tension bars in the bending tests with an ultimate deflection between 20 and 40 mm.

When the characteristic ultimate strain was adopted, the corroded beams failed through rupture of the corroded bars with a very limited ultimate deflection. However, when the average ultimate strain of the corroded bars was adopted, the beams failed due to concrete crushing if the cross-sectional loss of the tensile bars was smaller than 37%. When the cross-sectional loss of the tensile bars was over 37%, the beams failed due to rupture of the corroded tensile bars. The experimental results for the corroded beams were located within the intervals of the two models.

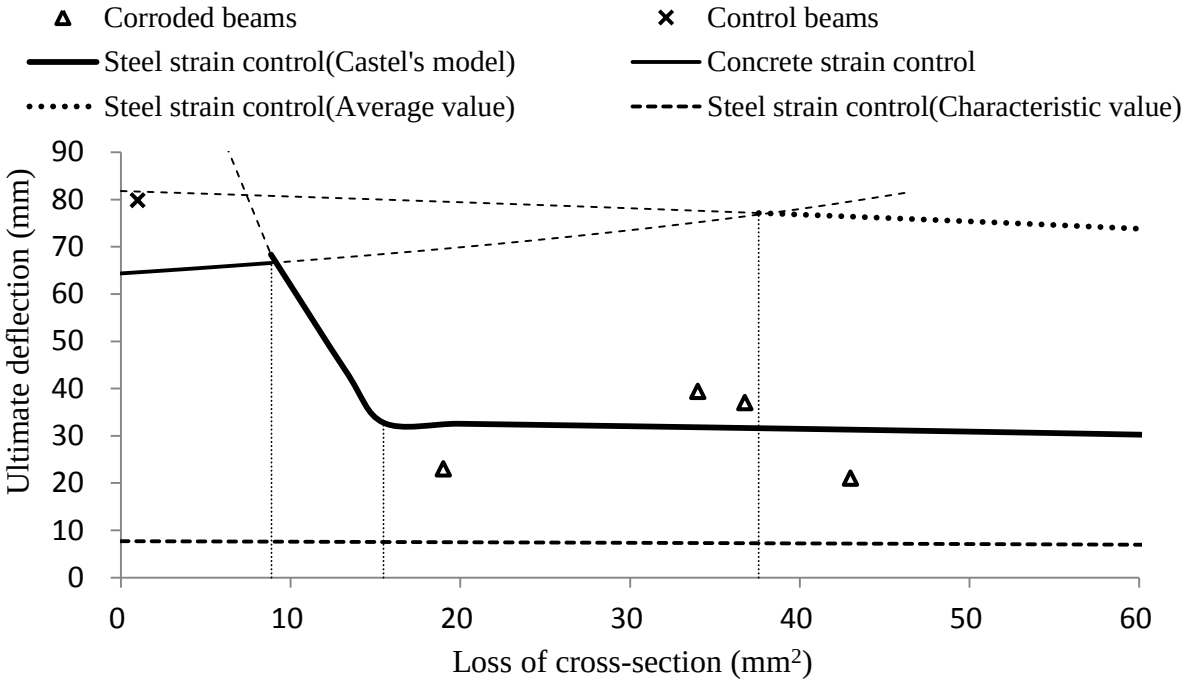

Figure 6-11 Ultimate deflection of the beams

The relative predicted ultimate deflection of the corroded beams was also used to compare with some other experimental results, including some other programs such as Maaddawy et

al. [19]. The results were shown in Figure 6-12.

According to Figure 6-12, the experimental results of most of the experimental results were located between the zone of characteristic value and average value when the corroded degree was larger than 8.8%. The results were still scattered through the trend of the results showed that the relative ultimate deflection decreased with the increase of the corrosion degree of the tension bars. However, the predicted zone of the ultimate deflection was still useful for the assessment of the existed corroded constructions.

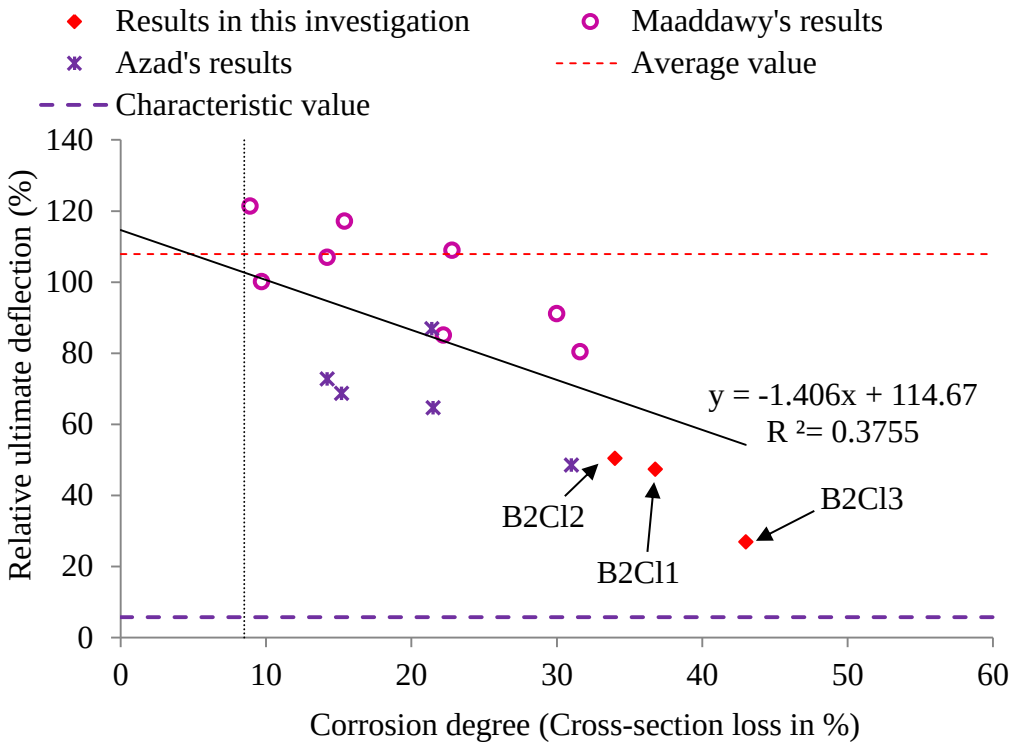

Figure 6-12 Comparison of experimental results with theoretical results [19]

The ductility index is the ratio of the total deformation at maximum load to the elastic limit deformation [23]. The deformation can be described in different ways. In this section, the deformation used is the deflection, and so the ductility index is defined as the ratio of the ultimate deflection over the deflection when the reinforcement yields. Figure 6-13 shows the influence of cross-sectional loss of the corroded tension bars on the relative ductility index, which was found from the ratio of the ductility index of the corroded beams to the average ductility index of the three non-corroded beams. The relative ductility index of the corroded beams was also reduced by the loss of cross-section of the tension bars. When compared with the ultimate deflection in Figure 6-11, the relative ductility index of the corroded beams was quite different. A possible explanation could be linked to the fact that both elastic deflection and ultimate deflection were reduced by the corrosion of the steel bars: for elastic deflection,

the steel cross-section was reduced by corrosion; for ultimate deflection, both steel cross-section and steel ductility decreased. In the ductility index calculation, both the numerator and the denominator decreased, which might give different results for the ductility index. As a result, the definition of ductility index may not be reliable to characterize the behaviour of corroded beams versus ductility. A new ductility index based on the ultimate deflection of corroded beams would be more accurate. More experiments and data from long-term corroded RC elements are still needed if a new ductility index is to be proposed.

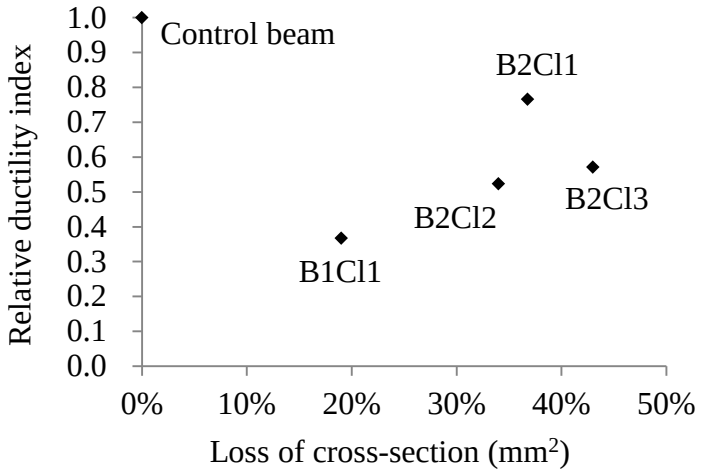

Figure 6-13 Relative ductility index of the corroded beams

6.5 Effect of corrosion duration

6.5.1 Cross-sectional loss in the reinforcement

The diameter losses of the tensile bars of all corroded beams are shown in relation to the corrosion duration in Figure 6-14, including pitting corrosion (the maximum loss) and general corrosion (the average loss of the whole tension bar). As discussed in previous literature on this programme [20], the initiation of corrosion in the tension bars was assumed to occur after about five years' exposure to the chloride environment, then the loss of steel bars increased gradually with the exposure time. In order to make the levels of corrosion of the tension bars clear, the theoretical corrosion of the reinforcement with current flow was also calculated by Faraday's law from the relationship between the corrosion period and the corrosion degree proposed by Rodriguez et al. [24].

$$\Phi=\Phi_0-\alpha\cdot 0.0115 I_{corr}\cdot t \qquad (6\text{-}2)$$

$$\Delta As(\%) = \left(1-\frac{\emptyset^2}{\emptyset_0^2}\right)\times 100\% \qquad (6\text{-}3)$$

Where: Φ is the residual diameter. Φ_0 is the nominal diameter. α is a coefficient. For general

corrosion, α=2 (in this case equation (5-2) corresponds to the model proposed by Andrade et al, [25]) while, for pitting corrosion, α ranges from 4 to 8. I_{corr} is the average value of the natural corrosion rate, which is usually assumed to be between 0.1-0.2 and 1–2 μA/cm^2 during time t (year).As shown in Figure 6-14, when I_{corr}=1.4 μA/cm^2, the calculated values of both the pitting corrosion and general corrosion match the experimental results for the corroded beams well.

According to the experimental results, the plots of the maximum cross-section loss and average cross-section loss versus the corrosion duration were close to straight lines. The most serious pitting corrosion developed at an average speed of about 1.85% maximum cross-section loss of the tensile bars per year.

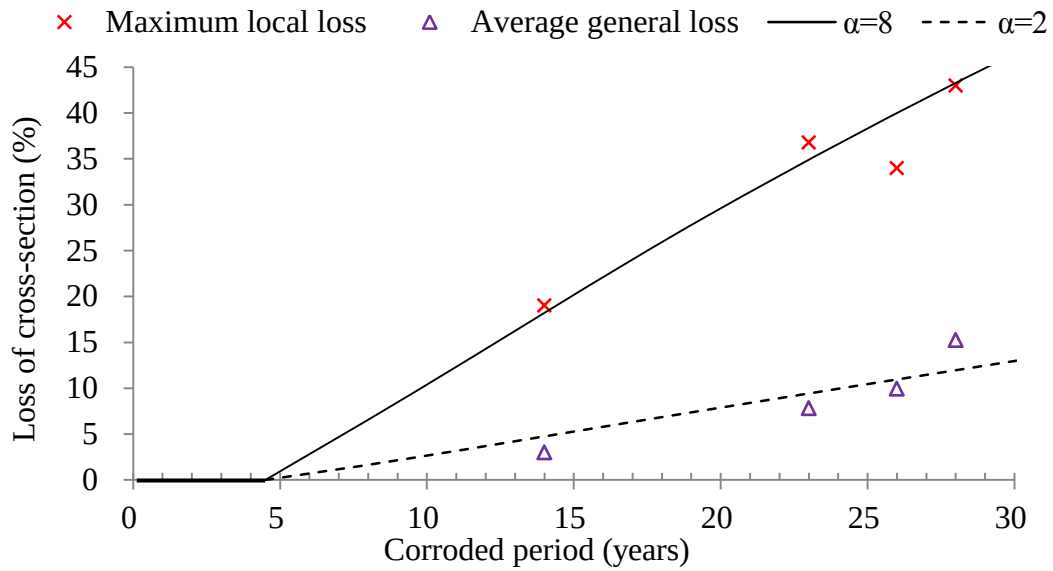

Figure 6-14 Diameter loss of the tension bars in relation to time with I_{corr}=1.4 μA/cm^2

6.5.2 Influence of corrosion period on capacity of the beams

The reductions of yield capacity and ultimate capacity of the corroded beams are shown in Figure 6-15. The first five years were assumed to be the initiation period for the corrosion cracking of the concrete cover. But it was necessary to point out that the initiate corrosion happened before the first corrosion crack. According to the program conducted at the moment, the initiation corrosion was supposed to happen at the 4.5th year. The corrosion speed between the period of corrosion initiation and the first corrosion crack was smaller than the corrosion speed after the cracking. However, as this period was relatively smaller than the whole corroded period, the corrosion speed in the following calculation was supposed to be constant

during the corrosion period. The yield capacity and ultimate capacity of the beams began to decrease from the 4.5th year, subsequent to the corrosion of the tension bars.

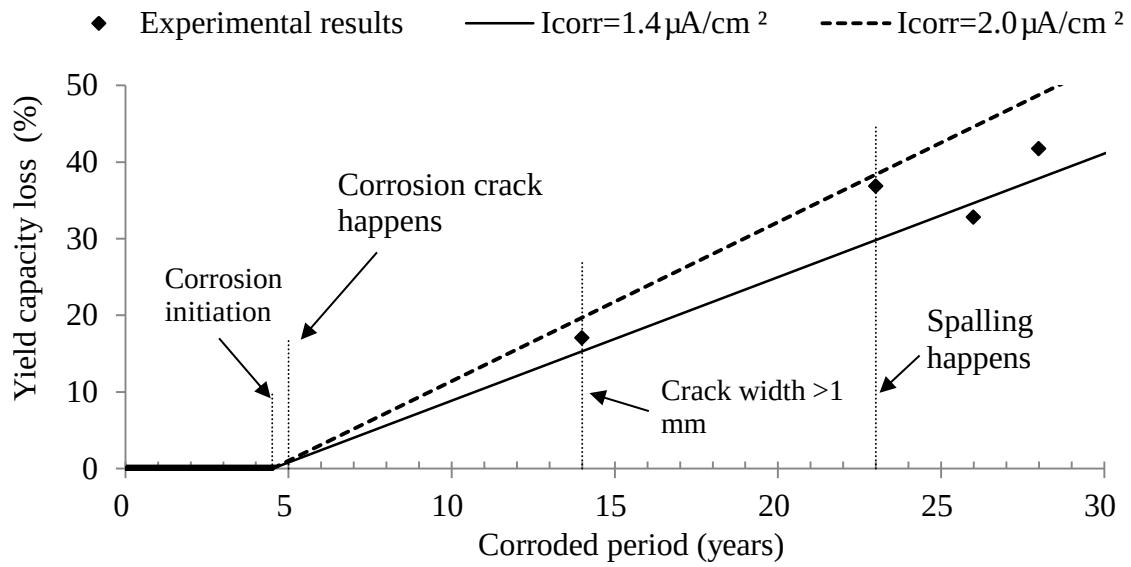

(a) Yield capacity reduction with corrosion duration

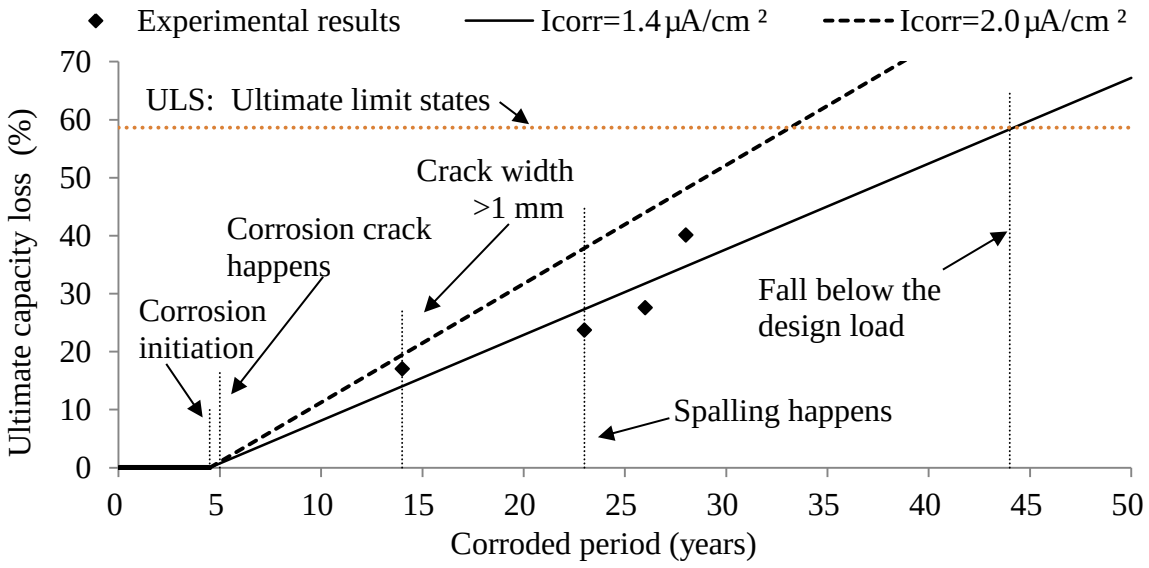

(b) Ultimate capacity reduction with corrosion duration

Figure 6-15 Reduction of yield capacity and ultimate capacity of the corroded beams

As shown in Figure 6-15, the loss of yield capacity of the corroded beams can also be estimated by Eq. (5-2). In the bending experiment, all the corroded beams failed, with the tensile bars ruptured in the mid-span. The failure points of the tensile bars were points of serious pitting corrosion. So in the estimation, α was assumed to be 8, and all the average values of yield strength and ultimate strength of the corroded bars were applied. The distributions of the yield capacity loss and ultimate capacity loss of the beams are shown in

Figure 6-15. All the experimental results are located below the values calculated with I_{corr}= 2 μA/cm^2. The experimental results are around the values calculated with I_{corr}= 1.4 μA/cm^2, which agrees with the conclusion of Figure 6-14 that I_{corr}= 1.4 μA/cm^2 would fit the experimental results best.

According to the experimental results, the beams in naturally corroded conditions were found follow the progression shown in Figure 6-15(b): the corrosion initiation began at the 4.5th year the corrosion cracks occurred at the 5th year; the corrosion crack width became larger than 1 mm at the 14th year; the spalling of concrete cover occurred at the 23rd year; and the ultimate capacity was thought to fall below the design load (ultimate limit state) at about the 44th year, which could be treated as the lifetime. It was worth noting that the lifetime was estimated by maximum cross-section loss of the tension bars and more experimental tests about long-term naturally corrosion were required.

6.6 Conclusion

The structural performance of four beams naturally corroded over a long time and three non-corroded beams was investigated in this section. The mechanical properties of the beams, including the yield capacity, the ultimate capacity and the ductility, were discussed in relation to the cross-sectional loss of the tensile bars due to chloride corrosion. The influence of the corrosion duration on the cross-sectional loss of the tensile bars and the ultimate capacity of the beams was also discussed. The following conclusions can be drawn:

(1) Loss of 1% of the cross-section of the tensile bars corresponds to about 1% reduction in yield capacity of the corroded beams. The ultimate capacity of the corroded beams was reduced significantly by the corrosion of the tension bar. However, it was still above the Ultimate Limit State of the beams despite the large cracks and spalling in the concrete cover.

(2) The maximum cross-sectional loss of the tensile bars was about 1.85% per year on average during the propagation phase of corrosion. The loss of ultimate deflection of the corroded beams was related to the loss of ductility of steel re-bars beyond a given loss of cross-section, which corresponded to a change in the failure mode from concrete crushing to steel bar brittle failure. For the beams presented, this threshold was 9%.

(3) In the very aggressive chloride environment, a simple calculation of maximum loss of cross-section versus time with I_{corr}= 2 μA/cm^2/year would allow a conservative estimation of the residual load-bearing capacity of the corroded beams.

6.7 References

[1] Page, C. L., Corrosion and its control in reinforced concrete, Sixth Sir Frederic Lea Memorial Lecture. *ICT Yearbook:* 1998-1999, Institute of Concrete Technology, Crowthorne, 1999, 37-51.

[2] Vu K. A. T., Stewart M. G., "Structural reliability of concrete bridges including improved chloride-induced corrosion models". *Struct safety*. 2000, 22(4): 313-33

[3] Raupach M., Chloride-induced macrocell corrosion of steel in concrete-theoretical background and practical consequences, *Construct Build Mater* 10(5), 1996, 329-38

[4] Mazars J., "A description of micro- and macroscale damage of concrete structures". *Eng Fracture Mechanics*. 1986, 25(5-6), 729-37

[5] Poupard O., L'Hostis V., Catinaud S., Petre-Lazar, E. "Corrosion damage diagnosis of a reinforced concrete beam after 40 years' natural exposure in marine environment." *Cem Concr Res*, 2006, 36(3), 504-20

[6] Broomfield J.P., Corrosion of steel in concrete, understanding, investigation and repair, (second ed.), *Taylor & Francis*, London (2007).

[7] Cairns J., Du Y., Law D., Structural performance of corrosion-damaged concrete beams, *Mag of concr res*. 2008, 60(5), pp.359-70

[8] Torres-Acosta A. A., Navarro-Gutierrez S., Terán-Guillén J., Residual flexure capacity of corroded reinforced concrete beams, *Eng Struct.* 2007; 29(6):1145-52

[9] El. Maaddawy T.; Soudki K., Effectiveness of impressed current technique to simulate corrosion of steel reinforcement in concrete. *J Mater in CivEng*, 2003; 15(1):41-7

[10] Malumbela G., Alexander M., Moyo P.. Variation of steel loss and its effect on the ultimate flexural capacity of RC beams corroded and repaired under load, *Construct Build Mater.* 2010; 24(6): 1051-9

[11] Ababneh A., Sheban M., Impact of mechanical loading on the corrosion of steel reinforcement in concrete structures, *Mater Struct*, 2011; 44(6): 1123-1137

[12] BS EN 1992-1-1 Eurocode 2, Design of concrete structures-Part 1-1 : General rules and rules for buildings, October 2005

[13] Vidal T., Castel A., François R., Corrosion process and structural performance of a 17-year-old reinforced concrete beam stored in chloride environment, *Cem Concr Res* 2007; 37(11) :1551-61

[14] Khan I.; François R., Castel A., Mechanical behaviour of long-term corroded reinforced concrete beam, *Modelling of corroding concrete structures* 2011; 5(10): 243-58

[15] ZHU W. J.; François R.; Coronelli D.; Cleland D., Effect of corrosion of reinforcement

on the mechanical behaviour of highly corroded RC beams, *Eng Struct,* 2013, 56, 544-54

[16] Castel A., François R., Arliguie G., Mechanical behaviour of corroded reinforced concrete beams—Part 1: experimental study of corroded beams, *Mater Struct*, 2000, 33(9): 539-44

[17] François R., Khan I., Dang V-H., Impact of corrosion on mechanical properties of steel embedded in 27-year-old corroded reinforced concrete beams, *Mater Struct*, 2013; 46(6), 899-910

[18] Zhu W. J., François, R., Effect of corrosion pattern on the ductility of tensile reinforcement extracted from a 26-year-old corroded beam, *Advances in Concrete Construction*, 2013, 1(2):121-37

[19] El Maaddawy T, Soudki K, Topper T. Long-term performance of corrosion-damaged reinforced concrete beams. *ACI Struct J*, 2005;102.

[20] Zhang R., Castel A., François R., Serviceability Limit State criteria based on steel-concrete bond loss for corroded reinforced concrete in chloride environment, *Mater Struct* 2009; 42(10):1407-21

[21] Vu N-A., Castel A., François R., "Response of post-tensioned concrete beams with unbonded tendon including serviceability and ultimate state", *Eng Struct,* 2010; 32(2) 556-69.

[22] Castel A., François R., Arligue G., Mechanical behaviour of corroded reinforced concrete beams—Part 2: bond and notch effects, *Mater Struct* 2000; 33(9):545-551

[23] Elchalakani M., Zhao X. L., Grzebieta R., Tests of cold-formed circular tubular braces under cyclic axial loading, *J Struct Eng*, ASCE, 2003; 129(4): 507-14

[24] Rodriguez J., Ortega L. M., Casal J., Diez J. M., Corrosion of reinforcement and service life of concrete structures, 7th International Conference on Durability of Building Materials and Components, Stockholm, 1996.

[25] Andrade A, Alonso C., Molina F.J., Cover cracking as a function of bar corrosion: Part I-Experimental test, *Mater Struct*, 1993, 26(8), 453-64

CHAPTER SEVEN

Mechanical performance of short-span beams

According to ACI 318-08 [1], deep beams are members loaded on one face and supported on the opposite face so that compression struts can develop between the loads and the supports, and have either: (a) clear spans, *l*n, equal to or less than four times the overall member depth; or (b) regions with concentrated loads within twice the member depth from the face of the support. However, Eurocode 2 [2] considers a member for which the span is less than 3 times the overall section depth as a deep beam. The member with the span between the deep beam and long beam is considered as short-span beams. Based on the Eurocode 2, this chapter mainly studies the residual mechanical performance of short-span beams.

This chapter describes an experimental investigation of the behaviour of corroded reinforced concrete short-span beams. These have been stored in a chloride environment for a period of 26 years and 28 years under service loading so as to be representative of real structural and environmental conditions. The corroded beams were tested until failure by a three-point loading system. Another four beams of the same age but without corrosion were also tested as control specimens. A short-span arrangement was chosen to investigate any effect of a reduction in the area and bond strength of the reinforcement on shear capacity. The relationship of load and deflection was recorded so as to better understand the mechanical behaviour of the corroded beams, together with the slip of the tensile bars. The residual mechanical behaviour of the beams is evaluated with the mechanical properties of the bars and the residual cross-section by different theories. The results show that the corrosion of the reinforcement in the beams induced by chloride has a very important effect on the mechanical behaviour of the short-span beams, as loss of cross-sectional area and bond strength have a very significant effect on the bending capacity. The failure mode of the short-span beams was changed gradually with the increase of the corrosion degree of the reinforcement.

7.1 Introduction

The problem of the deterioration of reinforced concrete structures due to chloride-induced corrosion of the steel reinforcement is considered one of the most important factors for the durability of reinforced concrete structures and has drawn great attention all over the world [3-6]. The major effect of the corrosion process is the formation of rust, whose volume is greater than steel (from two to six times depending on environmental conditions) [7] and this results in cracking and spalling of the concrete, which can influence various characteristics such as the mechanical performance and load capacity of the concrete structures.

Most experimental research deals mainly with the effect of steel corrosion on the flexural behaviour of reinforced concrete elements [8-11], in contrast little research has been done about the influence of corrosion on the shear behaviour of corroded reinforced concrete beams. Xia et al. [12] have studied the effect of the corroded stirrups on the shear performance of reinforced concrete beams and found that the shear failure mode of the beams could change from concrete crushing to stirrup failure with the increase of the corrosion level of the tension bars. Wang et al. [3, 13] have carried out some research on the impact of partial length corrosion on shear behaviour of reinforced concrete beams. Cairns [14] studies the shear capacity of RC beams which are corroded in different parts of the longitudinal reinforcement and suggests that the shear capacity of the corroded beams is increased when the reinforcement is exposed in all but the most lightly reinforced sections. Higgins et al. [15] investigate the impact of corrosion of stirrups on the shear capacity of the corroded RC beams and indicate that corrosion reduces shear capacity and overall deformation of the corroded beams.

However, most of these tests were carried out on beams subjected to accelerated corrosion due to an impressed electrical current and therefore the results may not be representative of concrete structures in service. Also it is difficult to find the relationship between the current-induced corrosion and the natural corrosion, which reduces the applicability of the research results.

7.2 Experimental tests on the corroded beams

This research program was mainly based on the four short-span beams obtained from beam B2Cl2 and B2Cl3. Bending tests had been carried out on Beams B2Cl2, B2Cl3, B2T2 and B2T3 at a 2850mm span. Bending failure occurred in the middle of the span as discussed in Chapter Five. Subsequently the residual beams were divided into two short-span beams

B2Cl2-1, B2Cl2-2, B2Cl3-1, B2Cl3-2, B2T2-1, B2T2-2, B2T3-1 and B2T3-2 as shown in Figure 7-1 by sawing to remove the middle cracked portion. The load tests were carried out on these short-span corroded beams directly once they were formed after sweeping the middle sections of the long-span beam, together with the two non-corroded beams. More detailed information about the short-span beams was shown in Table 7-1

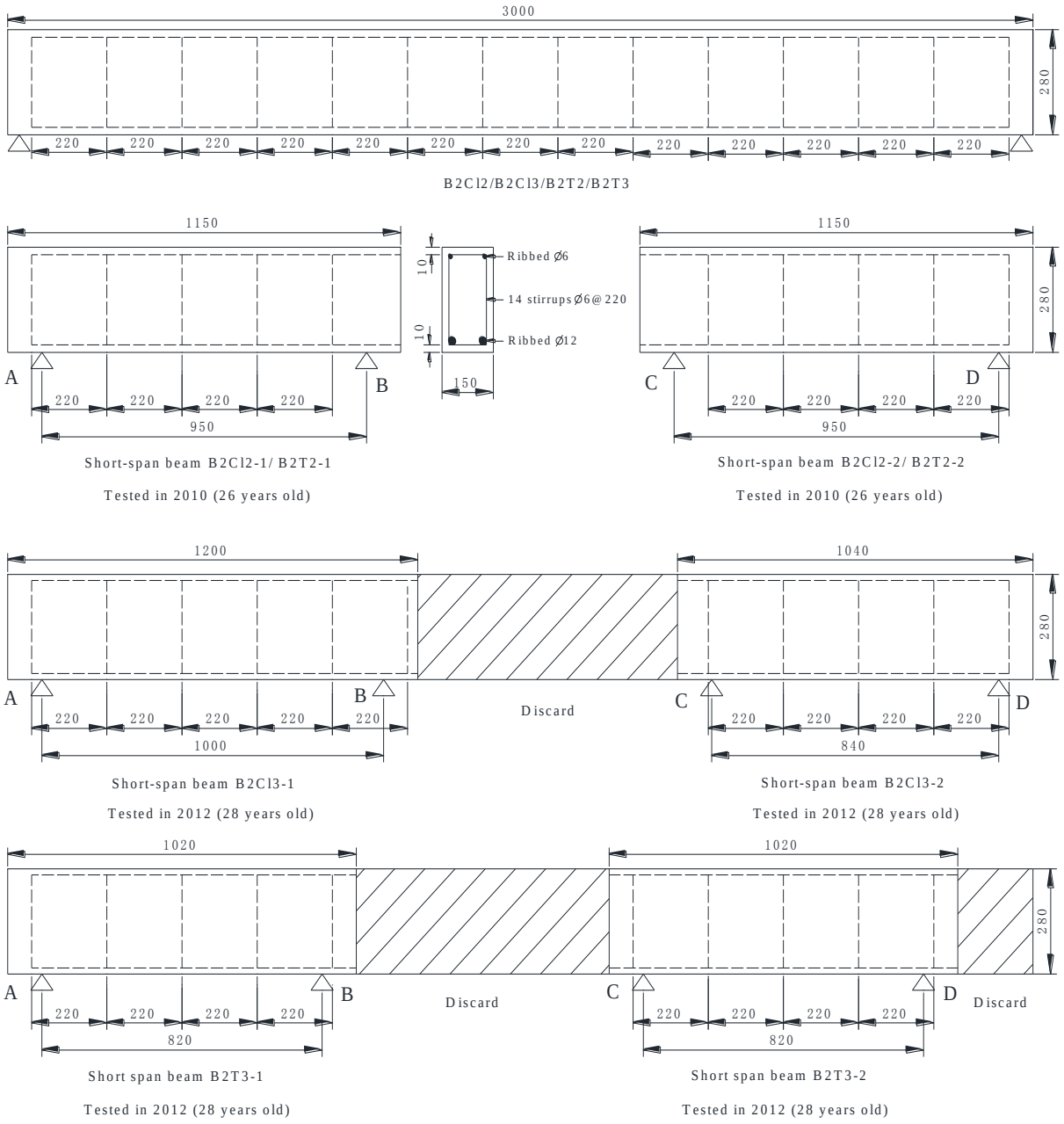

Figure 7-1 Layout of the reinforcement for the target beams (mm)

Table 7-1 Detailed information about the short-span beams

Beams	Age (years)	Length (mm)	Net span (mm)	Shear span to depth ratio	Status	Note
B2Cl2-1	26	1150	950	1.84	Corroded	According to Eurocode 2 [2], they belong to short-span beams
B2Cl2-2	26	1150	950	1.84	Corroded	
B2T2-1	26	1150	950	1.84	Non-corroded	
B2T2-2	26	1150	950	1.84	Non-corroded	
B2Cl3-1	28	1200	1000	1.94	Corroded	
B2Cl3-2	28	1040	840	1.63	Corroded	
B2T3-1	28	1020	820	1.59	Non-corroded	
B2T3-2	28	1020	820	1.59	Non-corroded	

7.2.1 Test arrangement and mechanical response of the beams

The load tests on the short-span beams were performed by increasing the mid-span load monotonically up to failure (Figure 7-2 and Figure 7-3). The load and deflection at the mid-span of the beams were recorded throughout the loading process, the latter by a linear variable differential transformer (LVDT) with an accuracy of 0.01mm.

During the load test, four other LVDT's were fixed at the ends of the concrete beam so that the sensor touched the ends of the bottom bars in Figure 7-2, where support A and support D correspond to the two ends showed in Figure 7-3, in order to obtain detailed information of the slip behaviour of the bars. For these sensors, the accuracy was $1x10^{-4}$ mm. At the end which was not sawn a small hole was drilled in the concrete so that the LVDT's could be located on the end of the reinforcing bar.

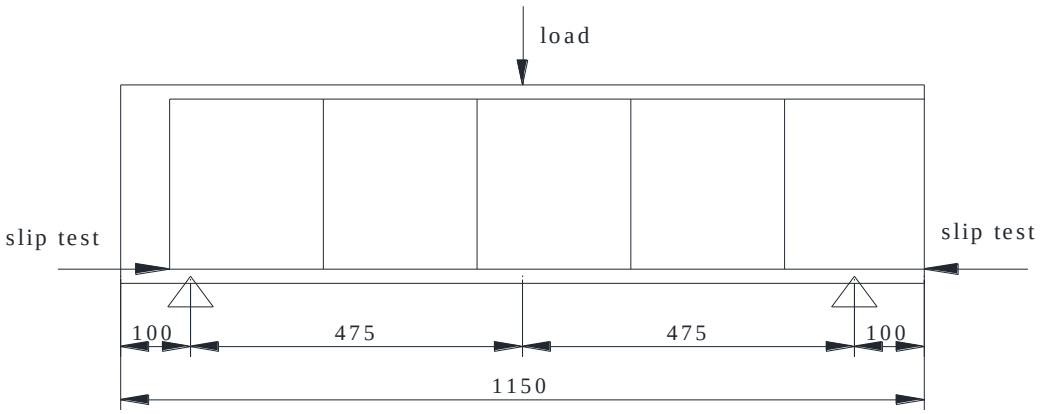

Figure 7-2 Three-point loading system and slip test

Figure 7-3 Support A/D

7.2.2 Mechanical response of the short-span beams

The behaviour under load and the failure modes of the corroded beams were different from those of the non-corroded beams. For the non-corroded beams without any previous damage, the first cracks appeared on the side faces of the beam. These were either vertical or inclined at a slight angle and started at the bottom close to mid-span and progressed upwards toward the location of the applied load. The failure of non-corroded beams B2T2-1 and B2T2-2 were shown in Figure 7-4. All the cracks propagated in both width and length, and then one main crack was formed, extending from the bottom of the beam to the loading point. With the crack widening progressively, failure occurred quite suddenly with the inclined crack opening wide. Surprisingly all of the main cracks appeared in the half of the beam with more stirrups. In Beam B2T2-2, simultaneously there was rupture in one of the main tension bars and two vertical legs of the stirrup, the latter close to the tension bar (Figure 7-5).

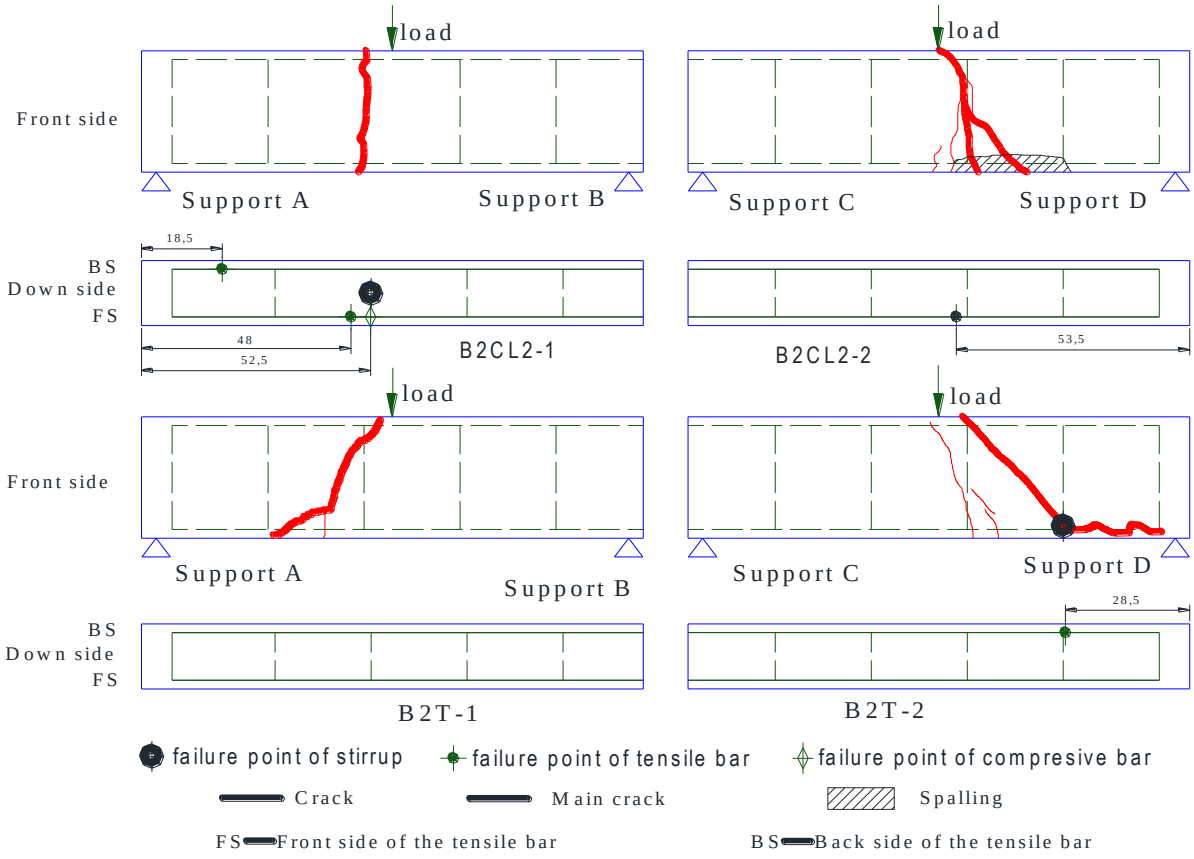

Figure 7-4 Failure points and the main cracks of the tests

Figure 7-5 Failure point of the stirrup of the non-corroded beam (B2T2-2)

Similarly, the non-corroded beams B2T3-1 and B2T3-2 behaved also brittle in the loading process. As shown in Figure 7-6, several inclined cracks appeared in the tension zones when the load was applied to the beam. With the load increased, the cracks climbed to the loading location at the compressive zone gradually, and the cracks got wider significantly. Finally, the

tension bars failed, leading to the rupture of beam B2T3-1. The failure points of the tension bars were not at the middle of the beam. It was at the root of the inclined cracks as Figure 7-6(a). As for B2T2-2, one stirrup failed as shown in Figure 7-6(b), which was also at the root of the inclined crack. No matter the beam failed due to the rupture of neither the tension bars nor the stirrup, all non-corroded beams were broken in shear failure mode.

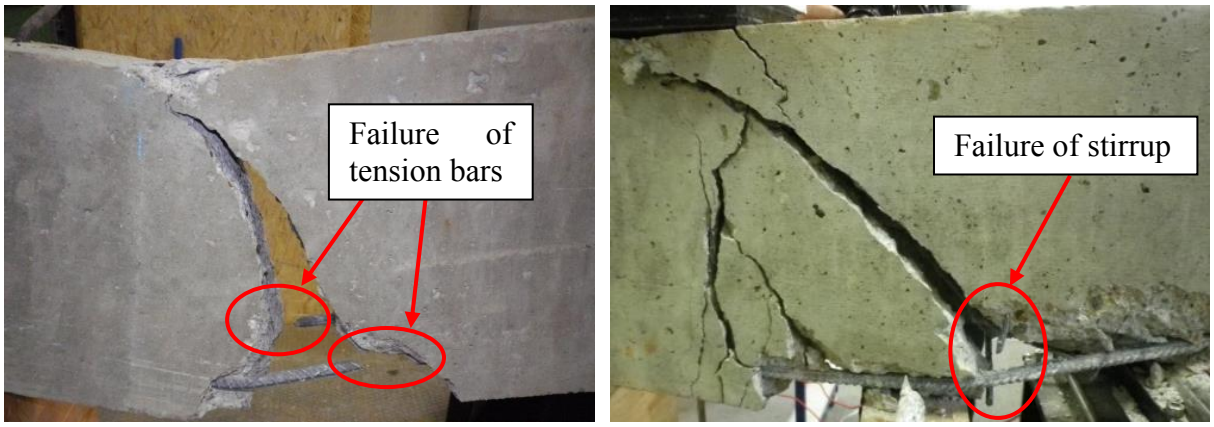

(a) Failure of non-corroded beam B2T3-1 (b) Failure of non-corroded beam B2T3-2

Figure 7-6 Typical rupture of short-span non-corroded beams

For the corroded beam B2Cl2-1, B2Cl3-1 and B2Cl3-2, the main crack was almost vertical along a stirrup nearest to the loading point, i.e. at mid-span of the short beam. The crack developed gradually from the bottom towards the top of the beam. As failure approached, the rate of deflection with load increased due to yielding of the tensile bars. Beam B2Cl2-1 failed due to the rupture of the two tension bars: one at the mid-span of the beam then followed by the failure of the other bar near the support (Figure 7-4 and Figure 7-7).

For the corroded beam B2Cl2-2, the main cracks divided into two branches on the sides of the beam. One crack inclined gradually in the diagonal direction at first, while with the load increasing, another transverse crack appeared gradually, parallel to the stirrup in the middle of the span. As the load increased, the concrete cover to the bottom reinforcement became delaminated from the parent concrete as illustrated in Figure 7-4. At last, the beam failed when the front side tension bar ruptured at the mid-span (Figure 7-4). It was worth noting that for the corroded beams B2Cl3-1 and B2Cl3-2, the tension bars failed at the mid-span, which was the characteristic of the bending failure mode.

(a) Failure of corroded beam B2Cl3-1

(The middle bar is designed to be the handle)

(b) Failure of corroded beam B2Cl3-2

(c) Failure of tension bar of B2Cl3-2

Figure 7-7 Failure of corroded beams due to bending(rupture of tension bar at mid-span)

As a result, it should be pointed out that all the corroded beams were in bending failure mode with tension bars failed. The rupture of tension bars near the mid-span showed that the post-yielding behaviour played a dominant role in the mechanical test of the corroded beams, and they finally failed after the beam had deflected considerably. The detailed information about the mid-span deflections of the beams was recorded together with load; the load-deflection curves are shown in Figure 7-8.

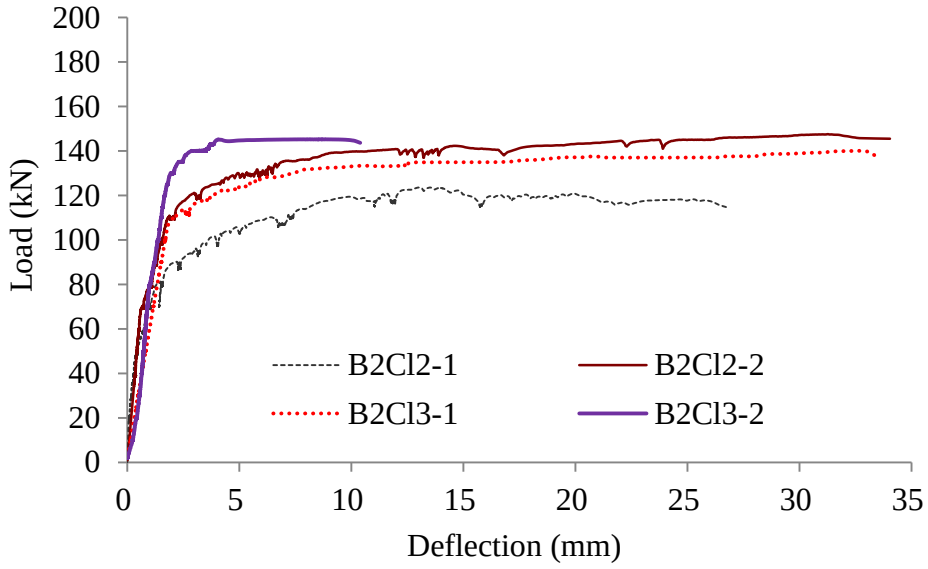

(a) Results of corroded short-span beams

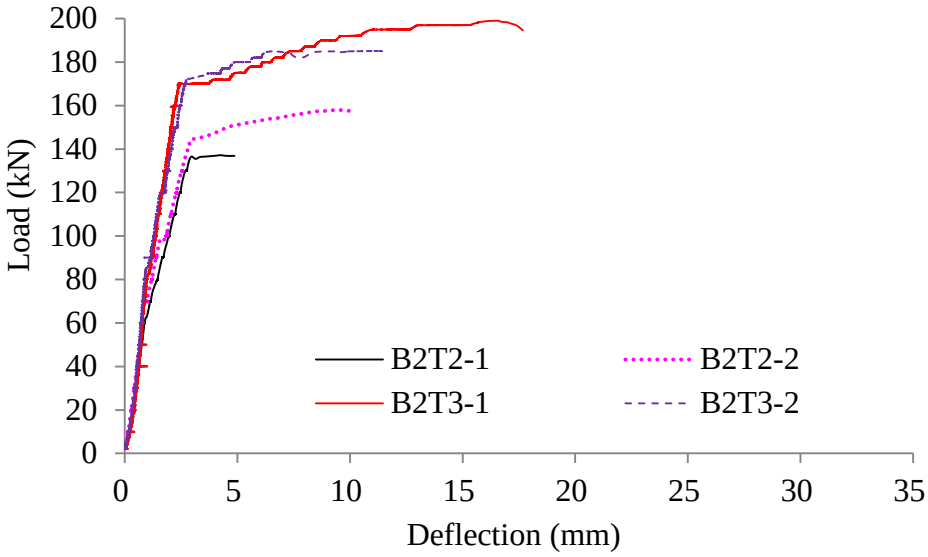

(b) Results of non-corroded short-span beams

Figure 7-8 Load-deflection curves of short-span bending tests

Surprisingly, the non-corroded beams exhibited less ductility than the corroded beams. This was illustrated in Figure 7-8 where the onset of yielding was clearly visible but the development of strain hardening of the reinforcement was shortened for all non-corroded beams. A possible explanation for this is that shear failure took place just after yielding of the longitudinal reinforcement. Another aspect which applied in the case of B2T2-1 was that the steel knife-edge load was acting on the beam directly without plate to transfer the load. As a result, the load was more concentrated and may have made a difference between the responses with other non-corroded beams. In the other non-corroded beams and corroded beams a steel plate of 150mm length and a rubber strip were used to transfer the load.

For the corroded beams, there was a considerable degradation of concrete cross-section (spalling, cracking), a loss of cross-section for longitudinal bars (tension and compression) and for stirrups. Usually the corrosion was assumed to lead to a more brittle behaviour of corroded RC elements. But as shown in Figure 7-4, the degradation due to corrosion led to an increase of ductility but with a small reduction in the ultimate capacity. When the corroded beams reached the yield point, the capacity still increased gradually with the development of large deflections until failure, which showed that the corroded beams retained good post-yielding characteristics while the increase of the capacity for the non-corroded beams was quite limited once the yield point was achieved.

These surprising results could be explained by a change in failure mode. Indeed, if a nonlinear model was used to compute the ultimate deflection of a short span beam in bending failure mode [16], 72 mm with a steel elongation of 7% corresponding to ultimate strain of steel bars would be found. Then the same model applied to the corroded beam taking into account the loss of cross-section and the reduction of ultimate strain at 3.5% would lead to an ultimate deflection of 36 mm which was closed to the experimental one. Thus the loss of steel ductility would lead to a loss of beam ductility for the same failure mode. However, the difference of failure mode between the corroded and non-corroded beams, i.e., bending versus shear, meant a more brittle behaviour of non-corroded beam even though the steel bars were more ductile. Nevertheless, for the non-corroded beams the failure mode involved interaction between flexure and shear, not untypical of short-span beams. For example yielding of the reinforcement began to take place but before strain hardening could develop shear failure occurred in the reduced compression zone. However with advanced corrosion the flexural capacity is reduced more than the shear capacity so that the failure mode changes to pure flexure.

The mechanical properties of all the short-span beams were extracted from the load-deflection curves of Figure 7-8 and sorted out in Table 7-2. The influence of the net span on the mechanical capacity of the non-corroded beams was more obviously than that of the corroded beams. Nevertheless, more information about the corrosion degree of the tension bars would be required in order to further identify the mechanical performance of the short-span beams.

Table 7-2 Results of the mechanical experiments on the short-span beams

Label	Net span (mm)	Yield capacity (kN)	Ultimate capacity (kN)	Deflection (mm)	Failure mode
B2Cl2-1	950	88.0	123.0	26.3	Bending
B2Cl2-2	950	110.0	148.0	34.0	Bending
B2T2-1	950	137.0	138.0	4.87	Shear
B2T2-2	950	145.0	159.0	9.77	Shear
B2Cl3-1	1000	113.8	140.2	33.3	Bending
B2Cl3-2	840	140.1	145.3	10.16	Bending
B2T3-1	820	170.1	199.0	16.6	Shear
B2T3-2	820	172.3	185.1	11.4	Shear

7.2.3 Slip of the tensile bars

The slips of the tension bars during the loading process on the beams were recorded by four LVDTs with an accuracy of 10^{-4} mm. The slip-force curves were made to show the process of the tension bars during the whole loading test. Figure 7-9 shows the curves of the corroded beams and Figure 7-10 shows the results of the non-corroded beams with the age of 26 years and 28 years old. The supports A, B, C, D stands for the ends of the beams which are shown in Figure 7-1. BS is short for the back side tension bar of the short-span beam. FS is short for front side tension bar of the short-span beams. For example, the legend BS Support A means the slip of the back side tension bar at the location near the support A.

According to Figure 7-9 and Figure 7-10, there were almost no slips for most of the corroded beams and non-corroded beams in the loading process except for B2Cl2-1 and B2T3-2. Slips of the tension bars only happened when the load reached the ultimate capacity, but the value was still very small even the short-span beams ruptured. This phenomenon supported the conclusion that the bond between the tension bars and concrete was still strong enough in the loading performance even though the beams were highly corroded and spalling occurred to some zones of the concrete cover.

However, it should be pointed out that the slip of B2Cl2-1 was due to the large spalling of the concrete cover near support B and almost extended throughout the length of the short-span beam as shown in the cracking map of B2Cl2 in Figure 5-4. According to Figure 7-9(a), the slip of tension bars occurred when the load reached 80 kN, which was coincided with a change in slope of the load-deflection curve of B2Cl2-1 in Figure 7-8(a). The slip increased rapidly which could also have contributed to the ultimate deflection of the beam. In spite of

the slip, the load which the beam was able to support increased slightly in a manner similar to the other corroded beams. Therefore, even with extensive spalling in the concrete cover there appeared to be sufficient anchorage to allow the corroded beam behave in a ductile mechanical performance.

Moreover, the slip of the front side tension bar near support C of B2T3-2 was relatively larger than that of the other results of non-corroded beams. It could be due to the damage of concrete cover near support C when the short-span beam was cut from the original beam as was shown in Figure 7-11.

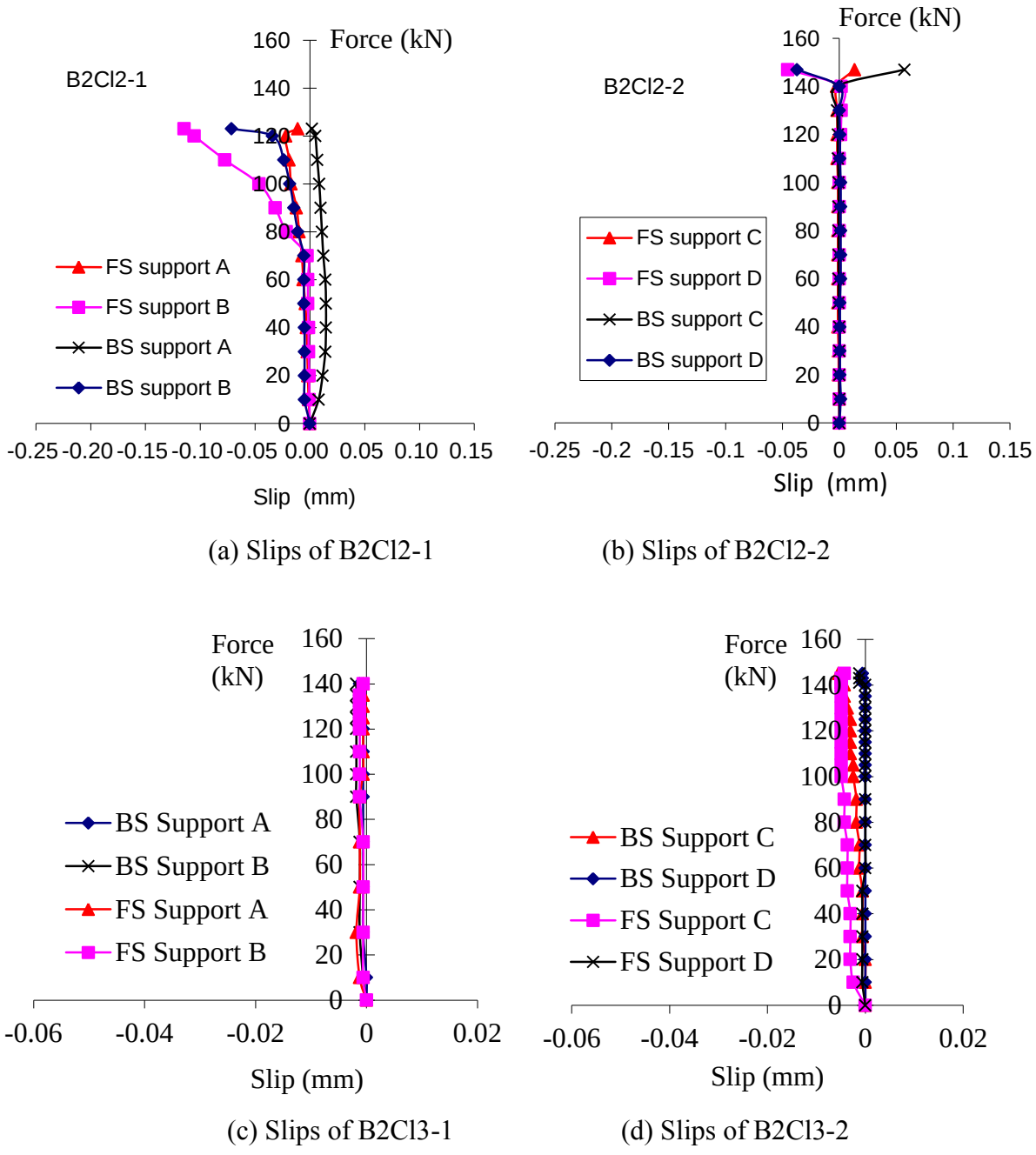

(a) Slips of B2Cl2-1 (b) Slips of B2Cl2-2

(c) Slips of B2Cl3-1 (d) Slips of B2Cl3-2

Figure 7-9 Load-slip behaviour for mechanical tests of the corroded beams

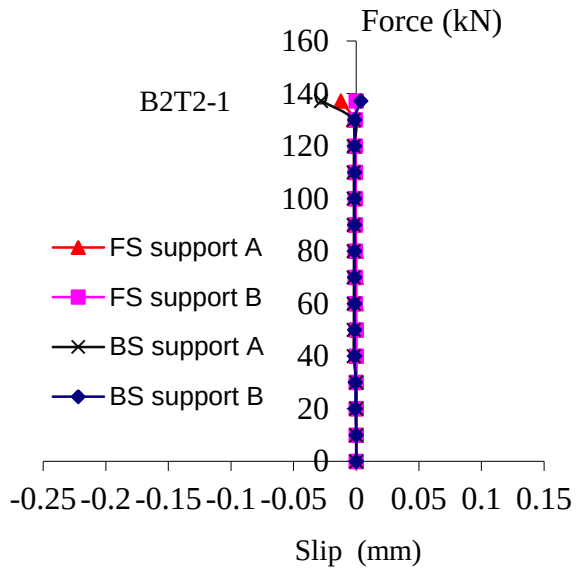

(a) Slips of B2T2-1

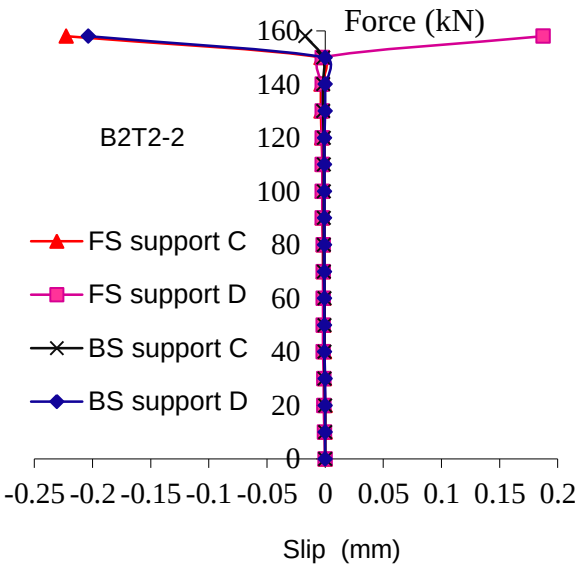

(b) Slips of B2T2-2

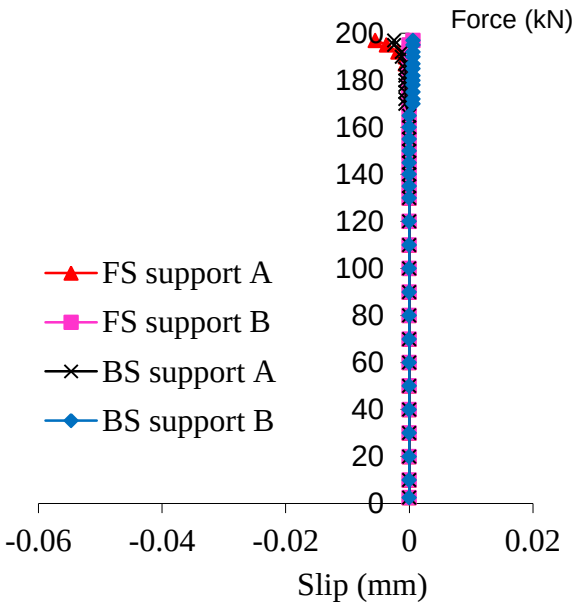

(c) Slips of B2T3-1

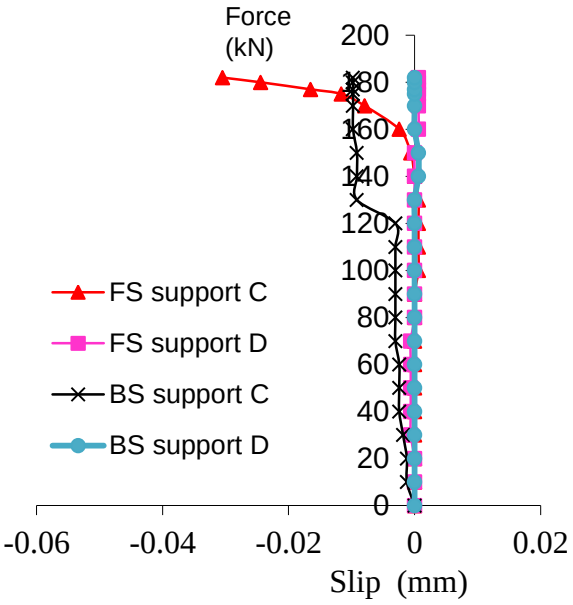

(d) Slips of B2T3-2

Figure 7-10 Load-slip behaviour for mechanical tests of the non-corroded beams

Figure 7-11 Damage of FS support C of B2T3-2

7.3 Discussion

The mechanical properties of the corroded bars were discussed in Chapter Four (previous literature [17]). The average results of the tension tests on the tension bars abstracted from the beams B2Cl2, B2Cl3, B2T2 and B2T3 were used to the calculation of the yield capacity and ultimate capacity of the short-span beams. Based on the previous research work, the yield strength of the corroded tension bars was considered to be 560 MPa, and the ultimate strength of the corroded bars was 770 MPa. While for the non-corroded bars, the yield strength and ultimate strength were 560 MPa and 620 MPa respectively.

7.3.1 Analytical model introduction

As the corroded beams and non-corroded beams failed in different failure mode, the yield capacity and ultimate capacity of all the short-span beams would be deduced in different ways. According to the experimental tests, the corroded short-span beams failed in bending failure mode, the yield capacity and ultimate capacity of the corroded beams were predicted by classical bending theory based on Eurocode 2 [2]. The non-corroded beams failed in shear failure mode. As a result, the capacities of the non-corroded beams were predicted by different shear models, including the cross-sectional shear, strut and tie model and arch effect model. The cross-sectional shear values were evaluated by the classical theories based on Eurocode 2 [2]. The strut and tie model and arch effect model would be introduced in this section.

According to Eurocode 2, the strut and tie model might be able to predict the shear capacity of the short-span beams, including the yield and ultimate capacities. Based on the experimental performance of the short-span beams, the strut and tie model of the short-span beams in this program was shown in Figure 7-12. The strut representing compressive stress fields was formed by the inclined diagonal cracks during the structural response. The ties corresponded for the tension reinforcement and the stirrups crossing the diagonal cracks.

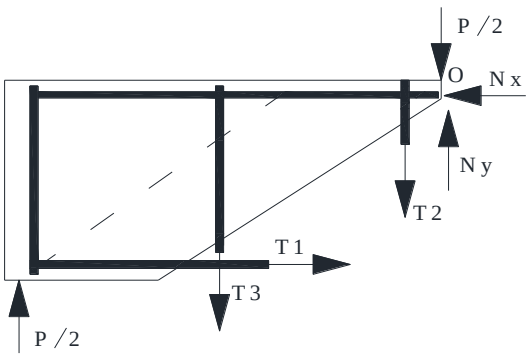

Figure 7-12 Strut and tie model of the short beams

By moment equilibrium about the loading point O, the force P applied to the beam is given by:

$$P = 2 \times \frac{f_{su\,1} \times l_1 \times A_{sw\,1} + \sum_{i=2}^{3} f_{sui} \times l_i \times A_{swi}}{l_0} \qquad (7\text{-}1)$$

Where:

l_i is respective lever arm to the forces of the tensile bars and the stirrups T_i from the top node O.

f_{sui} is the stress of the bar i, which will be discussed in detail in the next part.

A_{sw1} is the residual cross-section of the tensile bars.

A_{sw2}, A_{sw3} are the residual cross-sections of the stirrups.

The arch effect was also proposed to predict the mechanical capacity of the short-span beams [18]. The arch effect model was shown in Figure 7-13. Except for non-corroded beam B2T3-2 failed by the failure of the stirrup and the anchorage of the tension bar, all other short-span beams in this investigation were failed due to the failure of the tension bars, the capacity of short-span beams were considered to be mainly depended on the longitudinal steel reinforcement. As a result, the capacity P of the short-span beams could be deduced by the following equations:

$$P = 2 \times A_{sres} \times f \times \tan\theta \qquad (7\text{-}2)$$

While:

Asres is the residual cross-section of the tension bars;

f is the yield or ultimate strength of the tension bars;

θ is the angle of the arch body and the tension bars.

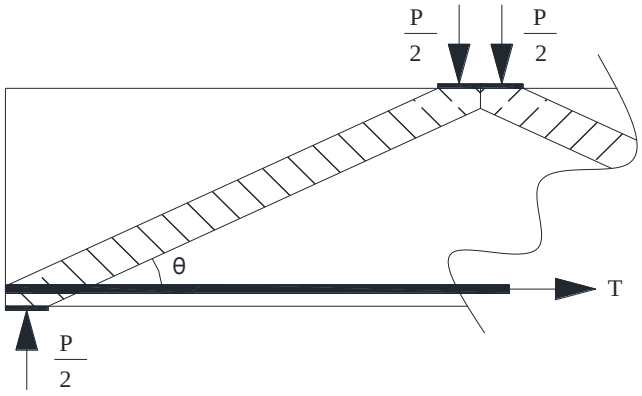

Figure 7-13 Arch effect model of the short beams in failure process

7.3.2 Comparison of yield capacity

The cross-section loss of the corroded tension bars was analysed in Chapter Four. The theoretical yield capacity of the short-span beams was deduced by different ways. The theoretical results of all the short-span beams are shown in Table 7-3. The results varied from each other significantly due to different theories. The value closer to experimental results was supposed to the net theoretical capacity for the short-span beams. The corresponding theory was treated as the predicted failure mode. According to Table 7-3, the predicted results of arch effect matched all the experimental yield capacity of the non-corroded short-span beams. Moreover, the predicted results of cross-sectional shear were also matched the experimental results of B2T2-1 and B2T2-2, which showed that the transition of the failure mode of the short-span beams when the span increased.

The influence of corrosion degree on the yield capacity of short-span beams is shown in Figure 7-14. As the yield capacities of the corroded short-span beams were predicted by bending theory, the trend lines of the theoretical results of the corroded short-span beams with different spans were shown in Figure 7-14. As shown in the figure, the residual yield capacity of the short-span beams was in linear relationship with the corrosion degree. Moreover, the span also played an important role in the mechanical performance of corroded beams. The yield capacity decreased with the increase of the span.

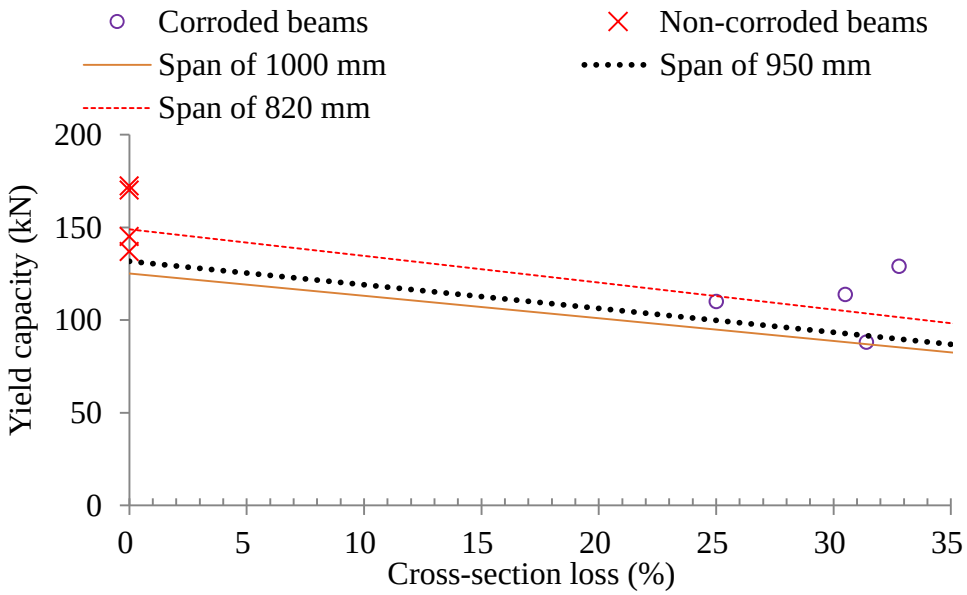

Figure 7-14 Corrosion influence on yield capacity of corroded beams (bending theory)

Table 7-3 Yield capacity of the short-span beams based on different theories

Label	ΔAs (%)	Span (mm)	P_E (kN)	Different theoretical results (kN)				P_T (kN)	P_T / P_E	Predicted failure mode
				Bending	CS	S&T	Arch			
B2Cl2-1	31.4	950	88.0	100.0	-	-	-	100.0	1.14	Bending
B2Cl2-2	25.0	950	110.0	109.1	-	-	-	109.1	0.99	Bending
B2T2-1	0	950	137.0	-	152.6	182.2	151.4	151.4/152.6	1.11/1.11	Arch/CS
B2T2-2	0	950	145.0	-	152.6	182.2	151.4	151.4/152.6	1.11/1.05	Arch/CS
B2Cl3-1	30.5	1000	113.8	95.8	-	-	-	95.8	0.84	Bending
B2Cl3-2	32.8	840	129.0	111.8	-	-	-	111.8	0.87	Bending
B2T3-1	0	820	170.0	-	152.6	192.1	187.3	187.3	1.10	Arch effect
B2T3-2	0	820	172.3	-	152.6	192.1	187.3	187.3	1.09	Arch effect

CS: cross-sectional shear; S&T: Strut and tie model; P_E: experimental results; P_T: net theoretical capacity

The influence of span on the yield capacity of the non-corroded and corroded (with a corrosion degree of 30% for the tension bars) short-span beams based on different models was shown in the Figure 7-15. The span played no influence on the predicted yield capacity of the short-span beams by cross-sectional shear theory. However, the span influenced on the yield capacity of the short-span beams significantly in the other prediction models. When the span increased, the yield capacity decreased in a non-linear way for both the corroded beams and non-corroded beams.

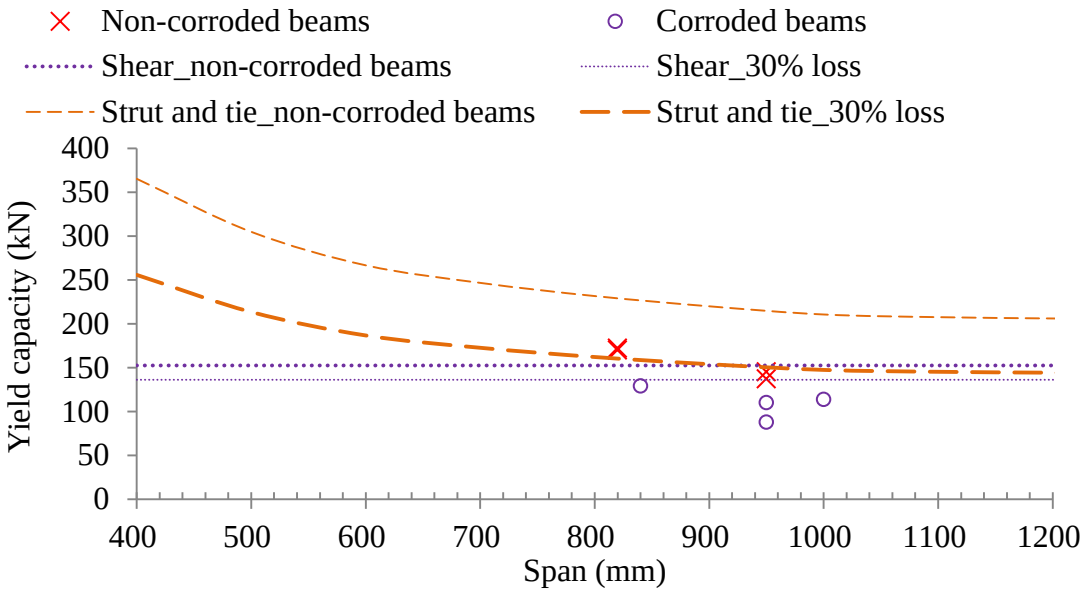

(a) Strut and tie model predictions

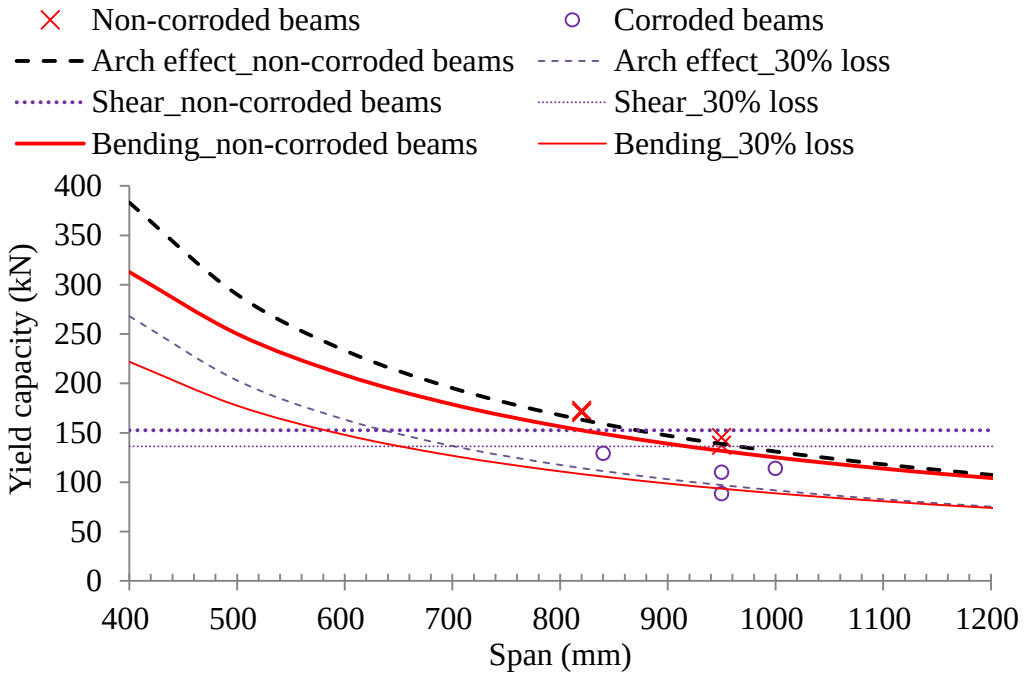

(b) Bending, cross-sectional shear and arch effect models

Figure 7-15 Influence of different factors on yield capacity of short-span beams

According to Figure 7-15(a), the strut and tie model overestimated the yield capacity for both the corroded short-span beams and non-corroded beams. The predicted values by cross-sectional shear theory matched the experimental results of non-corroded beams well, which differentiated the failure mechanism of the corroded short-span beams.

Figure 7-15 (b) showed that both the arch effect and bending theory could be applicable to the corroded short-span beams and non-corroded short-span beams. Indeed, when the span was over 800 mm, the prediction results of arch effect model and classical bending theory was very close to each other, which could be a sign of the transition of the failure modes. Moreover, the cross-sectional shear capacity of non-corroded beams was close to that of arch effect. The span between 800 mm and 950 mm could be treated as the failure mode transition zone for the non-corroded short-span beams, which agreed well with that of Table 7-3.

7.3.3 Comparison of ultimate capacity

The ultimate capacity of all the short-span beams was also evaluated by different theories. The theoretical results are shown in Table 7-4.

The corroded short-span beams were prediction by the classical bending theory. However, it should be noted that though the corroded beams showed the same bending failure mode, the ultimate mid-span deflection was quite different. As shown in Figure 7-9, the deflection of the corroded beam B2Cl3-2 was only 10.16 mm, much smaller than that of B2Cl3-1 with the value of 33.3 mm. The reason could be that the corroded beam B2Cl3-2 failed due to the brittle properties of the corroded tension bar. In fact, the failure points of the tension bars were checked carefully and found that there was a significant pitting corrosion at the zone of failure point of B2Cl3-2, while the uniform corrosion happened to the failure points of B2Cl3-1. According to the previous research [19], the asymmetrical distribution of residual cross-section of the reinforcement showed a more brittle performance than that of the reinforcement with uniform corrosion even though the corrosion degree was the same.

The non-corroded short-span beams failed in shear failure mode. However, as shown in the table, the prediction of cross-sectional shear theory was more closed to the short-span beams with span of 950 mm. But the short-span beams with span of 820 mm were more close to arch effect model, which showed that the span influenced the failure of the short-span beams significantly.

Moreover, the ultimate capacities of B2T3-1 and B2T3-2 were quite close to each other. In fact, the net span of the two beams was the same. But the reinforcement sketch was not the same. As shown in Figure 7-1, the transversal steel configuration of B2T3-1 was

dissymmetrical, and the transversal steel configuration of B2T3-2 was symmetrical but with defect of anchorage at one end. Finally, B2T3-1 showed shear failure mode with two tension bars failed at the end of the inclined cracks. B2T3-2 got deteriorated from the slip of the tension bars with damage of concrete cover at the end. Then one leg of the stirrups failed and the beam was broken. Though the two short-span beams behaved shear failure mode, the detailed factor still varied.

Table 7-4 Ultimate capacity of the short-span beams based on different theories

Label	ΔAs (%)	Span (mm)	P_E (kN)	Different theoretical results (kN)				P_T (kN)	P_T / P_E	Predicted failure mode
				Bending	CS	S&T	Arch			
B2Cl2-1	31.4	950	123.0	136.5	-	-	-	136.5	1.11	Bending
B2Cl2-2	25.0	950	148.0	148.8	-	-	-	148.8	1.01	Bending
B2T2-1	0	950	138.0	-	159.7	201	167.7	159.7	1.16	CS
B2T2-2	0	950	159.0	-	159.7	201	167.7	159.7	1.01	CS
B2Cl3-1	30.5	1000	140.0	130.8	-	-	-	130.8	0.93	Bending
B2Cl3-2	32.8	840	145.2	152.7	-	-	-	152.7	1.05	Bending
B2T3-1	0	820	199.0	-	159.7	213	207.4	207.4	1.04	Arch effect
B2T3-2	0	820	185.0	-	159.7	213	207.4	207.4	1.12	Arch effect

CS: cross-sectional shear; S&T: Strut and tie model;

P_E: experimental results; P_T: net theoretical capacity

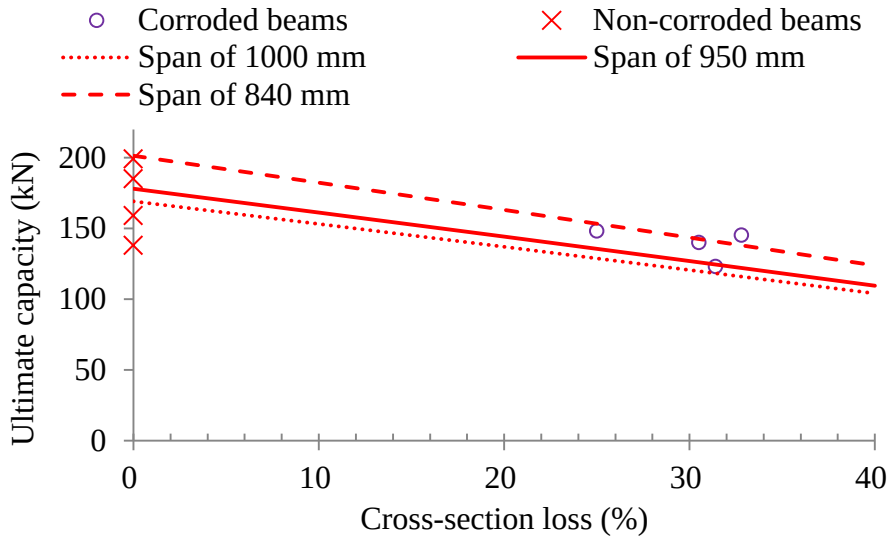

Figure 7-16 Corrosion influence on ultimate capacity of corroded beams (bending theory)

The ultimate capacities of the corroded beams were predicted by bending theory. The impacts

of corrosion degree on the ultimate capacity of the short-span beams with different spans were shown in Figure 7-16. The theoretical results showed that the ultimate capacity of the corroded beams was reduced in a linear relationship with the cross-section loss of the tension bars.

The theoretical results of the impact of spans with different cross-section losses are showed in Figure 7-17. The corroded beams were predicted by the corrosion degree of 30% of the two tension bars.

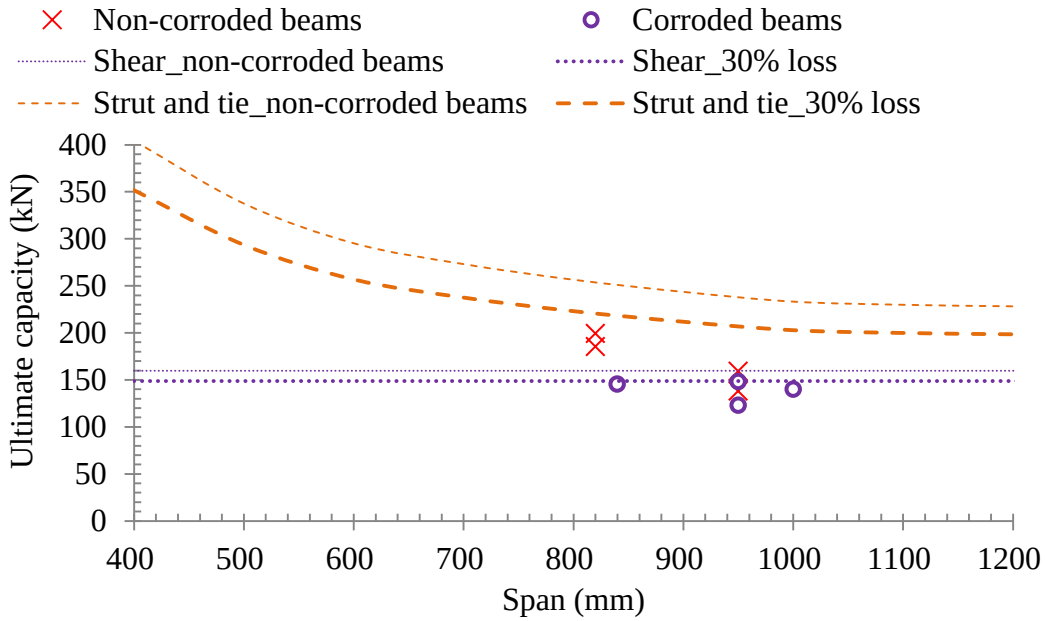

(a) Strut and tie model predictions

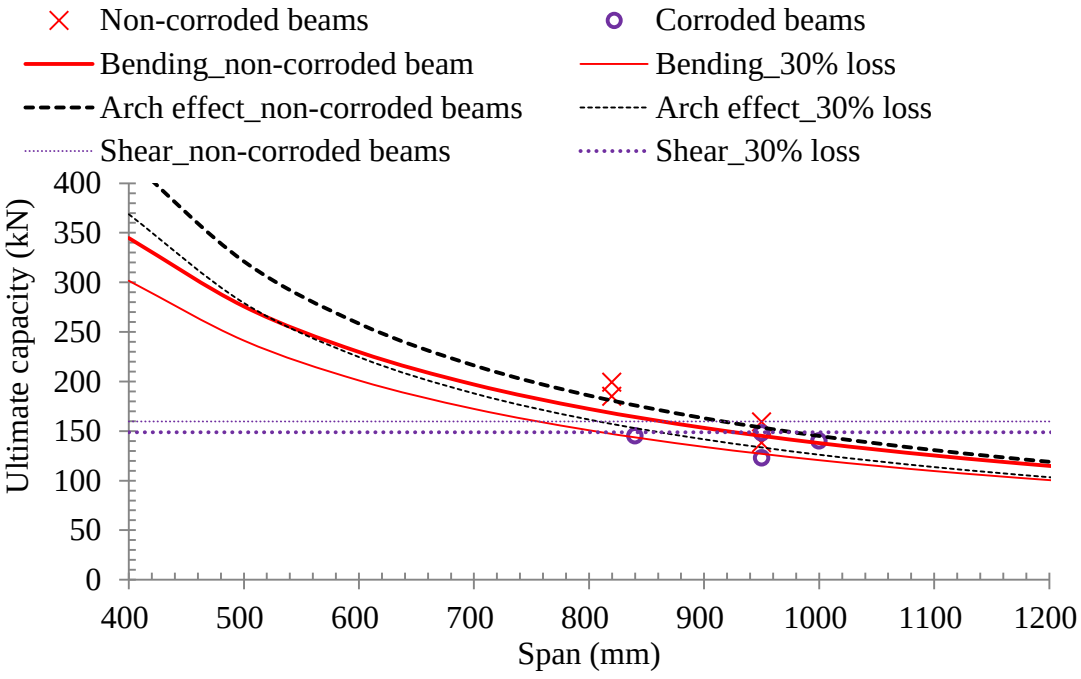

(b) Bending, cross-sectional shear and arch effect models

Figure 7-17 Influence of different factors on ultimate capacity of short-span beams

According to Figure 7-17(a), the results predicted by strut and tie model was over the experimental results of both the non-corroded short-span beams and the non-corroded short-span beams. The cross-sectional shear theory predicted the ultimate capacity of B2T3-1 and B2T3-2 well but a little smaller than that of the experimental results of B2T3-1 and B2T3-2.

Figure 7-17(b) showed that the predicted ultimate capacity of the short-span beams was in non-linear relationship with the span except for the cross-sectional shear values. It was clear that the ultimate capacity decreased when the span increased for both the corroded beams and non-corroded beams. With the increase of the span, the predicted results of bending theory got close to that of arch effect gradually, and the non-corroded short-span beams changed the failure modes from arch effect to cross-sectional shear gradually when the span increased to 950 mm.

It was interesting to find that the experimental results showed that the corroded short-span beams failed in bending failure mode as shown in Table 7-4, but the predicted value of both bending theory and arch effect were close to the experimental results, which showed the transition of the failure mode from arch effect to bending. Moreover, the transition zone of the span for the corroded short-span beams got smaller than that of the non-corroded beams.

7.3.4 Anchorage of the tension bars

The slip of the tension bars was in deep relationship with the anchorage of the bars in the residual concrete [20]. Based on previous research of Cosenza et al. [21] and Eligehausen et al. [22], Al-Mahmoud et al. [23] proposed an equation (7-3) to deduce the anchorage of the non-corroded tension bars. The results are shown in Table 7-5.

$$\tau_u = \frac{\sigma_{(max)} \cdot A}{\Sigma \cdot L_{anch}} \cdot \frac{1+\alpha}{1-\alpha} \qquad (7\text{-}3)$$

Where:

τ_u is the peak bond strength;

σ_{max} is the anchorage strength of the tension bars;

A is the cross-section of steel bar;

Σ is the perimeter of the tension bar;

α is curve-fitting parameter influencing the shape of the bond-slip curve in the ascending branch and obtained by equating the area underneath the ascending branch of the experimental curve to the value.

L_{anch} is the anchorage length. In this investigation, no hooks at the ends of all the tension bars,

as a result, the transmission length of 15 times the diameter of tension bars [2] was supposed to be the anchorage length for the undamaged beams.

But for the damaged non-corroded beam (Figure 7-11) and corroded beams, a new parameter was proposed to consider the reduction of corrosion on the bond strength. As a result, an improved equation was proposed as follow:

$$\tau_u = \frac{\sigma_{(max)} \cdot A}{\gamma \cdot \Sigma \cdot L_{anch}} \cdot \frac{1+\alpha}{1-\alpha} \qquad (7\text{-}4)$$

Where: γ is the coefficient considering the reduced perimeter length between the residual concrete and reinforcement, for the non-spalling bars, it was supposed to be 0.8, and for the anchorage with spalling zone, 0.6 was considered. Moreover, the anchorage length of the corroded or damaged zone, 20 times the diameter of tension bars were considered.

It was necessary to note that the ultimate stress kept the same when the anchorage length was larger than the transmission length according to the research of Al-Mahmoud et al. [23]. So in the following calculation, the transmission length of the corroded short-span beams and the non-corroded short-span beams in non-spalling and undamaged anchorage zones was in the same value.

Al-Mahmoud et al. [23] found that the peak bond strength was about 10 MPa. For the corroded short-span beams, the bond stresses of B-FS and B-BS of B2Cl1-1 were over this value, as a result, the slips occurred at these ends. But for the other location of the corroded short-span beams, the bond stresses were still under this criterion, and no slips were found in these zones as shown in Figure 7-9 and literature [24]. For the non-corroded short-span beams, the bond strength of C-FS of B2T3-2 was 12.92 MPa, which could explain the slip of the tension bars in Figure 7-10. However, the bond strength of most of the undamaged non-corroded short-span beams was around the criterion, which agreed well with the experimental results that most of the recorded value showed a sign of slips as shown in Figure 7-10.

7.3.5 Influence of corrosion on the ductility of the beams

As shown in Figure 7-8 and Table 7-2, the ductility of the corroded beams was much better than that of non-corroded beams, which could be due to the failure mode transitions. For the corroded beams, they failed in bending failure mode, but for the non-corroded beams, they failed in shear mode. However, it should be pointed out that the corroded beam B2Cl3-2 failed due to the damage at one of the support, which finally resulted in the failure with

relatively less deflection at the mid-span.

Table 7-5 Anchorage of the tension bars at the ends of all the beams

Beam	Location	L_{anch} (mm)	b_c	τ_u (MPa)	Location	L_{anch} (mm)	b_c	τ_u (MPa
B2Cl2-1	A-FS	240	0.8	8.42	B-FS	240	0.6	11.22
	A-BS	240	0.8	8.42	B-BS	240	0.6	11.22
B2Cl2-2	C-FS	240	0.8	8.42	D-FS	240	0.8	8.42
	C-BS	240	0.8	8.42	D-BS	240	0.8	8.42
B2T2-1	A-FS	180	-	10.33	B-FS	180	-	10.33
	A-BS	180	-	10.33	B-BS	180	-	10.33
B2T2-2	C-FS	180	-	10.33	D-FS	180	-	10.33
	C-BS	180	-	10.33	D-BS	180	-	10.33
B2Cl3-1	A-FS	240	0.8	8.42	B-FS	240	0.8	8.42
	A-BS	240	0.8	8.42	B-BS	240	0.8	8.42
B2Cl3-2	C-FS	240	0.8	8.42	D-FS	240	0.8	8.42
	C-BS	240	0.8	8.42	D-BS	240	0.8	8.42
B2T3-2	A-FS	180	-	10.33	B-FS	180	-	10.33
	A-BS	180	-	10.33	B-BS	180	-	10.33
B2T3-2	C-FS	240	0.6	12.92	D-FS	180	-	10.33
	C-BS	180	-	10.33	D-BS	180	-	10.33

Location A, B, C and D were shown in Figure 7-1

FS: front side tension bar; BS: back side tension bar

7.4 Conclusion

Based on the experimental tests on four long-term chloride corroded short-span beams and four non-corroded short-span beams, the mechanical performance of short-span beams were presented in this chapter. The corroded beams were stored in a chloride environment which was supposed to be the natural corrosion condition. Some conclusion could be drawn as follow:

(1) The mechanical performance of the short-span beams was changed. When the net span was the same, the corroded beams showed bending behaviour, while the non-corroded beams performed shear response (arch effect). The failure modes of the beams were transformed subsequently.

(2) The ductility of the short-span beams was improved significantly for the corroded beams. The non-corroded beams were rather brittle as the beams failed in shear. Nevertheless, the deflection of the corroded beams increased a lot due to the flexural response.

(3) With the increase of the span, the prediction value of arch effect model got close to bending theory gradually. For the corroded short-span beams, the span of the transition of the failure modes was smaller than that of the non-corroded short-span beams.

(4) The span influenced on the ultimate capacity of short-span beams significantly. The ultimate capacity of the short-span beams increased when the span got reduced.

(5) The corrosion spalling and mechanical damage of the anchorage increased the peak bond strength of the tension bars. As a result, slips occurred to the corresponding anchorage zones and finally lead to the failure of the short-span beams.

7.5 References

[1] 318 AC. Building Code Requirements for Structural Concrete (ACI 318-08) and Commentary. American Concrete Institute; 2008.

[2] Institution BS. Eurocode 2: Design of Concrete Structures: Part 1-1: General Rules and Rules for Buildings. British Standards Institution; 2004.

[3] Wang X. H., Gao X. H., Li B., Deng B. R., Effect of bond and corrosion within partial length on shear behaviour and local capacity of RC beam. *Construct Build Mater* 2011; 25(4): 1812-23

[4] Almusallam A. A., Effect of degree of corrosion on the properties of reinforcing steel bars, *Construct Build Mater.* 2001; 15(8) : 361-8

[5] ZHU W. J., François R., Coronelli D., Effect of corrosion of reinforcement on the coupled shear and bending behaviour of reinforced concrete beam. 6th International Conference on Bridge Maintenance, Safety and Management, Stresa, Lake Maggiore, Italy, July 8-12, 2012,

[6] Bhargava K., Ghosh A. K., Mori Y., Ramanujam S., Model for cover cracking due to rebar corrosion in RC structures, *Eng Struct*. 2006, 28(8): 1093-109

[7] Broomfield J. P., Corrosion of steel in concrete, understanding, investigation and repair, (second ed.), *Taylor & Francis*, London (2007).

[8] Rodriguez J., Ortega L. M., Casal J., Load carrying capacity of concrete structures with corroded reinforcement. *Construct Build Mater.* 1977; 11(4) : 239-48

[9] Chung L., Najm H., Balaguru P., Flexural behaviour of concrete slabs with corroded bars. *CemConcr Compos* 2008; 30(3) : 184-93

[10] Azad A. K., Ahmad S., Azher S. A., Residual strength of corrosion-damaged reinforced

concrete beams, *ACI Mater J.* 2007; 104(1) : 40-47

[11] Torres-Acosta A. A., Navarro-Gutierrez S., Terán-Guillén J.. Residual flexure capacity of corroded reinforced concrete beams, *Eng Struct* 2007; 29(6) : 1145-52

[12] Xia J., Jin W. L., Li L. Y., Shear performance of reinforced concrete beams with corroded stirrups in chloride environment. *Corros Sci* 2011; 53(5) : 1794-805

[13] Wang X. H., Li B., Gao X. H., Liu X. L., Shear behaviour of RC Beams with corrosion damaged partial length, *Mater Struct* 2012; 45(3): 351-79

[14] Cairns J. Strength in shear of concrete beams with exposed reinforcement. *Proc ICE-Struct Build* 1995; 110(2): 176–85.

[15] Higgins C., Farrow III W. C., Tests of reinforced concrete beams with corrosion-damaged stirrups. *ACI Struct J* 2006; 103(1): 133–41.

[16] Zhang R. J., Castel A., François R., Serviceability limit state criteria based on steel-concrete bond loss for corroded reinforced concrete in chloride environment, *Mater Struct*, 2009, 42(10) : 1407-21

[17] Zhu W. J., François R., Structural performance of RC beams corroded in chloride environment for a long period. *Mater Struct* accepted.

[18] Spinella N. Shear strength of full-scale steel fibre-reinforced concrete beams without stirrups. *Comput Concr* 2013; 11(5): 365–82.

[19] Zhu W. J., François R. Effect of corrosion pattern on the ductility of tensile reinforcement extracted from a 26-year-old corroded beam. *Adv Concr Constr* 2013; 1(2):121–37.

[20] AL-mahmoud F., Castel A., François R., Tourneur C., Effect of surface pre-conditioning on bond of carbon fibre reinforced polymer rods to concrete. *Cem Concr Compos* 2007; 29(9): 677–89.

[21] Cosenza E., Manfredi G., Realfonzo R., Behavior and modeling of bond of FRP rebars to concrete. *J Compos Construct*, 1997; 1(2): 40-51

[22] Eligehausen, Popov, Betero V. V., Local bond stress-slip relationships of deformed bars under generalized excitations, Report No. 83/23, EERC, University of California-Berkerley, Calif.; 1983. P. 162.

[23] Al-Mahmoud F., Castel A., François R., Failure modes and failure mechanisms of RC members strengthened by NSM CFRP composites–Analysis of pull-out failure mode. *Compos Part B Eng* 2012; 43: 1893–901.

[24] Zhu W. J. , François R., Coronelli D., Cleland D., Effect of corrosion of reinforcement on the mechanical behaviour of highly corroded RC beams. *Eng Struct* 2013; 56: 544–54.

CHAPTER EIGHT

Chloride-induced corrosion products of reinforcement embedded in concrete for 28 years

This chapter focuses on the composition of the corrosion products which were extracted from the chloride corroded reinforced concrete beam B2Cl3 with a corroded age of 28 years. The corrosion products were divided into several samples by the locations and reinforcement types, including the longitudinal reinforcement and the stirrups so as to study the influence of the service load on the corrosion products. X-ray diffraction and thermal analysis were conducted to investigate the composition of the corrosion products. The expansion coefficient corresponding to the corrosion products was calculated. The results show that the composition of the corrosion products was closed to the constituents found in the marine environment in Barcelona in Spain. Geothite and Akaganeite were found in considerable proportions in the corrosion products. The expansion coefficient of the corrosion products ranged from 2.97 to 3.15, which could be helpful for the research on the corrosion process of RC elements.

8.1 Introduction

Corrosion of reinforcement is one of the major causes of the premature degradation of reinforced concrete (RC) structures [1], especially for the buildings exposed to the marine environment with rich chloride ions [2]. The influence of the corrosion includes mainly three ways: (1) reduction of cross-section of the reinforcement; (2) deterioration of the bond between the reinforcement and the concrete; (3) the cracking and even spalling of concrete cover induced by the expansion of the corrosion products[3-4]. All of these will reduce the serviceability and load-bearing capacity of the structures significantly. Up to now, a lot of research has been conducted on the corrosion impact on the mechanical performance of the RC constructions [5-7]. However, the research on the corrosion products should also be interesting for better understand the mechanism of corrosion process in RC structures.

The investigations on the corrosion products induced by chloride ions in concrete structures have been carried out by some researchers. Syed et al. [8] discovered that the major constituent of the corrosion products formed in marine environment was Goethite (α-FeOOH), a large proportion of Lepidocrocite (γ-FeOOH) and small amounts of Ferrihydrite and Maghemite (γ-Fe_2O_3). Suda et al. [9] had almost the same conclusion that the corrosion products were mainly made up of Magnetite (Fe_3O_4), Goethite and Lepidocrocite for the concrete exposed to the marine environment for 5 years.

The volume of the corrosion products is much larger than that of original steel, which will result in the cracking even the spalling of the concrete cover. The ratio between the volume of corrosion products and iron consumed in the corrosion process is called expansion coefficient [1]. Tuutti [10] found that the expansion coefficient ranged from 2.2 to 6.4. Liu et al. [11] got the value of 4.0 from their concrete cracking model. Zhao et al. [12] proposed that the expansion coefficients of corrosion products varied from 2.9 to 3.3 due to different corroded environment. Nevertheless, it's a pity that most of the results were based on the corrosion products from the corroded elements such as ironwork directly. Some research work on the corrosion products of RC structures which was naturally corroded naturally for a long-time will be interesting.

Castel et al. [13] and Zhang et al. [14] found that the iron oxides and iron oxyhydroxides were principally composed of magnetite, hematite or Maghemite, Goethite, with a little amount of Lepidocrocite and Akaganeite. All the results were from the test of X-ray diffraction. However, as some of the diffraction patterns of the corrosion products are much too closed to each other, the proportion of the corrosion products and expansion coefficient of the corrosion products are not investigated.

This section studies the corrosion products from one beam of the program. The beam was labelled B2Cl3, with a corroded age of 28 years when the experiment was carried out in 2012. Both the corrosion products which came from tension reinforcement (bottom rebars), compressive reinforcement (top rebars) and stirrups were investigated by X-ray diffraction and thermal analysis respectively. Then the composition of the corrosion products was identified by the experimental results. The expansion coefficient was also deduced based on the experimental results.

8.2 Experimental procedure

Having been corroded for 28 years, beam B2Cl3 was highly corroded. The cracking of the concrete cover was well developed so that the corrosion products could move away from the interface of the reinforcement to the outside successfully as shown in Figure 8-1. In the bottom of the beam, spalling also happened in some zone along the longitudinal reinforcement.

Figure 8-1 Corrosion products in the outside surface of B2Cl3

8.2.1 Description of the samples of the corrosion products

The corrosion products were taken from the corroded reinforcement by a scalpel carefully. Six samples of corrosion products were gathered from different types of the corroded reinforcement. As shown in Figure 8-2, sample TFS-IV and sample TFS-V were both from the front side tensile bar which corresponded to large longitudinal cracks and spalling zone in the bottom surface (in the middle as shown in Figure 8-3) respectively. Sample TBS-IV responded to corrosion products from the tensile bar with a spalling of the concrete cover in the corner as shown in Figure 8-3. Sample CFS-IV represented the corrosion products from the compressive bars with a large longitudinal crack of about 1mm. Sample S-IV and sample

S-V standed for the corrosion products of the stirrups with transversal cracks.

It should be noted that all the samples were from the middle of the beam. As the corrosion was most seriously in this section, the corrosion products could be collected successfully. Moreover, the concrete composition was tried to avoid mixing into the corrosion products. Hence the corrosion products which had penetrated into the concrete were not considered in this section. As in Figure 8-3, only the layer of corrosion products was analysed here. In fact, the concrete around the corroded reinforcement which contained many corrosion products would be examined by SEM and be discussed in the following literatures.

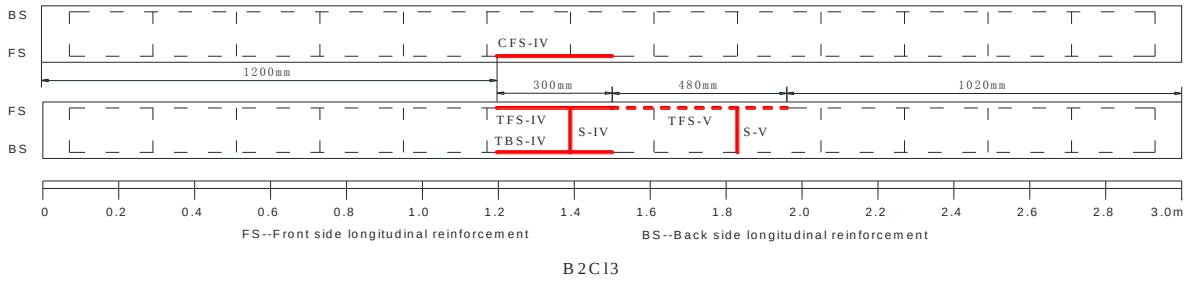

Figure 8-2 Location of the samples in beam B2Cl3

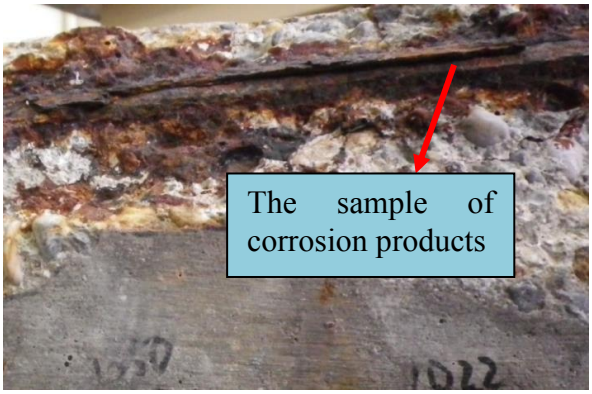

Figure 8-3 Sample TBS-IV at the spalling zone of tensile reinforcement

8.2.2 X-ray diffraction

All the six samples of the corrosion products were crushed into powder (<80μm). The X-ray diffraction (XRD) experiments were applied to the samples with COα-radiation. The wavelength was 1.78898. The data of the experiment was gathered over a 2θ varying from 4° to70°, with a speed of 0.02°/s.

8.2.3 Thermal analysis

The thermal analysis was also applied to all the samples. The samples were heated at a

heating rate of 10°C/min. All the qualitative and quantitative information about the temperature, sample quality and thermal energy were recorded until 1000°C.

8.3 Experimental results and discussion

8.3.1 X-Ray Diffraction (XRD) results

The XRD patterns for the corrosion products with different corroded ages are shown in this section. As part of the whole program, Castel et al. [15] and Zhang et al. [14] carried out the relative investigations on the corrosion products from the corroded beams which was stored in the same environment but with a corroded age of 14 years and 23 years respectively.

Figure 8-4 is the diffraction patterns of corrosion products from corroded beam B1Cl1 which was carried out by Castel et al.. Figure 8-5 is the diffraction patterns of corrosion products from corroded beam B2Cl1 which was conducted by Zhang et al.. The XRD patterns for sample TFS-IV of beam B2Cl3 with a corroded age of 28 years is shown as Figure 8-6. According to the comparison of the three figures, the composition of the corrosion products was almost the same although the relative proportion of the compositions was different from each other. The composition was mainly made up of iron oxides and iron oxyhydroxides. There were Magnetite (Fe_3O_4), Hematite (α-Fe_2O_3), Lepidocrocite (γ-FeOOH), Goethite (α-FeOOH), Akaganeite (β-FeOOH). A peak which was marked with several compositions means that at least one of them existed in the corrosion products such as Magnetite and Goethite at 2θ=62.5º.

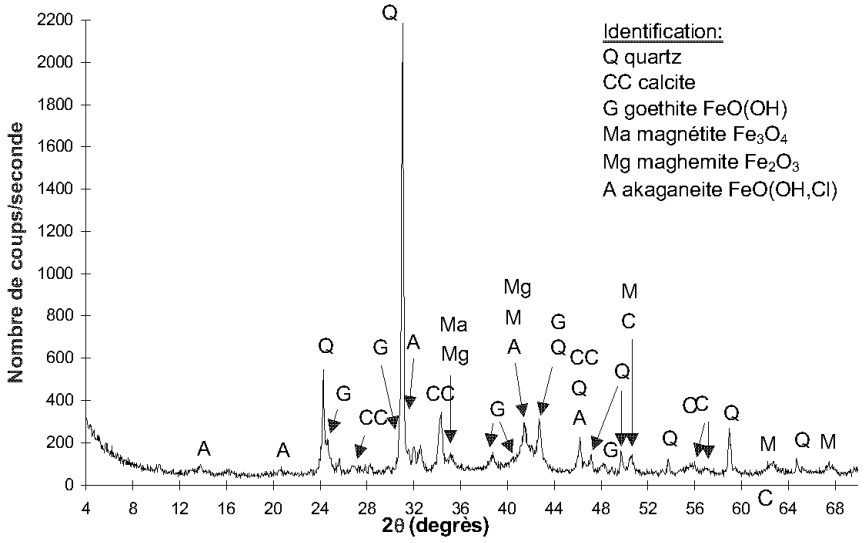

Figure 8-4 Castel's results for corrosion products of B1Cl1 at 14 years

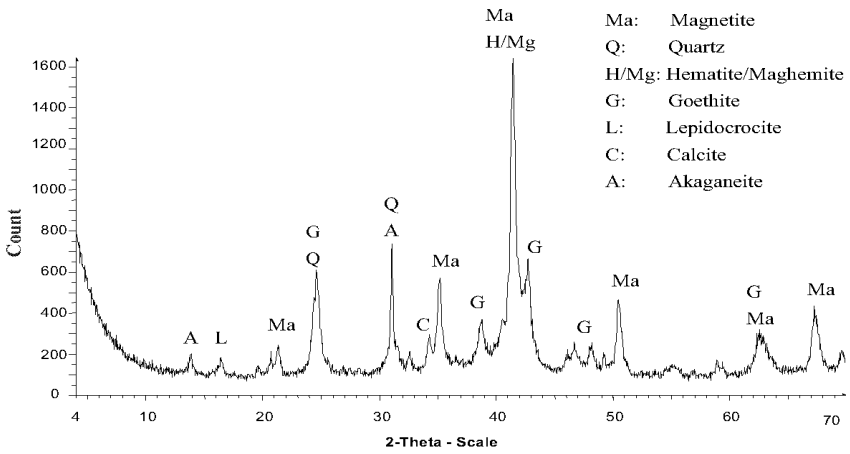

Figure 8-5 Zhang's results for corrosion products of B2Cl1 at 23 years

As the cement and concrete powder might mix into the corrosion product, the diffraction patterns of Quartz (SiO_2) and Calcite ($CaCO_3$) might exist in the whole diffraction patterns of the corrosion products. For example, the diffraction patterns of both Goethite and Quartz may exist at 2θ of 24.5º. In Figure 8-4, the existence of Quartz was sure and played a significant role in the sample of B1Cl1 at 14 years. The existence of Calcite was sure at 2θ of 34ºfor sample of B2Cl1 at 23 years. However, the content of concrete and cement powders in the sample decreased obviously according to the comparison of the diffraction pattern figures. The existence of Quartz and Calcite was not sure for the sample of B2Cl3 at 28 years, as the peak of diffraction patterns was the same to the corrosion products of Goethite and Hematite as Figure 8-6. In order to make difference of the corrosion products from the cement and concrete powder more clearly, the XRD was conducted for all the samples of corrosion products from beam B2Cl3 when the thermogravimetric (TG) analysis was finished.

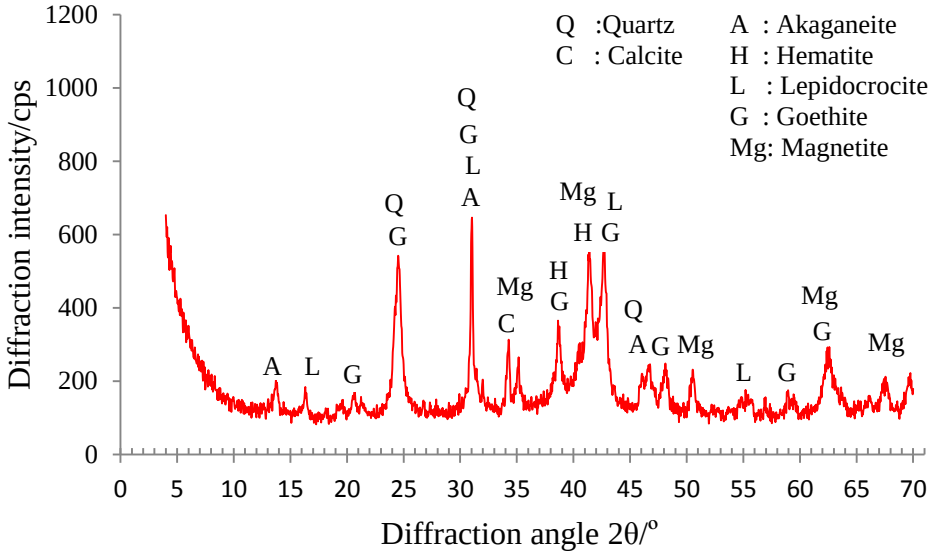

Figure 8-6 XRD patterns of sample TFS-IV

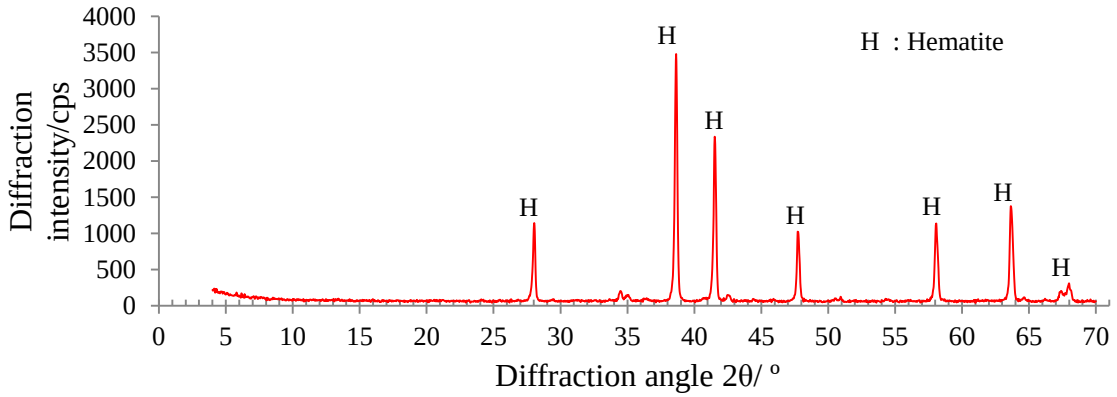

Figure 8-7 XRD patterns of TFS-IV heated sample

As discussed by Chang et al. [16], the Calcite will be destroyed when it was heated to the temperature between 550ºC and 950ºC as Eq. (7-1). So the peak of diffraction pattern for Calcite will disappear and a new peak for Calcia (CaO) will show up in the diffraction patterns of heated sample if Calcite existed in the original sample of TFS-IV. However, in Figure 8-7, no peak of diffraction pattern for Calcia could be found as shown in Figure 8-7. That means that no Calcite existed in the corrosion product sample of TFS-IV.

$$CaCO_3 \rightarrow CaO + CO_2 \qquad (8\text{-}1)$$

The Quartz will stay stable during the heating process. But the peak of diffraction pattern corresponding to the possible existence of Quartz vanished from Figure 8-7. In fact, all the peaks of diffraction patterns are confirmed to be the presence of Hematite. So the samples could be considered to be the composition of pure corrosion products of iron oxides and iron oxyhydroxides.

In the sample TFS-IV, no cement and concrete powder was mixed into the corrosion products. This can be due to the highly corrosion of the reinforcement in B2Cl3 at 28 years. Pure corrosion products around the reinforcement were enough to be collected from the corroded bars, which can be helpful for the following analysis on the properties of corrosion products.

The diffraction patterns of the heated samples of TFS-IV and TBS-IV were improved in Figure 8-8. As shown in the figure, the Goethite played a major role in the corrosion products. The existence of Akaganeite was also obvious, which could match well with the conclusions of Fuente et al.[17] that the rust generated from chloride environment contained Akaganeite. Ishikawa et al. [18] found that Lepidocrocite could transform into Geothite gradually in normal conditions. So Lepidocrocite was not the dominating constituent in the corrosion products. Espada et al.[19] found that Akaganeite was gradually transformed into Magnetite

on the reinforcement interface. That could be the reason that the relative quantity of Magnetite was found in Figure 8-8.

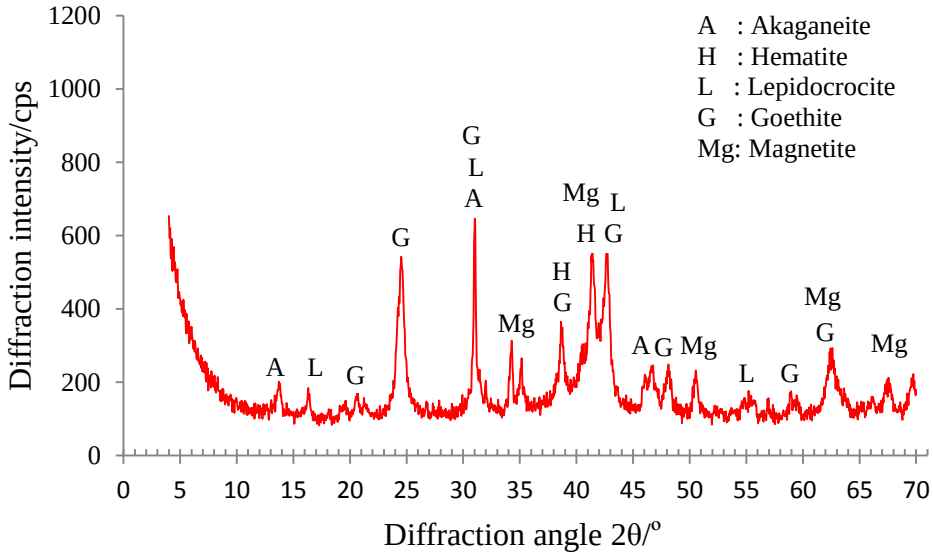

(a) Improved XRD patterns of sample TFS-IV

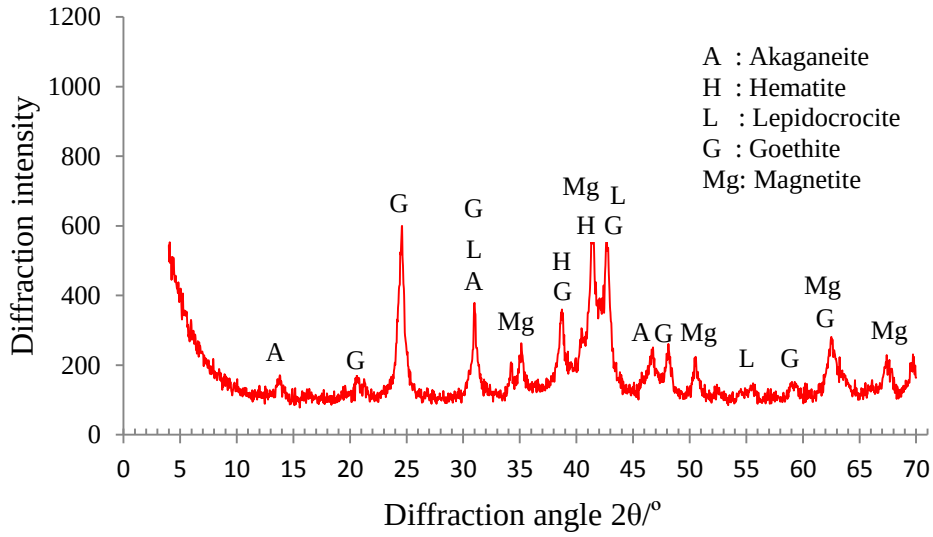

(b) Improved XRD patterns of sample TBS-IV

Figure 8-8 Improved XRD patterns of all the samples from B2Cl3 at 28 years

By comparing with Figure 8-4 of sample from B1Cl1 at 14 years, Figure 8-5 of sample from B2Cl1 at 23 years and Figure 8-8 of sample from B2Cl3 at 28 years, the constituents of the corrosion products were not changed with the corrosion age. Nevertheless, the corrosion period could change the proportions of the constituents of the corrosion products such as the transformation of Akaganeite to Magnetite, which could agree well with the conclusion of Fuente et al. [19]

It is necessary to point out that Hematite was also found in the corrosion products in Figure

8-8. According to Cornell et al. [20], Hematite was considered to be the composition of the mill scale which was formed before corrosion initiation rather than the corrosion process of the reinforcement, as Hematite was formed at a very high temperature.

As shown in Figure 8-8, the diffraction patterns of the two samples were almost the same, which showed that the composition of the corrosion products was close to each other. XRD could identify the constituents of the corrosion products. However, as some peak of the diffraction patterns could correspond to several constituents, the quantity of each constituent was unable to investigate by this experiment. Then thermogravimetric was applied for the samples to collect more information to differentiate the compositions.

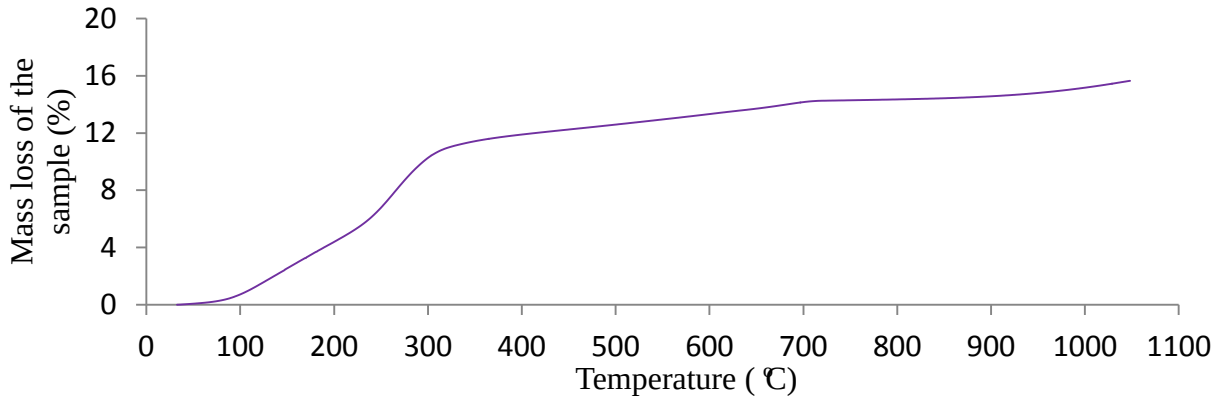

(a) Relative mass loss of the sample TFS-IV

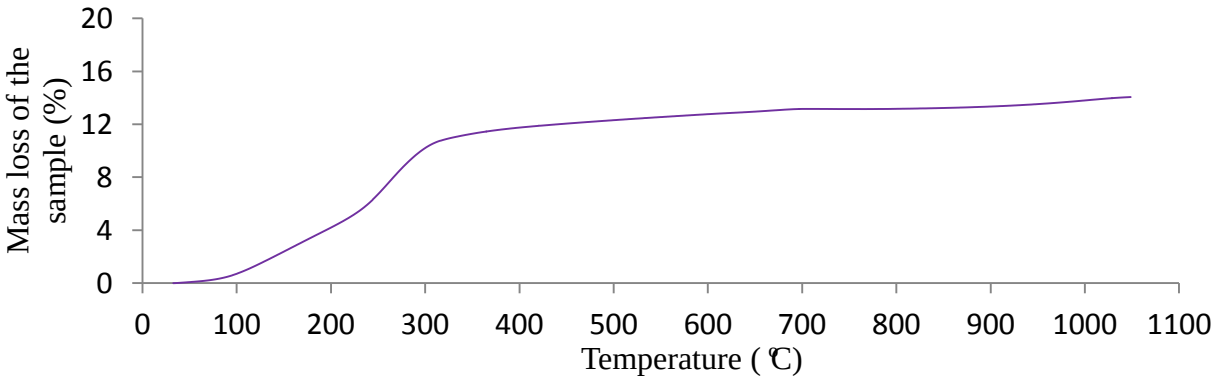

(b) Relative mass loss of the sample TBS-IV

Figure 8-9 Characteristic curves of corrosion products in TG tests

8.3.2 Thermogravimetric (TG) test results

Figure 8-9 and Figure 8-10 show the TG and DTG curves of both samples of TFS-IV and TBS-IV. The figures contain the information about the mass loss of the samples with the increase of the temperature from 30ºC (room condition) to over 1000ºC. The departure of water in the two samples was also recorded in the whole process and showed in Figure 8-11.

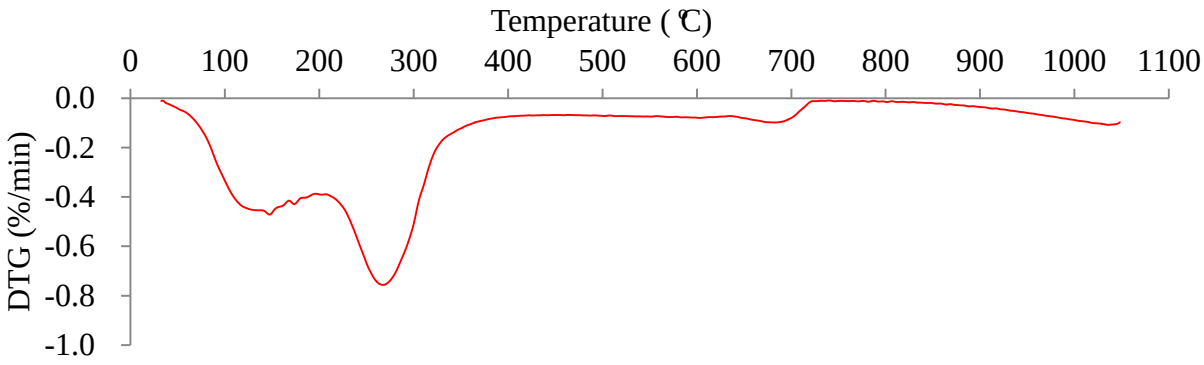

(a) TFS-IV

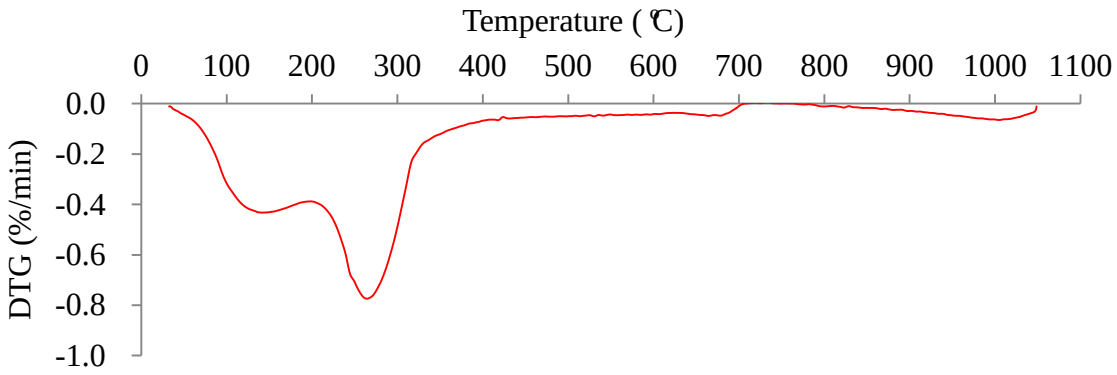

(b) TBS-IV

Figure 8-10 DTG of the corrosion samples

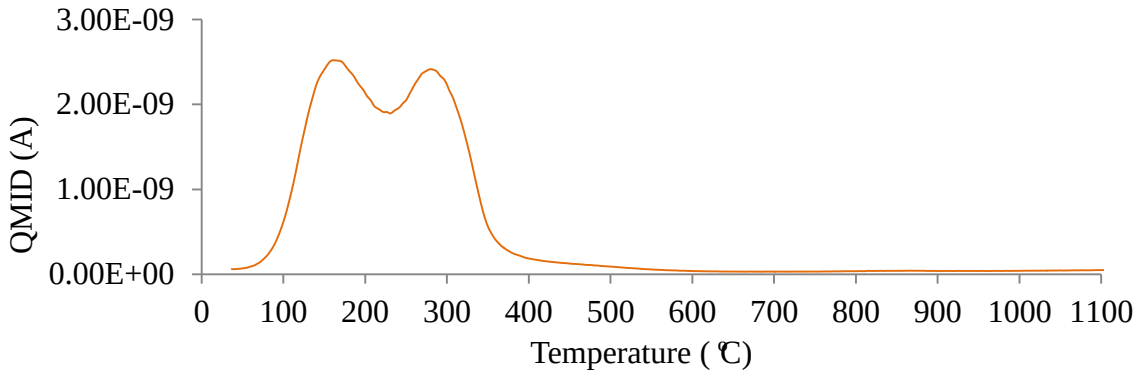

(a) TFS-IV

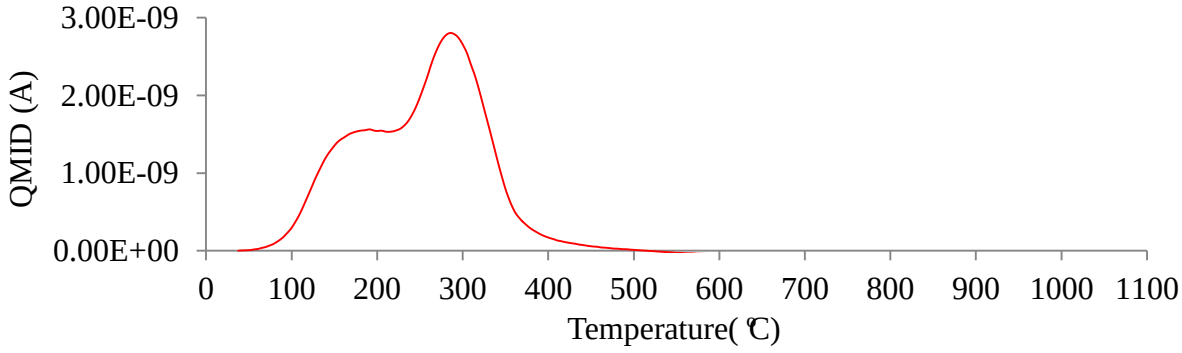

(b) TBS-IV

Figure 8-11 Loss of H_2O in the TG tests

According to the curves of the departure of water, the heating could be divided into two steps. One was the evaporation of physically absorbed water in the corrosion product samples, which corresponded to the peak at about 130ºC and ranged from room condition to about 200ºC. The other was the dehydration of the corrosion products of iron oxyhydroxides. The peak of this dehydration process was about 260ºC and the process could range from 200ºC to about 400ºC. After 400ºC, the water departure was less than 0.05% with the temperature and the mass loss of the sample was less than 2% in the range from 400ºC to 1100ºC. As a result, this process was not considered in the following research. The dehydration process could be expressed as Eq. (8-2) [20].

$$2Fe(OH) \rightarrow Fe_2O_3 + H_2O \qquad (8\text{-}2)$$

In the heating process, some transformation also happened to the iron oxides. According to Cornell et al. [20], when the temperature reached 200ºC, Magnetite (Fe_3O_4) began to oxidize to Maghemite (γ-Fe_2O_3) gradually. Nevertheless, it was just an intermediate compound. As once the temperature was higher than 300ºC, the iron oxides would finally transform into Hematite (α-Fe_2O_3). The whole reaction process could be expressed as follow:

$$\text{Magnetite } (Fe_3O_4) \xrightarrow{200ºC-300ºC} \text{Maghemite } (\gamma - Fe_2O_3) \xrightarrow{>300ºC} \text{Hematite } (\alpha - Fe_2O_3) \quad (8\text{-}3)$$

According to Eq. (8-3), Maghemite was only the intermediate compound. Finally, all the iron oxides and iron oxyhydroxides would transform into Hematite, which could well agree with the XRD results of the heated samples as shown in Figure 8-7. Though the transformation process of the iron oxides (Magnetite) was complicated, it could still be simplified as follow:

$$4Fe_3O_4 + O_2 \rightarrow 6Fe_2O_3 \qquad (8\text{-}4)$$

As shown in Eq. (8-4), the oxygen became the constituent of the compound of Hematite, which increased the mass of the sample. However, as it combined with the dehydration reaction of the iron oxyhydroxides.

According to Eq.(8-2)-Eq.(8-4) and the information of the experimental results, the composition of corrosion products could be identified. For example, the hydroxy-oxides, Magnetite and Hematite in the sample of corrosion products could be deduced by the thermogravimetric results. The hydroxyl-oxides included three types of the constituents, Geothite, Akaganeite and Lepidocrocite as referred in the XRD figures in Figure 8-8.

Nevertheless, the proportion of the three hydroxyl-oxides could be differentiated from XRD results. However, as the Hematite was formed in a high temperature [21], the existence of Hematite should come from the mill scale. Finally, the Hematite and the water departure at the temperature of lower than 230ºC was excluded in the constituents of the corrosion products.
However, it should be noted that as part of the experimental results could only be used for qualitative analysis, the quantitative analysis was not precise. For the precise results, some more experiments for quantitative analysis are required.

Table 8-1 Compositions in the samples

	Sample mass (mg)	Geothite α-FeOOH (mg)	Akaganeite β-FeOOH (mg)	Lepidocrocite γ-FeOOH (mg)	Magnetite Fe_3O_4 (mg)	Hematite α-Fe_2O_3 (mg)	Water H_2O (mg)
TFS-IV	1112.452	437.3	249.9	267.2	80.7	9.1	68.3
TBS-IV	971.283	414.2	205.1	131.2	140.8	21.4	58.5
TFS-II	1359.794	412.0	478.9	334.7	59.15	9.8	65.3
TBS-II	2344.159	1043.5	495.5	481.0	203.9	13.7	106.5
S-V	1635.138	522.3	461.3	482.3	90.1	7.1	72.1

8. 3.3 Comparison of the corrosion compositions

The composition of the corrosion products are compared with the results of Fuente et al. [18] and Zhao et al. [12] as shown in Table 8-2. According to the table, the composition of corrosion products could still vary from different locations in the world, especially for Lepidocrocite and Magnetite/Maghemite.
The composition of all the samples was shown as Table 8-2. The composition of the corrosion products was close to the results in mild marine environment in Barcelona, Spain, especially for the phenomenon that Akaganeite was found in considerable proportions in marine environment. The hydroxyl-oxides played a significant role in the corrosion products. While for the three forms of the hydroxyl-oxides, Geothite was in considerable proportion, and then followed by Akaganeite. Lepidocrocite was relatively weaker. The content of Lepidocrocite was still higher than Magnetite.
Moreover, the composition of the corrosion products in the five samples from different location and different bars was close to each other. The service load played little influence to the composition of the corrosion products.

Table 8-2 Comparison of the corrosion products

Environment and Location	Geothite %	Akaganeite %	Lepidocrocite %	Magnetite/ Maghemite%
Rural, El Escorial, Spain	24.6	--	60.6	14.8
Urban, Madrid, Spain	24.6	--	60.6	14.8
Industrial, Bilbao, Spain	18.9	--	46.5	11.4
Marine (mild), Barcelona, Spain	15.8	35.5	39.1	9.6
Marine (severe), Alicante, Spain	17.5	39.3	43.2	--
Urban, Shanghai, China	32.4	36.3	6.7	24.6
Marine, Ningbo, China	22.8	41.5	5.5	30.2
Marine, Yokosuka, Japan	10.7	57	4.9	27.4
TFS-II	32.1	37.3	26.0	4.6
TBS-II	46.9	22.3	21.6	9.2
TFS-IV	42.2	24.1	25.8	7.8
TBS-IV	46.5	23.0	14.7	15.8
S-V	33.6	29.6	31.0	5.8

8.4 Expansion coefficient of the corrosion products

As in the corrosion process, the Fe was transformed into hydroxyl-oxides and oxides. The expansion coefficient of the corrosion products could be calculated with the help of the density and the molar mass of the constituent of the corrosion products. Finally, the expansion coefficient of each corrosion composition and the total expansion coefficient of each sample could be calculated as Table 8-3:

The expansion coefficient of the corrosion products was close to each other, ranging from 2.97 to 3.15, which could be helpful for the further research work on the corrosion of the reinforcement and the cracking of the concrete cover.

Table 8-3 Expansion coefficient of the corrosion products

Geothite	Akaganeite	Lepidocrocite	Magnetite	
2.95	3.53	3.07	2.10	
TFS-II	TBS-II	TFS-IV	TBS-IV	S-V
3.15	3.02	3.05	2.97	3.11

8.5 Conclusions

The corrosion products retrieved from a beam with a 28-year-old corroded beam were investigated in this section. XRD experiments and thermogravimetry were applied to differentiate the constituents of the corrosion products. According to the experiments, the proportion of the composition was found to be close to the corrosion products in marine environment in Barcelona, Spain. Both Geothite and Akaganeite played a most important role in the composition. The expansion coefficient of the corrosion products could range from 2.97 to 3.15, which could be helpful for the further study about the influence of the corrosion behaviour of the reinforcement on the cracking process of the concrete cover.

8.6 References

[1] Caré S., Nguyen Q. T., L'Hostis V., Berthaud Y., Mechanical properties of the rust layer induced by impressed current method in reinforced mortar, *Cem Concr Res*, 2008; 38(8-9), 1079-91

[2] Neville A., Chloride attack of reinforced concrete : an overview. *Mater Struct*, 1995, 28(2):63-70

[3] Coronelli D., Gambarova P., Structural assessment of corroded reinforced concrete beams: modeling guidelines. *J Struct Eng ASCE.* 2004, 130(8), 1214-24

[4] Auyeung Y. B., Balaguru P., Chung L., Bond behavior of corroded reinforcement bars. *ACI Mater J.* 2000, 97(2), 214-20

[5] Stewart M. G., Spatial variability of pitting corrosion and its influence on structural fragility and reliability of RC beams in flexure, *Struct saf*, 2004; 26(4):453-70

[6] Castel A., François R., Arliguie G. Mechanical behaviour of corroded reinfroced concrete beams, part. 1: Experimental study of corroded beams. *Mater Struct*, 2000; 33(9):539-44

[7] Castel A., François R., Arliguie G. Mechanical behaviour of corroded reinfroced concrete beams, part. 2: Bond and notch effects. *Mater Struct*, 2000; 33(9):545-51

[8] Syed S., Atmospheric corrosion of hot and cold rolled carbon steel under field exposure in Saudi Arabia, *Corros Sci* 2008; 50(6): 1779-84

[9] Suda K., Misra S., Motohashi K., Corrosion products of reinforcing bars embedded in concrete, *Corros Sci* 1993; 35(5-8): 1543-9

[10] Tuutti K., Corrosion of steel in concrete, Report 4, Swedish Cement and Concrete Research Institute, Stockholm, Sweden, April 1982, p.82.

[11] Liu Y., Weyers R. E., Modeling the time to corrosion cracking in chloride contaminated reinforced concrete structures, *ACI Mater J* 1998; 95(6): 675-81

[12] Zhao Y. X., Ren H. Y., Dai H., Jin W. L., Composition and expansion coefficient of rust based on X-ray diffraction and thermal analysis, *Corros Sci* 2011; 53(5): 1646-58

[13] Castel A., Couplage mécanique et corrosion dans les éléments en béton armé, Thèse de Doctorat de l.Université Paul Sabatier de Toulouse, 2000

[14] Zhang R. J., Phase d'initiation et de propagation de la corrosion dans les structures en béton armé et leurs conséquences sur la durée de vie, Thèse de doctorat de l'Institut National des Sciences Appliquées de Toulouse, 2008

[15] Castel A., Couplage mecanique et corrosion dans les elements de béton armé, Thèse de doctorat de l'Institut National des Sciences Appliquées de Toulouse, 2000

[16] Chang C. F., Chen J. W., The experimental investigation of concrete carbonation depth. *Cem Concr Res* 2006, 36(9):1760-7

[17] de la Fuente D., Diaz I., Simancas J., Chico B., Morcillo M., Long-term atmospheric corrosion of mild steel, *Corros Sci*, 2011, 53(2): 604-17

[18] Ishikawa T., Takeuchi K., Kandori K., Nakayama T., Transformation of γ-FeOOH to α-FeOOH in acidic solution containing metal ions, *Colloids and Surfaces A: Physicochemistry Engineering Aspects* 2005, 266:155-9

[19] Espada L., Merino P., González A., Sánchez A., Atmospheric corrosion in marine environments, in : Proceedings of the 10th International Congress on Metallic Corrosion, vol. 1, Oxford and IBH Publishing Co, New Delhi, 1987, pp.3-7

[20] Cornell R. M., Schwertmann U., The iron oxides, VHC Verlagsgesellschaft, Weinhaim, Germany, 1996

GENERAL CONCLUSIONS

This dissertation is based on the experimental tests on the corroded beams B2Cl2 and B2Cl3 which have been stored in a chloride environment for a period of 26 years and 28 years respectively. The research is carried out mainly in the following four sections:

The first section focused on the residual mechanical properties of the corroded bars. The strength of the corroded bars was calculated by the residual gravimetrical cross-section which was found stronger than that of the non-corroded bars. The corrosion deteriorated the ductility more significantly. The corroded bars became brittle when the corrosion degree was high enough. Moreover, the residual shape of the cross-section of the reinforcement was found to be an important factor for the ductility of the steel bars. Some new simulations of the non-corroded bars in different residual shapes and different diameters were conducted. The results showed that the asymmetrical residual cross-section reduced the ductility of the reinforcement more obviously even though the corrosion degree was the same.

The second section paid attention to the flexural performance of the corroded beams. As the beams were highly corroded, corrosion cracks occurred to the beams throughout the spans and spalling happened to some zones in the tension sections. The bending tests showed that the corrosion reduced the yield capacity, ultimate capacity and ductility of the corroded beams significantly. The theoretical capacities of the corroded beams were deduced by the classical method. The results showed that 1% cross-sectional loss of the tension bars corresponded to 1% loss of yield capacity and about 0.84% loss of ultimate capacity. The natural corrosion at the maximum cross-sectional loss corresponded to a corrosion speed of 1.3$\mu A/cm^2$/year. The lifetime was also predicted to be 45 years by the average corrosion properties.

The third mainly section fixed on the shear performance of the short-span beams. According to the experimental tests, the non-corroded short-span beams was typically in shear failure mode, however, the corroded beams showed a bending failure mode, the ductility was increased significantly. The results showed that the corrosion could change the failure modes of the short-span beams due to the arc effect.

In the last section, the corrosion products were investigated in order to check the expansion coefficient. Based on XRD and TG tests on the corrosion products which were collected from B2Cl3, the chemical compositions were deduced, which was found to be quite close to the results got from the marine constructions. The results would be important for the further research on the cracking mechanism of the RC constructions due to chloride corrosion.

LIST OF PUBLICATIONS

ZHU W., François R., Coronelli D., Cleland D., Effect of corrosion of reinforcement on the mechanical behaviour of highly corroded RC beams, *Engineering Structures*, 2013, 56: 544-54,

ZHU W., François R., Effect of corrosion pattern on the ductility of tensile reinforcement extracted from a 26-year-old corroded beam, *Advances in Concrete Construction*, 2013, 1(2): 121-36

ZHU W., François R., Corrosion of the reinforcement and its influence on the residual structural performance of a 26-year-old corroded RC beam, *Construction and Building Materials*, 2014, 51, 461-72

ZHU W., François R., Structural performance of RC beams corroded in chloride environment for a long period, *Materials & Structures*, Accepted

ZHU W., François R., Assessment of the residual capacity of natural corroded RC beam by the real tension stress of the corroded bars, *Engineering Structures*, submitted in July, 2013

International conferences:

ZHU W., François R., Coronelli D., Effect of corrosion of reinforcement on the coupled shear and bending behaviour of reinforced concrete beam, 6th International Conference on Bridge Maintenance, Safety and Management, IABMAS, July 8-12, 2012, Streso, Lake Maggiore, Italy

ZHU W., François R., The residual structural performance of RC beams damaged by 28 years of natural corrosion in chloride environment, 11th International Conference on Structural Safety & Reliability, ICOSSAR June 16-20, 2013, Columbia University, New York, USA

ZHU W., François R., Residual structural performance of a 26-year-old corroded reinforced concrete beam, 3rd International Conference on Concrete Repair, Rehabilitation, and Retroffiting, ICCRRR, Sep. 3-5, 2012, Cape Town, South Africa)